

BUCKLING STRENGTH OF COLD FORMED STEEL SECTIONS APPLIED IN PALLET RACK STRUCTURES

Teză destinată obținerii
titlului științific de doctor inginer
la

Universitatea "Politehnica" din Timișoara
în domeniul Inginerie Civilă
de către

ing. Nicolae Andrei Crișan

Conducător științific: Prof. Dr HC. Dr. Ing. Dan Dubina,
M.C. al Academiei Române

Referenți științifici: Prof. Dr. Ing. Dinar Camotim
Prof. Dr. Ing. Dan Crețu
Conf. Dr. Ing. Viorel Ungureanu

Ziua susținerii tezei: 09.09.2011.

Seriile Teze de doctorat ale UPT sunt:

- | | |
|------------------------|---|
| 1. Automatică | 7. Inginerie Electronică și Telecomunicații |
| 2. Chimie | 8. Inginerie Industrială |
| 3. Energetică | 9. Inginerie Mecanică |
| 4. Ingineria Chimică | 10. Știința Calculatoarelor |
| 5. Inginerie Civilă | 11. Știința și Ingineria Materialelor |
| 6. Inginerie Electrică | |

Universitatea „Politehnica” din Timișoara a inițiat seriile de mai sus în scopul diseminării expertizei, cunoștințelor și rezultatelor cercetărilor întreprinse în cadrul școlii doctorale a universității. Seriile conțin, potrivit H.B.Ex.S Nr. 14 / 14.07.2006, tezele de doctorat susținute în universitate începând cu 1 octombrie 2006.

Copyright © Editura Politehnica – Timișoara, 2006

Această publicație este supusă prevederilor legii dreptului de autor. Multiplicarea acestei publicații, în mod integral sau în parte, traducerea, tipărirea, reutilizarea ilustrațiilor, expunerea, radiodifuzarea, reproducerea pe microfilme sau în orice altă formă este permisă numai cu respectarea prevederilor Legii române a dreptului de autor în vigoare și permisiunea pentru utilizare obținută în scris din partea Universității „Politehnica” din Timișoara. Toate încălcările acestor drepturi vor fi penalizate potrivit Legii române a drepturilor de autor.

România, 300159 Timișoara, Bd. Republicii 9,
tel. 0256 403823, fax. 0256 403221
e-mail: editura@edipol.upt.ro

Foreword

The thesis was developed during my activity (2008 – 2011) within the Department of Steel Structures and Structural Mechanics (CMMC), the Center of Excellence in the Mechanics of Materials and Safety of Structures (CEMSIG), from the “Politehnica” University of Timișoara.

I would like to express my gratitude and thanks to my advisor, Prof. PhD. Eng. Dr. H.C. Dan Dubină, C.M. of Romanian Academy for all his support and guidance throughout my research activity. His advices and comments along these years made it possible for me to conclude my work.

I would like to thank to Assoc. Prof. PhD. Eng. Viorel Ungureanu for his support and assistance. His valuable advices helped me with the development of the experimental program and numerical simulations.

Special thanks to Senior Lecturer PhD.Eng. Adrian Dogariu for his valuable help with numerical analyses. During these three years of research activity, his patience and attitude encouraged me to finalize the thesis.

Thanks to eng. Diana Duma, PhD. Student Eng. Iulia Juca, PhD. Student. Eng. Cristian Vulcu and Dan Scarlat for their help with the laboratory work.

My thanks also go to my colleagues, Ph.D. eng. Filip Vacarescu Norin, Ph.D. eng. Danku Gelu, Ph.D. eng. Neagu Calin and Ph.D. eng. Both Ioan, for their advices and support.

My thanks to Prof. PhD. Eng. Daniel Grecea, Assoc. Prof. PhD. Eng. Raul Zaharia, Assoc. Prof. PhD. Eng. Aurel Stratan, Assoc. Prof. PhD. Eng. Adrian Ciutina, Assoc. Prof. PhD. Eng. Adrian Ivan, PhD. Eng. Ramona Gabor, PhD. Eng. Sorin Bordea, PhD. Student Eng. Lucian Gilea and eng. Viorel Popa for their assistance and suggestions.

And last, but not least, I am grateful to my parents and my brother for all the unconditional support. I hope I have made them proud.

Timișoara, Septembrie 2011

Eng. Crișan Nicolae Andrei

Crișan Nicolae Andrei

Buckling strength of cold formed steel sections applied in pallet rack structures

Studiul formelor de instabilitate a structurilor din profile de oțel cu pereți subțiri formate la rece pentru sisteme de depozitare paletizată

Teze de doctorat ale UPT, Seria 5, Nr. 76, Editura Politehnica, 2011, 234 pagini, 141 figuri, 72 tabele.

ISSN: 1842-581X

ISBN: 978-606-554-327-0

Keywords:

thin walled sections, cold formed profiles, perforated pallet rack upright, yield strength, tensile strength, residual stress, local buckling, distortional buckling, overall buckling, flexural buckling, torsional buckling, interactive buckling, reduced slenderness, critical buckling length, critical buckling load, erosion factor, imperfection coefficient, Erosion of Critical Bifurcation Load, coupling length, coupling point, coupling range,

Abstract:

This thesis brings in discussion the simple and coupled instability phenomenon of cold formed steel section used for pallet rack structures. An experimental program has been developed in order to observe the influence of the geometric and material imperfections on the ultimate axial load capacity of the cold formed sections, together with the effect of the perforations. Four pallet rack upright section, with and without perforations, have been tested in accordance with the European pallet rack design code.

The experimental output has been used calibrate and validate a numerical model, in order to study the effects of different imperfection combinations and to determine the critical imperfection from the point of view of interactive buckling.

Based on the experimental and numerical results, a design procedure has been proposed, for the determination of buckling strength of perforated sections used for pallet rack structures.

Table of Content

Table of content	5
List of figures	7
List of tables	11
Summary	13
Rezumat	15
1 INTRODUCTION	17
1.1 Thin walled members	17
1.2 Thesis objectives	18
1.3 Thesis outline	19
2 INTERACTIVE BUCKLING OF THIN WALLED MEMBERS	21
2.1 Cold-formed steel sections	21
2.2 Storage systems	28
2.2.1 Definitions and components	28
2.2.2 Loads for storage systems	31
2.3 Some peculiar characteristics of cold-formed thin-walled steel sections	33
2.3.1 Strain hardening and change of yield strength due to the cold forming	33
2.3.2 The Bauschinger effect	36
2.3.3 Residual stresses	36
2.3.4 Geometric imperfections	40
2.4 Peculiar problems of cold-formed steel design	42
2.4.1 Buckling strength of cold-formed members	42
2.4.2 Torsional rigidity	46
2.4.3 Web crippling	47
2.4.4 Ductility and plastic design	48
2.4.5 Design assisted by testing	48
2.5 Distortional buckling: summary review	48
2.6 Interactive buckling	55
2.6.1 Theoretical background	55
2.6.2 Models and methods	67
2.7 Design Code Provisions	85
2.7.1 European Buckling curves: summary review	85
2.7.2 Design according to EN 15512: „Steel static storage systems – Adjustable pallet racking systems - Principles for structural design“	96
2.8 Concluding Remarks	102
3 EXPERIMENTAL PROGRAM	103
3.1 Introduction	103
3.2 Summary of EN15512 provisions for testing compressed members	105
3.3 Experimental testing program	110
3.3.1 Geometry and material	110
3.3.2 Material testing. Yield strength variation	111
3.3.3 Residual stresses	115
3.3.4 Geometrical imperfections	118
3.3.5 Stub column testing	122
3.3.6 Upright testing	127
3.3.7 Distortional buckling specimens testing	131

3.3.8 Interactive buckling specimens tests	136
3.4 Tests summary and interpretation	145
3.4.1 Material properties	145
3.4.2 Sectional and overall imperfections	148
3.4.3 Compression tests results	150
3.5 Concluding remarks	157
4 NUMERICAL STUDIES	161
4.1 Introduction	161
4.2 Geometrical characteristics of cross-section	161
4.3 Model calibration and validation	162
4.4 Imperfection sensitivity study	177
4.5 Erosion of critical bifurcation erosion and imperfection factor evaluation	182
4.6 Concluding remarks	189
5 BUCKLING CHECKING OF PERFORATED COLD-FORMED STEEL SECTIONS IN COMPRESSION.	191
5.1 Introduction	191
5.1.1 Experimentally based design procedure	194
5.1.2 FE based design procedure	196
5.2 Proposed design procedure – 1	198
5.3 Proposed design procedure – 2	206
5.4 Concluding Remarks	208
6 CONCLUSIONS	215
6.1 Conclusions	215
6.1.1 Thesis objective	215
6.1.2 Synthesis of chapters conclusions	215
6.1.3 Concluding remark	217
6.2 Personal contributions	218
6.3 Publications	219
6.4 Acknowledgements	220
REFERENCES	221

List of Figures

- Fig. 2.1 Stand cold reduction mill
Fig. 2.2 Stages in roll forming a simple section
Fig. 2.3 Industrial roll forming lines
Fig. 2.4 Forming steps in press braking process
Fig. 2.5 Industrial brake press
Fig. 2.6 Forming of folding
Fig. 2.7 Typical upright frames
Fig. 2.8 General system components
Fig. 2.9 Pallet rack beam sections
Fig. 2.10 Pallet rack upright sections
Fig. 2.11 Pallet rack upright perforation types
Fig. 2.12 Beam to column connections
Fig. 2.13 Effects of strain hardening and strain aging on σ - ε characteristics of carbon steel: (a) global σ - ε diagram; (b) apparent σ - ε diagram for a cold-formed member)
Fig. 2.14 Influence of manufacturing process on yield strength
Fig. 2.15 (a) Bauschinger effect; (b) Inverse Bauschinger effect
Fig. 2.16 Idealisation of residual stresses
Fig. 2.17 Measurement of residual stresses in a cold rolled C profile:
(a) residual "flower"; (b) slicing method; (c) curvature method
Fig. 2.18 Residual flower for plain channel and lipped channel sections
Fig. 2.19 Measured residual stress in cold-formed steel sections:
(a) cold-rolled angle; (b) cold-rolled C profile; (c) press braked U profile [21]
Fig. 2.20 Definition of local imperfections
Fig. 2.21 Buckling modes for a lipped channel in compression Single modes:
(a) local (L); (b) distortional (D); (c) flexural minor axis (F); (d) flexural major axis (F); (e) flexural-torsional (FT) Coupled (interactive) modes: (f) L + D; (g) F + L; (h) F + D; (i) FT + L; (j) FT + D; (k) F + FT; (l) F + FT + L; (m) F + FT + D
Fig. 2.22 Buckling strength versus half-wavelength for a lipped channel in compression
Fig. 2.23 Behaviour of (a) slender tick-walled and (b) thin-walled compression bar
Fig. 2.24 Failure mode of a lipped channel in compression
Fig. 2.25 Effect of local buckling on the member capacity
Fig. 2.26 Torsional deformations
Fig. 2.27 Stability and instability of structures
Fig. 2.28 Erosion of critical bifurcation load
Fig. 2.29 Stable and unstable components
Fig. 2.30 Post-critical behaviour as result of the sum of the two components
Fig. 2.31 Natural coupled instability: example for lipped channel section analysed with a spline finite strip buckling program
Fig. 2.32 Coupled instability by design: example for T section with test evidences
Fig. 2.33 Similarities between plastic buckling and coupled instability
Fig. 2.34 Load-displacement curves found using different analyses of the same structure

- Fig. 2.35 Elastic bifurcation and geometrically nonlinear effects in structural systems
- Fig. 2.36 Load-deflection paths in imperfect structural systems
- Fig. 2.37 Square simply supported thin plate in compression
- Fig. 2.38 Local buckling of component walls of a cold-formed thin-walled section
- Fig. 2.39 Post buckling behaviour of stiffened and unstiffened plate element (Hancock, 1998)
- Fig. 2.40 Consecutive stress distribution in stiffened compression elements: (a)-pre-critical stage; (b)-intermediate post-critical stage; (c)-ultimate post-critical stage
- Fig. 2.41 Behaviour of ideal and actual simply supported plate in uniaxial stress
- Fig. 2.42 Stress distribution in simply supported plate, uniaxially compressed:(a) actual stress distribution; (b) equivalent stress distribution based on the "effective width" approach
- Fig. 2.43 Change of effective width in terms of maximum edge stress
- Fig. 2.44 Reduction factor, ρ , vs. relative plate slenderness, $\bar{\lambda}_p$, relationship
- Fig. 2.45 In-plane configurations of C-section deformation modes: (a) discretization no. 1; (b) discretization no. 2 [44]
- Fig. 2.46 GBT-based column buckling: (a) P_b vs. L curves ($L > 100$ cm), (b) modal participation diagrams and (c) in-plane shapes of 3 buckling and deformation modes
- Fig. 2.47 The interactive buckling model based on the ECBL theory
- Fig. 2.48 Theoretical and practical interaction of two buckling modes
- Fig. 2.49 The erosion of bar buckling curve
- Fig. 2.50 Relation between ψ erosion factor and α coefficient of imperfection
- Fig. 2.51 Relation between α , \bar{N}_L and ψ
- Fig. 2.52 The interactive buckling model based on the ECBL theory
- Fig. 2.53 (a) Imperfect bar member in compression; (b) load - deflection path
- Fig. 2.54 Buckling length L_{cr} as a function of the real length L of the column
- Fig. 2.55 $\sigma - \lambda$ relationship of a compressed member
- Fig. 2.56 Torsional buckling and flexural-torsional buckling
- Fig. 2.57 Results of experimental tests in real members
- Fig. 2.58 European design buckling curves
- Fig. 2.59 Shift of neutral axis due to effective cross-section
- Fig. 2.60 Examples of distortional buckling modes
- Fig. 2.61a Examples of elastic critical stress for various buckling modes as function of half-wave length and examples of buckling modes
- Fig. 2.62b Examples of elastic buckling load and buckling resistance as a function of member length
- Fig. 2.63 Mono-symmetric cross-sections susceptible to torsional-flexural buckling
- Fig. 2.64 Distortional mode controlled by simple lips
- Fig. 2.65 Distortional mode not controlled by simple lips
- Fig. 2.66 Stub column test arrangement
- Fig. 2.67 Alternative arrangements for compressive tests on uprights
- Fig. 3.1 STUB column test arrangement
- Fig. 3.2 RS125x3.2 cross-section - brut and perforated

Fig. 3.3 RS95x2.6 cross-section – brut and perforated
 Fig. 3.4 Behaviour curves for base material
 Fig. 3.5 Section partition in strips
 Fig. 3.6 Behaviour curves for RS95 section strips
 Fig. 3.7 Behaviour curves for RS125 section strips
 Fig. 3.8 Definition of flexural and membrane residual stress
 Fig. 3.9 Strips partition for residual stresses measurements
 Fig. 3.10 Vic3D measuring system.
 Fig. 3.11 Measured geometry and approximation function for residual stresses measurement
 Fig. 3.12 Spring-back effect
 Fig. 3.13 Measured geometry and measurement sections
 Fig. 3.14 Proposed and considered imperfections
 Fig. 3.15 Measured global rectilinear deviations for upright specimens
 Fig. 3.16 Set up for measuring imperfections of upright specimens
 Fig. 3.17 Measuring device for geometric imperfections
 Fig. 3.18 Considered sectional and global bow imperfection
 Fig. 3.19 Stub column test setup
 Fig. 3.20 Experimental curves for ST-125 a) brut and b) net stub column specimens.
 Fig. 3.21 Experimental curves for ST-95 a) brut and b) net stub column specimens.
 Fig. 3.22 UPRIGHT tests setup
 Fig. 3.23 Experimental curves for UP-125 a) brut and b) net upright specimens.
 Fig. 3.24 Experimental curves for RS95 a) brut and b) net upright specimens.
 Fig. 3.25 Uniform stress distribution over the effective net section
 Fig. 3.26 DISTORTIONAL tests setup
 Fig. 3.27 Experimental curves for DIST-125 a) brut and b) net specimens
 Fig. 3.28 Experimental curves for DIST-95 specimens
 Fig. 3.29 Interactive buckling for studied members in compression
 Fig. 3.30 Displacement transducers setup
 Fig. 3.31 Schematic test setup for interactive buckling specimens
 Fig. 3.32 Test setup for interactive buckling specimens
 Fig. 3.33 Maximum experimental load vs. axial shortening curves for RS125 interaction specimens
 Fig. 3.34 Experimental load vs. axial shortening curves for RS95 interactive buckling specimens
 Fig. 3.35 Yield limit increase due to cold forming
 Fig. 3.36 Yield stress increase due to cold forming ($\%f_y$)
 Fig. 3.37 Ultimate strength increase due to cold forming ($\%f_u$)
 Fig. 3.38 Average bending residual stresses ($\%f_y$)
 Fig. 3.39 Average residual stresses for press braked sections(%)
 Fig. 3.40 Residual stress distribution ($\%f_y$)
 Fig. 3.41 Sectional imperfections
 Fig. 3.42 Modal classification for RS125B section
 Fig. 3.43 Modal classification for RS125N section (t_{eq} experimental)
 Fig. 3.44 Modal classification for RS95B section
 Fig. 3.45 Modal classification for RS95N section (t_{eq} experimental)

- Fig. 4.1 Material behaviour curves defined in FE models for RS125 models
- Fig. 4.2 End constrains
- Fig. 4.3 Mesh details for RS125 STUB specimen
- Fig. 4.4 Behaviour curves for different FE types
- Fig. 4.5 Behaviour curves for RS125 stub specimens
- Fig. 4.6 Behaviour curves for RS95 stub specimens
- Fig. 4.7 Coupling of simple buckling modes
- Fig. 4.8 Behaviour curves for RS125 upright specimens
- Fig. 4.9 Behaviour curves for RS95 specimens
- Fig. 4.10 Behaviour curves for RS125 INTERACTIVE specimens
- Fig. 4.11 Behaviour curves for RS125 INTERACTIVE specimens
- Fig. 4.12 The ECBL interactive buckling model for distortional and Euler bar instabilities
- Fig. 4.13 Example of considered simple imperfections (f and d)
- Fig. 4.14 Example of considered coupled imperfections (f and d)
- Fig. 4.15 The interactive buckling model based on the ECBL Theory
- Fig. 4.16 Interaction curves for RS125B section
- Fig. 4.17 Interaction curves for RS125N section
- Fig. 4.18 Interaction curves for RS95B section
- Fig. 4.19 Interaction curves for RS95N section
- Fig. 5.1 The ECBL interactive buckling model for distortional and Euler bar instabilities
- Fig. 5.2 Buckling strength curves for RS125N section
- Fig. 5.3 Buckling strength curve for RS95N section
- Fig. 5.4 Buckling capacity curve for RS125N section – experimental method, $\gamma_{M1}=1.0$
- Fig. 5.5 Buckling capacity curve for RS95N section – experimental method, $\gamma_{M1}=1.0$
- Fig. 5.6 Buckling capacity curve for RS125N section – experimental procedure, $\gamma_{M1}=1.1$
- Fig. 5.7 Buckling strength curve for RS95N section – experimental procedure, $\gamma_{M1}=1.1$
- Fig. 5.8 Buckling capacity curve for RS125N section – numerical procedure, $\gamma_{M1}=1.0$
- Fig. 5.9 Buckling capacity curve for RS95N section – numerical procedure, $\gamma_{M1}=1.0$
- Fig. 5.10 Type 2 sectional imperfection (d_2) for distortional specimens.

List of Tables

- Table 2.1 Influence of manufacturing process on the basic strengths of hot and cold-formed profiles
- Table 2.2 Type magnitude of residual stress in steel sections
- Table 2.3 Coupled instabilities in bar members
- Table 2.4 Imperfection factors for buckling curves
- Table 2.5 Appropriate buckling curve for various types of cross-section
- Table 2.6 Imperfection factor α for different types of cold-formed section
- Table 3.1 Specimen codification for considered sections
- Table 3.2 Base material properties for section RS95
- Table 3.3 Base material properties for section RS125
- Table 3.4 Comparison of mechanical characteristics for RS95B section
- Table 3.5 Comparison of mechanical characteristics for RS125B section
- Table 3.6 Average residual stresses distribution
- Table 3.7 STUB test specimen lengths
- Table 3.8 Maximum loads and failure mode for RS125B stub column specimens
- Table 3.9 Maximum load and failure mode for ST-125N net stub specimens
- Table 3.10 Maximum load and failure mode for ST-95B specimens
- Table 3.11 Ultimate load and failure mode for ST-95N specimens
- Table 3.12 Ultimate load and failure mode for UP-125B specimens
- Table 3.13 Maximum load and failure mode for UP-125N upright specimens
- Table 3.14 Maximum load and failure mode for ST-95B upright specimens
- Table 3.15 Maximum load and failure mode for UP-95N upright specimens
- Table 3.16 Distortional critical buckling load and equivalent thickness of perforated sections; half wave lengths of studied sections
- Table 3.17 Length for distortional specimens
- Table 3.18 Maximum load and failure mode for DIST-125B specimens
- Table 3.19 Ultimate load and failure mode for DIST-125N specimens
- Table 3.20 Ultimate load and failure mode for DIST-95B specimens
- Table 3.21 Ultimate load and failure mode for DIST-95N specimens
- Table 3.22 Sectional capacity of RS95 and RS125 section
- Table 3.23 Coupling length for RS95 and RS125 section
- Table 3.24 Specimens length for interactive buckling study
- Table 3.25 Failure loads and failure mode for INT-125B specimens
- Table 3.26 Failure loads and failure mode for INT-125N specimens
- Table 3.27 Failure load and failure mode for INT-95B specimens
- Table 3.28 Failure load and failure mode for INT-95N specimens
- Table 3.29 Mean value of base material properties
- Table 3.30 Sectional measured imperfections (d_2) for short specimens
- Table 3.31 Sectional imperfections d_2 INTERACTIVE specimens
- Table 3.32 Measured loading eccentricities
- Table 3.33 Local buckling ratios
- Table 3.34 Experimental test review
- Table 3.35 Effective areas and equivalent thickness for STUB column specimens
- Table 3.36 Distortional critical buckling load and section's capacity
- Table 3.37 Effective areas for distortional and upright tests
- Table 3.38 Experimental distortional failure loads and section strength

Table 3.39 Erosion coefficient for RS125 sections based on experimental approach

Table 3.40 Erosion coefficient for RS95 sections based on experimental approach

Table 4.1 Measured imperfections and load eccentricities for RS125B stub specimen

Table 4.2 Ultimate load and analysis time per element type

Table 4.3 Ultimate loads for different imperfection factors

Table 4.4 Cases considered for parametric analysis

Table 4.5 Numerical model validation for STUB specimens

Table 4.6 Failure mode for STUB specimens: Experimental vs. numeric

Table 4.7 Numerical model validation for UPRIGHT specimens

Table 4.8 Failure mode for UPRIGHT specimens: Experimental vs. numeric

Table 4.9 Numerical model validation for INTERACTIVE specimens

Table 4.10 Failure mode for INTERACTIVE specimens: Experimental vs. numeric

Table 4.11 "Theoretical" distortional capacity of RS95 and RS125 section

Table 4.12 The effects of normalized geometric imperfections – absolute values

Table 4.13 The effects of normalized geometric imperfections – difference

Table 4.14 Erosion and imperfection coefficients for considered imperfections

Table 4.15 Coupling length and resulted erosion for RS125B section

Table 4.16 Coupling length and resulted erosion for RS125N section

Table 4.17 Coupling length and resulted erosion for RS95B section

Table 4.18 Coupling length and resulted erosion for RS95N section

Table 4.19 Coupled instabilities for structural elements

Table 5.1 Assumptions for FE-methods

Table 5.2 Properties used for ECBL approach

Table 5.3 Considered coupling length and coupling interval

Table 5.4 Interactive buckling interval results

Table 5.5 Design procedures – results

Table 5.6 Maximum geometric imperfections for RS125N interactive buckling specimens

Table 5.7 Maximum geometric imperfections for RS95N interactive buckling specimens

Summary

Nowadays, the stability verifications for cold formed thin walled members is made using European buckling curves developed in the '60, based on an ample experimental program. The buckling curves were developed for hot rolled profiles and their use was further extend for cold formed thin walled members, even if it is well known, that the physical-mechanical properties and behaviour of cold formed profiles are very different to those of hot rolled profiles.

The main objective of this thesis is to develop a procedure to determine the buckling strength of cold formed steel sections applied in pallet rack structures.

In chapter 2 are presented the specific problems regarding the cold formed thin walled steel elements behaviour and their applications. There are presented the effects of cold forming process on mechanical properties of base material, the problem of geometrical imperfections, the strain hardening as an effect of cold working, the Bauschinger effect and residual stresses, specific to this type of profiles. It is also analysed the walls slenderness effect on the stability resistance for this sections.

Simple and coupled instabilities for elements under axial compression are reviewed together with theoretical considerations, current models and design procedures, for Direct Strength Method (DSM), Generalised Beam Theory (GBT) the Erosion of Critical Bifurcation Load (ECBL) and FE numerical models.

Also, are presented the storage structural systems together with their components, including specific design problems. Current European design standard and literature review was made in order to underline the current problems regarding the design of this type of structures.

In Chapter 3 is presented the experimental program carried out at in the CEMSIG testing facility at "POLITEHNICA" University of Timișoara, Construction Faculty, Department of Steel Constructions and Structural Mechanics (CMMC). There have been studied four types of cross-sections, with and without perforations. Experimental program have been developed in accordance with provision of the European pallet rack design code, and includes:

- Material tensile tests
- Geometric imperfection measurements
- Short (STUB column) specimen centric compression tests
- Long (UPRIGHT column) specimen centric compression tests
- "Distortional" specimen centric compression tests
- Centric compression tests on specimens having the length in the interactive buckling domain

Chapter 4 deals with the numerical model developed for thin walled members, with and without perforations. It describes the steps for finite element procedure used to calibrate and validate the numerical model. Using the calibrated and validated finite element model against the experimental tests, a parametric study was conducted in order to determine the influence of geometric, sectional and global imperfections, on the ultimate capacity of a thin walled member and to determine the dominant imperfection for the case for pallet rack upright sections.

Based on ECBL approach, simple and coupled imperfections that are critical for member ultimate capacity will be determined and together with α imperfection coefficients that take into account these initial imperfections.

In chapter 5 is presented the design procedure in accordance with EN1993-1-1 specifications adapted for the case of distortional-flexural interactive buckling.

Concluding the results from previous chapters, a new design procedure based on ECBL approach is proposed.

The ECBL approach is a newly developed procedure that permits the evaluation erosion of critical bifurcation load as result of interactive buckling. It allows considering the interaction of sectional (local or distortional buckling) with global (flexural, torsional or flexural-torsional) instabilities.

For this study, the distortional-flexural coupled instability was considered. Using the ECBL approach, two design procedure based on EN1993-1-1/EN1993-1-3 buckling strength checking were developed: an experimentally based procedure and a numerically based procedure.

It was observed that the resulting buckling strength curve determined using the experimentally based procedure describe optimally the strength of the tested specimens. The design procedure based on numerical models is more conservative, due to the fact that the imperfections considered for the numerical approach were coupled with their maximum values. This approach was considered due to the fact that the loading eccentricities were disregarded, while in practice they are inerrant.

The obtained results are compared with experimental tests results for the two studied sections, with perforations.

Further on, in the final chapter are presented the research concluding remarks together with the author's contributions.

Taking into account that the imperfection coefficients for the European buckling curves (EN1993-1-1) have been experimentally determined for hot-rolled sections and the factor $\alpha \lambda^{-0.2}$ have been calibrated by Rondal and Maquoi in '70s for the same type of profiles, it is not normal that these values to be used for cold formed steel sections.

The values of imperfection coefficients presented in EN1993-1-1 are influenced by the cross-sectional shape in direct relation with the membrane residual stresses. For the case of thin walled section, the membrane residual stresses are significantly lower than the flexural residual stresses, on one hand, and on the other hand the influence of geometric imperfections, due to wall slenderness has a more pronounced effect than the residual stresses.

Considering these, imperfection coefficients specifically determined for thin walled sections together with a proper calibration of safety coefficient, γ_{M1} , is required. For this purpose, appropriate α imperfection factors can be calibrated based on experimental tests, numerical simulations or a combination of the two by using ECBL approach.

The final conclusion of this study is that it is really possible to adapt the European buckling curves and use the design checking procedure for stability problems from EN1993-1-1 and EN1993-1-3 for verification of upright type members in compression.

Rezumat

În prezent, verificarea la stabilitate a profilelor cu pereți subțiri, formate la rece, se face pe baza curbelor de flambaj Europene. Aceste curbe de flambaj au fost determinate în urma unui amplu program experimental desfășurat în anii '60. Curbele de flambaj au fost determinate pentru profilele grele, formate la cald, iar mai apoi, folosirea acestor curbe a fost extinsă pentru calculul barelor cu pereți subțiri chiar dacă proprietățile fizico-mecanice ale acestora diferă în mod fundamental de cele ale profilelor formate la cald.

Obiectivul principal al acestei lucrări, este de a dezvolta o metoda de calcul pentru determinarea rezistenței la flambaj a profilelor perforate formate la rece folosite pentru structura de rezistență a sistemelor de depozitare paletizată.

Capitolul 2 prezintă studiul monografic realizat pentru a sintetiza problemele de specifice de comportament ale profilelor cu pereți subțiri formate la rece împreună cu principalele domenii de utilizare. În continuare, se prezintă efectele procesului de formare la rece asupra proprietăților mecanice ale materialului de bază. De asemenea se studiază problematica imperfecțiunilor geometrice, efectul de ecruisare, efectul Bauschinger și efectul tensiunilor reziduale, specifice acestor tipuri de profile. Se analizează, în același timp, efectul zvelteții pereților secțiunii asupra stabilității secțiunii.

Se trec în revistă instabilitățile simple și cuplate pentru elementele supuse la compresiune, împreună cu considerațiile teoretice, modele și proceduri de calcul pentru DSM (Direct Strength Method) – Metoda Rezistenței Efective,GBT (Generalised Beam Theory) – Teoria Grinzii Generalizate, ECBL (Erosion of Critical Bifurcation Load) – Eroziunea Încărcării Critice de Bifurcare și a modelelor numerice cu element finit.

În continuare se prezintă structurile de depozitare împreună cu elementele componente, inclusiv probleme specifice de calcul ale acestor structuri. De asemenea se prezintă procedura de calcul din norma europeană de proiectare a sistemelor de depozitare paletizată pentru a sublinia problemele actuale cu privire la acest tip de structuri.

Capitolul 3 prezintă programul experimental desfășurat în cadrul laboratorului „CEMSIG” din cadrul Facultății de Construcții, din Universitatea „PLOTEHNICA” din Timișoara. S-au studiat patru tipuri de secțiuni, cu și fără perforații. Programul a fost dezvoltat în conformitate cu prevederile normei europene de proiectare a sistemelor de depozitare paletizată. Programul experimental cuprinde următoarele tipuri de teste:

Teste pe material

Măsurători pentru determinarea imperfecțiunilor geometrice

Teste de compresiune pe tronsoane scurte (STUB Column Tests)

Teste de compresiune pe tronsoane cu lungimea egală cu distanța dintre două noduri succesive ale unui panou transversal al structurii de rezistență a sistemului de depozitare paletizată

Deoarece scopul lucrării de față este studiul formelor de instabilitate a profilelor perforate formate la rece, iar pe baza rezultatelor se urmărește propunerea unei proceduri de verificare a stabilității acestor profile, programul experimental a fost completat cu:

- teste pe tronsoane cu lungimea egală cu lungimea de semiundă a flambajului prin distorsiune

- teste pe tronsoane cu lungimea în intervalul de cuplare al flambajului prin distorsiune cu flambajul global (prin încovoiere). Lungimea de cuplare a fost determinată pe baza procedurii ECBL.

În continuare, în capitolul 4, pe baza rezultatelor obținute în urma programului experimental, se trece la calibrarea și validarea unui model numeric pentru profilele cu și fără perforații.

Folosind modelul numeric cu element finit calibrat s-a efectuat un studiu parametric pentru a determina influența diferitelor tipuri de imperfecțiuni geometrice asupra capacității ultime a profilelor cu pereți subțiri perforați solicitate la compresiune. Folosind procedura ECBL s-au determinat imperfecțiunile critice pentru aceste profile, s-au determinat factorii de eroziune maximi, iar pe baza valorii lor de calcul s-au determinat coeficienții de imperfecțiune, α .

În partea finală a lucrării, se propun două metode de calcul (1) bazate pe o abordare experimentală, în conformitate cu prevederile normei europene, adaptate însă pentru considerarea cuplării modurilor de instabilitate și (2) bazate pe o abordare numerică pentru a limita numărul de teste necesare. Curbele obținute cu ambele metode propuse sunt comparate cu rezultatele testelor experimentale.

Curbele de flambaj determinate cu ajutorul metodelor propuse pe baza procedurilor definite în normele europene, EN1993-1-1/EN1993-1-3, descriu optim comportamentul observat pentru specișenele încercate experimental.

Metoda folosită pentru calibrarea coeficientului de imperfecțiune, α , este o metodă nouă care permite determinarea acestui coeficient pe baza valorii de calcul a factorului de eroziune, determinat în intervalul de cuplare a modurilor de flambaj considerate. În acest caz s-a considerat cuplarea flambajului prin distorsiune cu flambajul global prin încovoiere.

Lucrarea se încheie cu concluziile trase pe baza analizei rezultatelor obținute, atât pe cale experimentală cât și pe cale numerică. Ținând seama de faptul că factorii de imperfecțiune folosiți pentru trasarea curbelor de flambaj europene au fost determinați în urma unui amplu program experimental, desfășurat în anii '60, pentru profilele formate la cald, iar factorul $\alpha \bar{\lambda} - 0.2$ a fost calibrat de Rondal și Maquoi pentru același tip de profile, nu este normal ca aceste valori să fie folosite pentru calculul secțiunilor formate la rece.

Valorile factorilor de imperfecțiune definite de EN1993-1-1 sunt în principal influențate de forma secțiunilor transversal în relație directă cu tensiunile reziduale membranare. În cazul profilelor formate la rece, tensiunile membranare sunt semnificativ mai reduse decât cele de încovoiere, pe de o parte, iar pe de altă parte, influența imperfecțiunilor geometrice, datorită zvelteții pereților, are un efect mai important decât tensiunile reziduale.

Din acest motiv, pentru barele cu pereți subțiri, se impun factori de imperfecțiune determinați în mode specific și calibrarea corespunzătoare a coeficientului de siguranța aferent.

La finalul acestui studiu se poate spune ca prin folosirea metodologiei propuse de ECBL, este posibilă adaptarea curbelor de flambaj europene, specificate în EN1993-1-1 și EN1993-1-3, pentru calculul profilelor formate la rece.

1 INTRODUCTION

1.1 Thin walled members

Nowadays, the stability verifications for cold formed thin walled members is made using European buckling curves developed in the '60, based on an ample experimental program. The buckling curves were developed for hot rolled profiles and the use was further extend for cold formed thin walled members, even if is well known that the physic-mechanical properties and behaviour of cold formed profiles are very different to those of hot rolled profiles.

These differences refer mainly to:

- different origin of imperfections: the stability of hot rolled profiles is substantially influenced by residual stresses as a result of hot rolling process, while cold formed members are much more sensitive to geometric imperfections than to residual stresses, which are substantially lower and partially compensated by strain hardening due to cold working.
- because of walls high slenderness there is always an interaction between sectional and global instabilities. Due to this interaction, the critical buckling load is eroded, with a maximum effect in the coupling point.

In these conditions, it is obvious that for cold formed thin walled steel elements is required the use of specialized buckling curves. The use of present buckling curves, determined for hot rolled steel profiles, is a temporary solution adopted in the '70 because of the increasing use of thin walled members in structural elements.

The buckling curves for interactive buckling concept based on erosion of critical buckling load was for the first time presented by Dubina in 1990, followed by an analysis, attempting to classify the thin walled sections from the point o view of the erosion of critical interactive buckling load sensitivity.

It's worth mentioning that the study of coupled instabilities, which are characteristic especially to thin walled structures, is a worldwide trend.

The use of thin walled members in a wide range of applications is conditioned, firstly, by a correct evaluation of stability resistance hence the need for design relations. These relations must embed the real behaviour of these profiles and they must be, in the same time, simple enough to be included in design standards and to be used in current design of such profiles.

The understanding of the instability phenomena of thin walled profiles (which is the principal criterion for design) can extend the use of these profiles in more structural engineering applications. It is known that the use of thin walled members is more economic and less time consuming compared to the use of hot rolled profiles.

1.2 Thesis objectives

This thesis has the following objectives:

- The main objective of this thesis is to develop a procedure to determine the buckling strength of perforated cold formed steel sections applied in pallet rack structures
- The development of an experimental program for:
 - determination of base material properties, yield limit and strength increase due to cold forming together with the residual stress magnitude and distribution.
 - geometric imperfection measurement
 - short (STUB) specimens: in order to determine the influence of local buckling and perforations on cross sections capacity.
 - long (UPRIGHT) specimens: in order to determine the influence of distortional buckling on the upright capacity.
 - “distortional” specimens: in order to determine the distortional capacity of studied sections, with and without perforations.
 - specimens having the length in the interactive buckling domain. The purpose of these tests is to experimentally determine the erosion due to instability coupling and geometric and material imperfections.
- To understand the behaviour of thin walled members with perforations from the point of view of simple and coupled instabilities
- To calibrate and validate of FE numerical models using the software package ABAQUS in order conduct a imperfection sensitivity numerical study to determine the dominant combination of imperfections.
- To develop a model for interactive buckling (distortional buckling and global flexural buckling) based on ECBL (Erosion of Critical Bifurcation Load) approach
- To evaluation the erosion of distortional capacity as result of coupled instabilities, geometric and material imperfections
- To determine the α imperfection coefficient based on ψ erosion coefficient for interactive buckling i.e. distortional buckling and global flexural buckling for profiles with and without perforations
- To propose a design method based on the erosion of critical bifurcation load approach able to predict accurately the compressive capable force for thin walled profiles with perforations

1.3 Thesis outline

The thesis lineout is closely related to above mentioned objectives:

Chapter 1

In this chapter are presented the current general state of knowledge in the cold formed steel sections stability field together with the points of interest that justify the research. There are also presented the thesis objectives.

Chapter 2

In this chapter are analyzed the specific problems regarding the cold formed thin walled steel elements behaviour and their applications. There are presented the effects of cold forming process on mechanical properties of base material, the problem of geometrical imperfections, the strain hardening as an effect of cold working, the Bauschinger effect and residual stresses, specific to this type of profiles. It is also analysed the walls slenderness effect on the stability resistance for this sections.

Simple and coupled instabilities for elements under axial compression are reviewed together with theoretical considerations, current models and design procedures, for Direct Strength Method (DSM), Generalised Beam Theory (GBT) the Erosion of Critical Bifurcation Load (ECBL) and FE numerical models.

In this chapter are also presented the storage structural systems together with their components, including specific design problems.

Current European design standard and literature review was made in order to underline the current problems regarding the design of this type of structures.

Chapter 3

In this chapter is presented the experimental program carried out at in the CEMSIG testing facility at "POLITEHNICA" University of Timișoara, Construction Faculty, Department of Steel Constructions and Structural Mechanics (CMMC). Experimental program includes:

- Material tensile tests, in order to experimentally determine the base material properties, yield limit and strength increase due to cold forming together with the residual stress magnitude and distribution.
- Geometric imperfection measurements
- Short (STUB column) specimen centric compression tests: in order to determine the influence of local buckling and perforations on cross sections capacity in accordance with EN15512:2009 specifications.
- Long (UPRIGHT column) specimen centric compression tests: in order to determine the influence of distortional buckling on the upright capacity in accordance with EN15512:2009 specifications.
- "Distortional" specimen centric compression tests: in order to determine the distortional capacity of studied sections, with and without perforations.
- Centric compression tests on specimens having the length in the interactive buckling domain. The purpose of these tests is to experimentally determine the erosion due to instability coupling and geometric and material imperfections.

Chapter 4

This chapter deals with the numerical model developed for thin walled members, with and without perforations. It describes the steps for FE procedure used to calibrate and validate the numerical model. Using the calibrated and validated FE model against the experimental tests, a parametric study was conducted in order to determine the influence of geometric, sectional and global imperfections, on the ultimate capacity of a thin walled member and to determine the dominant imperfection for the case for pallet rack upright sections.

Based on ECBL approach, simple and coupled imperfections that are critical for member ultimate capacity will be determined and together with α imperfection coefficients that take into account these initial imperfections.

Chapter 5

This chapter presents the design procedure in accordance with EN1993-1-1 specifications adapted for the case of distortional-flexural interactive buckling. Concluding the results from previous chapters, a new design procedure based on ECBL approach is proposed.

The obtained results will be compared with experimental tests results for the two studied sections, with perforations.

Chapter 6

In this chapter are presented the research concluding remarks together with the author's contributions.

2 INTERACTIVE BUCKLING OF THIN-WALLED SECTIONS

2.1 Cold-formed steel sections

Cold-formed steel products are found in all aspects of modern life. The use of these products are multiple and varied, ranging from "tin" cans to structural piling, from keyboard switches to mainframe building members. Nowadays, a multiplicity of widely different products, with a tremendous diversity of shapes, sizes, and applications are produced in steel using the cold forming process.

The use of cold-formed steel members in building construction began on about the 1850s in both the United States and Great Britain. However, such steel members were not widely used in buildings until 1940.

In the recent years, it has been recognised that cold-formed steel sections can be used effectively as primary framing components. In what concerns cold-formed steel sections, after their primary applications as purlins or side rails, the second major one in construction is in the building envelope. Options for steel cladding panels range from inexpensive profiled sheeting for industrial applications, through architectural flat panels used to achieve a prestigious look of the building. Light steel systems are widely used to support curtain wall panels. Cold-formed steel in the form of profiled decking has gained widespread acceptance over the past fifteen years as a basic component, along with concrete, in composite slabs. These are now prevalent in the multi-storey steel framed building market. Cold-formed steel members are efficient in terms of both stiffness and strength. In addition, because the steel may be even less than 1 mm thick, the members are light weight. The already impressive load carrying capabilities of cold-formed steel members will be enhanced by current work to develop composite systems, both for wall and floor structures.

The term *storage racking* covers an extremely wide range of products that have as their purpose the storage of material in a secure and easily accessible manner. Storage racking systems range from small shelving systems to extremely large rack-clad buildings. The components used in storage racking are largely of cold-formed steel, and the storage racking industry is one of the major users of cold-formed steel.

The forerunners of the modern storage structures were slotted-angle products first introduced in the 1930s. These consisted of cold-formed angle sections with perforations to provide a means whereby the designer could utilize the simplicity and flexibility of connections thus permitted to produce storage systems in a variety of shapes and configurations. By this means simple shelving could be provided for warehouses of any size. From these beginnings, natural evolution leads to the present-day situation [1]. It was found that for many systems bolted connections could be beneficially replaced by clips or other specific connections, and a wide variety of alternative connection methods were developed for different systems. Although perforated angles had much in their favour for some purposes, particularly for smaller storage systems, the requirements for bracing in these torsionally weak members meant that for many purposes other shapes of cross-sections were superior. Nowadays slotted angles are still widely used for shelving

systems, but in larger storage racking systems other perforated members, generally mono-symmetric, are used as columns, while normally unperforated members are used as beams.

The use of cold-formed steel structures is increasing throughout the world with the production of more economic steel coils particularly in coated form with zinc or aluminium / zinc coatings. These coils are subsequently formed into thin-walled sections by the cold-forming process. They are commonly called "Light gauge sections" since their thickness has been normally less than 3 mm. However, more recent developments have allowed sections up to 25 mm to be cold-formed, and open sections up to approximately 8mm thick are becoming common in building construction. The steel used for these sections may have a yield stress ranging from 250 MPa to 550 MPa [2]. The higher yield stress steels are also becoming more common as steel manufacturers produce high strength steel more efficiently.

It should be mentioned that, in some cases, the thickness of base material is obtained by cold reducing (rolling) of the virgin material. Rolling is an indirect compression process. Normally the only force or stress applied is the radial pressure from the rolls; this deforms the metal and pulls it through the roll gap. Rolling is the most widely used deformation process and for the reason that there are so many versions the process has its own classification. In Fig 2.1 is presented, schematically a rolling process according to one of California Steel Industries (<http://www.californiasteel.com>).

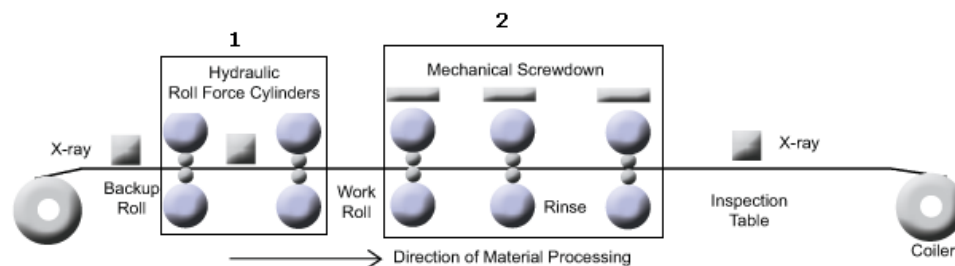


Fig. 2.1 Stand cold reduction mill

The process is controlled by three X-Ray units, which provide feed-forward and feedback strip thickness to the automatic gauge control computer. Large, fast acting hydraulic roll force cylinders on first two stands provide consistent strip thickness on the downstream stands (1). Last three stands operate in a more gradual acting manner, reacting to strip's current thickness and customer requirements (2).

Cold-formed members are normally manufactured by one of three processes. These are:

- Cold roll forming;
- Press braking process;
- Cold folding.

Cold roll forming consists of feeding a continuous steel strip through a series of opposing rolls to progressively deform the steel plastically to form the desired shape. Each pair of rolls produces a fixed amount of deformation in a sequence of type shown in Fig 2.2a. Each pair of opposing rolls is called a stage as shown in Fig 2.2. In general, the more complex the cross-sectional shape, the greater the number of stages required. In the case of cold-formed rectangular hollow sections,

the rolls initially form the section into a circular section and a weld is applied between the opposing edges of the strip before final rolling (called sizing) into a square or rectangular shape.

Fig 2.3 (a and b) shows two industrial roll forming lines for long products profiles and sheeting, respectively.

A significant limitation of roll forming is the time taken to change rolls for a different size sections. Consequently, adjustable rolls are often used which allows a rapid change to a different section width or depth.

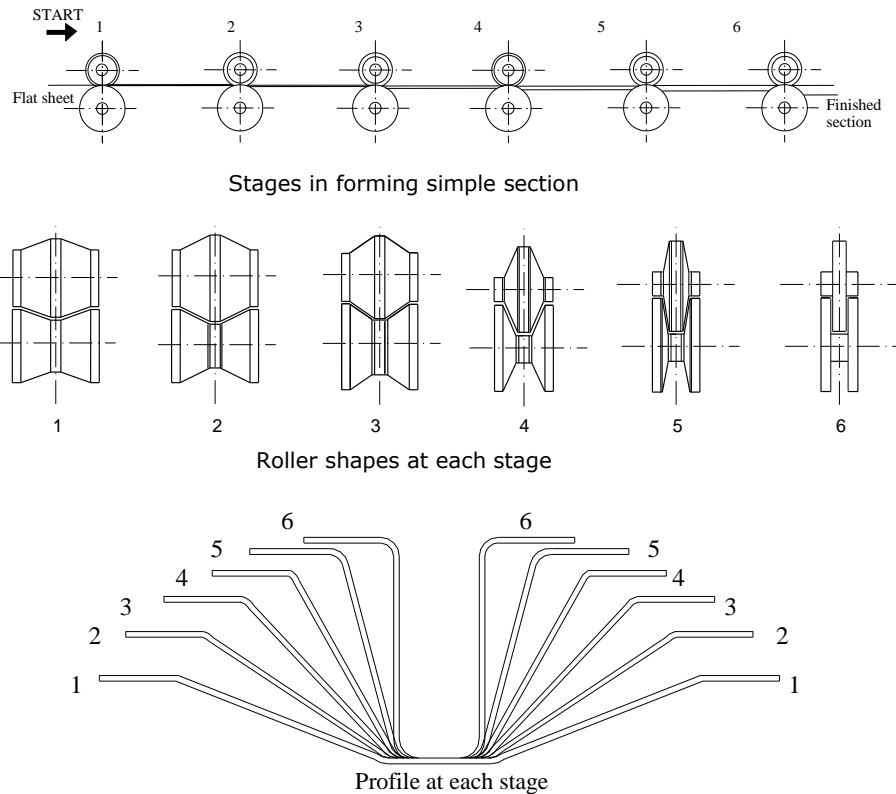


Fig. 2.2 Stages in roll forming a simple section [3]

A simple section may be produced by as few as six pairs of rolls. However, a complex section may require as many as 15 sets of rolls. For rack uprights, which contain arrays of holes along the profiles length, a perforation stage is required.

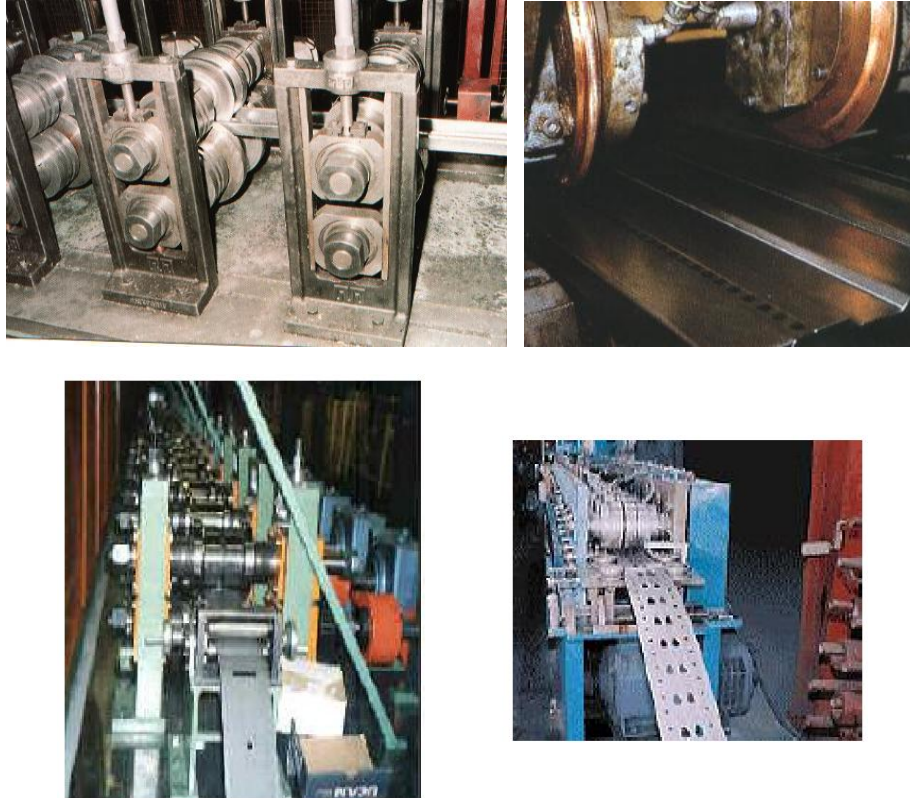


Fig. 2.3 Industrial roll forming lines

Press-braking is more widely used, and a greater variety of cross-sectional forms can be produced by this process. Here a section is formed from a length of strip by pressing the strip between shaped dies to form the profile shape (see Fig 2.4). Usually each bend is formed separately. The set-up of a typical brake press is illustrated in Fig 2.5. This process also has limitations on the profiled geometry which can be formed and, often more importantly, on the lengths of sections which can be produced. Press-braking is normally restricted to sections of length less than 5 m although press brakes capable of production 8 m long members are in use in industry.

Roll forming is usually used to produce sections where very large quantities of a given shape are required. The initial tooling costs are high but the subsequent labour content is low. Brake pressing is normally used for low volume production where a variety of shapes are required and the roll forming costs cannot be justified.

The press brake operation may be used under the following conditions:

- The section is of simple configuration.
- The required quantity is less than about 90m/min.
- The section to be produced is relatively wide 450mm such as roof sheets and decking units.

Simple sections such as angles, channels and Z-sections are formed by press brake operation from sheet, strip, plate, or bar in not more than two operations. More complicated sections may take several operations.

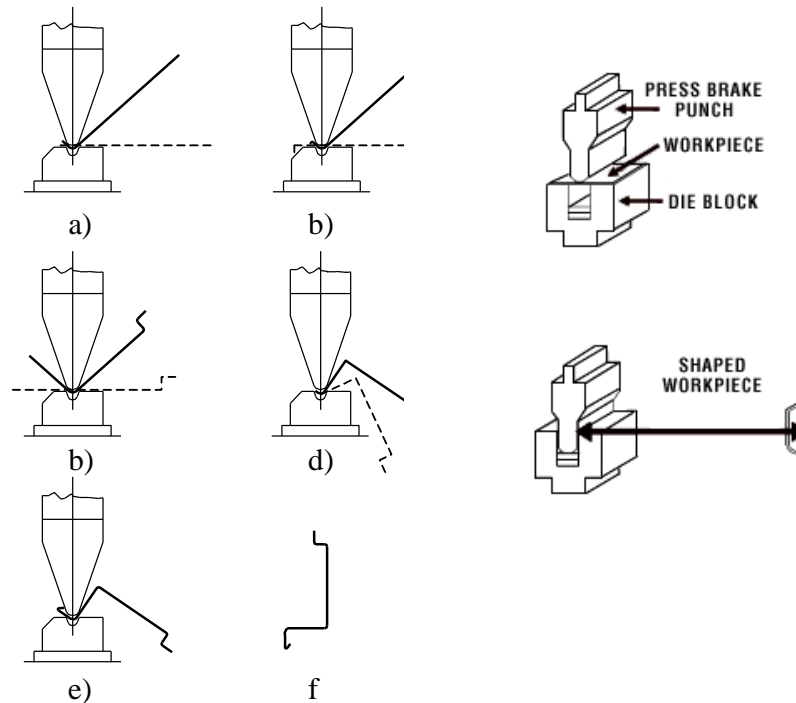


Fig. 2.4 Forming steps in press braking process

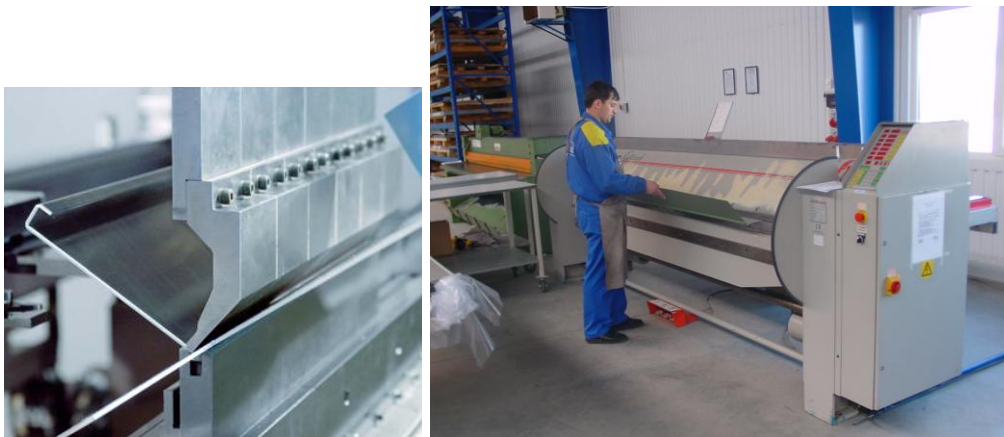


Fig. 2.5 Industrial brake press

Folding is the simplest process, in which specimens of short lengths and of simple geometry are produced from a sheet of material by folding a series of bends (see Fig 2.6). This process has very limited application.

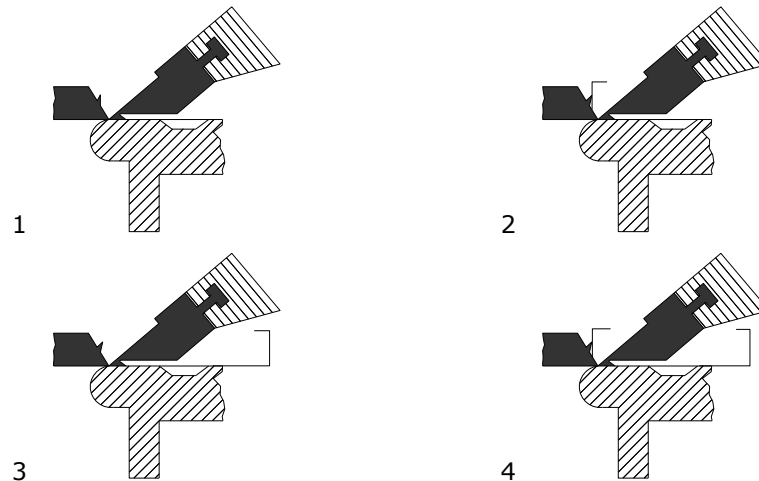


Fig. 2.6 Forming of folding

The use of thinner sections and high strength steels leads to design problems for structural engineers which may not normally be encountered in routine structural steel design. Structural instability of sections is most likely to occur as a result of the sections, leading to a reduced buckling loads (and stresses), and the use of higher strength steel makes the buckling stress and yield stress of the thin-walled sections approximately equal. Further, the shapes which can be cold-formed are often considerably more complex than hot-rolled steel shapes such as I-sections and unlipped channel sections. The cold-formed sections commonly have mono-symmetric or point symmetric shapes, and normally have stiffening lips on flanges and intermediate stiffeners in wide flanges and webs. Special design standards have been developed for these sections.

In the USA, the Specification for the design of cold-formed steel structural members of the American Iron and Steel Institute was first produced in 1946 and has been regularly updated based on research to the most recent 1996 edition [4] , [5] . The first edition of the unified *North American Specification* [6] was prepared and issued in 2001, followed by *Supplement 2004: Appendix 1, Design of Cold-Formed Steel Structural Members Using Direct Strength Method* [7] . It is applicable to the United States, Canada and Mexico for the design of cold-formed steel structural members. In 2007, the second edition of the *North American Specification for the Design of Cold-Formed Steel Structural Members* was issued [8] . The document was prepared on the basis of the 2001 edition of the Specification, the Supplement 2004 to the 2001 Specification, and subsequent developments. The new and revised provisions provide the up-to-date information for the design of cold-formed steel structural members, connections, assemblies, and systems

In Europe, the ECCS Committee TC7 originally produced the European Recommendations for the design of light gauge steel members in 1987 [9] . This European document has been further developed and published in 2006 as the European Standard Eurocode 3: *Design of steel structures. Part 1-3: General Rules. Supplementary rules for cold-formed thin gauge members and sheeting* [10] .

In Australia and New Zealand, a new limit states design standard AS/NZS 4600 for the design of cold-formed steel structures was published in December 2005 [11] .

In general, cold-formed steel sections provide the following advantages in building construction [12] :

- As compared with thicker hot-rolled shapes, cold-formed steel members can be manufactured for relatively light loads and/or short spans;
- Unusual sectional configurations can be produced economically by cold-forming operations, and consequently favourable strength-to-weight ratios can be obtained;
- Nestable sections can be produced, allowing for compact packaging and shipping;
- Load-carrying panels and decks can provide useful surfaces for floor, roof, and wall construction, and in other cases they can also provide enclosed cells for electrical and other conduits;
- Load-carrying panels and decks not only withstand loads normal to their surfaces, but they can also act as shear diaphragms to resist force in their own planes if they are adequately interconnected to each other and to supporting members.

Compared with other materials such timber and concrete, the following qualities can be realised for cold-formed steel structural members.

- Lightness;
- High strength and stiffness;
- Ability to provide long spans, up to 10 m [3] ;
- Ease of prefabrication and mass production;
- Fast and easy erection and installation;
- Substantial elimination of delays due to weather;
- More accurate detailing;
- Non-shrinking and non-creeping at ambient temperatures;
- Formwork unneeded;
- Termite-proof and rot-proof;
- Uniform quality;
- Economy in transportation and handling;
- Non-combustibility;
- Recyclable material.

The combination of the above-mentioned advantages can result in cost saving in construction.

2.2 Storage systems

From the industrial point of view, the warehouse storage is nothing more than the place where raw material and the finite or semi finite products are stored. The storage is, in fact, an integral part of production process.

This approach led to a continuous development of complex storage systems where the product, or a part of it, is not just stored, but sorted or packed or even prepared for selling. In order to satisfy these demands, the storage system must be organized in such a way that the products are efficiently stored and sufficiently accessible. For this, storage systems were designed to reduce the occupied space to the minimum, with an adequate safety factor. Along the years, automated handling systems controlled by computers were developed to help manoeuvring the stored goods. In the same time, simple shelving structures loaded and unloaded by hand are used for small amount of goods.

The storage systems varies from small shelves to palletized storage systems up to 30m high loaded and unloaded by computer controlled systems.

Nowadays storage systems have their origins in slotted angle profiles introduced in the '30s. The perforations of these thin walled profiles enabled the quick and easy connection together with the freedom for the designer to conceive various configurations. These simple profiles were the starting point for today's upright sections.

There is available a wide range of storage systems. They can be classified based on storage time of a specific product, storage type, handling equipment, etc., but for a structural engineer is important the structural system that withstand the loads.

Storage systems varies from simple shelves of few metres with two or three spans, loaded manually with relatively lightweight products, to palletized storage systems with bigger spans that can rise up to 30m, loaded and unloaded by computer controlled cranes with heavy mechanical components or bulky products. The most usual storage pallet rack systems are up to 6m high, served by forklifts or other equipments having a capacity of about 2 tons per level per bay.

2.2.1 Definitions and components

Besides the terms and definitions used for normal thin-walled structures, used in EN1993-1-3:2006, new terms and definitions are used for pallet rack storage systems. Specific terms and definitions for adjustable pallet racking are defined in [13] and [14].

Upright frame are two (often perforated) upright sections linked together by a system of bracing members. Different available frame types are presented in Fig 2.7. In Fig 2.8 are presented the general storage system components.

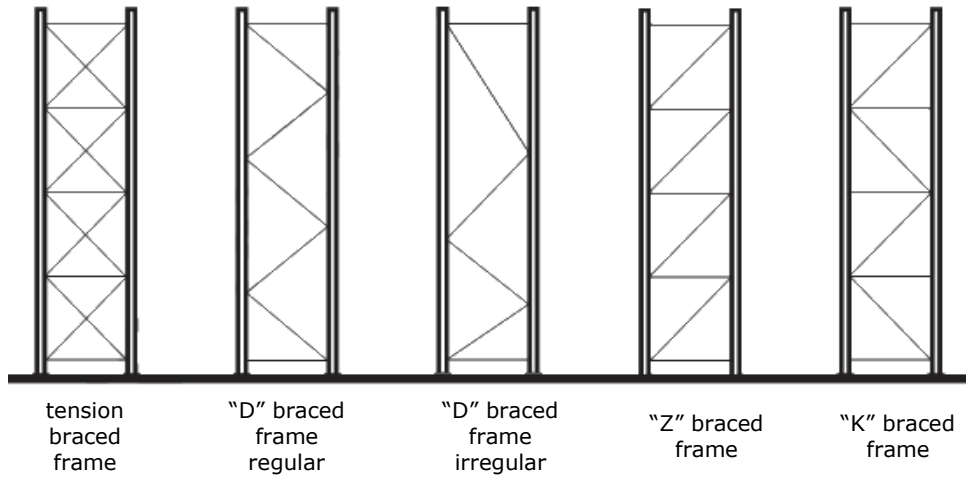


Fig. 2.7 Typical upright frames

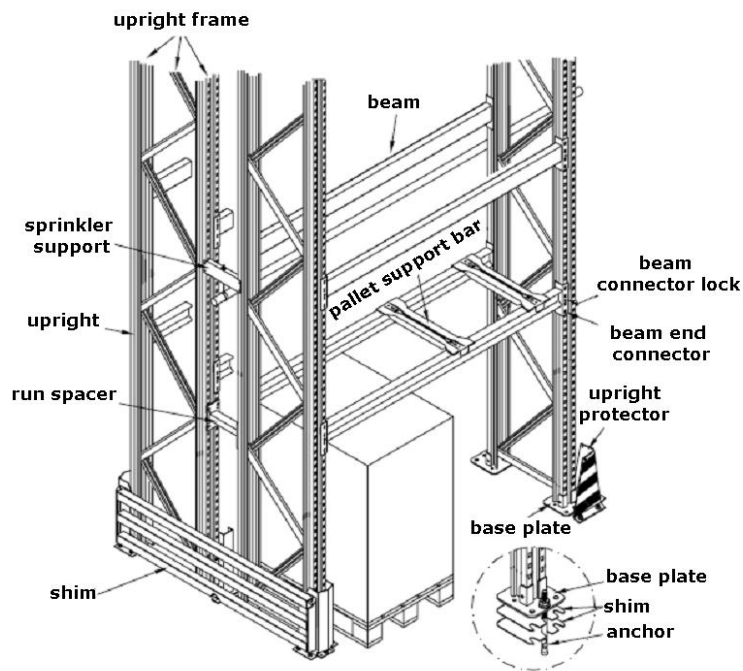


Fig. 2.8 General system components

Beams are the horizontal member linking adjacent frames and lying in the horizontal direction parallel to the operating aisle. In Fig 2.9 are presented usual beam sections for storage systems.

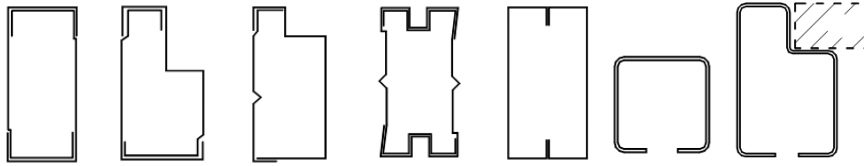


Fig. 2.9 Pallet rack beam sections

For usual spans the beams dimensions are limited by its bending capacity. The beams failure occurs by local buckling of compressed flange. Usually, closed sections are more efficient than open ones due to a better material distribution. Lateral beam stability is not an issue generally, but in the case of open step sections they can twist under load.

In the beginning the upright sections were a perforated "C" type profile because of the ease of production. Due to industrial development upright sections changed into more complex shape with better load bearing capacity. The resulted complex shape is determined based on two considerations i.e. ease of assembling and structural efficiency (cost effective). Usually, upright sections are open section as presented in Fig 2.10.

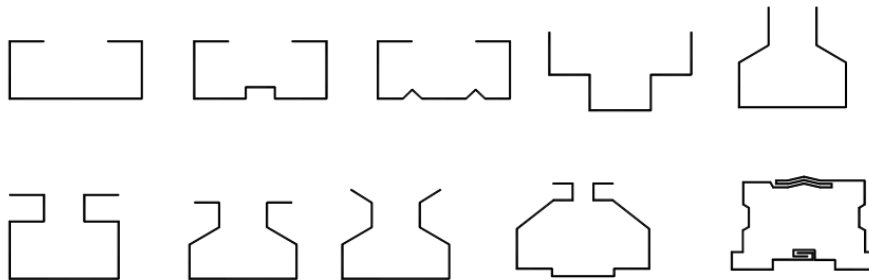


Fig. 2.10 Pallet rack upright sections

The upright sections usually contain arrays of holes that enable beams to be clipped into position at heights that are not pre-determined before manufacture. Different perforation arrays, as specified in EN15512:2009 provisions are presented in Fig 2.11.

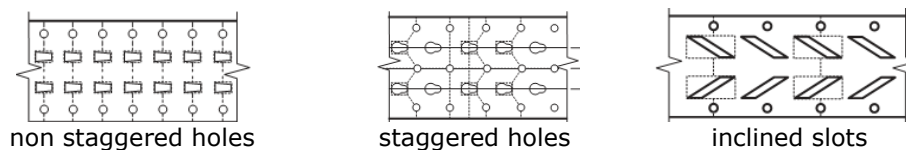


Fig. 2.11 Pallet rack upright perforation types

From structural point of view, the connections behaviour can be classified as built-in, pinned and semi-rigid. A semi-rigid connection has certain elasticity and is usually done by welding or bolts. Pallet rack systems use clamped semi-rigid connections.

The clips can be components of beam end assembly or can be individual parts. The clip shape determines the hole geometry on the upright. The tolerances are a compromise between the wedge up effect that enables connections rigidity

and adequate behaviour under loading and the ease of assembly. In Fig 2.12 are presented different types of beam to upright connections.

Another very important connection is the base connection. For light weight storage systems, no base connection is necessary, but in the case of heavy weight storage systems the base connection is imperative. The base connection can be pinned or built in, depending on the structural type chosen for the storage system. A built in connection increase the structural stability and load bearing capacity. Usually, the baseplate connection is protected against impact.



Fig. 2.12 Beam to column connections

2.2.2 Loads for storage systems

Permanent actions. All European design codes use the Ultimate Limit State criteria. Storage systems make no exception. For pallet rack storage systems, the permanent actions include the actual weights of materials and constructions. Additional, the weight of fixed service equipment, such as sprinklers, electrical feeders, and heating, ventilating, and air conditioning systems, shall be taken into account if such equipment is supported by the structural members of the rack.

Variable actions. The variable actions include the unit loads, vertical placement loads, horizontal placement loads, rack-guided equipment loads, floor and walkway loads, thrusts on handrails, actions from imperfections (i.e. frame, bracing, member, loading), impact and accidental loads, wind loads, snow loads and seismic actions. The specified weight of unit load shall not be less than 80% of the maximum weight of unit load. In upright design the worst case load distribution shall be considered where maximum weight of unit load shall be applied to the upper storage positions up to the specified bay load.

Actions due to impact (accidental loads). In the design of pallet rack storage systems the live loads and placement loads must be assumed to include adequate allowance for ordinary impact conditions. Impact damage caused by fork-lift trucks or other moving equipment against rack-uprights shall be avoided by appropriate operator training and safety measures. Rack components directly above a unit load shall be able to absorb an accidental vertical force. In general, this force is applied at the end of a beam in order to verify that the connector does not disengage. Upward placement loads are accidental variable actions and must be considered with a load factor. Also, an accidental overload in the horizontal direction must be considered.

Wind loads. Wind loads are determined in accordance with relevant national regulations. When a rack is exposed to wind, no account will be taken of the shielding effects of fully or partially loaded racks upwind of the run in consideration. Each individual row of racking (between adjacent aisles) shall be designed to resist the full wind pressure, suction and wind friction forces. The fully or partially loaded

rack shall be considered to be impermeable to wind in the loaded areas unless the effect of permeability can be quantified.

Snow loads. Snow loads are determined in accordance with relevant national regulations.

Seismic actions. There are different seismic provisions documents around the world. In USA there is AISC standard, in Europe is EN1998, in Romania there is P100-1:2006. Different seismic requirements for each of the above mentioned seismic design code, for a multi-storey structure, are presented in [17] .

Racking systems are not regular buildings but a very particular form of steel construction. They differ from buildings in terms of their use, the loads that are supported, the geometrical dimensions and the components used in their construction. These components are normally thin-gauge cold-formed profiles and, in the case of uprights, are typically continuously perforated. This gives the required functionality, adaptability and flexibility needed to cope with the great variation in the different types of goods that are stored.

Whilst the basic technical description of an earthquake is obviously the same for all structures it is of great importance to define whether or not it is possible to apply the "general design rules" to a storage system. It is necessary to consider how to modify the general principles and technical requirements, in order to take into account the peculiarities of storage system and to achieve the requested safety level. To this purpose, in September 2010 a Code of Practice FEM 10.2.08 was issued as the outcome of a working group initiated by European Racking Federation. The new code of practice considers 3 levels of requirements:

- No collapse requirement.
- Damage limit state requirement.
- Movement of unit loads.

The reference return period of the design earthquake such as defined in EN1998-1 is managed through an importance factor scaling the design spectrum. Specific importance classes are defined for racks, with associated importance factor:

- Class I: Warehouses with fully automated storage operation or with low occupancy;
- Class II: Standard warehouse conditions;
- Class III: Retail areas with public access;
- Class IV: Hazardous product storage.

Design codes. In Europe, the design code EN15512 replaced in 2009 the FEM 10.2.02 code of practice for the design of steel static pallet racking. In USA the Rack Manufacturing Institute released in 2008 a revision of MH16.1 design code, 2004 edition. In Australia, the AS4048 standard from 1993 is in use.

The European design code is based on experimental testing. In the case of compression members the effects of perforations is taken into account by relevant test methods. The design provisions of the European design code for the storage systems uprights are presented in subchapter 2.6.2. The test procedures will be further discussed in Chapter 3.

2.3 Some peculiar characteristics of cold-formed thin-walled steel sections

2.3.1 Strain hardening and change of yield strength due to the cold forming

The manufacturing process plays a governing role in some characteristics that have an influence on the buckling behaviour of the profiles. First of all, it leads to a modification of the stress-strain curve of the steel. With respect to the virgin material, cold-rolling provides an increase of the yield strength and, sometimes, of the ultimate strength that is important in the corners and still appreciable in the flanges, while press braking let these characteristics nearly unchanged in the flanges. Obviously, such effects do not appear in case of hot-rolled sections, as shown in Table 2.1 [15] .

Table 2.1 Influence of manufacturing process on the basic strengths of hot and cold-formed profiles

Forming method		Hot rolling	Cold forming	
			Cold rolling	Press braking
Yield strength	Corner	--	high	high
	Flange	--	moderate	--
Ultimate strength	Corner	--	high	high
	Flange	--	moderate	--

The increase of the yield strength is due to strain hardening and depends on the type of steel used for cold rolling. On the contrary, the increase of the ultimate strength is related to strain aging that is accompanied by a decrease of the ductility and depends on the metallurgical properties of the material.

Results of investigations conducted by Winter, Karren, Chajes, Britvec, and Uribe [16] , [18] , [19] , [20] on the influence of cold work indicate that the changes of mechanical properties due to cold work are caused, mainly, by strain hardening and strain aging, as illustrated in Fig 2.13 [16] in which curve A represents the behaviour curve of the virgin material, curve B is due to unloading in the strain-hardening range, curve C represents immediate reloading and curve D is the behaviour curve of reloading after strain aging. It can be observed that the yield points of both curves C and D are higher than the yield point of the virgin material and that the ductility decrease after strain hardening and strain aging.

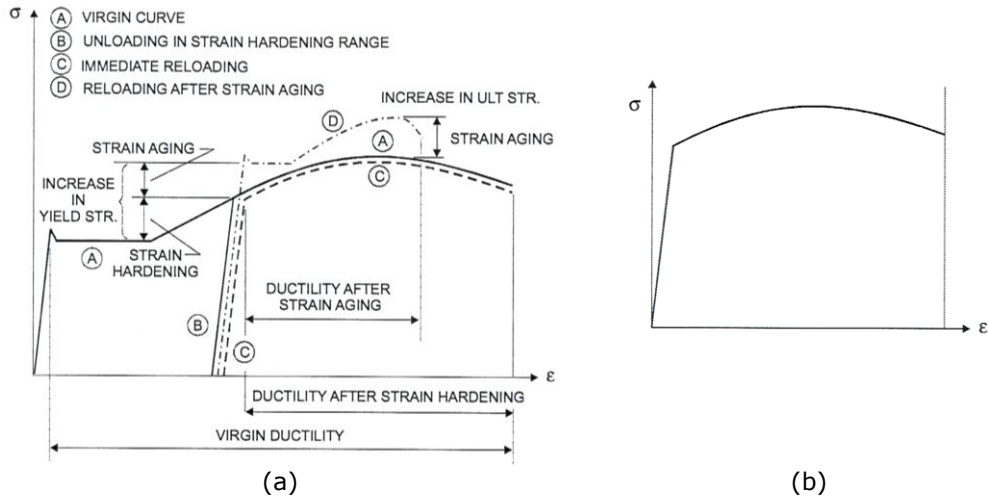


Fig. 2.13 Effects of strain hardening and strain aging on σ - ϵ characteristics of carbon steel: (a) global σ - ϵ diagram; (b) apparent σ - ϵ diagram for a cold-formed member)

Due to the forming process strain-hardening can vary considerably along the cross-section as shown in Fig 2.14.

For design the increase in yield strength can be taken into account by using an average yielding strength.

Karren [23] and Karren & Winter [24] have proposed the following equation for the corner yield strength:

$$f_{yc} = \frac{k \cdot g}{(r/t)^h} \tag{2.1}$$

with $g = 0.945 - 1.315 \cdot q$ (2.2)

$$h = 0.803 \cdot q \tag{2.3}$$

where t is the thickness of the sheet, r is the inside bend radius, k and q are the parameters of the hardening law which are given by:

$$k = 2.80 \cdot f_u - 1.55 \cdot f_{yb} \tag{2.4}$$

$$q = 0.225 \cdot \frac{f_u}{f_{yb}} - 0.120 \tag{2.5}$$

where f_u is the virgin ultimate strength and f_{yb} the virgin yield strength of the sheet.

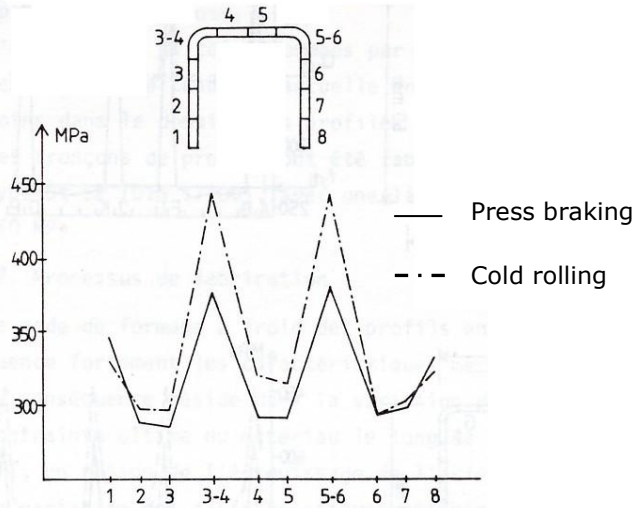


Fig. 2.14 Influence of manufacturing process on yield strength [27]

With regard to the full-section properties, the average tensile yield strength may be approximated by using a weighted average as follows [24] :

$$f_{ya} = A_c \cdot f_{yc} + (1 + A_c) \cdot f_{yb} \quad (2.6)$$

where A_c is the ratio of corner area to total cross-sectional area.

In accordance to EN1993-1-3 provisions, the average yield strength is calculated with Eq. (2.7):

$$f_{ya} = f_{yb} + \left(f_{yu} - f_{yb} \right) \frac{knt^2}{A_g}, \text{ but } f_{ya} \leq \frac{(f_{yu} + f_{yb})}{2} \quad (2.7)$$

where:

- A_g is the gross cross sectional area,
- k is the numerical coefficient that depends on the type of forming (7 for cold rolling, 5 for other methods),
- n is the number of 90° bends in the cross-section with and internal radius $r \leq 5t$,
- t is the nominal core thickness t_{cor} of the steel material before cold forming, exclusive of zinc or organic coatings

In the European standard EN1993-1-3 is also specified that the increase in yielding strength due to cold forming shall be taken into account only for the following cases:

- in axially loaded members in which the effective cross-sectional area A_{eff} equals to gross area A_g ;
- in other cases in which it can be shown that the effects of cold forming lead to an increase in the load carrying capacity.

2.3.2 The Bauschinger effect

The Bauschinger effect refers to the property of materials where the material's behaviour change as a result of the microscopic stress distribution. For example, an increase in tensile yield strength is done at the expense of compressive yield strength. The basic mechanism for the Bauschinger effect is related to the dislocation structure in the cold-worked material. As deformation occurs, the dislocations will accumulate at barriers and produce dislocation pileups and tangles.

In addition to strain hardening and strain aging, the changes in mechanical properties produced by cold work are also caused by the direct and inverse Bauschinger effect. The Bauschinger effect refers to the fact that the longitudinal compression yield strength of the stretched steels is smaller than the longitudinal tension yield strength, as shown in Fig. 2.15a. The inverse Bauschinger effect produces the reverse situation in transverse direction, as shown in Fig. 2.15b , [12]

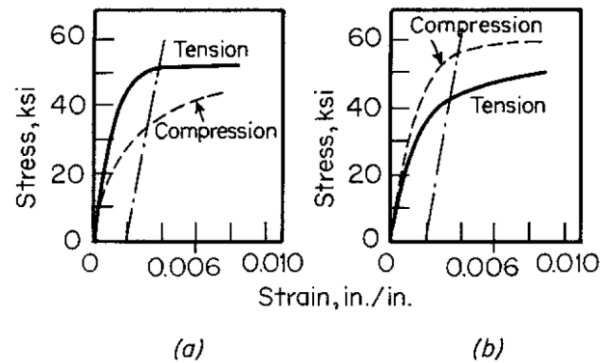


Fig. 2.15 (a) Bauschinger effect; (b) Inverse Bauschinger effect [12]

2.3.3 Residual stresses

Residual stresses are stresses that exist in the member as a result of manufacturing and fabricating processes. In the past, the distribution of residual stresses and the effect of such stresses on the load-carrying capacity of steel members have been studied extensively for hot-rolled wide-flange shapes and welded members. For these structural shapes, the residual stresses are caused by uneven cooling after hot rolling or welding. These stresses are often assumed to be uniform across the thickness of the member.

In hot-rolled steel members residual stresses do not vary markedly through the thickness, which means the membrane residual stresses are dominant, while in cold-formed steel members residual stresses are dominant by a "flexural", or through thickness variation. This variation of residual stresses may lead to early yielding on the faces of cold-formed steel plates and can influence their local buckling strength.

Residual stresses can be idealised as a summation of two types: flexural (FRSs) and membrane (MRSs) (see Fig. 2.16).

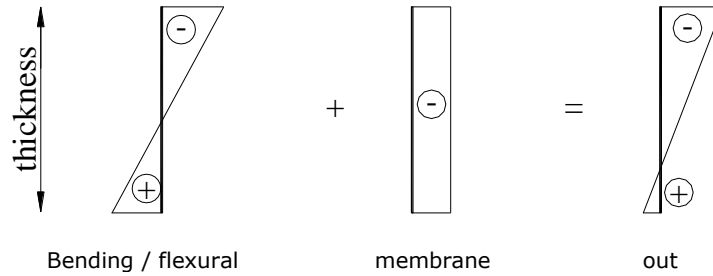


Fig. 2.16 Idealisation of residual stresses (Schafer & Peköz 1998)

Experimental evidence shows more complex actual distributions of residual stresses. Fig. 2.17 presents the distribution of measured residual stress for a cold-formed steel lipped channel section [21], while Fig. 2.18 provide evidence for residual flower for plain and lipped channel sections [21].

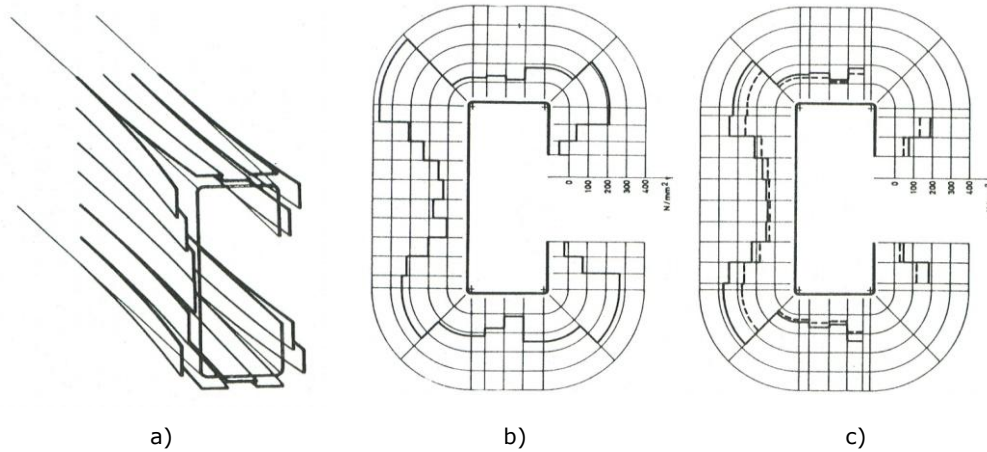


Fig. 2.17 Measurement of residual stresses in a cold rolled C profile: (a) residual "flower"; (b) slicing method; (c) curvature method [21]

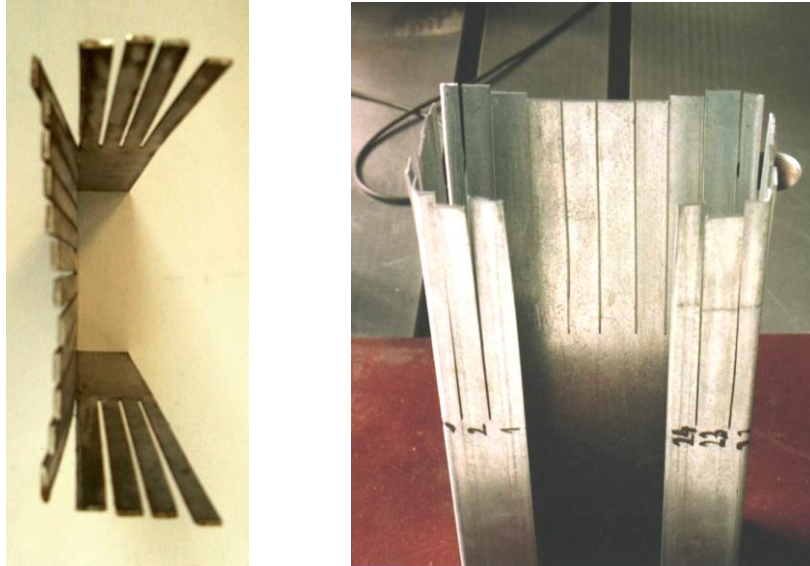


Fig. 2.18 Residual flower for plain channel and lipped channel sections

Hot-rolled profiles are affected by residual stresses, which result from air cooling after hot-rolling. These stresses are mostly of membranar type; they depend by the shape of sections and have a significant influence on the buckling strength. Therefore, residual stresses are the main factor which caused the framing of hot-rolled sections on different buckling curves in European design codes [29] .

In case of cold-formed sections the residual stresses are mainly of flexural type, as Fig. 2.18 demonstrates, and their influence on the buckling strength is less important than membranar residual stresses as Table 2.2 shown [15] .

On the other hand, cold rolling produce different residual stresses in the section when compared with press braking, as shown in Table 2.2, so the section strength may be different in cases where buckling and yielding interact [15]

Table 2.2 Type magnitude of residual stress in steel sections

Forming method	Hot rolling	Cold forming	
		Cold rolling	Press braking
Membranar residual stresses (σ_m)	High	low	low
Flexural residual stresses (σ_{rf})	low	high	low

Experimental evidence shows more complex actual distributions of residual stresses. Fig. 2.19 (a to c) presents the distribution of measured residual stress for a cold-formed steel angle, channel and lipped channel [21] .

As in Fig. 2.19 is shown the thickness of sheet section are quite large for a cold-formed section. In fact, experimentally measuring through thickness residual stress variation of thin plate is very difficult, for not saying infeasible. The only available experimental measurements for thin plates (0~1 mm) are at the faces of the plate.

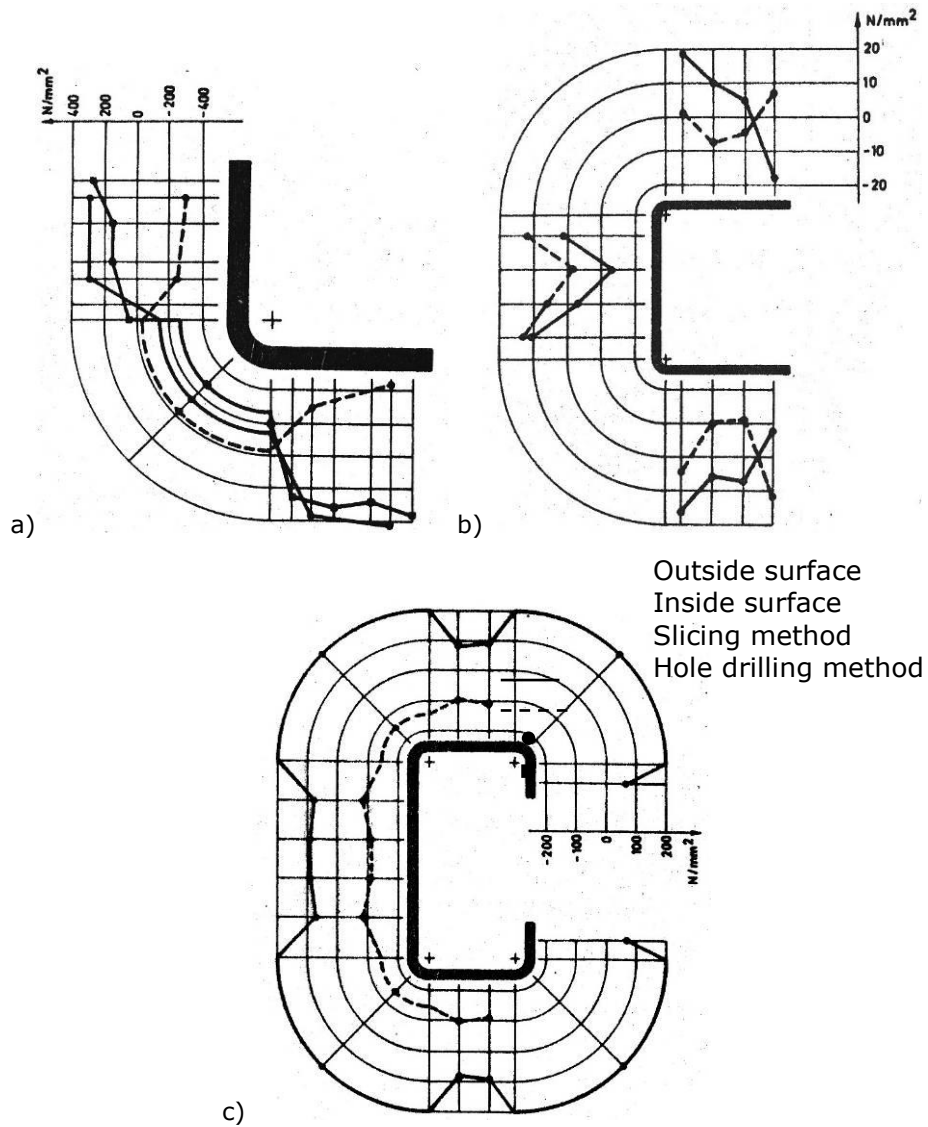


Fig. 2.19 Measured residual stress in cold-formed steel sections: (a) cold-rolled angle; (b) cold-rolled C profile; (c) press braked U profile [21]

The actual European buckling curves have been calibrated using test results on hot formed (rolled and welded) steel sections, obtained during a large experimental campaign around the Europe in 1960's [25]. These curves are based on the well-known Ayrton-Perry formula, in which the imperfection factor α was correspondingly calibrated [26].

Due to the fact the mechanical properties of cold-formed sections – e.g. cold-forming effect and residual stresses – are different to those of hot formed ones, different buckling curves should be justified. Nowadays there are available both

numerically and experimentally approaches to calibrate appropriate α factors for cold-formed sections [27] but, for the sake of simplicity of design process, the same buckling curves as for hot sections are still used (EN 1993-1-1 and EN 1993-1-3).

2.3.4 Geometric imperfections

For a cold-formed thin-walled member, the geometric imperfections refer to deviations of the real element from the "perfect geometry". The imperfections can be of several types: flexural (bow) imperfections, flexural-torsional imperfections, as global imperfections and local or sectional imperfections.

Global flexural (bow) imperfections about minor inertia axis

Systematic measurements for cold-formed angle profiles imperfections were presented in by [29] , [30] . The imperfections were measured for cold rolled and press braked profiles. The values scattering resulted from a statistical analysis of measured imperfections indicates a good control of geometrical characteristics in the fabrication process. The obtained values for initial bow imperfection of approximately $f_0/L=1/1000$ for cold-rolled profiles are in accordance with the ECCS (1978) specifications and less than the limit imposed for fabrication allowance of $L/750$ mentioned in European standard EN1090-2:2008. For cold braked profiles, the measured initial imperfections were significantly lower ranging from $f_0/L=1/2100$ down to $1/2700$.

Batista [27] measured initial imperfection for "U" and "C" type sections and found an initial bow imperfection of $f_0/L=1/2530$. The results of initial imperfection measurements revealed that there are two types of bow imperfections: single half wave imperfections and multiple half wave imperfections. Based on initial imperfection measurements the following conclusions can be drawn:

- the initial imperfections of most interest are those measured along the elements axis, near the corner, due to the fact that these imperfections have a big influence on the gravity centre position;
- imperfections measured along profile's free edges have a lower impact on the overall bar behaviour and they can be considered as sectional imperfections;
- instead of using the measured initial imperfections, it is preferable to use an equivalent sinusoidal imperfection due to the fact that the initial imperfections can be compared with sinusoidal amplitude.

Further on, examining the result of imperfection measurements for 66 "U" and "C" profiles was observed that:

- equivalent initial bow imperfections were less than $L/1000$ (where L is profile's length), this being the limit mentioned by ENV1993-1-3;
- the absolute values of measured initial bow imperfections are below the imposed limit, $L/1000$.

Moreover, the values of initial imperfections, measurements done by Young [34] were found to be in ranging from $L/1300$ to $L/1100$ for cold-formed "C" profiles with fixed ends and from $L/2800$ to $L/1800$ for same profile with pinned ends. For "U" profiles, the measured imperfection values were found to be ranging from $L/2500$ to $L/1400$ for the profiles with fixed ends, while for profiles with pin ends the maximum bow imperfection in the middle span was found to be ranging from $L/5000$ to $L/2200$.

Global torsional imperfections

Costa Ferreira [30] observed that the value for initial torsional deviations for the cold formed profiles are about $0.53^0/m$, below the imposed manufacturing allowance of $1^0/m$.

Current design codes do not specify a reference value for initial torsional imperfections. This is because a torsional imperfection less than $1^0/m$ does not influence the overall profile’s stability.

Still, the Australian design code, AS4100 propose the following formulas for initial bow and torsional imperfections:

$$1000 \cdot f_0/L = 1000 \cdot \phi_0 \cdot \left(M_{cr} / N_{cr} \cdot L \right) = -1, \quad \text{for } \bar{\lambda}_{LT} \geq 0.6 \tag{2.8}$$

$$1000 \cdot f_0/L = 1000 \cdot \phi_0 \cdot \left(M_{cr} / N_{cr} \cdot L \right) = -0.001, \quad \text{for } \bar{\lambda}_{LT} < 0.6 \tag{2.9}$$

where:

- N_{cr} is the Euler buckling load about minor inertia axis;
- M_{cr} is the flexural-torsional critical bending moment;
- $\bar{\lambda}_{LT}$ is the reduced slenderness for flexural-torsional buckling.

Local (sectional) imperfections

Many researchers measured the local imperfections for thin-walled cold-formed steel profiles, but none of these studies proposed limit values for local imperfections. Schafer & Pekoz [36] , [37] proposed a classification of local geometric imperfections for thin walled profiles in compression and/or bending:

- maximum local imperfections, in the case of stiffened elements (Fig. 2.2a);
- deviations from the straight, in case of flanges, stiffened of unstiffened (Fig. 2.20b).

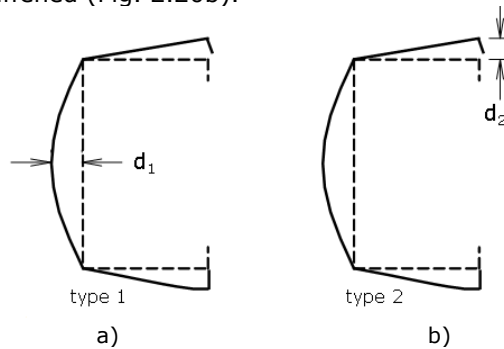


Fig. 2.20 Definition of local imperfections

Type 1 imperfections are characteristic for local buckling, while **type 2** imperfections initiate distortional buckling.

2.4 Peculiar problems of cold-formed steel design

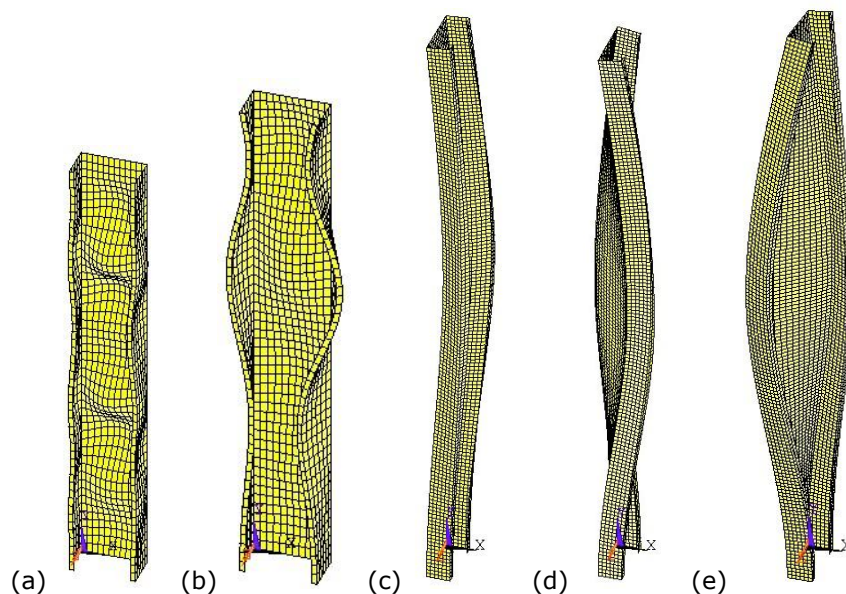
The use of thin-walled sections and cold-forming manufacturing effects can result in special design problems not normally encountered when hot-rolled sections are used. A brief summary of some special problems in cold-formed steel design are reviewed on the following.

2.4.1 Buckling strength of cold-formed members

Steel sections may be subject to one of four generic types of buckling, namely local, global, distortional and shear. Local buckling is particularly prevalent in cold-formed steel sections and is characterised by the relatively short wavelength buckling of individual plate element. The term "global buckling" embraces Euler (flexural) and flexural-torsional buckling of columns and lateral-torsional buckling of beams. It is sometimes termed "rigid-body" buckling because any given cross-section moves as a rigid body without any distortion of the cross-section. Distortional buckling, as the term suggests, is buckling which takes place as a consequence of distortion of the cross-section. In cold-formed sections, it is characterised by relative movement of the fold-lines. The wavelength of distortional buckling is generally intermediate between that of local buckling and global buckling.

It is a consequence of the increasing complexity of section shapes that local buckling calculation are becoming more complicated and that distortional buckling takes on increasing importance.

Local and distortional buckling can be considered as "sectional" modes, and they can interact with each other as well as with global buckling [38]. Fig. 2.21 shows single and interactive (coupled) buckling modes for a lipped channel section in compression. The results have been obtained using an elastic eigen-buckling FEM analysis.



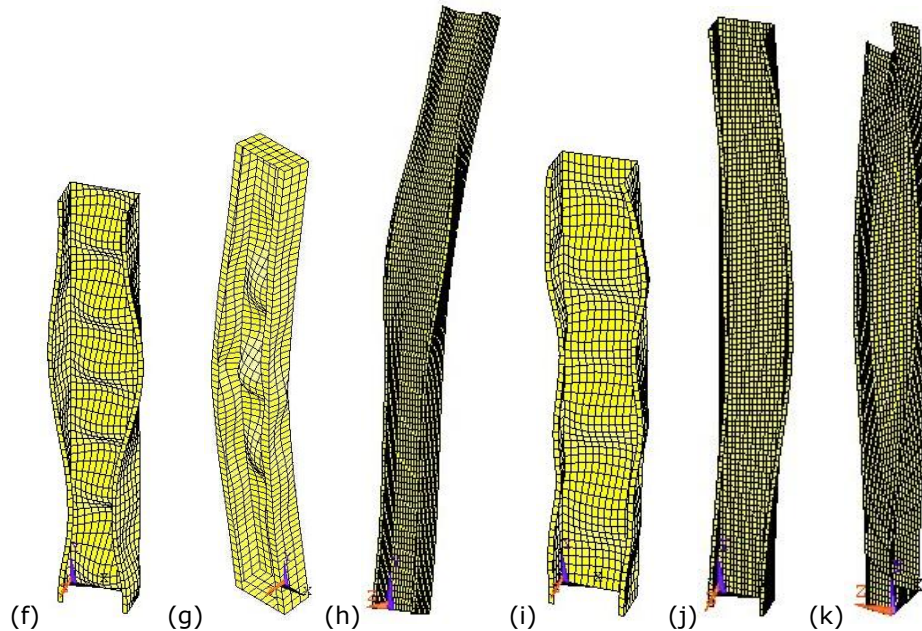


Fig. 2.21 Buckling modes for a lipped channel in compression
 Single modes: (a) local (L); (b) distortional (D); (c) flexural minor axis (F); (d) flexural major axis (F); (e) flexural-torsional (FT)
 Coupled (interactive) modes: (f) L + D; (g) F + L; (h) F + D; (i) FT + L; (j) FT + D; (k) F + FT; (l) F + FT + L; (m) F + FT + D

For given geometrical properties of member cross-section, the different buckling modes depend by the buckling length, as shown in Fig 2.22 [39]. The curves shown in Fig 2.22 have been obtained using elastic Finite Strip (FS) software, analysing and describing the change of buckling strength versus buckle half-wavelength. A first minimum (Point A) occurs in the curve at a half-wavelength of 65 mm and represents *local* buckling in the mode shown. The local mode consists mainly of deformation of the web element without movement of the line junction between the flange and lip stiffener. A second minimum also occurs at a point B at a half-wavelength of 280 mm in the mode shown. This mode is the *distortional* buckling mode since movement of the line junction between the flange and lip stiffener occurs without a rigid body rotation or translation of the cross-section. In some papers, this mode is called a *local-torsional* mode. The distortional buckling stress at point B is slightly higher than the local buckling stress at point A, so that when a long length fully braced section is subjected to compression, it is likely to undergo local buckling in preference to distortional buckling. The section buckles in a flexural or flexural-torsional buckling mode at long wavelengths, such as at points C, D and E. For this particular section, flexural-torsional buckling occurs at half-wavelengths up to approximately 1800 mm beyond which flexural buckling occurs. The dashed line in Fig. 2.22, added to the original figure, qualitatively shows the pattern of *all modes* or *coupled mode*.

The effect of interaction between sectional and global buckling modes consists in increasing sensitivity to imperfections, leading to the erosion of theoretical buckling strength (see hatched zones in Fig. 2.22). In fact, due to the

inherent presence of imperfection, buckling mode interaction always occurs in case of thin-walled members.

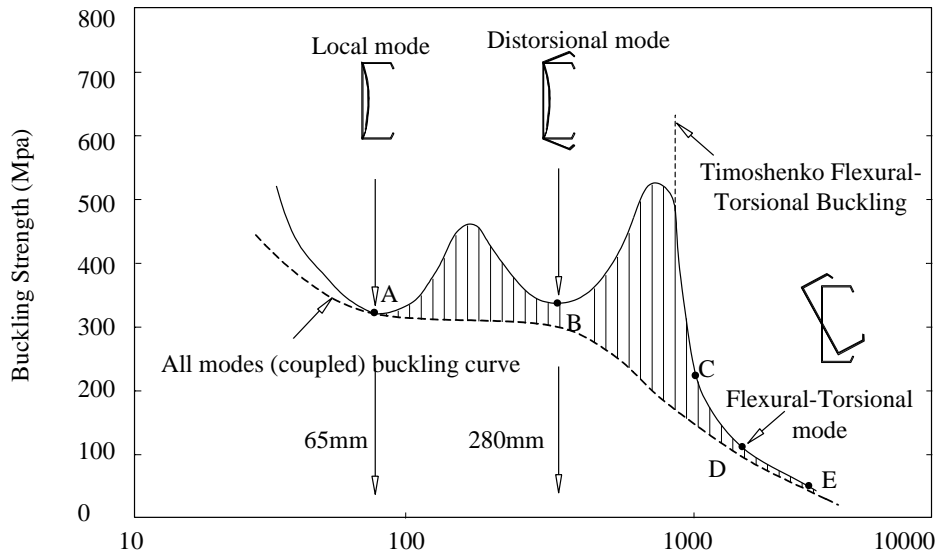


Fig. 2.22 Buckling strength versus half-wavelength for a lipped channel in compression [22]

Fig. 2.23 shows the difference in behaviour of a *tick-walled* slender bar in compression (Fig. 2.23a), and a *thin-walled* one (Fig. 2.23b); they are assumed, theoretically, to have the same value of their gross areas. Both cases of ideal perfect bar and imperfect one are presented.

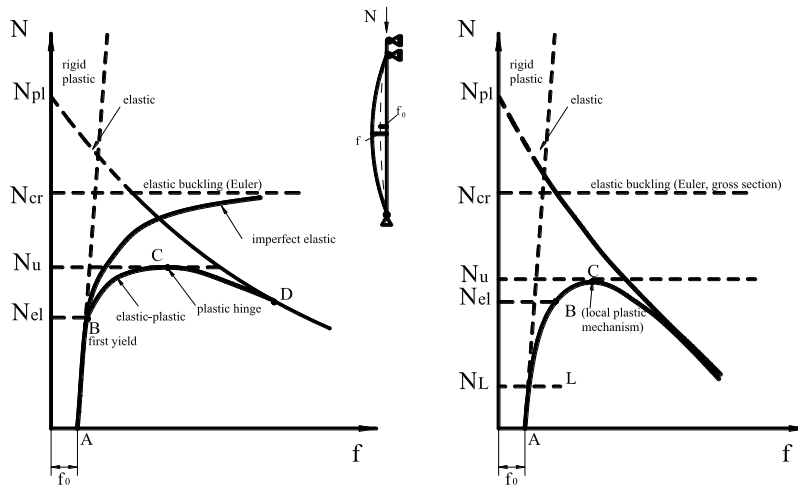


Fig. 2.23 Behaviour of (a) slender tick-walled and (b) thin-walled compression bar

Looking to the behaviour of actual *tick-walled* bar it can be seen that it begins to depart from the elastic curve at point B when the first fibre reaches the

yield stress, N_{e1} , and it reaches its maximum (ultimate) load capacity, N_u , at point C (e.g. plastic hinge is formed); after which it declines and the curve approaches the theoretical rigid-plastic curve asymptotically. The elastic theory is able to define the deflections and stresses up to the point of first yield and to define the load at which first yield occurs. The position of rigid-plastic curve determinates the absolute limit of load carrying capacity, for above it is a region in which the structures cannot carry a load and remain in a state of equilibrium. It intersects the elastic line as if to say "thus far and no further" [39] .

In case of thin-walled bar the sectional buckling, either local or distortional buckling, N_L , occurs prior to the initiation of plastification, N_{e1} . Sectional buckling is characterised by the stable post-critical path and bar does not fail when it occurs, but significantly lose from its stiffness. The yielding starts at the corners of cross-section, a few time before the failure of the bar, when sectional buckling changes into local plastic mechanism quasi-simultaneously with global buckling occurrence [41] . Fig. 2.24, obtained by advanced FEM simulation, clearly shows the failure mechanism of a lipped channel bar in compression [41] .

In fact, when sectional buckling phenomenon occur prior to global buckling – for very slender members, even they are thin-walled, no local or distortional modes can appear before flexural or flexural-torsional global modes – a "softening" (e.g. weakening of both capacity and stiffness of the bar), the practical design operates with reduced geometrical characteristics of cross-section, i.e. reduced or effective area, moments of inertia, radius of gyration.

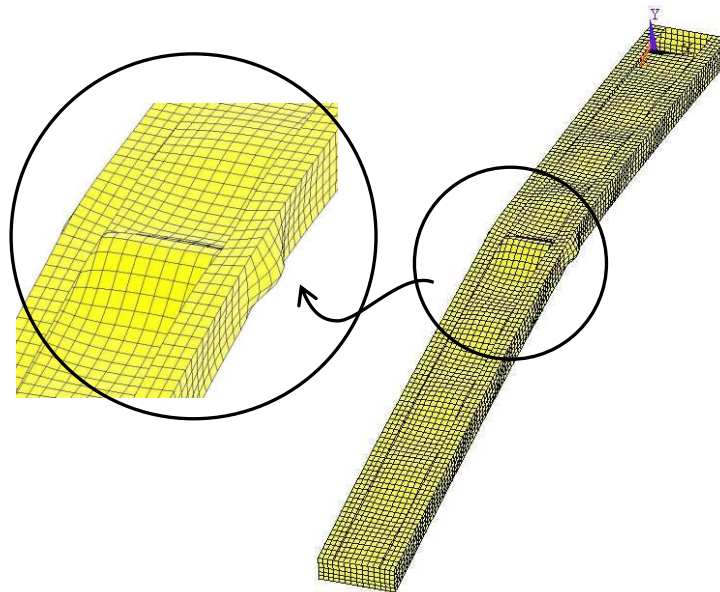


Fig. 2.24 Failure mode of a lipped channel in compression

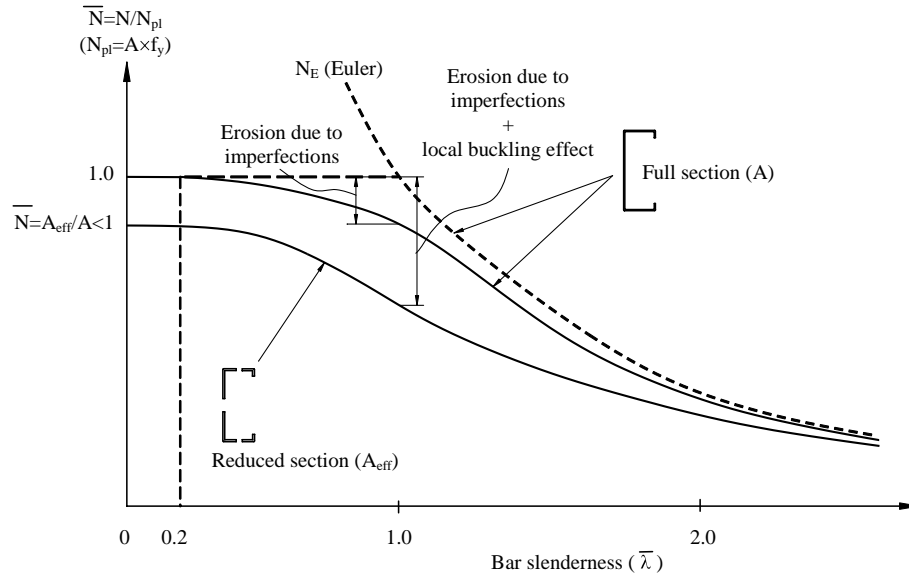


Fig. 2.25 Effect of local buckling on the member capacity

In Fig. 2.25 are shown the comparison between the buckling curves of a lipped channel member in compression, calculated according to EN 1993-1-3, considering the full effective cross-section (e.g. no local buckling effect) and the reduced (effective) cross-section (e.g. when the local buckling occurs and interacts with global buckling).

However the effectiveness of thin-walled sections, expressed in terms of load carrying capacity and buckling strength of compression walls of beam and columns can be improved considerably by the use of edge stiffeners or intermediate stiffeners.

2.4.2 Torsional rigidity

Cold-formed sections are normally thin and consequently they have a low torsional stiffness. Many of the sections produced by cold-forming are mono-symmetric with their shear centre eccentric from their centroid as shown in Fig. 2.26a. Since the shear centre of a thin-walled beam is the axis through which it must be loaded to produce flexural deformation without twisting, than any eccentricity of the load from this axis will generally produce considerable torsional deformations in a thin-walled beam as shown in Fig. 2.26a.

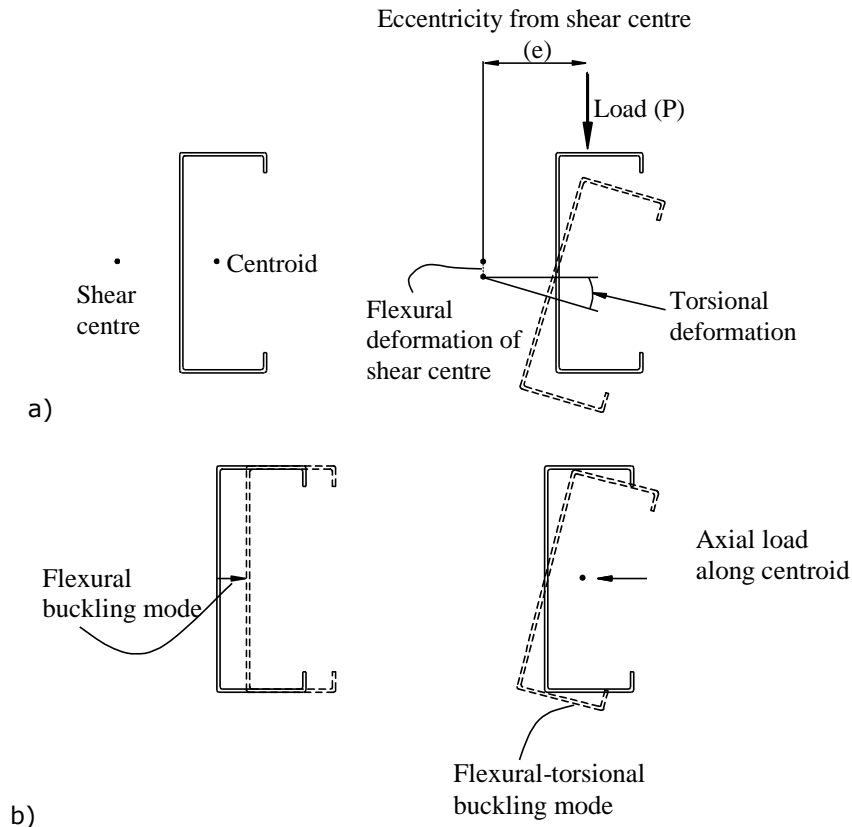


Fig. 2.26 Torsional deformations

Consequently beams usually require torsional restraints either at intervals or continuously along them to prevent torsional deformations. Often, this is the case of beams such as Z- and C- purlins which may undergo flexural-torsional buckling because of their low torsional stiffness, if are not properly braced.

In addition, for columns axially loaded along their centroid axis, the eccentricity of the load from the shear centre axis may cause buckling in the flexural-torsional mode as shown in Fig. 2.26b at a lower load than the flexural buckling mode also shown in Fig. 2.26b. Hence the checking for the flexural-torsional mode of buckling is compulsory in such a case, too.

2.4.3 Web crippling

Web crippling at points of concentrated load and supports can be a critical problem in cold-formed steel structural members and sheeting for several reasons. These are:

- in cold-formed steel design, it is often not practical to provide load bearing and end bearing stiffeners. This is always the case in continuous sheeting and decking spanning several support points;
- the depth-to-thickness ratios of the webs of cold-formed members are usually larger than hot-rolled structural members;

- in many cases, the webs are inclined rather than vertical;
- the intermediate element between the flange, onto which the load is applied, and the web of a cold-formed member usually consists of a bend of finite radius. Hence the load is applied eccentrically from the web.

Web crippling is really a very peculiar feature of the behaviour of thin-walled cold-formed sections and special design provisions are included in design codes in order to manage this phenomenon.

2.4.4 Ductility and plastic design

Due to the sectional buckling phenomena mainly (cold-formed sections are of class 4 or class 3, at the most), but also due to the effect of cold-forming by stress hardening, the cold-formed steel sections possess a low ductility and are not generally allowed for plastic design. Therefore, the previous discussion related to Fig. 2.23b revealed the low inelastic capacity reserve for these sections, after the yielding was initiated. However, for members in bending, design codes allow to use the inelastic capacity reserve of their cross-section part which is working in tension. Moreover, because of their reduced ductility, cold-formed sections cannot dissipate energy in seismic resistant structures. Cold-formed sections can be used in seismic resistant structures because there are structural benefits coming from their reduced weight, but only elastic design is allowed and no reduction of shear seismic force is possible. Hence, in seismic design, a reduction factor $q=1$ has to be taken as stated in EN 1998-1:2004.

2.4.5 Design assisted by testing

Cold-forming technology makes available production of unusual sectional configurations. However, from the point of view of structural design, the analysis and design of such unusual members may be very complex. Structural systems formed by different cold-formed sections connected one to each other (pallet rack systems, like purlins and sheeting, for instance) can also lead to complex design situations, not entirely covered by design code procedures. Of course, numerical FEM analysis is always available, but for some simply practical situations, modelling could be very complicate. For such complex design problems, modern design codes permit to use testing procedures to evaluate structural performances. Testing can be used either to replace design by calculation or combined with calculation. Only officially accredited laboratories, by competent authorities, are allowed to perform such tests and to delivery relevant certificates.

2.5 Distortional buckling: summary review

On the following, based on the reviews done by Schafer and Hancock [43] and Camotim and Silvestre [44], a history of distortional buckling of cold-formed steel columns will be presented and updated for the period 2000 until present.

Research in the behaviour of cold-formed steel columns spans approximately fifty years. Through that time distortional buckling, under many different names, has come in and out of the spotlight. This brief account highlights the major experimental work in cold-formed steel column research. Theoretical

trends are also briefly mentioned, particularly as they relate to distortional buckling. Though distortional buckling in beams and columns is intimately tied together an attempt is made to focus only on the column research.

Summary [43]

	Overall	Distortional Buckling
1940's and 1950's	<ul style="list-style-type: none"> Elastic plate stability formalized Experimental work begins Effective width for ultimate strength 	<ul style="list-style-type: none"> Known phenomena Too complicated to predict analytically
1960's	<ul style="list-style-type: none"> Early design methods formalized Cold-formed steel material properties Prediction of overall (global) buckling 	<ul style="list-style-type: none"> Approximate analytical methods from Aluminum researchers Folded plate theory for distortional buckling
1970's	<ul style="list-style-type: none"> Local and overall interaction Design methods for unstiffened and edge stiffened elements Finite Elements 	<ul style="list-style-type: none"> Observed in experiments, but often intentionally restricted Elastic buckling criteria not accurate for predicting failure mode
1980's	<ul style="list-style-type: none"> Imperfections and residual stresses Effective width formalized Finite strip Distortional buckling problems 	<ul style="list-style-type: none"> Hand methods for elastic prediction Experiments with unrestricted distortional buckling performed Postbuckling reserve discovered
1990's	<ul style="list-style-type: none"> Distortional buckling problems Distortional buckling design Interaction & column boundary conditions Generalized Beam Theory 	<ul style="list-style-type: none"> Hand methods for elastic prediction Interaction of distortional with other buckling modes examined Design: column curve or effective width? Heightened imperfection sensitivity? Inclusion in Design Standards
	Overall	Distortional Buckling
2000 to Present	<ul style="list-style-type: none"> Generalized Beam Theory – extensive developments CUFSM tool Direct Strength Method (DSM) Erosion of Critical Bifurcation Load (ECBL) 	<ul style="list-style-type: none"> DSM included in Appendix 1 to the North American Specification for the Design of Cold-Formed Steel Structural Members (2004) and AS/NZS4600:2005 Interaction of distortional with other buckling modes examined Sensitivity of distortional-overall interactive buckling to sectional imperfections

The 1940's and 1950's

Cold-formed steel column research began in the 1940's with proprietary testing at Cornell University [45], [46]. In [47] is summarized the state of the art for the 1940's. Chilver [48], [49] and Harvey [50] summarized the experimental

and theoretical thin-walled column research in Britain. After fifty years of progress, modern column research is still similar to Chilver's work: elastic stability solutions for local plate buckling and "effective width" for the ultimate strength.

The elastic plate buckling solution was based on Lundquist and Stowell [58] who extended the work of Timoshenko and Gere [59] by providing practical methods for calculating the stability of connected plates. The "effective width" solution was based on von Kármán et al. [60] and the experimental corrections of Winter [61]. Notably, both Chilver and Harvey properly included the interaction of elements in determining the local buckling stress. Also, for lipped channels Chilver stated that the reinforcing "lip" should be sufficiently stiff to insure local buckling (and thus avoid distortional buckling), but gave no criteria for achieving this.

The 1960's

At Cornell, cold-formed steel column research in the 1960's primarily ignored distortional buckling as work focused on material properties, and the behaviour of long columns [55], [56]. Karren showed significant variation in engineering properties around the cross-section; notable, since this fact is widely ignored in current research on distortional buckling. The experimental method used by Karren – compression testing of back-to-back connected specimens – would also later be used by Cornell researchers. At the same time researchers in Canada examined optimizing the geometry of cold-formed columns and edge stiffeners [62], [63].

Aluminum researchers in the 1960 have investigated lipped channels and hats experimentally [70] and analytically [71]. Sharp presented an early theoretical treatment of distortional buckling, or as he termed it "overall" buckling. Under simplifications about the rotational restraint at the web/flange juncture the distortional buckling stress of a lipped channel was approximated. Dwight's experiments were used for verification.

A folded plate method was developed at Purdue University [72] to predict the lateral and torsional buckling of thin-walled beams including sectional distortion. The method demonstrated distortional buckling of open sections under both compressive axial and bending load. At about the same time, an exact stiffness method was developed in the UK by Wittrick [73], [74] for studying the buckling of stiffened panels in compression. Although only stiffened panels, and not open section members, were investigated, distortional buckling modes (called torsional modes) were discovered.

The 1970's

Across the world, column research in the 1970's focused on the interaction between local and overall (i.e, global – flexural, torsional, flexural-torsional) buckling modes ([63], [64], [68], [77]). At Cornell, work also continued on unstiffened elements [78]) and on intermediate and edge stiffeners [79]. In Germany isolated edge stiffeners were studied experimentally and analytically by physically replacing the web/flange juncture with a simple support, thus providing known boundary conditions [65].

Desmond's (1977) work forms the basis for the modern AISI (1996) Specification on edge stiffened elements. In that work, the term "stiffener" buckling describes the distortional mode. For design purposes, Chilver stated that a "lip" should have sufficient stiffness to insure that local buckling occurs. Desmond recognized that elastic buckling criteria (i.e, ensuring that "stiffener" buckling is a higher critical stress than local buckling) does not meet Chilver's criteria. Using

experimental data Desmond empirically formulated rules for an adequate “lip” stiffener. An adequate stiffener is not always economical and thus Desmond provided a single empirical solution for the buckling coefficient, k , of an edge stiffened element in either local or “stiffener” buckling. As a result, distortional buckling was incorporated into the AISI Specification as another local mode and was not treated as explicitly different from local plate buckling. Desmond’s (and Kalyanaraman’s) experimental studies, followed Karren, and thus the specimens were formed by connecting two members back to back. In the resulting specimen, the web thickness is twice that of the flange. The distortional buckling stress is artificially elevated due to higher than normal rotational stiffness at the web/flange juncture provided by the web.

In Sweden, Thomasson [167] performed experiments on lipped channels with slender webs. In order to elevate the local buckling stress of the webs small groove stiffeners were folded in. This eliminated the local buckling problem, but created what Thomasson called a “local-torsional” problem – i.e, distortional buckling. This is a recurring theme for distortional buckling – optimization to remove a local mode creates a distortional problem. Thomasson considered this “local-torsional” mode undesirable and thus put closely spaced braces from lip to lip, insuring that distortional buckling did not occur and therefore making the local mode again dominant.

The 1980’s

At Cornell research focused on imperfections and residual stresses [80] , [81] , local buckling interaction [82] , beam-columns [83] , and the formalization of a unified effective width approach [84] . Mulligan [82] encountered distortional buckling in testing, and followed Thomasson’s terminology thus calling the mode “local-torsional”. Mulligan observed that Desmond’s adequate moment of inertia criteria did not appear to restrain this local-torsional mode in many cases. However, in the end, Mulligan chose to provide braces in a manner similar to Thomasson and distortional buckling was restricted in order to study local buckling phenomena

In Europe, researchers such as [88] continued to provide strong evidence for interaction of local and overall column buckling. At the University of Strathclyde research on local and overall interaction continued ([89]) as well as studies on the behavior of isolated lip stiffened elements [90] , [91] . Lim [90] took the same experimental approach as [65] . The “torsional” mode (distortional buckling) for these flanges may be accurately predicted due to the special boundary conditions.

In the 1980’s some researchers began to focus on distortional buckling. This trend was most evident at the University of Sydney. The need to investigate the behavior of cold-formed steel storage racks lead to work on distortional buckling [92] , [93] . The optimized nature of storage rack columns insured that distortional buckling often dominated. Hancock [66] extended and popularized the finite strip analysis as a tool for understanding the buckling modes in thin-walled members. The specific version of the finite strip method which could account for both plate flexural buckling and membrane buckling in thin-walled members was developed by [75] . Lau extended the finite strip buckling capabilities to the spline finite strip method [67] to allow for fixed-ended boundary conditions, performed experiments in which distortional buckling was the failure mechanism [139] and generated a hand method [76] for predicting the elastic distortional buckling stress. The hand method used classical analytical techniques similar to Sharp [85] but included web instability in the model which had not been considered by Sharp.

In Japan, several authors (Hikosaka, Takami and Maruyama, Takahashi) published papers [86] [87] on the prediction of distortional buckling of thin-walled members with polygonal crosssection.

In the USA, Sridharan [96] developed the finite strip method to study post-buckling in the distortional mode (called local-torsional) and demonstrated the rapid increase in membrane stress at the tips of edge-stiffening lips after distortional buckling. This indicated that the postbuckling reserve in the distortional mode may not be as great as the local mode since yielding would occur earlier in the post-buckling range.

The 1990's

In Europe, column testing continued, [97] Eurocode 3 Part 1.3 (1996) provided a method for predicting the distortional buckling of simple lipped sections such as channels accounting for the restraint provided by the web and the flange to the lip buckling as a strut. This method accounted for the distortional deformations of the web and flange but used a column curve for the failure of the lip so that there was no post-buckling reserve in the distortional mode. Testing of HSS Channels was performed at the Technical Research Centre of Finland [98] and the sections underwent distortional buckling in some cases. The results were compared with the Eurocode method including modifications to improve it.

At the University of Missouri-Rolla work on the effect of strain rate on columns was conducted [158]. At Cornell, further research on load eccentricity effects and web perforations were conducted [99]. Research in Canada and at Texas-Austin examined Z section columns and provided further experimental evidence of distortional failures and problems in the AISI Specification [100], [101], [102].

University of Sydney research on distortional buckling continued in the 1990's [103], [104], [105]. Kwon conducted experiments on lipped channels with and without groove stiffeners in the web. The distortional mode was unrestricted and the tests showed that interaction of distortional buckling with other modes is weak. Distortional buckling was experimentally observed to have lower post-buckling capacity than local buckling. The results were summarized and new column strength curves suggested for distortional failures in [22]. Research also continued on local and overall column buckling interaction. In [35] is presented the importance of different end fixity on the post-buckling behaviour. Young (1997) experimentally demonstrated that fixed ended columns do not suffer the same interaction problems as pin ended columns. Young also observed that the interaction of distortional buckling with other modes is weak.

The University of Strathclyde conducted studies directly related to "torsional" buckling, i.e., distortional buckling [107], [108], [109]. Seah investigated hats and channels with compound lips. Seah developed hand methods for the prediction of distortional buckling similar to Lau's and Sharp's treatments. For ultimate strength Seah and Rhodes's treated the distortional mode in a manner similar to local buckling. Thus, they proposed an effective width approach rather than the column curve approach proposed by Sydney researchers. In addition [110] summarized the state of the art prediction abilities of cold-formed steel design specifications. Limitations and discrepancies were found in all major design specifications.

In the 1990's Generalized Beam Theory (GBT) (theory:[111], [112]) has become a useful tool to study distortional buckling of columns (applications:[113], [117]). Generalized Beam Theory is an extension to conventional engineering beam

theory that allows cross-section distortion to be considered. Stability analysis of thin-walled members may also be performed using GBT. Using GBT, Davies and Jiang argued that distortional buckling has weak interactions with other modes. GBT is currently only applicable in elastic problems, but Davies and Jiang endorsed the column strength curves of [118] for ultimate strength prediction.

Using finite strip and finite element analysis Schafer (1997) demonstrated that the distortional mode has greater imperfection sensitivity than local modes. Schafer also observed that distortional failures have lower post-buckling strength than local failures. New hand methods for predicting distortional buckling that are a hybrid of the finite strip method and the classic hand methods used by Sharp (1966) are presented and verified. [119] explicitly showed that the AISI Specification equations (via Desmond) over-predict the distortional buckling stress, particularly as the ratio of the web height to flange width becomes large.

The Australian Standard for Steel Storage Racking (1993) and the Australian/New Zealand Standard for Cold-Formed Steel Structures (1996) were developed to contain explicit design rules for distortional buckling in compression.

2000 to Present

In the last decade, the research team of Professor Camotim at IST (Technical University of Lisbon) has devoted a very significant amount of research work to the development, numerical implementation, application and worldwide dissemination of novel GBT formulations that considerably broaden the scope of this theory, by enabling the performance of several additional analyses and covering a wider range of structural systems [125], [126], [127], [128], [129], [130]. In particular, it is now possible to carry out (i) first-order, buckling, post-buckling, vibration and dynamic analyses of metal and FRP members with open and closed cross-sections, and (ii) first-order, buckling and post-buckling analyses of thin-walled steel frames. Generalized Beam Theory has a user friendly program for use developed at the Technical University of Lisbon called GBTUL (Bebiano et al. 2008, <http://www.civil.ist.utl.pt/gbt/>), that performs elastic buckling (bifurcation) and vibration analyses of prismatic thin-walled members.

Another alternative to study the elastic buckling analysis of thin-walled members is CUFSM tool (<http://www.ce.jhu.edu/bschafer/cufsm/>). CUFSM employs the semi-analytical finite strip method to provide solutions for the cross-section stability of such members [131], [132]. Recently, an extension to the conventional FSM solution have been explored, i.e. the constrained finite strip method, or cFSM. A cFSM solution provides a means for (1) stability solutions to be focused only a given buckling mode (*modal decomposition*), or (2) a conventional FSM stability solution may be classified into the different fundamental buckling modes (*modal identification*).

The Direct Strength Method is an entirely new design method for cold-formed steel and was adopted in 2004 as Appendix 1 to the *North American Specification for the Design of Cold-Formed Steel Structural Members*. The Direct Strength Method does not rely on effective width, nor require iteration for the determination of member design strength. Instead, the engineer must determine the elastic buckling load in local, distortional, and global buckling. This information along with the load that causes first yield are then employed in a series of simple equations to “directly” provide the strength prediction. The primary complication with the method lies in determining the elastic local, distortional, and global buckling loads; once these values are determined application of the method is straightforward. Computational tools, such as the freely available open source

program CUFSM, can provide the elastic buckling loads that the Direct Strength Method requires [131] , [132] .

Leece and Rasmussen [171] carried out experimental data and simulated FEA models to assess current design guidelines for distortional buckling of stainless steel lipped channel members in compression. Channels with and without intermediate stiffeners were examined. The majority of tests showed distortional buckling as the critical failure mode, with one shorter length channel experiencing local and distortional buckling interaction.

At the PU Timisoara, Dubina and Ungureanu [133] , [134] characterize and codify the geometrical imperfections and residual stresses and also assess their influence on the cold-formed steel member strength. They found that the different shapes of local-sectional imperfections have a different effect on the member buckling strength and emphasised that the sine shape of these imperfections not always represents the appropriate mode to be introduced into the non-linear analysis. Also, they shown a higher sensitivity of the distortional-overall interactive buckling to sectional imperfections, due to the lower post-critical strength reserve of the distortional mode, compared with the local one. Their ultimate goal is to provide a set of reliable and easy-to-use guidelines aimed both (1) fabricators (establishment of manufacturing tolerance limits) and (2) designers (clear definition of the member initial state that must be included in the FEA.

2.6 Interactive buckling

2.6.1 Theoretical background

The behaviour of a structure is known if the three sequence of load-deformation curve are well defined: pre-critical, critical, and post-critical paths (Fig. 2.27).

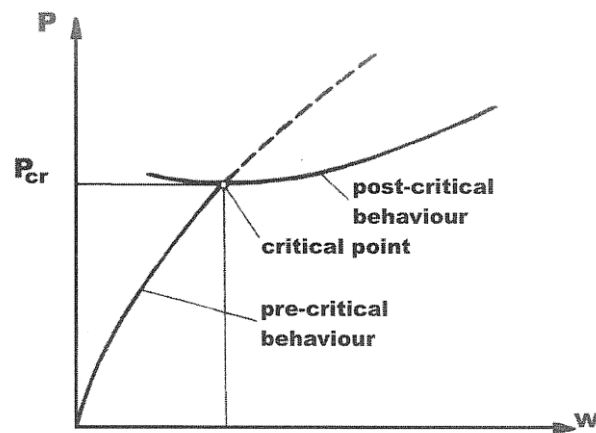


Fig. 2.27 Stability and instability of structures [136]

In function of considered type of behaviour, today conceptions and trends in the structural stability shows that the investigations have tended to fall into one of the following directions [136] :

Practical design direction, in which methods of analysis, specific for stability problems related to some structural forms, are developed. These studies are invaluable since they aim is to provide solutions to practical problems, to supply designers with data useful for design and to prepare norms, specifications or codes. In this field of structural stability work the engineers who believe especially in the physical sense of the phenomena than in the mathematical results. All the researches in this direction are based on *Euler's concept*, which considers that an analysis for stability is restricted to determining the buckling load and all the structural members have the same sensitivity to the imperfections as the standard bar hinged at both ends, and the difference between buckling and bifurcation loads is due to the influence of mechanical and geometrical imperfections.

Theoretical direction, in which the main problem is the study of phenomena with aid of theoretical methods. This direction is concerned with a more profound understanding of the phenomenon of instability, especially in the post-critical range. This approach, which has led to the *Theory of Post-critical Behaviour of the Structures* is less familiar to designers. A wide range of research has gone into these theories: mathematicians and mechanical engineers specialized in applied mathematics and mechanics, engineers who have been working in the field of space and naval constructions rather in building and industrial constructions, have all contributed to it. The start of this research direction was the Koiter's doctoral thesis (1967). Koiter showed that, beside Euler's type of bifurcation, there are other types

of structural behaviour at the critical point, connected with the post-critical curve and that the collapse load of the actual structure, with its geometrical imperfections, is in direct connection with the post-critical behaviour. Hence *Koiter's concept* demands that, besides determining the critical load, the post-critical behaviour of the structure should be studied so as to determine to what extent the structure is sensitive to imperfections. This concept, applied to struts, plates and shells, explained their fundamental different response. It seems fair to say that the Koiter's post-buckling theory represents one of most important contributions in the field of stability of elastic systems since the initial investigations of Euler.

Instability of evolving systems. For systems governed by a gradiental potential, Thorn (1972) developed a very important theory, the well-known *Theory of Catastrophes*. Other two theories, which deal with stability and instability of systems, were developed in the same time. The concept of *Dissipative Systems* elaborated by Prigogine and Stengers in 1979 covers all natural phenomena which occur far from its initial equilibrium as they can appear beyond a critical value, in the domain of non-linear processes. The second theory, developed by Haken (1978) and known as the *Synergetics*, deals with the co-operation of the individual parts of a system, both in the equilibrium and instability ranges. These theories are interdisciplinary fields of research works, which aid the better understanding of the instability phenomena. Therefore, the instability theory interacted vigorously for the last years with these general theories.

2.6.1.1. Erosion of the Critical Bifurcation Load

In ideal structure loses its stability through bifurcation. The critical bifurcation load is reached at the point of intersection between the pre-critical curve and the post-critical one. An actual structure, i.e. one with imperfections, loses stability through limit point equilibrium (Fig. 2.28). Normally, since structures inevitably have imperfections, the limit load ought to be determined. But this task is very difficult even with very powerful computers due to the geometrical and physical nonlinearities are very pronounced when the limit load is reached. Computation of the limit load by means of complicated and time-consuming computer programs will remain the task of research works only. In practice of structure design the critical bifurcation can be determined by means of much simpler methods than the ones required for determining the limit load. Therefore, for future, the computation of bifurcation load remains the methodology used in practice. The main problem is the correction of this bifurcation load considering the influence of geometrical and mechanical imperfections.

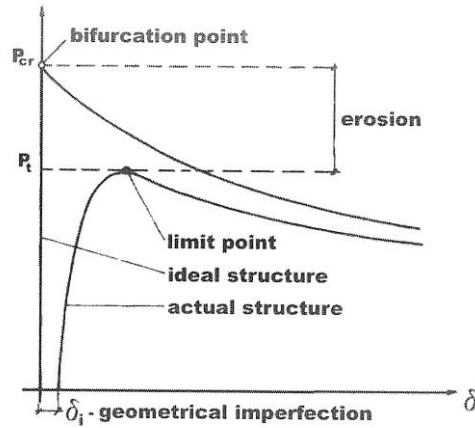


Fig. 2.28 Erosion of critical bifurcation load

The difference between the critical bifurcation load and the limit load is the *erosion of the critical load*. This erosion may be more or less pronounced, depending on the type of structure and the size of the imperfections. Thus if one accept the critical bifurcation load as the basic value, the main problem will be the determination of this erosion. Since this erosion is little in some structures and significant in others, the idea is now that the critical bifurcation load consists of two components, a stable and an unstable one, the latter being the only one that is eroded by imperfections (Fig. 2.29). The degree of the erosion depends on the imperfection size and on the ratio of the unstable to the stable component. So, the two aspects of instability, the critical bifurcation load and the post-critical behaviour, can be considered as a result of the sum of the two components (see Fig. 2.30):

Critical bifurcation load = Stable component + Unstable component

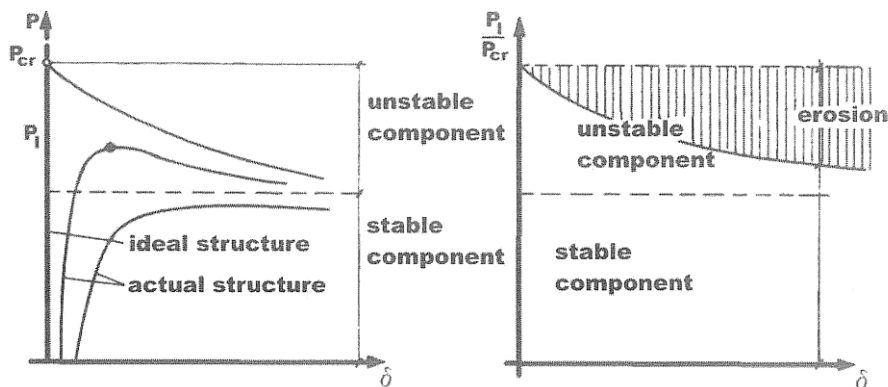


Fig. 2.29 Stable and unstable components

The stable component presents a stable symmetric post-critical behaviour, while the unstable component can show an unstable symmetric or asymmetric post-critical behaviour. By superposing these two components, result the post-critical behaviour of structure. If the both components are symmetrical ones, the post-

critical behaviour results symmetrical too, but in function of the characteristics of the two components, the behaviour can be stable or unstable. If the unstable component presents an asymmetric post-critical behaviour, the result of the superposing is always an unstable asymmetric post-critical behaviour.

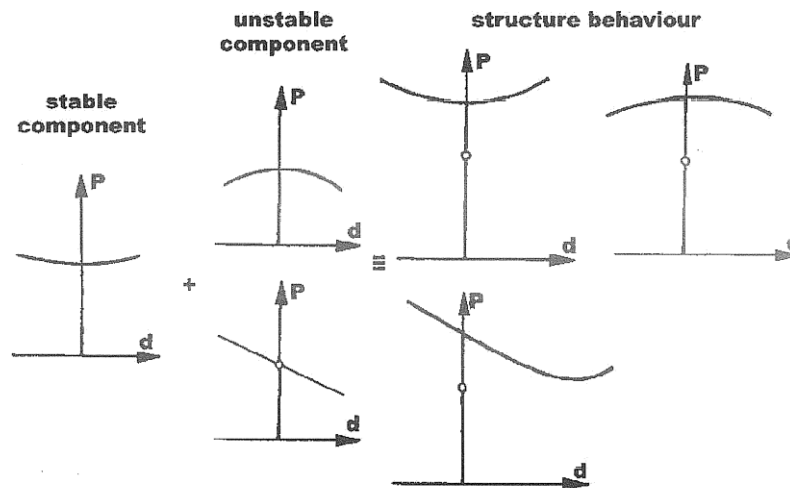


Fig. 2.30 Post-critical behaviour as result of the sum of the two components

This idea is not really new. The isolated bar has been analysed on the similar principle, the European buckling curves representing, in fact, the erosion of the bifurcation load as a function of the bar slenderness, which introduces the size of unstable component due to plastic deformations, eroded by geometrical and mechanical imperfections. The concept of reduced components is also used in the analysis of thin-walled members. Thus, the bearing capacity is considerably reduced by coupling the buckling of walls with the global buckling of the bar. A number of methods account for this effect, such as the well-known active width, which suggests that the stiffness of the bar be reduced by eliminating part of the bar walls as an effect of their buckling.

An analysis of these studies shows that the idea of taking into account the unstable component eroded by imperfections has introduced satisfactory results for many types of structures. Since each of these studies is rather particular in character, a more general approach to the problem is now required to provide a unitary concept for all types of structures. In the first analysis it is necessary to determine the factors that account for unstable components in the critical bifurcation load. An analysis carried out by Gioncu (1986) has established that the stable component is introduced by bending stresses, while the unstable component is produced by the following factors:

- extensional deformations;
- elastic lateral supports,
- coupled instabilities;
- plastic deformations.

Once these factors are known, a method applicable in design practice must be found to eliminate the actual difficulties of the stability analysis of structures.

Coupled instabilities. The instability behaviour of bar members is generally characterised by stable post-critical modes. However the interaction of two stable symmetric post-critical modes may generate an unstable coupled asymmetric mode, rendering the member highly sensitive to imperfections. In such case a significant erosion of critical load occurs. Examining the cases of coupled instability, it was found that two very different types exist [140] :

- *naturally coupled instabilities*; which result in garland curves. Two forms of instabilities are possible in the intersection points of these curves. The post-critical curves can be stable for uncoupled modes, but by coupling, they become unstable. The phenomenon of buckling patterns change in plates and shells, due to this mode interaction, is well known, but, in some way, it may be found also in the case of thin-walled members (Fig. 2.31).
- *coupling due to design*; when the geometric dimensions of structure are chosen such as two or more buckling modes are simultaneously possible (Fig. 2.32). For this case, the optimisation based on the simultaneous mode design principle plays a very important role and the attitude of the designer towards this principle is decisive. This type of coupling is the most interesting in practice.

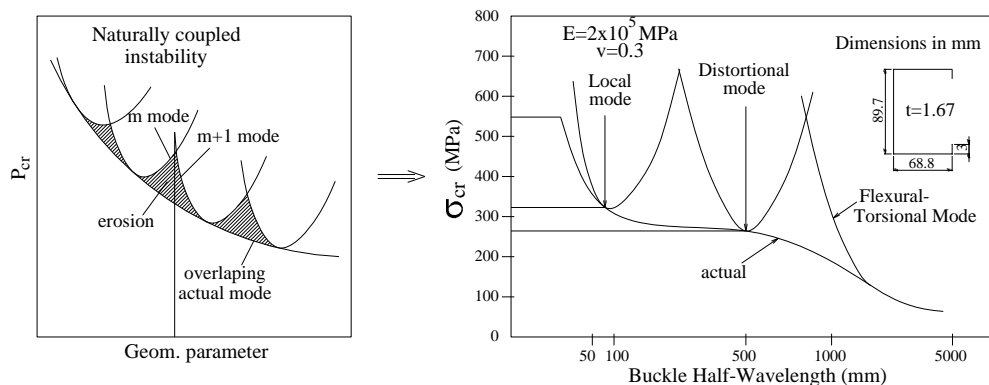


Fig. 2.31 Natural coupled instability: example for lipped channel section analysed with a spline finite strip buckling program [139]

Another classification of coupled instabilities refers to the linearity or non-linearity of coupling:

- *linear coupling*; this occurs when two modes are coupling from the origin, independently of the presence of imperfections. An example is the interaction between flexural and torsional buckling of mono-symmetrical sections;
- *non-linear coupling*; this exist for some geometrical proportions of structures only, and the presence of the geometrical imperfections is indispensable for coupling; this coupling doesn't exist for ideal structure. For instance, this is the case of the interaction between flexural buckling and torsional-flexural buckling of some mono-symmetrical cross-section (Fig. 2.32).

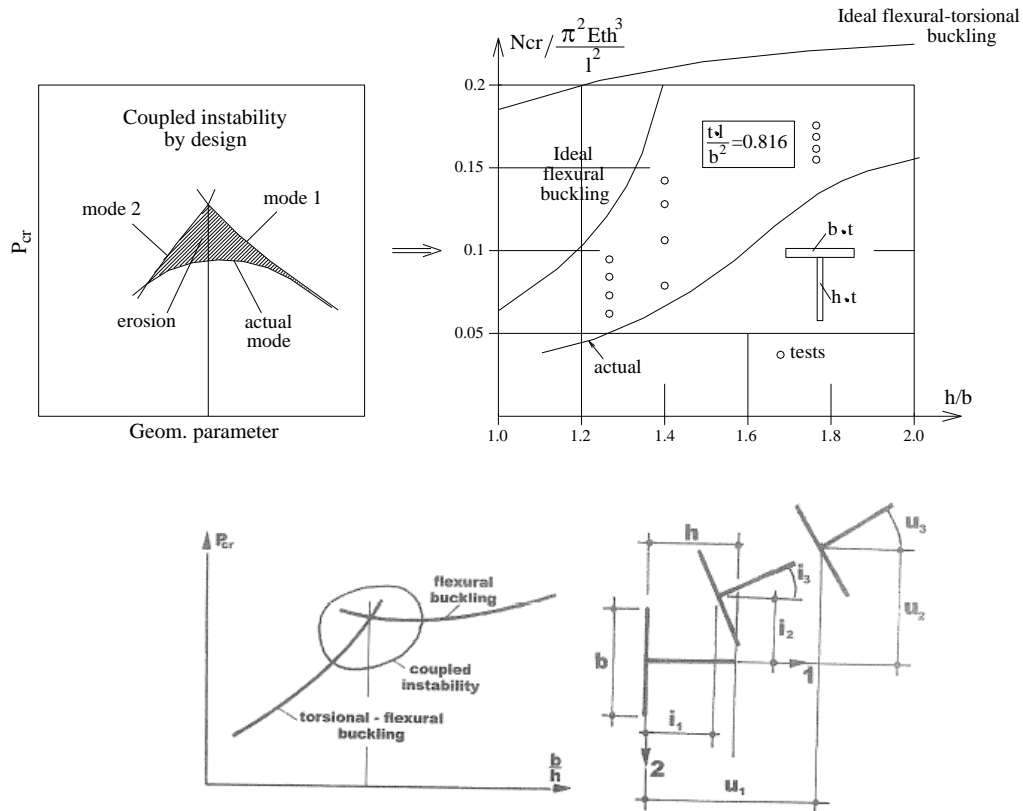


Fig. 2.32 Coupled instability by design: example for T section with test evidences [140]

The general meaning of coupled instability phenomenon is related, in fact, to non-linear coupling. Due to the imperfections, an interaction erosion of critical bifurcation load occurs. This erosion is maximum in the coupling point vicinity. For bar members, an interactive slenderness range, in which sensitivity to imperfections is increased, may be identified. Classes of interaction types, separated by specific levels of erosion intensity, may be defined.

Given a compression member, we are assuming two simultaneous buckling modes may occur. If N_u is the critical ultimate load, and N_{cr} the ideal critical one, the following relation may be written:

$$N_u = (1-\psi)N_{cr} \tag{2.10}$$

The *erosion factor* ψ was introduced as a *measure* of erosion of critical load. Gioncu (1994) has classified the interaction types by means of this erosion factor, as follows:

- class I: weak interaction (W), $\psi \leq 0.1$;
- class II: moderate interaction (M), $0.1 < \psi \leq 0.3$;
- class III: strong interaction (S), $0.3 < \psi \leq 0.5$;
- class IV: very strong interaction (VS), $\psi > 0.5$.

Obviously, an appropriate framing of each coupled instability into the relevant class is very important because the methods of analysis used for design have to be different from one class to another. In case of week or moderate

interaction, structural reliability will be provided by simply using of design code safety coefficients, while in case of strong or very strong interaction, special methods are needed.

If large number of local buckling modes occurs simultaneously under the same local critical load, two types of interaction are produced. The first is due to local multiple local modes and gives rise to an unstable post-critical behaviour. The second interaction of the local buckling modes with the global buckling mode yields to a very unstable post-critical behaviour, with great erosion due to the imperfections. Thus, this case of the multiple-buckling modes interaction causes very destabilizing effects. Strong and very strong interaction is the result of this coupled instability. For this type of interaction, very special design methods must be developed. This is the case of compression thin-walled columns.

Regarding the post-critical behaviour of an elastic structure and the elasto-plastic curve, one can see many similarities (see Fig. 2.33): the same plateau and hardening path and the same effects of imperfections. The similarities are most pronounced if the curves from Fig. 2.33b are examined. In the first figure one can see the well-known elasto-plastic buckling curves, for an ideal and actual member, while in the second, the coupling between two instability modes, with the effects of the geometrical imperfections. The analogy is almost perfect, the yield stress playing the same role as the local buckling stress. These observations confirm that the elasto-plastic buckling can be considered as a coupled instability between the local bifurcation and the elastic buckling of the column.

Table 2.3 summarises the main coupled instability cases, which may appear within the bar members.

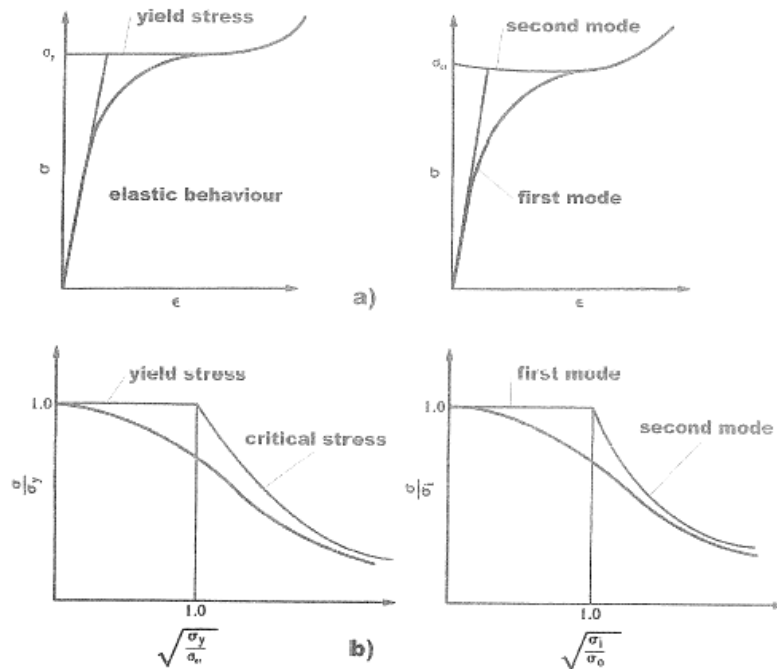


Fig. 2.33 Similarities between plastic buckling and coupled instability (Gioncu 2004)

Table 2.3 Coupled instabilities in bar members

No.	Bar member type	Instability modes	Class of interaction
1.	Mono-symmetrical columns	$F + FT = FFT$	W to M $\psi \leq 0.3$
2.	Built-up columns	$F + L = FL$	M $0.1 < \psi \leq 0.3$
3.	Thin-walled columns	$F + L = FL$	S to VS
		$FT + L = FTL$	$\psi \geq 0.3$
		$F + FT + L = FFTL$	
4.	Thin-walled beams	$F + D = FD$	M to S
		$FT + D = FTD$	$0.3 \leq \psi \leq 0.5$
		$F + FT + D = FFTD$	
		$LT + L = LTL$	M
		$LT + D = LTD$	$\psi \leq 0.3$

Legend: F = flexural buckling ; FT = flexural-torsional buckling;
 L = local buckling ; D = distortional buckling
 W = weak interaction ; M = moderate interaction ; S = strong interaction;
 VS = very strong interaction

2.6.1.2. Different computational analyses and different structural behaviours [114]

The key categories of computational analysis that were first devised for use in EN 1993-1-6 are recommended for wide use for all structures:

- LBA: Linear elastic bifurcation analysis, obtaining the lowest eigenvalue for the system;
- MNA: Materially nonlinear analysis, using small displacement theory (no change of geometry), and an ideal elastic-plastic constitutive model for the material;
- GNA: Geometrically nonlinear analysis of the elastic perfect structure;
- GMNA: Geometrically and materially nonlinear analysis of the perfect structure;
- GMNIA: Geometrically and materially nonlinear analysis with explicit imperfections.

“Geometrically nonlinear” means an analysis that takes full account of the change in geometry, both in kinematic and equilibrium relationships, whether this be a small change in one dimension or a gross inversion of the complete structure. Similarly it is expected that in a GMNA or GMNIA analysis, the material model will be fully nonlinear and not simply an ideal elastic-plastic model, unless this truly represents the material response. The classic image of the load-displacement curves given by these analyses is shown in Fig. 2.34.

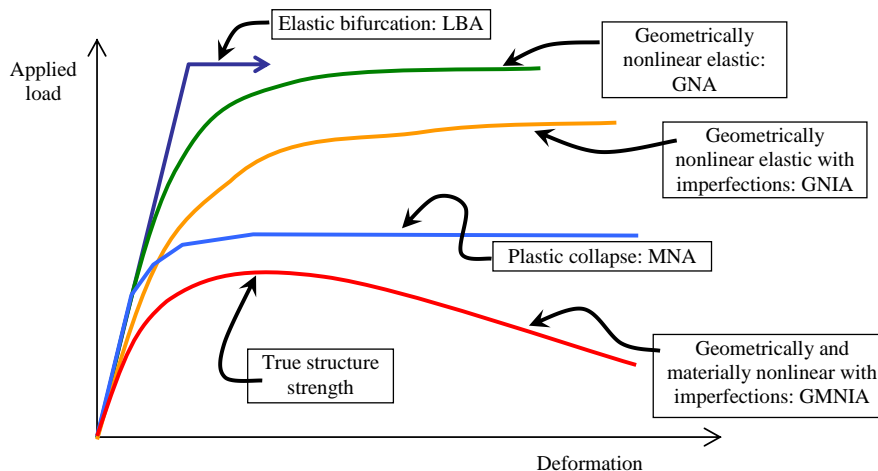


Fig. 2.34 Load-displacement curves found using different analyses of the same structure [114]

The images in Fig. 2.34 are substantially misleading for many non-standard structures since the load-displacement curves all asymptote to a maximum or pass through a maximum load, so that the “strength” derived from each analysis is unambiguous. But in more complex structures, such as space frames, plate assemblies and shells, a GMNIA analysis can lead to a much greater variety of behaviours as is later illustrated in Figs. 2.35 and 2.36.

More complex innovative structures may exhibit many different behaviours under materially and geometrically nonlinear analysis. The following gives a short

indication of some of the phenomena that may appear and so must find a place in any more general all-embracing description.

The classic images of the behaviour of member, plate and shell structures are shown in Fig. 2.35a, whilst the geometrically nonlinear elastic snap-through buckling of arches, shallow space trusses and shells is illustrated in Fig. 2.35b. The consequences of imperfections, coupled with the question of whether the post-buckling behaviour is stiffening or softening, are illustrated in Figs. 2.35c and d.

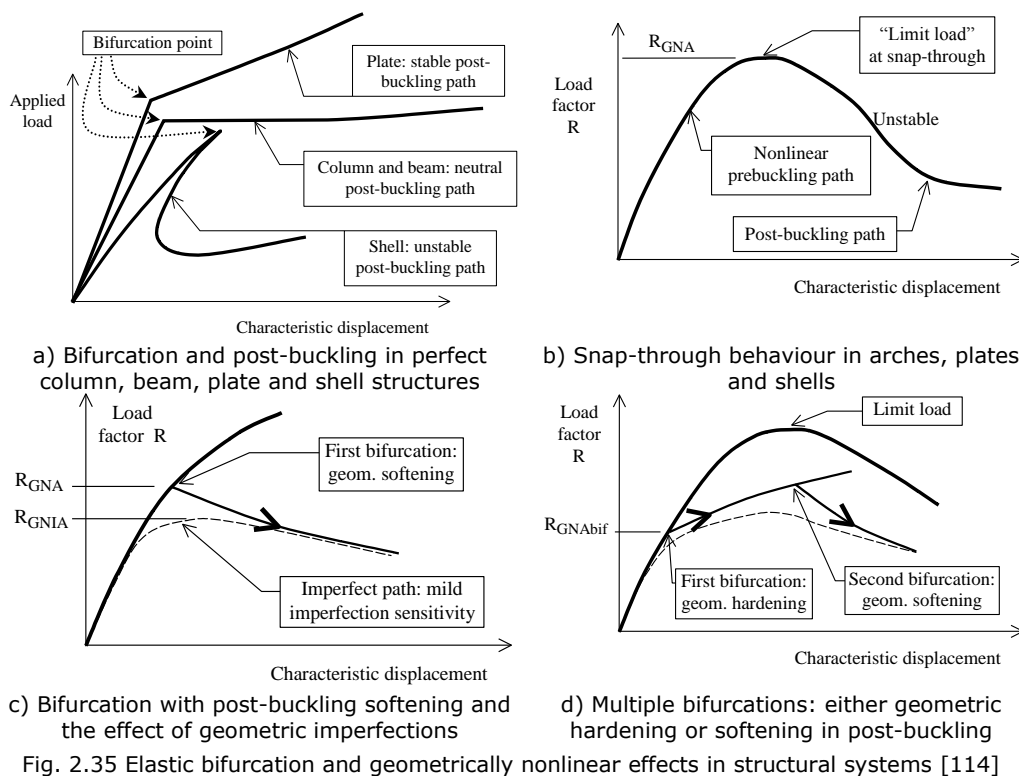


Fig. 2.35 Elastic bifurcation and geometrically nonlinear effects in structural systems [114]

These phenomena become trickier when the geometric imperfections simply cause progressively growing deformations, as shown in Fig. 2.36a, where no bifurcation is detected, but a limit load may occur. Finally Fig. 2.36b illustrates the problem that the perfect structure may bifurcate with a clear peak load; the same structure when slightly imperfect may show reduced strengths with a limit load; but as the imperfection amplitude increases, the limit load may disappear to be replaced by a smooth transition from prebuckling to large displacements in the post-buckling mode. It is not easy to define what is meant by failure here, and a simple reliance on the maximum achieved load is not helpful. The above phenomena may occur in elastic or elastic-plastic structures. They also have implications for tolerance specifications.

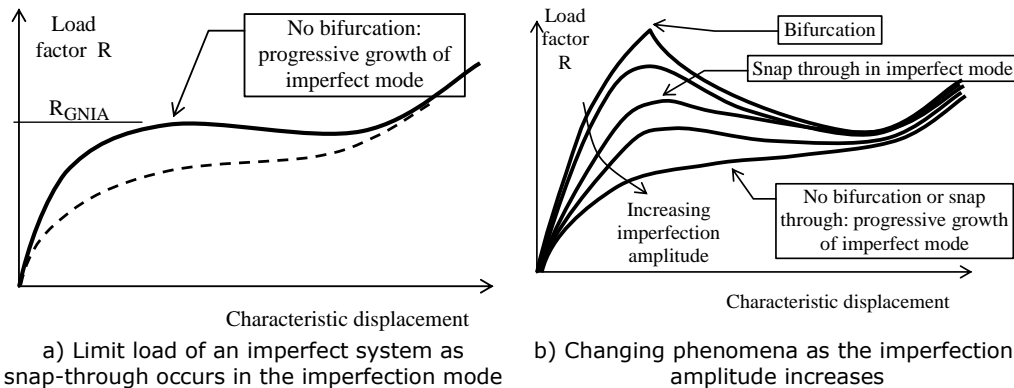


Fig. 2.36 Load-deflection paths in imperfect structural systems [114]

2.6.1.3. Summary of design methods

The methods used for interactive buckling analysis of thin-walled steel members in compression can be classified in four categories [135] i.e.

- *Analytical methods*, based on the asymptotic or perturbation theory of post-critical behaviour of members; however such methods can be used for theoretical purposes, only;
- *Semi-analytical methods*, by which the modelling of the local buckling is based on the “plate effective width” and the non-linear equations are used to describe the bar members behaviour (ECBL);
- *Semi-empirical methods*, which modify the bar member buckling curves by means of reduced or effective geometrical properties of cross-section on the base of “effective width” concept; the “effective width” method is actually used in design codes. As an alternative to that, the “effective stiffness” can be used (DSM);
- *Numerical methods* based on Finite Element Method (FEM) or Finite Strip Method (FSM). Simple eigenbuckling analysis can be used to obtain the uncoupled paths of buckling modes and their corresponding critical loads or the advanced non-linear inelastic analysis to simulate the real behaviour. Linear and non-linear *General Beam Theory (GBT)* can be also framed in this category.

Various methods have been used by engineers to design cold-formed steel members, and some of the more recent methods are summarised as follows [115]

- **FEA (Finite Element Analysis) Method**
 - An initial model representing the structure or structural component is built within the computer software.
 - Load can be placed at any point on the member and in any direction.
 - Once solved for the given load, the software provides solutions of the governing differential equations and calculates the reactions and deflections over the length of the member.
 - The reactions and deflections are examined to determine if the structure or structural component has the required design capacity.
 - The analysis solvers can incorporate non-linear stress-strain relationship and non-linear geometry.

- Point-contact elements, links, and/or compression only members can be used to model the contact between connected components.
 - Perforations can be included if required.
 - Complex boundary conditions can be examined if required.
 - With increasing computer speeds and memory, FEA now takes less computer time to carry out.
- **FSM (Finite Strip Method)**
 - Semi-analytical, semi-numerical approach.
 - Similar to FEA but requires less time to build the model, uses less memory and has faster solve times.
 - Based on half sine wave displacement functions.
 - Assumes simple pinned end supports.
 - Axial load or constant bending moment is applied to give constant stress resultant.
 - This method is used in the program Thin-Wall [116]
 - **GBT (Generalised Beam Theory)**
 - Essentially the separation of the behaviour of a prismatic member into a series of orthogonal displacement modes.
 - All buckling modes and their interaction are examined.
 - Each buckling mode or interaction of modes has a relatively simple equation in terms of the generalised section properties and the material properties.
 - Can separate and combine individual buckling modes and their associated buckling components.
 - Axial load or constant bending moment is applied to give a constant stress resultant.
 - **Effective Width Method**
 - Effective widths on individual parts of the full section are calculated from first understanding the stress distribution within the member. This includes calculating the element buckling stress from simple plate theory with edges supported (by stiffeners) or free (no stiffeners).
 - The effective widths are then combined to determine an overall effective section.
 - Depending on the applied stresses, a new centroidal axis is equated.
 - A new effective section is determined based on the new centroid of the section, and the iterative process is continued until the solution converges.
 - Depending on the slenderness of the member, different equations are then used to determine buckling capacities for each mode of buckling.
 - **DSM (Direct Strength Method)**
 - Relatively new semi-empirical method being brought into some design codes, AISI, including the NAS and AS/NZS 4600:2005.
 - In essence, this method replaces the effective width concept with an effective stress concept.
 - Uses full section properties therefore no calculations required for effective width/section.

- Uses FSM to obtain the elastic critical buckling loads for each mode type.
 - Depending on the slenderness of the member, a simple equation for the ultimate strength can be derived for each buckling mode.
 - **ECBL (Erosion of Critical Bifurcation Load)**
 - Semi-analytical method based on plate effective width.
 - Introduces the local failure mode of thin-walled sections into the global behaviour of the member (local-overall buckling interaction).
 - Introduces an erosion factor to accurately determine the imperfection factor.
 - Successfully used to predict behaviour of perforated sections.
- On the following, the most important methods will be presented.

2.6.2 Models and methods

2.6.2.1. Effective width method

Considering a simply supported square plate subjected to uniform compression stress in one direction, it will buckle in a single curvature shape curvature in both directions, as shown in Fig. 2.37.

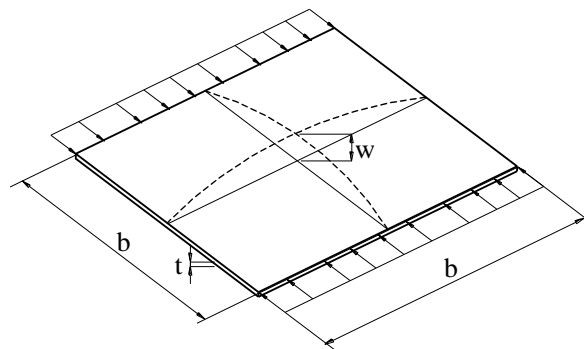


Fig. 2.37 Square simply supported thin plate in compression

However, in case of an individual compression wall of a cold-formed thin-walled section the length of the element is much larger than the width (see Fig.2.38). This type of buckling is called "local" because the length of buckles which form are comparable to the dimensions of the cross-section.

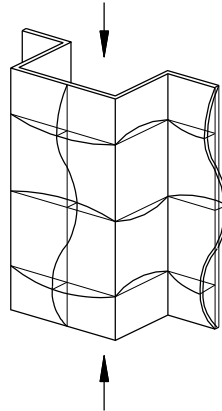


Fig. 2.38 Local buckling of component walls of a cold-formed thin-walled section

A plate subjected to uniform compressive strain between rigid frictionless platens will deform after buckling as shown in Fig. 2.39a and will redistribute the longitudinal membrane stress from uniform compression to those shown in Fig 2.39b.

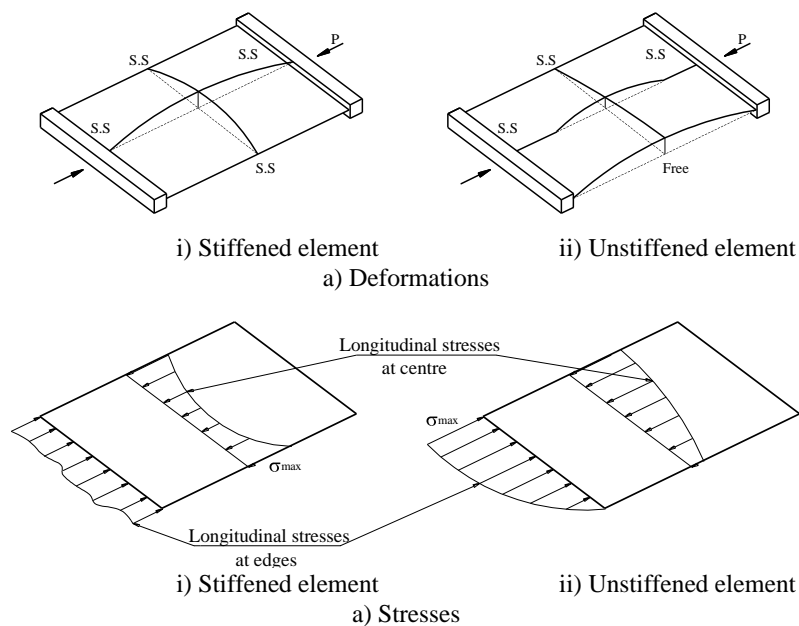


Fig. 2.39 Post buckling behaviour of stiffened and unstiffened plate element (Hancock, 1998)

In the pre-buckling phase stresses are uniformly distributed (see Fig. 2.40a); after buckling occurred they become non-uniform (see Fig. 2.40b) and continuously concentrate and increase towards edges as load increases, until the yield strength is reached (see Fig. 2.40c), when the plate starts to fail.

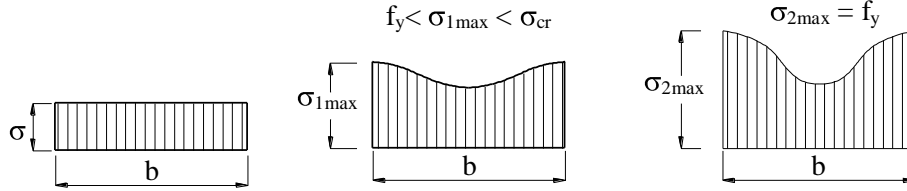


Fig. 2.40 Consecutive stress distribution in stiffened compression elements: (a)-pre-critical stage; (b)-intermediate post-critical stage; (c)-ultimate post-critical stage

The behaviour of an ideal (e.g. perfect) and an actual (imperfect) plate is shown in Fig. 2.41.

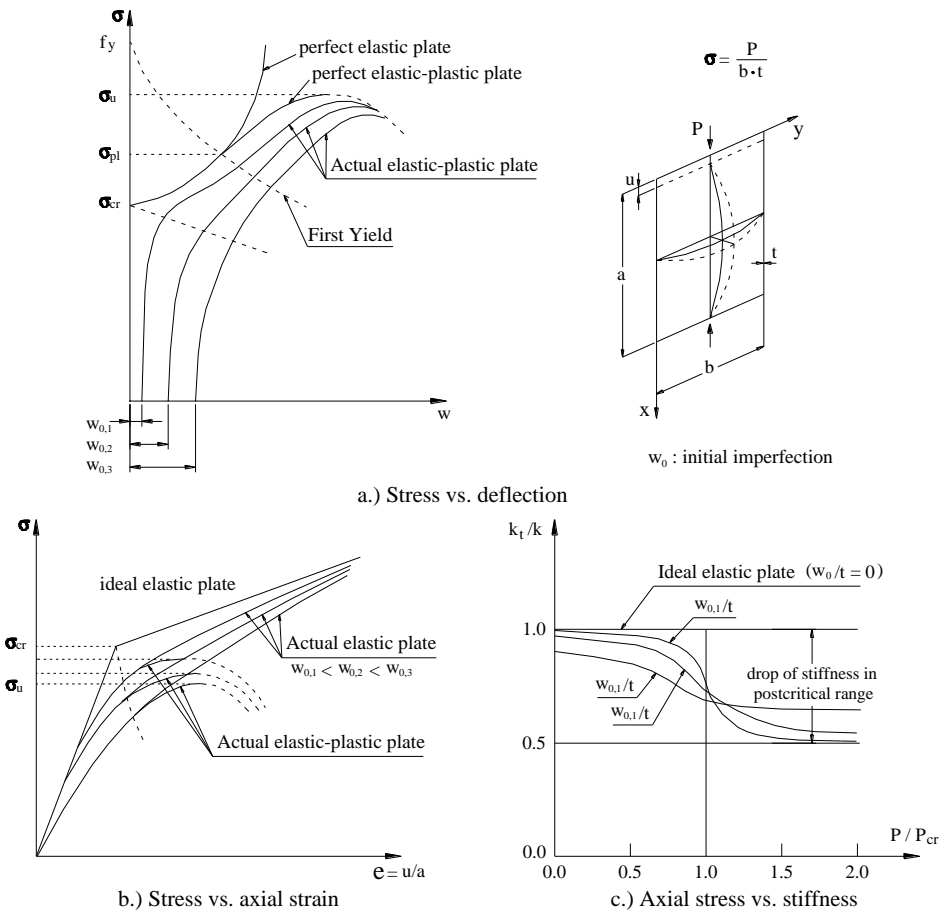


Fig. 2.41 Behaviour of ideal and actual simply supported plate in uniaxial stress

Looking to the path of ideal plate stress deflection curve it can be observed: in the pre-critical range $\sigma < \sigma_{cr}$, the plate has a linear behaviour characterised by a plane stress state; when the critical stress point is reached, $\sigma = \sigma_{cr}$, the plate

suddenly lose its rigidity (see Fig. 2.41b) and significant increase of deflection occurs. Consequently, in that range, the large deformation theory has to be used in order to describe the plate behaviour, and the post-critical behaviour is generated by tangent axial stiffness, K , e.g. $K = dP/dU$, instead of first order elastic stiffness, $K = P/U$. The post-critical path depends by restraining edge conditions, stress distribution (e.g. uniform or non-uniform compression) and material characteristic. The behaviour continues to remain elastic ($\sigma_{cr} < \sigma < f_y$) and due to "membrane lag" effect a stabilizing action occurs due to which the post-critical stress reserve is available. The behaviour of the plate in this range is described by non-linear equation of stress equilibrium and strain compatibility, well known as Von Karman-Marguerre equations ([119], [120]). The "membrane lag" is the explanation for the non-linear elastic behaviour within this range.

When the first yield is reached in the point $\sigma = \sigma_{pl}$, the curve change the curvature, and the plate starts its elastic-plastic behaviour. In the domain $\sigma \leq \sigma_{pl}$, the unloading path is fully reversible. For this reason, the point $\sigma = \sigma_{pl}$ is also called "reversibility" point [121]. The behaviour in this point corresponds to the stress distribution (c) in Fig. 2.40.

In the range $\sigma > \sigma_{pl}$ the plate loses rapidly its stiffness and reaches the ultimate strength, f_u . To account for the reduces stiffness of the plate, into the post-critical range, the plate behaviour within this range will not governed by the elastic modulus, E , but by the "tangent modulus", E_t , or by the "secant modulus" E_s . In fact, due to its small thickness, the post-elastic strength reserve of such a type of plate is not significant to be considered in practice. Therefore, for practical design purposes, the ultimate strength reference point is $\sigma = \sigma_{pl}$. Consequently one speaks about the "post-critical" strength of the thin steel plates, but does not speak about their post-elastic strength.

When both geometrical and material imperfections are present (e.g. initial deflections and residual stresses for instance), which is the case of actual plate, its behaviour is characterised by a continuous deformation process, as seen in Fig. 2.41: more increase of the initial deflection w_0 (to be regarded here as an equivalent imperfection), more smooth is the $\sigma - w$ curve. In fact, in practice it is really difficult to catch the points σ_{cr} and σ_{pl} , and often during tests σ_u is taken as σ_{cr} and vice versa. Therefore for the actual thin plate, the $\sigma_{cr} - \sigma_u$ range is quite reduced.

The post-buckling behaviour of the plate can be analysed by using large deflection theory. The following differential equation for large deflection buckling of a plate was introduced by von Karman in 1910:

$$\frac{\partial^4 \omega}{\partial x^4} + 2 \cdot \frac{\partial^4 \omega}{\partial x^2 \partial y^2} + \frac{\partial^4 \omega}{\partial y^4} = \frac{t}{D} \cdot \left(\frac{\partial^2 F}{\partial y^2} \cdot \frac{\partial^2 \omega}{\partial x^2} - 2 \cdot \frac{\partial^2 F}{\partial x \partial y} \cdot \frac{\partial^2 \omega}{\partial x \partial y} + \frac{\partial^2 F}{\partial x^2} \cdot \frac{\partial^2 \omega}{\partial y^2} \right) \quad (2.11)$$

where F is the Airy, a stress function defining the median fibre stress of the plate, and

$$\sigma_x = \frac{\partial^2 F}{\partial y^2} \quad (2.12)a$$

$$\sigma_y = \frac{\partial^2 F}{\partial x^2} \quad (2.12)b$$

$$\tau_{xy} = \frac{\partial^2 F}{\partial x \partial y} \quad (2.12)c$$

It has been found that the solution of the differential equation for large deflection theory has little application in the practical design because of its complexity. For this reason, a concept of the "effective width" was introduced by von Karman *et al.* in 1932 [60]. In this approach, instead of considering the non-uniform distribution of stress, $\sigma_x(y)$, over the entire width of the plate b , it was assumed that the total load, P , is carried by a fictitious effective width, b_{eff} , subjected to a uniform distributed stress equal to the edge stress, σ_{max} , as shown in Fig 2.42. The width b_{eff} is selected so that the area under the curve of the actual non-uniform stress distribution is equal to the sum of the two parts of the equivalent rectangular shaded area with a total width b_{eff} and an intensity of stress equal to the edge stress σ_{max} , that is,

$$P = \sigma_{med} \cdot b = \int_0^b \sigma_x(y) dy = \sigma_{max} \cdot b_{eff} \quad (2.13)$$

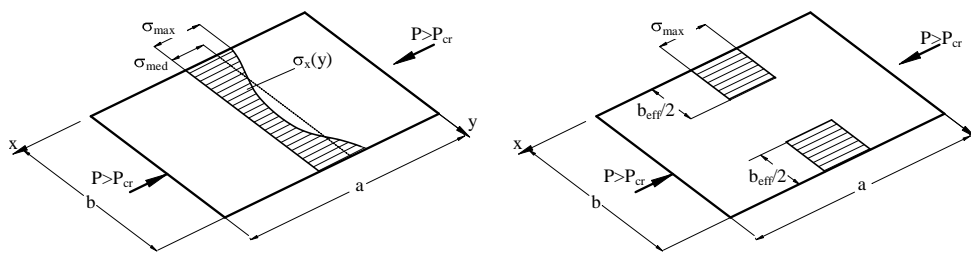


Fig. 2.42 Stress distribution in simply supported plate, uniaxially compressed: (a) actual stress distribution; (b) equivalent stress distribution based on the "effective width" approach

The magnitude of effective width, b_{eff} , changes as the magnitude of σ_{max} change (see Fig 2.43). Therefore the minimum effective width results for σ_{max} equals to f_y (see Fig 2.40c).

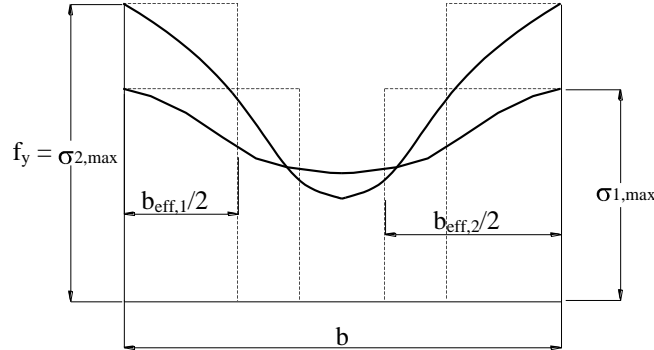


Fig. 2.43 Change of effective width in terms of maximum edge stress

At limit, it may also be considered that the effective width b_{eff} represents a particular width of the plate which just buckles when the maximum compressive stress reaches the yield point of steel. Therefore for a long plate, the theoretical value of b_{eff} may be determined from Eq. (2.11) as follows:

$$\sigma_{cr} = \sigma_{max} = f_y = \frac{k_{\sigma} \cdot \pi^2 \cdot E}{12 \cdot (1 - \nu^2) \cdot (b_{eff} / t)^2} \quad (2.14)$$

$$b_{eff} = \frac{k_{\sigma} \cdot \pi^2}{\sqrt{12 \cdot (1 - \nu^2)}} \cdot t \cdot \sqrt{\frac{E}{f_y}} \quad (2.15)$$

$$b_{eff} = C \cdot t \cdot \sqrt{\frac{E}{f_y}} \quad (2.16)$$

$$C = \sqrt{k_{\sigma} \cdot \pi^2 / 12 \cdot (1 - \nu^2)} \quad (2.17)$$

is a constant for a given type of plate element, depending of the value of buckling coefficient, only

If $k = 4$ and $\nu = 0.3$ are taken, $C=1.9$, and Eq. (2.16) becomes:

$$b_{eff} = 1.9 \cdot t \cdot \sqrt{\frac{E}{f_y}} \quad (2.18)$$

which represents the von Karman formula for design of the stiffened elements derived in 1932.

Since the critical elastic buckling stress of the complete plate is given by eq. (2.19) e.g.

$$\sigma_{cr} = \frac{k_{\sigma} \cdot \pi^2 \cdot E}{12 \cdot (1 - \nu^2) \cdot (b_{eff} / t)^2} \quad (2.19)$$

then by substitution

$$\frac{b_{eff}}{b} = \sqrt{\frac{\sigma_{cr}}{f_y}} \quad (2.20)$$

If the relative or reduced plate slenderness, $\bar{\lambda}_p$, is defined as:

$$\bar{\lambda}_p = \sqrt{\frac{f_y}{\sigma_{cr}}} = \frac{1.052}{\sqrt{k}} \cdot \frac{b}{t} \cdot \sqrt{\frac{f_y}{E}} = \frac{b/t}{28,4 \cdot \varepsilon \cdot \sqrt{k}} \quad (2.21)$$

where: $\varepsilon = \sqrt{235/f_y}$.

If one notes, $\rho = b_{eff}/b$, the ratio between effective width and full width, b , which represents the reduction factor of the plate within the post-buckling range, finally it can be written

$$b_{eff} = \rho \cdot b \quad (2.22)$$

with

$$\rho = \frac{b_{eff}}{b} = \frac{1}{\bar{\lambda}_p} \leq 1 \quad (2.23)$$

Equation (2.22) is in fact another form of the initial formula of von Karman. Formula (2.15) and correspondingly eq. (2.20), gives the effective width in the ultimate post-buckling range (see Fig. 2.40c). In the intermediate post-buckling stage, when $\sigma_{cr} < \sigma_{max} < f_y$, (see Fig. 2.40b) the effective width can be obtained with formula

$$b_{eff} = C \cdot t \cdot \sqrt{\frac{E}{\sigma_{max}}} \quad (2.24)$$

or

$$\frac{b_{eff}}{b} = \sqrt{\frac{\sigma_{cr}}{\sigma_{max}}} \quad (2.25)$$

with the corresponding relative slenderness of the plate

$$\bar{\lambda}_p = \sqrt{\frac{\sigma_{cr}}{\sigma_{max}}} \quad (2.26)$$

The expression (2.17) of C , which leads for simply supported plates (e.g. $k_\sigma=4$ for stiffened elements) to the value 1.9, was confirmed by test only for large b/t ratios. Consequently in 1946 Winter proposed to replace that formula with

$$C = 1.9 \cdot \left[1 - 0.415 \cdot \left(\frac{t}{b} \right) \cdot \sqrt{\frac{E}{f_y}} \right] \quad (2.27)$$

which leads to the well-known actual formula of effective width, e.g.

$$\rho = \frac{b_{eff}}{b} = \sqrt{\frac{\sigma_{cr}}{f_y}} \cdot \left(1 - 0.22 \cdot \sqrt{\frac{\sigma_{cr}}{f_y}} \right) \leq 1 \quad (2.28)$$

or, in terms of relative plate slenderness, $\bar{\lambda}_p$,

$$\rho = \frac{b_{eff}}{b} = \frac{1}{\bar{\lambda}_p} \cdot (1 - 0.22 / \bar{\lambda}_p) \quad (2.29)$$

Effective width depends on both edge stress σ_{max} and b/t ratio. The plate is fully effective when $\rho = 1$, e.g. $b = b_{eff}$, and it is easy to show that it happens when $\bar{\lambda}_p \leq 0.673$ (see Fig. 2.44) or

$$\frac{b}{t} > \left(\frac{b}{t} \right)_{lim} = 16.69 \cdot \varepsilon \cdot \sqrt{k} \quad (2.30)$$

with

$$\varepsilon = \sqrt{235 / f_y} \quad (2.31)$$

If $k_\sigma = 4$ and $k_\sigma = 0.425$ are replaced in eq. (2.30) for simply supported plates – edge stiffened or web type elements, and for the plates with a free longitudinal edge – unstiffened or flange type elements, respectively, it gives:

- web type elements

$$\left(\frac{b}{t} \right)_{lim} = 38.3 \cdot \varepsilon \quad (2.32)$$

- flange type elements

$$\left(\frac{b}{t} \right)_{lim} = 12.5 \cdot \varepsilon \quad (2.33)$$

The effective or equivalent width method is a powerful one, leads to very simple design rules and gives an indication of the behaviour of the plate as ultimate conditions are approached. However, it is difficult to prove the validity of this approach, especially due to approximate nature of the initial assumptions made by von Karman in regard with the two “edge strips” which concentrate the active part of the plate. Therefore, Winter semi-empirically adopted the von Karman formula (i.e. the eq. (2.29)) replaced eq. (2.22) in order to fit better with test results.

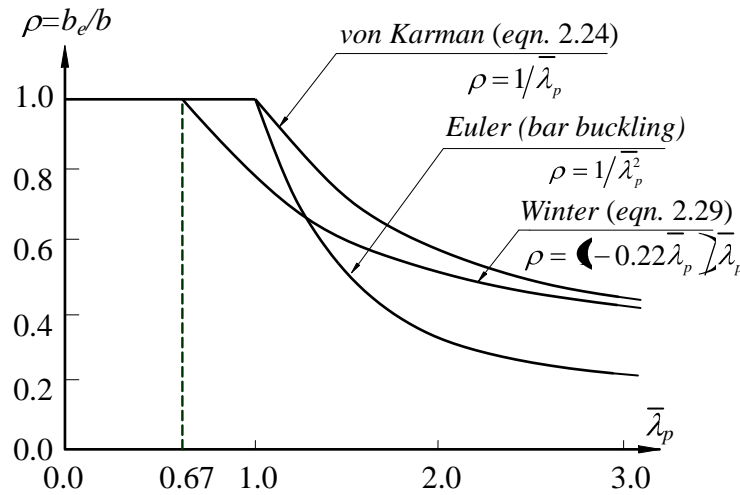


Fig. 2.44 Reduction factor, ρ , vs. relative plate slenderness, $\bar{\lambda}_p$, relationship

The Winter formula (2.29) for the effective width is actually used in all relevant design code provisions thin walled steel structures (EN1993-1-3:2006, AISI-2007, AS/NZS 4600:2005).

Despite of its semi-empirical characteristic this formula leads to quite satisfactory results for 4-sided simply supported plates (web type). However, for 3-sided simply supported plates (flange type), this formula used with a buckling coefficient equal to 0.425 or 0.43 is too conservative both for strength and stiffness, and alternative proposals were made by several authors (von Karman *et al.*[60] Fischer & Zhu, 1996).

2.6.2.2. Direct Strength Method

Schafer & Pekoz (1998) have proposed a new procedure which works only with the gross properties of the cross-section of a member and can take into account the interaction between local and global buckling and also the interaction between distortional and global buckling.

The Direct Strength Method is a new design procedure for cold-formed steel member design. The Direct Strength Method does not use effective width, nor require iteration for determining effective properties, instead the method uses member elastic buckling solutions based on gross properties to determine the member strength in three key limit states: global buckling, local buckling (including interaction with global buckling), and distortional buckling.

Direct Strength Method is an extension of column curves to other models such as local and distortion buckling, developed both for columns and beams, and proposed by Schafer (2001). The method has been adopted in 2004 as Appendix 1 of *North American Specification for the Design of Cold-Formed Steel Structural Members (AISI, 2004)* and in 2005 by the *Australian/New Zealand Standard for Cold-formed steel structures (AS/NZS4600:2005)*.

The key information that the engineer must provide is the elastic buckling loads in global (P_{cre}), local (P_{cr1}), and distortional (P_{crd}) buckling, these, along with the squash load (P_y), provide the strength. The easiest means for finding the elastic

buckling loads is the use of the freely available, open source, software, CUFSM, (www.ce.jhu.edu/bschafer/cufsm, Schafer and Ádány [131]). However, CUFSM is not required for the Direct Strength Method as (1) closed formed solutions are provided for standard shapes in the DSM Design Guide, and (2) other software packages are available that provide the same solution.

On the following only the method for columns is presented.

The nominal axial strength, P_{ne} , for flexural, torsional, or flexural-torsional buckling is:

$$\lambda_c \leq 1.5 \quad P_{ne} = (0.658^{\lambda_c^2}) P_y \quad (2.34a)$$

$$\lambda_c > 1.5 \quad P_{ne} = \left(\frac{0.877}{\lambda_c^2} \right) P_y \quad (2.34b)$$

where

$$\lambda_c = \sqrt{P_y / P_{cre}}$$

$$P_y = A f_y$$

P_{cre} = minimum of the critical elastic column buckling load in flexural, torsional or flexural-torsional buckling

The nominal axial strength, P_{nl} , for *local buckling* is:

$$\lambda_l \leq 0.776 \quad P_{nl} = P_{ne} \quad (2.35a)$$

$$\lambda_l > 0.776 \quad P_{nl} = \left[1 - 0.15 \left(\frac{P_{crl}}{P_{ne}} \right)^{0.4} \right] \left(\frac{P_{crl}}{P_{ne}} \right)^{0.4} P_{ne} \quad (2.35b)$$

$$\text{where } \lambda_l = \sqrt{P_{ne} / P_{crl}}$$

P_{crl} = critical elastic local column buckling load

The nominal axial strength, P_{nd} , for *distortional buckling* is:

$$\lambda_d \leq 0.561 \quad P_{nd} = P_y \quad (2.36a)$$

$$\lambda_d > 0.561 \quad P_{nd} = \left[1 - 0.25 \left(\frac{P_{crd}}{P_y} \right)^{0.6} \right] \left(\frac{P_{crd}}{P_y} \right)^{0.6} P_y \quad (2.36b)$$

$$\text{where } \lambda_d = \sqrt{P_y / P_{crd}}$$

$$P_y = A f_y$$

P_{crd} = critical elastic distortional column buckling load

Because DSM is based on an abstraction of the cross-section type, it is important for the users to be aware of the types of cross-sections which are included in the derivation of a particular DSM. Hence, the concept of pre-qualified sections was introduced. Sections which fall within specific geometric and material limitations can be designed using DSM with the proscribed safety factors. DSM has been extensively developed for cold-formed simple lipped sections

Recent research by Moen and Schafer [122] is focused on extending the use of DSM to perforated thin walled sections.

2.6.2.3. Generalised Beam Theory (GBT)

In the 1990's Generalized Beam Theory (GBT) (theory: Schardt 1989, Davies et al. 1994) has become a useful tool to study distortional buckling of columns (applications: Schardt 1994, Davies and Jiang 1996). Generalized Beam Theory is an extension to conventional engineering beam theory that allows cross-section distortion to be considered. Stability analysis of thin-walled members may also be performed using GBT. In the last decade, the research team of Professor Camotim at IST (Technical University of Lisbon) has devoted a very significant amount of research work to the development, numerical implementation, application and worldwide dissemination of novel GBT formulations that considerably broaden the scope of this theory, by enabling the performance of several additional analyses and covering a wider range of structural systems (Camotim et al. [125] , [126] , [127] , [128] , [129] , [130]). In particular, it is now possible to carry out (i) first-order, buckling, post-buckling, vibration and dynamic analyses of metal and FRP members with open and closed cross-sections, and (ii) first-order, buckling and post-buckling analyses of thin-walled steel frames. Generalized Beam Theory has a user friendly program for use developed at the Technical University of Lisbon called GBTUL (Bebiano et al. [142] , <http://www.civil.ist.utl.pt/gbt/>), that performs elastic buckling (bifurcation) and vibration analyses of prismatic thin-walled members.

Generalised Beam Theory (GBT) may be viewed as either (i) a *bar theory* incorporating cross-section in and out-of-plane deformations or (ii) a *folded plate theory* that includes plate rigid-body motions ([111] , [128]). By decomposing the member deformed configurations or buckling/vibration mode shapes into linear combinations of longitudinally varying cross-section *deformation modes*, GBT provides a general and elegant approach to obtain accurate solutions for several structural problems involving prismatic thin-walled members – moreover, one also obtains the contributions of each deformation mode, a feature enabling a much clearer interpretation of the structural response under consideration.

For example Fig. 2.45 shows the modes obtained for a C section for two different nodal discretizations in a cross-section analysis: (A) no intermediate nodes (apart from the two associated with the two extremities (see Fig. 2.45a), and (B) one intermediate node at each flange and three at the web (see Fig. 2.45b). As the figure shows, (i) although the first 6 modes are fairly similar for both discretizations, for the finer one (*i.e.*, (A)) (ii) modes 7-8 display a better “quality” and (iii) there were obtained 4 additional modes, namely 9-13.

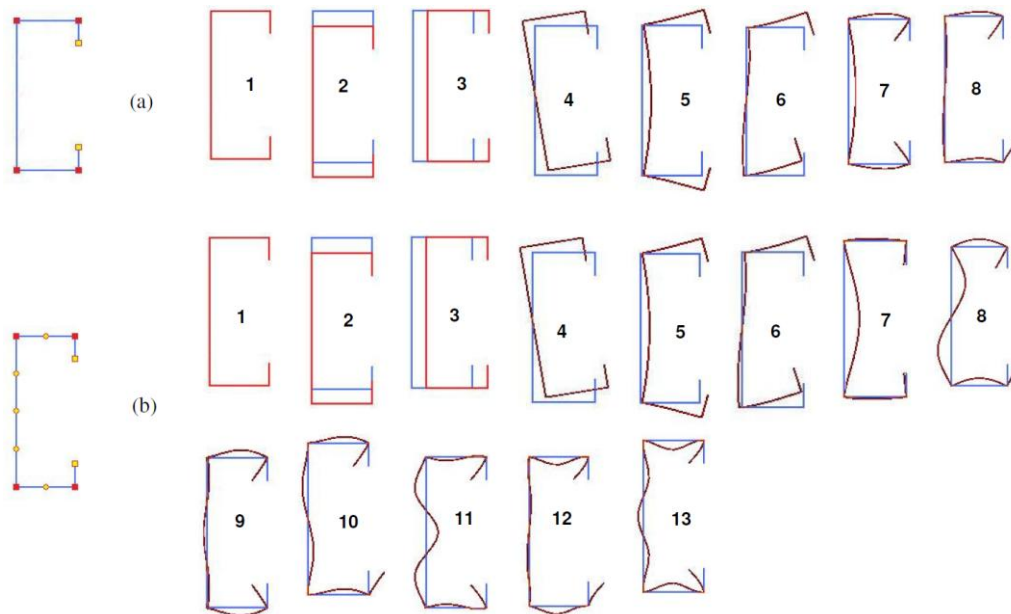


Fig. 2.45 In-plane configurations of C-section deformation modes: (a) discretization no. 1; (b) discretization no. 2 [44]

After performing the cross-section analysis and the ensuing mode selection, buckling/vibration analysis of members using 4 different types of support (boundary) can be done. The 4 support conditions are: (i) simply supported ("S-S"), (ii) clamped-free (or cantilever, "C-F"), (iii) clamped-clamped ("C-C") and (iv) clamped supported ("C-S"). Once problem solution is found, GBTUL 1.0b provides, deformed configurations, corresponding to the member buckling or vibration modes, by both (i) graphical 2D and 3D representations, and (ii) modal participation factors and diagrams.

Fig. 2.46 shows, as an example, the output of GBTUL 1.0b for the case of a lipped channel section in compression [123]. The curves shown in Fig. 2.46(a) provide the variation of the buckling load P_b with the column length L ($L \geq 222$ cm). Fig. 2.46(b) displays the GBT-based column modal participation diagram (for single halfwave buckling), providing the contributions of each GBT deformation mode to the column buckling modes. Finally, Fig. 2.46(c) shows the buckling mode shapes yielded by the GBT analyses for columns with lengths $L = 222, 300, 900$ cm, as well as the in-plane shapes of the 3 deformation modes that participate in them.

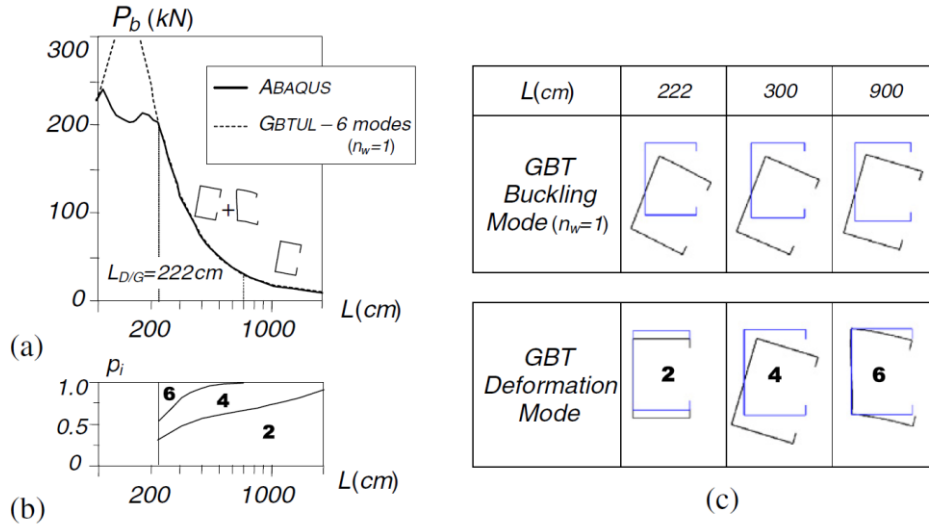


Fig. 2.46 GBT-based column buckling: (a) P_b vs. L curves ($L > 100$ cm), (b) modal participation diagrams and (c) in-plane shapes of 3 buckling and deformation modes

2.6.2.4. Erosion of Critical Bifurcation Load (ECBL) approach

On the basis of Erosion of Critical Bifurcation Load (ECBL) concept [135] a new approach was proposed to evaluate the ultimate strength in local – overall interactive buckling. This approach, really based on the background of coupled instability phenomenon, enables to use the European buckling curve format and to calibrate appropriate buckling curves for any kind of interactive overall-local/sectional buckling mode.

Assuming the two theoretical simple instability modes that couple in a thin-walled compression member, are the Euler bar instability mode, $\bar{N}_E = 1/\bar{\lambda}^2$ (e.g. $\bar{\lambda}$ can be the flexural, $\bar{\lambda}_F$, or flexural-torsional, $\bar{\lambda}_{FT}$, slenderness) and the local instability mode, $\bar{N}_L = A_{eff}/A = Q$ (see Fig. 2.47), then the maximum erosion of critical load, due both, to the imperfections and coupling effect occurs in the coupling point $\bar{\lambda}_C = 1/\sqrt{\bar{N}_L}$.

The interactive buckling load, $\bar{N}(\bar{\lambda}, \bar{N}_L, \psi)$, pass through this point and the corresponding value of ultimate buckling load is $\bar{N}_{erod,E} = (1-\psi)\bar{N}_L$, where ψ is the erosion factor.

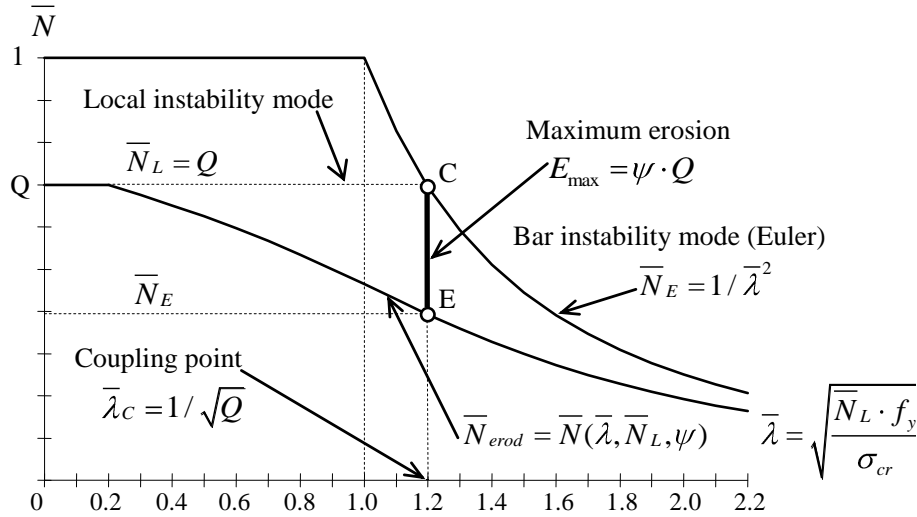


Fig. 2.47 The interactive buckling model based on the ECBL theory

It must be underlined that \bar{N}_L not represents rigorously the theoretical local buckling curve, but it can be assumed, being the lower-section strength as a reference or a practical strength of the cross-section corresponding to the local buckling mode. On the basis of this assumption, it is possible to evaluate the ultimate strength of the stub column. One might call the *coupling point* C, obtained according to this mode, the *practical interaction point*. Similarly, the same approach can be applied for the case where the interaction occurs between the distortional mode, $\bar{N}_D = N_D / N_{pl}$, $N_{pl} = A \cdot f_y$, and overall mode.

To understand better these *engineering* assumptions, one considers the theoretical elastic buckling modes (bifurcation) characterising the instability of a thin-walled member in compression. The local mode could be local buckling (L) or distortional buckling (D), and the relevant value (e.g. of lower critical load will be considered). Similarly, the overall mode will be either flexural (F) or flexural-torsional one (FT).

For instance, in Fig. 2.48, D and FT modes will be assumed in order to identify, qualitatively, the interaction and compare with the actual, elastic-plastic behaviour curve.

Modes (D) and (FT) are interacting into the theoretical coupling point C_{th} , while mode $N=N_{D,cr}$ with (FT) into practical coupling point C_{pr} . Correspondingly to the two coupling points and related to the actual elastic-plastic $N(L)$ curve will be the theoretical, E_{th} , and practical, E_{pr} , erosions.

The use of practical interaction has the advantage to give the possibility to use Ayrton-Perry model and the European buckling curve format in order to obtain interactive buckling curves as it will be shown in the following.

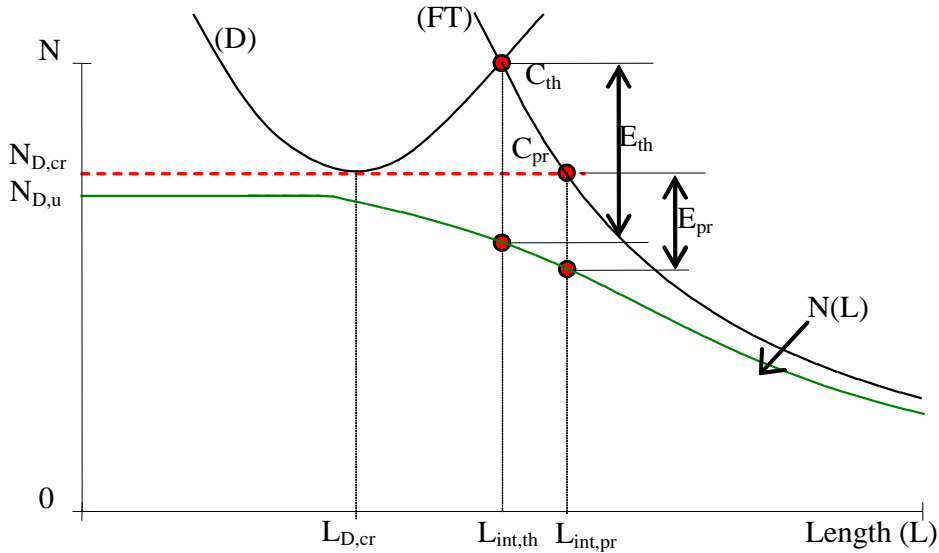


Fig. 2.48 Theoretical and practical interaction of two buckling modes

The Ayrton-Perry equation (2.37) can be written in the form:

$$(1 - \bar{N}) (1 - \bar{N} \bar{\lambda}^2) = \alpha \bar{N} (\bar{\lambda} - 0.2) \tag{2.37}$$

It is easy to show the relation between the imperfection and erosion factor. The *negative sign* solution of eq. (2.37), in the particular point $\bar{\lambda} = 1$ has to be taken equal with $1 - \psi$, because it corresponds to the maximum erosion of the Euler curve when no local buckling occurs (see Fig. 2.49), e.g.

$$\bar{N}(\bar{\lambda} = 1, \alpha) = \frac{1}{2} [2 + 0.8\alpha - \sqrt{(2 + 0.8\alpha)^2 - 4}] = 1 - \psi \tag{2.38}$$

that gives:

$$\alpha = \frac{\psi^2}{0.8(1 - \psi)} \tag{2.39}$$

or

$$\psi = 0.4(\sqrt{5\alpha + \alpha^2} - \alpha) \tag{2.40}$$

In this case the *erosion* can be associated to the plastic-elastic interaction between the *rigid plastic mode* (plastic strength) of stub column and the overall elastic buckling mode of the bar, given by Euler formula.

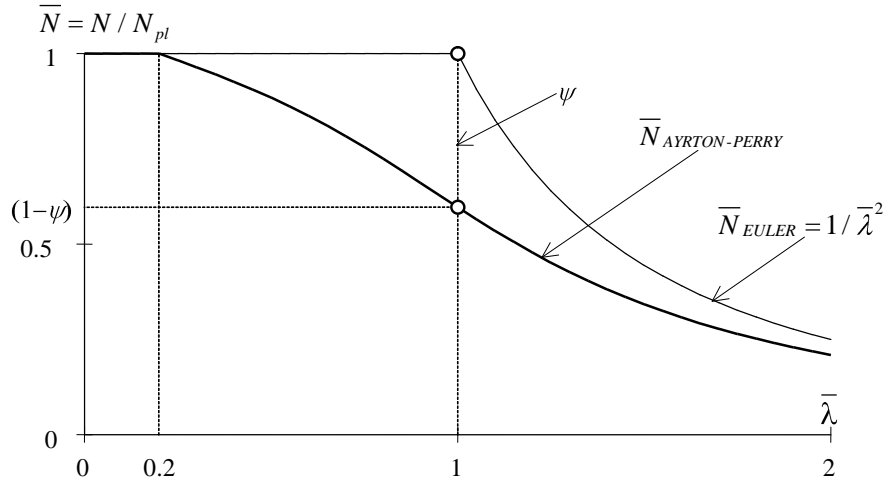


Fig. 2.49 The erosion of bar buckling curve

Fig. 2.50 shows the change of ψ erosion factor depending on α coefficient of imperfection in European buckling curves.

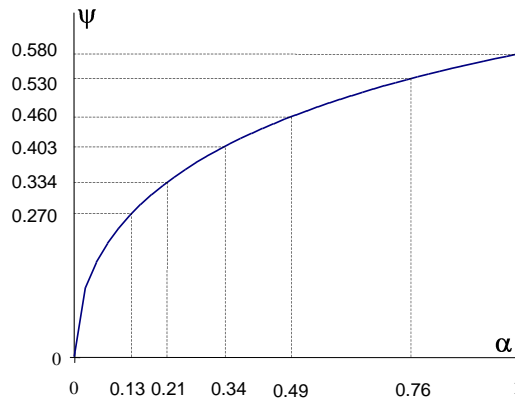


Fig. 2.50 Relation between ψ erosion factor and α coefficient of imperfection

When local buckling occurs prior to bar buckling, then the corresponding solution of eq. $(\bar{N}_L - \bar{N})(1 - \bar{\lambda}^2 \bar{N}) = \alpha(\bar{\lambda} - 0.2)\bar{N}$, in the coupling point, E (see Fig. 2.47) is:

$$\bar{N} = \frac{1 + \alpha(\bar{\lambda} - 0.2) + \bar{N}_L \bar{\lambda}^2}{2\bar{\lambda}^2} - \frac{1}{2\bar{\lambda}^2} \sqrt{[1 + \alpha(\bar{\lambda} - 0.2) + \bar{N}_L \bar{\lambda}^2]^2 - 4\bar{N}_L \bar{\lambda}^2} = (1 - \psi)\bar{N}_L \quad (2.41)$$

which leads to

$$\alpha = \frac{\psi^2}{1 - \psi} \cdot \frac{\sqrt{\bar{N}_L}}{1 - 0.2\sqrt{\bar{N}_L}} \quad (2.42)$$

This represents the new formula of α imperfection coefficient, which should be introduced in European buckling curves in order to adapt these curves to local – overall buckling. Fig. 2.51 (a and b) show the change of α depending on ψ and \bar{N}_L .

When one speaks about the erosion of theoretical buckling curve in the coupling point distinction should be made between the *erosion*, expressed by ψ , which refers to the effect of both imperfections and coupling, and the reduced ultimate strength of member, due to local buckling which is introduced by \bar{N}_L factor. Once more, one notice this approach applies similarly to the case where the sectional mode is distortion instead of local buckling. In fact, since the squash load for the same section is the same, it buckles by local buckling of walls or by distortion, the basic Ayrton-Perry formula, eq. (2.37) does not change.

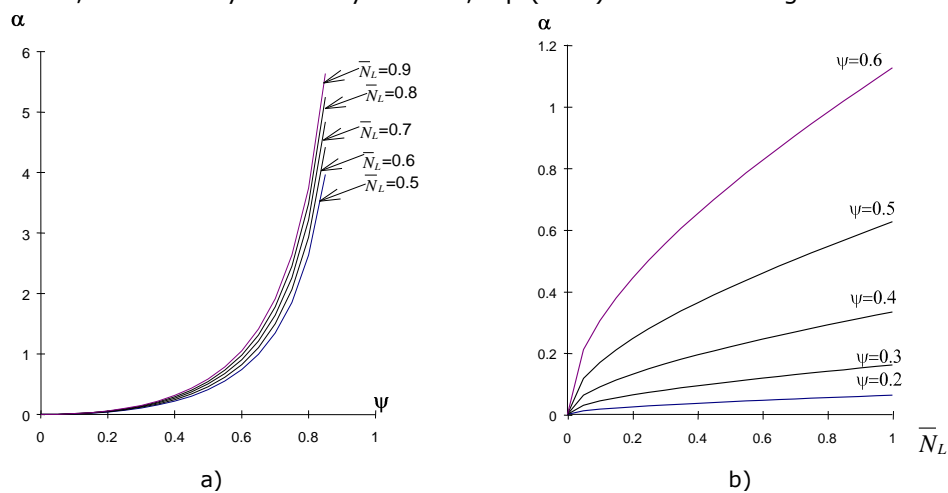


Fig. 2.51 Relation between α , \bar{N}_L and ψ

It appears easier to evaluate experimentally and/or numerically the ψ erosion factors for specific types of cold-formed steel sections and, on this basis, to calibrate relevant α imperfection factors, in order to be implemented in the Eurocode 3 approach. Examples of calibration of α imperfection factor are presented by [134].

An extension of ECBL approach was plastic-elastic interactive model which naturally describes the phenomenon of the interactive buckling of thin-walled members. Ungureanu and Dubina [135] have shown that stub columns form "*local plastic mechanisms*", the stub column fails by forming plastic hinge and/or plastic zone, as effect of the localisation of buckling pattern. Consequently, the local-global interactive buckling is of *plastic-elastic* type, not an *elastic-elastic* one. Fig. 2.52 shows the ECBL approach adapted to plastic-elastic interactive buckling.

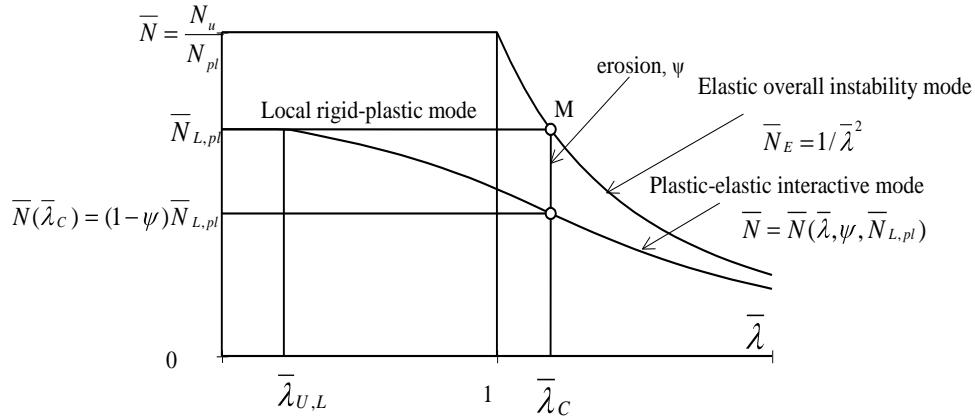


Fig. 2.52 The interactive buckling model based on the ECBL theory

where:

- N_u = ultimate compression strength;
- N_{pl} = $A \times f_y$ full plastic strength of thin-walled cold-formed members;
- $N_{pl,m}$ = the local plastic buckling (mechanism) strength;
- A = the gross area of cross section;
- $\bar{\lambda}$ = relative slenderness in overall buckling;
- $\bar{\lambda}_c$ = relative slenderness in the coupling point.

Following exactly the same way as for the elastic local-overall interactive buckling, the α imperfection factor for the plastic-elastic interactive buckling results:

$$\alpha = \frac{\psi^2}{1-\psi} \cdot \frac{\sqrt{\bar{N}_{L,pl}}}{1-0.2\sqrt{\bar{N}_{L,pl}}} \quad (2.43)$$

where

$$\bar{N}_{L,pl} = \frac{N_{pl,m}}{A \cdot f_y} \quad (2.44)$$

Another important application of ECBL approach was the systematic study of the influence of size and shape of sectional geometrical imperfections on the ultimate buckling strength of plain and lipped channel sections, both in compression and bending [134]. Special attention was paid on the characterisation and codification of imperfections for non-linear FEM simulation. Based on the ECBL approach and using an advanced non-linear inelastic analysis, the erosion of theoretical buckling strength, due to geometrical imperfections, in single and coupled instability modes was evaluated. According to the authors' knowledge, this is the first attempt to identify quantitatively the erosions of theoretical buckling strength due to the imperfections and coupling effect in the interactive buckling.

In Chapter 5 of the thesis the ECBL approach will be adapted for distortional-overall interaction mode, for the case of rack upright sections.

2.7 Design Code Provisions

2.7.1 European Buckling curves: summary review

The theoretical model applied in EN 1993-1-1 for the design approach against buckling of bars in compression is based on the so called *divergence model*, which considers the imperfect pinned bar (see Fig. 2.53) and takes into account for the 2nd order effect of axial force N which, due to the eccentricity represented by the initial imperfection e_0 , generates a bending moment M , and transform the compression problem in a compression – bending one.

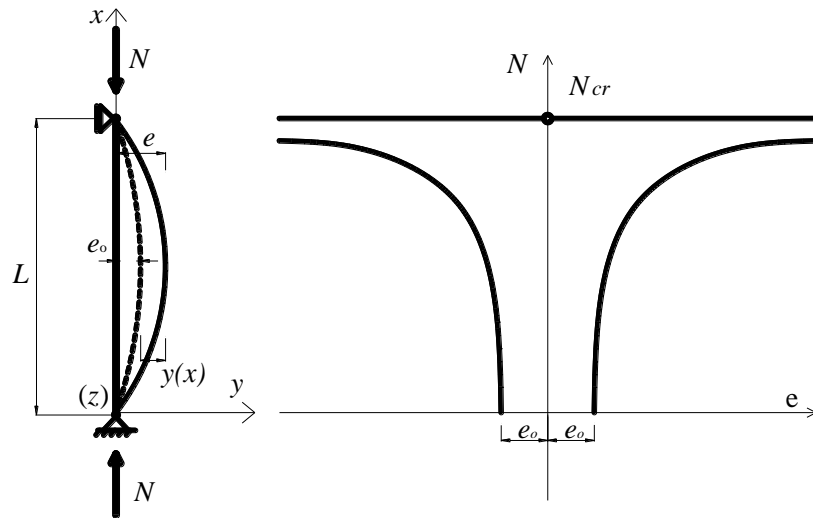


Fig. 2.53 (a) Imperfect bar member in compression; (b) load – deflection path

The critical load is:

$$N_{cr} = \frac{\pi^2 EI}{L^2} \quad (2.45)$$

For other support conditions, the critical load can be obtained following a similar way, considering adequate support conditions. Alternatively, the critical load may be obtained directly from eq. (2.45), replacing the real length L by the buckling length L_{cr} . The buckling length L_{cr} of a member is defined as the length of a fictitious equivalent pinned member with the same critical load. Fig. 2.54 illustrates the buckling lengths for isolated members, for several support conditions, considered as fundamental cases.

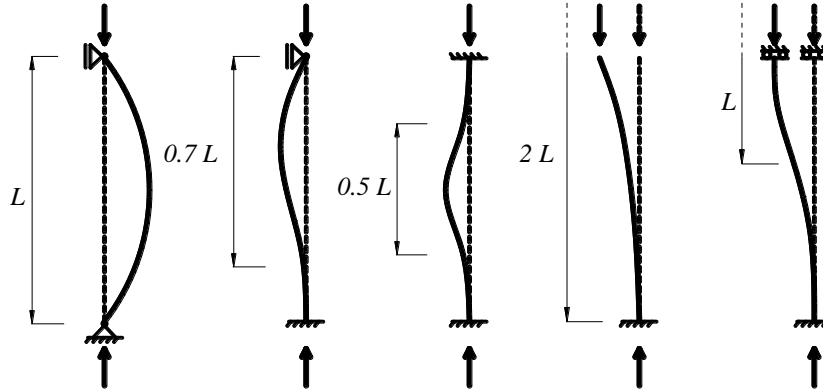


Fig. 2.54 Buckling length L_{cr} as a function of the real length L of the column

To generalize, one can use L_{cr} in the Euler's formula (2.45), and write

$$L_{cr} = \mu L \quad (2.46)$$

where μ is the buckling length multiplier, which takes the values corresponding to the fundamental cases presented in Fig. 2.54, or others.

$$N_{cr} = \frac{\pi^2 EI}{L^2} \quad (2.47)$$

By dividing Euler's critical load by the area of the cross-section (A), the critical stress is obtained:

$$\sigma_{cr} = \frac{\pi^2 EI}{A L_{cr}^2} = \frac{\pi^2 E}{\lambda^2} \quad (2.48)$$

where, $\lambda = L_{cr}/i$ is the slenderness coefficient and $i = \sqrt{I/A}$ is the radius of gyration of the section.

In a member without imperfections, composed of a material with elastic-perfectly plastic behaviour (i.e. mild steel), failure will only occur by buckling in the elastic range if Euler's critical stress is lower than the yield stress f_y . For a short member (with a low slenderness coefficient λ), failure occurs by yielding of the cross-section, when the applied stress equals the yield stress, that is, when $\sigma = N/A = f_y$. The limit between the two types of behaviour is defined by a value of the slenderness coefficient, denoted as λ_1 , given by:

$$\sigma_{cr} = \frac{\pi^2 E}{\lambda_1^2} = f_y \Rightarrow \lambda_1 = \pi \sqrt{\frac{E}{f_y}} \quad (2.49)$$

Based on the slenderness coefficient λ_1 , the non-dimensional slenderness coefficient $\bar{\lambda}$ is defined as:

$$\bar{\lambda} = \frac{\lambda}{\lambda_1} = \pi \sqrt{\frac{A f_y}{N_{cr}}} \quad (2.50)$$

The behaviour of a compressed bar member, without imperfections, for the full slenderness range, is represented in Fig 2.55.

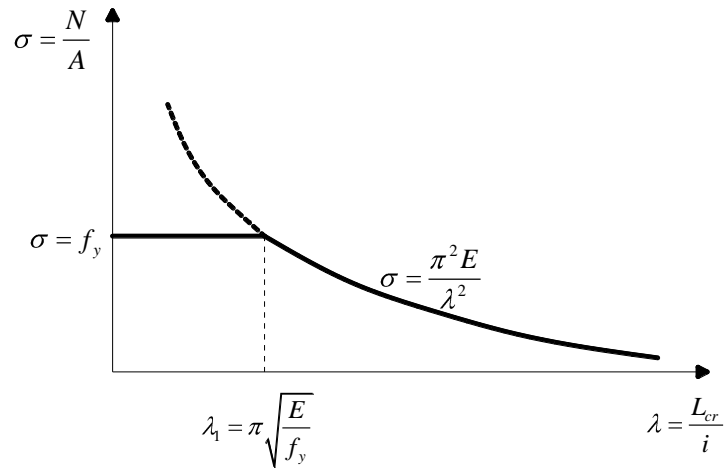
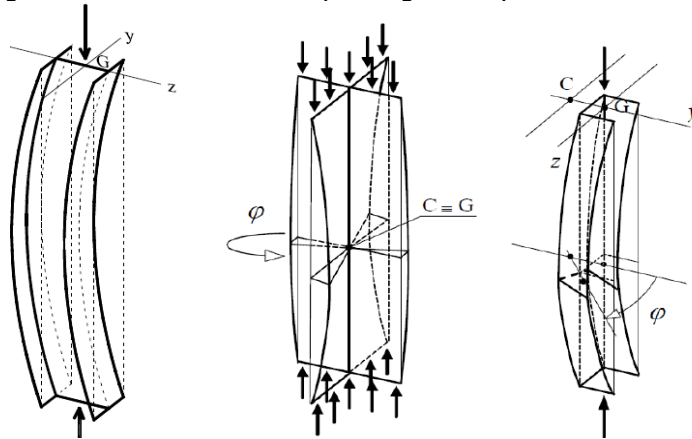


Fig. 2.55 $\sigma - \lambda$ relationship of a compressed member

The solution represented by Euler’s formula (2.47) corresponds to flexural buckling, according to which the instability is caused by deflection (e.g. transverse deformation related to the axis of the bar member). The lowest value of critical load corresponds to the buckling plane characterised by the lowest slenderness of the bar.

However, in case of members in compression of thin-walled open cross-section (and hence low torsional stiffness), not only flexural buckling may occur (see Fig. 2.57a) but also other instability phenomena may, as torsional buckling or flexural-torsional buckling. Torsional buckling is due to the rotation of cross-sections around the axis of the member, as illustrated in Fig. 2.57b; flexural-torsional buckling consists of the simultaneous occurrence of torsional and bending deformations along the axis of the member (see Fig. 2.57c).



(a) flexural buckling (b) torsional buckling (c) flexural-torsional buckling

Fig. 2.56 Torsional buckling and flexural-torsional buckling

The instability modes illustrated in Fig. 2.57 are characteristic of thin-walled open cross-sections, such as channels, angles or cruciform cross-sections. The torsional mode is considered, in general, a theoretical one, mainly important as component of the naturally coupled flexural-torsional buckling mode.

For members of symmetric cross-section with respect to the y axis, the torsional buckling critical load is given by:

$$N_{cr,T} = \frac{1}{i_o^2} \left(GI_t + \frac{\pi^2 EI_w}{L_{cr,T}^2} \right) \quad (2.51)$$

For the same type of cross-sections, the flexural-torsional buckling critical load is given by:

$$N_{cr,TF} = \frac{N_{cr,y}}{2\beta} \left[1 + \frac{N_{cr,T}}{N_{cr,y}} - \sqrt{\left(1 - \frac{N_{cr,T}}{N_{cr,y}}\right)^2 + 4 \left(\frac{y_o}{i_o}\right)^2 \frac{N_{cr,T}}{N_{cr,y}}} \right] \quad (2.52)$$

where,

G is the shear modulus;

I_t is the torsion constant of the gross cross-section;

I_w is the warping constant of the gross cross-section;

i_y is the radius of gyration of the gross cross-section about the $y - y$ axis;

i_z is the radius of gyration of the gross cross-section about the $z - z$ axis;

$L_{cr,T}$ is the buckling length of the member for torsional buckling;

y_o, z_o are the shear centre co-ordinates with respect to the centroid of the gross cross-section.

i_o is the radius of polar gyration given by

$$i_o^2 = i_y^2 + i_z^2 + y_o^2 + z_o^2 \quad (2.53)$$

$N_{cr,y}$ is the critical load for flexural buckling about the $y - y$ axis;

β is a factor given by

$$\beta = 1 - (y_o / i_o)^2 \quad (2.54)$$

In real structures, imperfections are unavoidable and they represent deviations from the theoretical behaviour previously described; under these circumstances, the theoretical critical load, in general, is not reached. Imperfections can be divided into two types: (i) geometrical imperfections (initial bowing, warping, twisting, local deviations characterised by dents and regular undulations in component walls, eccentricity of the loads) and (ii) material imperfections (change of yield strength, residual stresses).

Fig. 2.58 illustrates the results of experimental tests on axially compressed members with several slenderness coefficients $\bar{\lambda}$ and compares them with the theoretical behaviour (ECCS, 1976). It can be observed that for low values of $\bar{\lambda}$, failure occurs essentially by plastification of the section and values of σ / f_y higher than 1.0 are obtained experimentally due to strain-hardening. For slender bars, of high values of $\bar{\lambda}$, failure occurs by buckling in the elastic range, the imperfections not having much influence. For intermediate values of $\bar{\lambda}$, failure occurs by elastic-

plastic instability, and it is in this slenderness domain that imperfections have more influence (the experimental results deviate most from the theoretical curve).

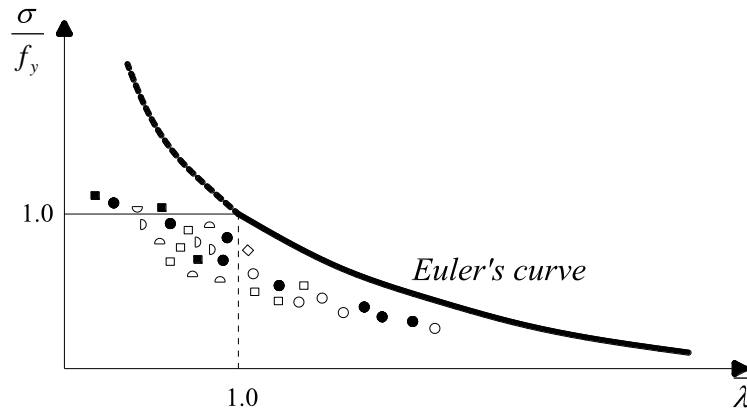


Fig. 2.57 Results of experimental tests in real members

The resistance of compressed members is based on the "European design buckling curves" that relate the ratio $\chi = \sigma / f_y$ with the non-dimensional slenderness $\bar{\lambda}$. These (five) curves (see Fig. 2.59) were the result of an extensive experimental and numerical research programme conducted on hot-rolled and welded sections, that accounted for all imperfections in real compressed members (initial out-of-straightness, eccentricity of the loads, residual stresses).

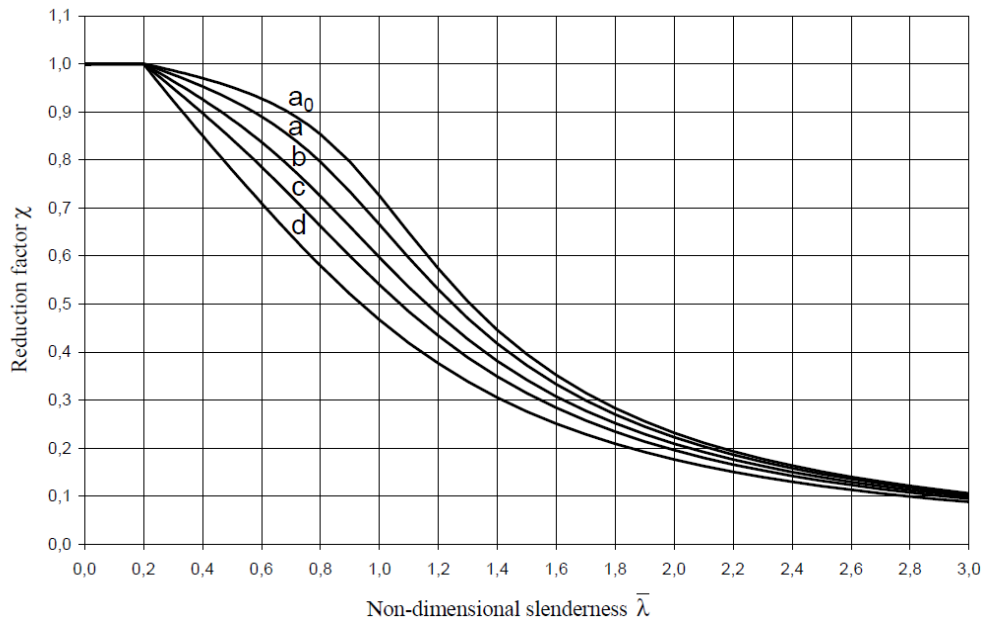


Fig. 2.58 European design buckling curves

The analytical formulation of the buckling curves was derived by Maquoi & Rondal (1978), and is based on the Ayrton-Perry formula, considering an initial sinusoidal deformed configuration corresponding to an "equivalent initial deformed configuration" where the amplitude was calibrated in order to reproduce the effect of all the imperfections.

$$(1 - \chi) \frac{1 - \chi \bar{\lambda}^2}{\bar{\lambda}^2} = \frac{e_o A}{W_{el}} \chi = \eta \chi \quad (2.55)$$

which constitutes the basic form of the Ayrton-Perry equation. η represents the generalized initial imperfection that can be used to estimate the effects on the buckling strength of initial imperfections such as geometrical, material or mechanical. Because the influence of some of these initial imperfections is linked with the length of the member, it has been chosen to express η as follows (Maquoi & Rondal, 1978):

$$\eta = \alpha(\bar{\lambda} - 0.2) \quad (2.56)$$

where the imperfection factor α depends on the shape of the cross-section, buckling plane, etc. and 0.2 defines the length of the plateau along which $\chi = 1.0$. Based on the previous relations, the Ayrton-Perry equation (2.55) can be written in the form:

$$1 - \chi \bar{\lambda}^2 (1 - \chi) = \eta \chi = \alpha \chi (\bar{\lambda} - 0.2) \quad (2.57a)$$

or in terms of normalised or non-dimensional axial force, $\bar{N} = N/N_{pl}$ becomes:

$$(1 - \bar{N}) \frac{1 - \bar{N} \bar{\lambda}^2}{\bar{\lambda}^2} = \alpha \bar{N} (\bar{\lambda} - 0.2) \quad (2.57b)$$

Equation (2.57) is a quadratic equation in χ , from which the minimum solution only is relevant:

$$\chi = \frac{\phi - \sqrt{\phi^2 - \bar{\lambda}^2}}{\bar{\lambda}^2} \quad (2.58)$$

with

$$\phi = 0.5 \left[1 + \alpha(\bar{\lambda} - 0.2) + \bar{\lambda}^2 \right] \quad (2.59)$$

By multiplying the numerator and the denominator of the previous expression by the conjugated term $\phi + \sqrt{\phi^2 - \bar{\lambda}^2}$, the expression from EN19933-1-1 is obtained, which gives the χ factor (reduction factor accounting for the potential of flexural buckling) as a function of the non-dimensional slenderness coefficient $\bar{\lambda}$ and of the imperfection factor:

$$\chi = \frac{1}{\phi + \sqrt{\phi^2 - \bar{\lambda}^2}} \quad (2.60)$$

The European buckling curves, modelled by Eq (2.56) are displayed in Fig. 2.59, together with the corresponding value of α imperfection factors in Table 2.4.

Table 2.4 Imperfection factors for buckling curves

Buckling curve	a_0	a	b	c	d
Imperfection factor α	0.13	0.21	0.34	0.49	0.76

This approach runs for class 1 to 3 cross-sections. For class 4, the case of thin-walled sections, interaction between local or distortional buckling with overall buckling occurs.

2.7.1.1. Class 4 sections: local-global interactive buckling

As shown in EN1993-1-1 the Ayrton-Perry formula, experimentally calibrated for hot-rolled sections, is used for calculation of the buckling strength of columns under compression [26].

To take into account the interaction between local and global buckling in case of thin-walled sections (class 4), the calculation of the load bearing capacity it has to be based upon the effective cross-section, calculated for uniform compression. For practical reason, the same approach was applied in EN1993-1-3 for thin-walled cold-formed sections. In fact, the same buckling curves, based on hot-rolled section tests are used for cold-formed sections too, even in this case are different due to different fabrication technology, the nature and influence of imperfections.

A member is subjected to concentric compression if the line of action goes through the neutral axis of the effective cross-section. If this line does not coincide with the centroidal axis of its gross cross-section, bending moments corresponding to the shift of the centroidal axes (see Fig. 2.60) should be taken into account.

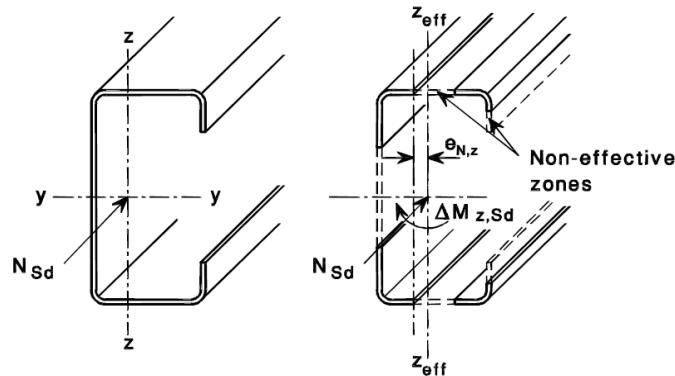


Fig. 2.59 Shift of neutral axis due to effective cross-section

To take into account for the effect of local buckling in eq. (2.57) will be simple to introduce:

$$N = A_{eff} f_y \quad (2.61)$$

where A_{eff} is the effective area of cross-section, calculated using the effective width approach.

If consider $A_{eff} = QA$, where A is the area of gross cross-section and Q is the reducing factor of gross cross-section calculated on the basis of effective width principle, the *effective* or *reduced* cross-section plastic strength can be written as:

$$N = A_{eff} f_y = Q A f_y \quad (2.62)$$

and, as a consequence, equation (2.57b) becomes:

$$(Q - \bar{N})(1 - \bar{\lambda}^2 \bar{N}) = \alpha(\bar{\lambda} - 0.2)\bar{N} \quad (2.63)$$

with

$$\bar{\lambda} = \sqrt{\frac{A_{eff} f_y}{N_{cr}}} = \frac{\lambda}{\lambda_1} \sqrt{Q} \quad (2.64)$$

Equation (2.64) represents the Ayrton-Perry formula for *Local-Overall Interactive Buckling*.

There are also other approaches to apply for interactive buckling of thin-walled members which, in some way, are replicating better the nature of interactive phenomenon. Two of these approaches are summarised on the following.

2.7.1.2. Design according to EN1993-1-3

The effects of distortional buckling should be allowed for in cases such as those indicated in Fig. 2.61(a), (b) and (c). In these cases the effects of distortional buckling should be determined using numerical methods or column stub tests.

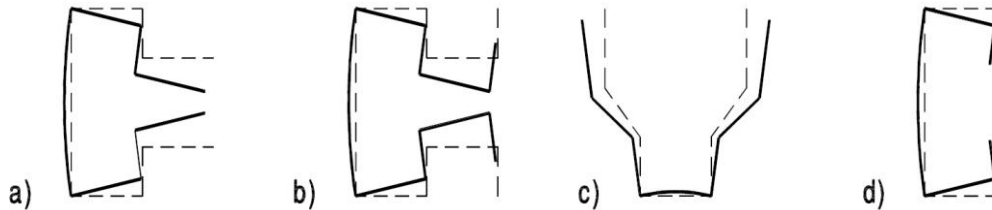


Fig. 2.60 Examples of distortional buckling modes

The distortional buckling for elements with edge or intermediate stiffeners as indicated in Fig. 2.61(d) is treated in Section 5.5.3 of EN1993-1-3 for Plane elements with edge or intermediate stiffeners. The design of compression elements with edge or intermediate stiffeners shall be based on the assumption that the stiffener behaves as a compression member with continuous partial restraint, with a spring stiffness that depends on the boundary conditions and the flexural stiffness of the adjacent plane elements.

When a numerical method is used to calculate the elastic buckling stress the following procedure may be used:

1) For the wavelength up to the actual member length, calculate the elastic buckling stress and identify the corresponding buckling modes, see Fig. 2.62a.

2) Calculate the effective width(s) according to 5.5.2 of EN1993-1-3 for locally buckled cross-section parts based on the minimum local buckling stress, see Fig. 2.62b.

3) Calculate the reduced thickness of edge and intermediate stiffeners or other cross-section parts undergoing distortional buckling based on the minimum distortional buckling stress, see Fig. 2.62b.

4) Calculate overall buckling resistance (flexural, torsional or lateral-torsional buckling depending on buckling mode) for actual member length and based on the effective cross-section from 2) and 3).

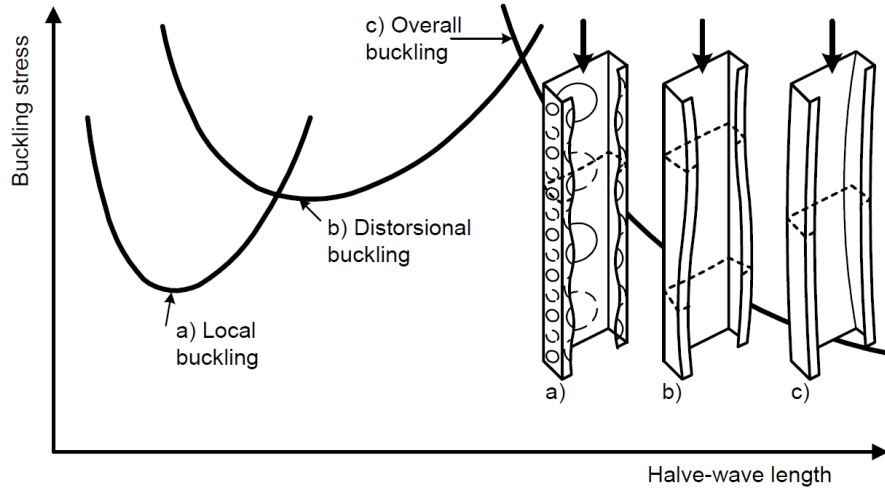


Fig. 2.61a Examples of elastic critical stress for various buckling modes as function of half-wave length and examples of buckling modes

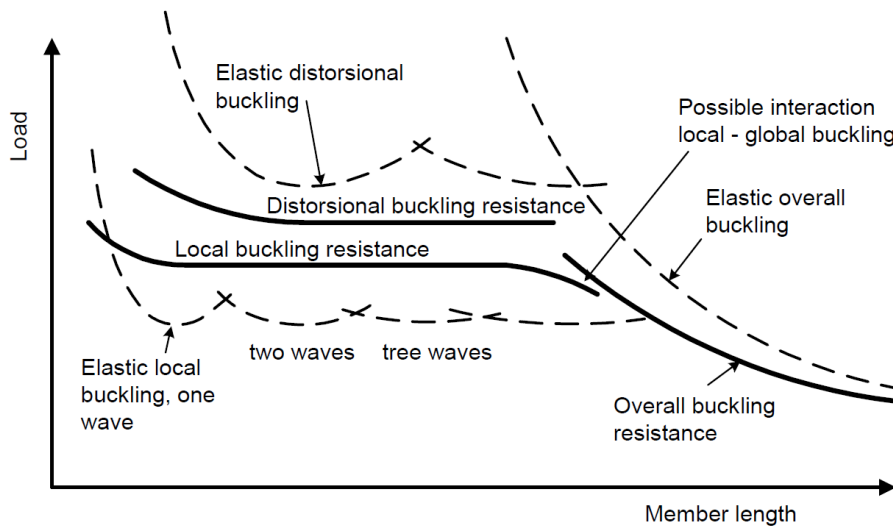


Fig. 2.62b Examples of elastic buckling load and buckling resistance as a function of member length

The provisions in EN1993-1-1 (paragraph 6.3.1 of the code) for buckling resistance of uniform members with cross-sections of Class 4 in compression have to be combined with the relevant provisions of EN1993-1-3 (paragraph 6.2.1 of the code).

A member in compression should be verified against buckling using the following equation:

$$\frac{N_{Ed}}{N_{b,Rd}} \leq 1 \quad (2.65)$$

where

N_{Ed} is the design value of the compression force;

$N_{b,Rd}$ is the design buckling resistance of the compression member.

The design buckling resistance of a compression member with Class 4 cross-section should be taken as:

$$N_{b,Rd} = \frac{\chi A_{eff} f_y}{\gamma_{M1}} \quad (2.66)$$

where χ is the reduction factor for the relevant buckling mode.

For members with non-symmetric class 4 sections, the additional moment ΔM_{Ed} should be taken into account due to the eccentricity of the centroidal axis of the effective section, as shown in Fig. 2.60.

For axial compression in members the value of χ for the appropriate non-dimensional slenderness $\bar{\lambda}$ should be determined from the relevant buckling curve according to:

$$\chi = \frac{1}{\phi + \sqrt{\phi^2 - \bar{\lambda}^2}}, \text{ but } \chi \leq 1 \quad (2.67)$$

where $\phi = 0.5 \left[1 + \alpha \bar{\lambda} - 0.2 + \bar{\lambda}^2 \right]$ and $\bar{\lambda} = \sqrt{\frac{A_{eff} f_y}{N_{cr}}}$ for class 4 cross-

sections.

α is an imperfection factor;

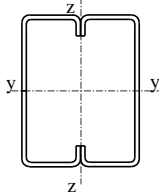
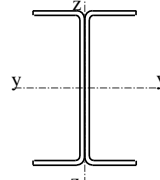
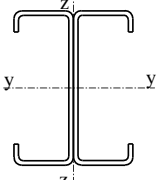
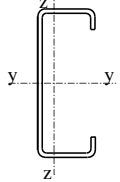
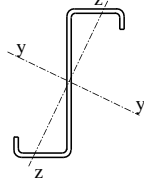
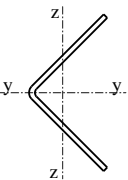
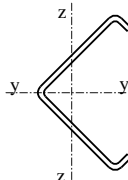
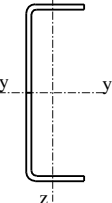
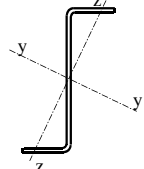
N_{cr} is the elastic critical force for the relevant buckling mode based on the gross cross-sectional properties.

The imperfection factor α corresponding to the appropriate buckling curve should be obtained from Table 2.4 and Table 2.5.

For slenderness $\bar{\lambda} \leq 0.2$ or for $N_{Ed} / N_{cr} \leq 0.04$, the buckling effects may be ignored and only cross-sectional checks apply.

The design buckling resistance $N_{b,Rd}$ for flexural buckling should be obtained from EN 1993-1-1 using the appropriate buckling curve according to the type of cross-section, axis of buckling and yield strength used. For flexural buckling the appropriate buckling curve should be obtained from Table 2.5. The buckling curve for a cross-section not included in Table 2.5 may be obtained by analogy.

Table 2.5 Appropriate buckling curve for various types of cross-section

Type of cross-section	Buckling about axis	Buckling curve
	if f_{yb} is used	any
	if f_{ya} is used ^{*)}	any
	y - y	a
	z - z	b
	any	b
	any	b
	any	c
	any	c
	any	c
	or other cross-section	

^{*)} The average yield strength f_{ya} should not be used unless $A_{eff} = A_g$

The appropriate non-dimensional slenderness $\bar{\lambda}$ could be written as:

$$\bar{\lambda} = \sqrt{\frac{A_{eff} f_y}{N_{cr}}} = \frac{L_{cr}}{i} \sqrt{\frac{A_{eff}}{A}} \quad \lambda_1 = \pi \sqrt{\frac{E}{f_y}} \quad (2.68)$$

where

L_{cr} is the buckling length in the buckling plane considered;

i is the radius of gyration about the relevant axis, determined using the properties of the gross cross-section;

For members with point-symmetric open cross-sections (e.g Z-purlin with equal flanges), account should be taken of the possibility that the resistance of the member to torsional buckling might be less than its resistance to flexural buckling.

For members with mono-symmetric open cross-sections, as shown Fig. 2.63, account should be taken of the possibility that the resistance of the member to torsional-flexural buckling might be less than its resistance to flexural buckling.

For members with non-symmetric open cross-sections, account should be taken of the possibility that the resistance of the member to either torsional or torsional-flexural buckling might be less than its resistance to flexural buckling.

The design buckling resistance $N_{b,Rd}$ for torsional or torsional-flexural buckling should be obtained using eq. (2.66) and the relevant buckling curve for buckling about the $z-z$ axis obtained from Table 2.5.

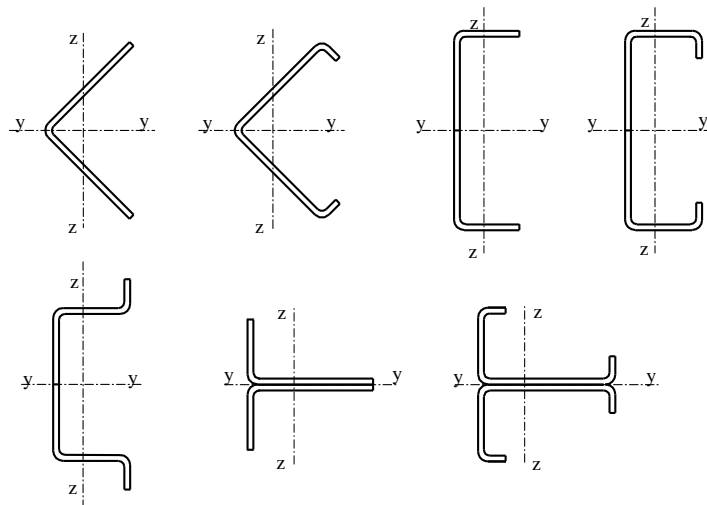


Fig. 2.63 Mono-symmetric cross-sections susceptible to torsional-flexural buckling

The buckling length l_T for torsional or torsional-flexural buckling should be determined taking into account the degree of torsional and warping restraint at each end of the system length L_T .

2.7.2 Design according to EN 15512: „Steel static storage systems - Adjustable pallet racking systems - Principles for structural design“

In Europe, the design code EN15512 replaced in 2009 the FEM 10.2.02 code of practice for the design of steel static pallet racking. In USA the Rack Manufacturing Institute released in 2008 a revision of MH16.1 design code, 2004 edition. In Australia, the AS4048 standard from 1993 is in use.

On the following are summarized the design provisions of the European design code, EN15512, for the storage systems uprights. The European design code is based on experimental testing. In the case of compression members the effects of perforations is taken into account by relevant test methods. The effect of perforation on the thin-walled section behaviour is very difficult to be accounted using an analytical approach.

Compression members of open cross-section are subject to three buckling modes, which are, in order of wavelength (see EN 1993-1-3):

- local buckling;
- distortional buckling;
- lateral torsional buckling.

When calculating the load bearing capacity and stiffness, the effect of local buckling shall be taken into account by using the effective cross-sectional properties calculated on the basis of the effective width of individual elements in compression. Effective section properties are used in strength calculations and shall be calculated for non-perforated members in accordance with EN 1993-1-3 or determined by stub column tests according to A.2.1 of EN15512.

Compression elements with perforations shall be designed on the basis of tests (see A.2.1, A.2.2, A.2.3 of EN15512 – presented in details in Chapter 3 of the thesis). Compression elements without perforations may be assumed to be fully effective if the width to thickness ratio complies to the following limits:

- element supported on two longitudinal edges;

$$\frac{b_p}{t} \leq 1.28 \sqrt{\frac{E}{f_y}} \quad (2.69)a$$

- element with only one edge supported;

$$\frac{b_p}{t} \leq 0.42 \sqrt{\frac{E}{f_y}} \quad (2.69)b$$

The stub test is used to observe the influence of perforations and local buckling on the compressive strength of a short column. This test cannot be used to observe the influence of distortional buckling. The test procedure will be further discussed in Chapter 3.

For members of intermediate effective length, as are generally encountered in the upright frames of typical pallet racks, the distortional mode is likely to be the most critical.

If the upright is perforated, its performance with respect to distortional buckling shall be determined by test. If the upright is not perforated, two cases shall be considered:

Case 1: The distortion mode is controlled by simple lips. For sections of the type shown in Fig. 2.64, which generally have four folds, the procedures given in EN 1993-1-3 for the design of edge stiffeners shall be deemed to include the distortional mode as well as the local buckling mode.

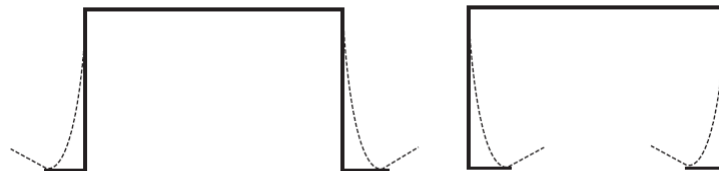


Fig. 2.64 Distortional mode controlled by simple lips

Case 2: General case of the distortional mode. For sections typified by Fig. 2.65 which generally have more than four folds and where the distortional mode is not controlled by simple lips, the strength with regard to the distortional mode shall be determined by rational analysis which includes for member imperfections or by testing according to A.2.2 of EN15512.

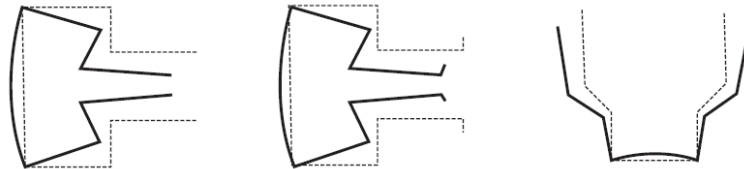


Fig. 2.65 Distortional mode not controlled by simple lips

Distortional buckling is extremely sensitive to the end conditions (fixed or simply supported with respect to the distortional mode) and care should be taken to ensure that the boundary conditions in either analysis or testing correspond to those in the prototype member. The wavelength for distortional buckling is significantly longer than that for local buckling. This means that distortional buckling is not usually identified by a conventional stub-column test. Furthermore, if a stub-column test exhibits a distortional failure mode, it is unlikely that the length is sufficient to determine the minimum distortional buckling load.

The design procedure for perforated compression members shall take proper account of the presence of regular arrays of holes or slots. Three alternative procedures are available.

- Design by testing according to the specifications of the annexes A.2.1 and A.2.3 of the design code EN15512 (presented in details in Chapter 3 of the thesis);
- A fully theoretical procedure which takes rational account of the perforations (e.g. by using finite elements) together with local, global and distortional buckling and imperfections. The way imperfections are taken into account shall be validated by test. It is implicit that the design of continuously perforated members requires testing; however, this is not intended to restrict the development of analytical procedures (e.g. using finite elements) for predicting the performance of members containing regular arrays of holes or slots. Where rational analysis can be shown to be sufficient, it may be used as an alternative to the use of the relevant test procedures;
- A calculation procedure, which is based on the use of the experimentally-determined effective area, A_{eff} , modified for distortional buckling as follows:
 1. A distortional buckling test shall be carried out according to annex A.2.2 of EN15512 on a column length equal to the length of the single bracing panel closest to one meter to give a design strength value $N_{db,Rd}$. Where a frame has a variable panel length then each panel length per upright combination shall be checked. The number of tests may be minimized by the use of finite element analysis. The test results shall be used to validate the finite element model. The test procedure will be further discussed in Chapter 3 of the thesis.
 2. The design strength, $N_{b,Rd}$, at this column length, in the absence of distortional buckling, shall be calculated using the effective area and

the nominal values of yield stress and thickness and taking account of flexural and flexural-torsional buckling. The flexural buckling lengths shall be equal to the distance between the centres of support of the member and the torsional buckling length shall be half the length of cold-formed section in the sample.

3. The ratio $\varepsilon = N_{db,Rd}/N_{b,Rd}$ is then determined. If $\varepsilon \geq 1,0$ no adjustment to the effective area shall be made.
4. If $\varepsilon < 1,0$ the value of A_{eff} shall be reduced to a new value at which the calculated value of $N_{b,Rd}$ is equal to the value obtained from the distortional buckling test, $N_{bd,Rd}$ and $\varepsilon = 1$. This new value of A_{eff} shall be used in all subsequent calculations.

Annexes A.2.1, A.2.2, A.2.3 of EN15512 present the design of elements with perforations in compression on the basis of tests. Annex A.2.1 is devoted to stub column compression tests. The test shall be used to observe the influence of such factors as perforations and local buckling on the compressive strength of a short column. This test shall not be used to observe the influence of distortional buckling.

The test specimen shall be prepared as follows and as shown in Fig. 2.66 (details are presented in Chapter 3 of the thesis).

a) Its length shall be greater than three times the greatest flat width of the section (ignoring intermediate stiffeners). It shall include at least five pitches of the perforations.

b) It shall be cut normal to the longitudinal axis, midway between two sets of perforations.

c) The base and cap plates shall be bolted or welded to each end of the stub upright.

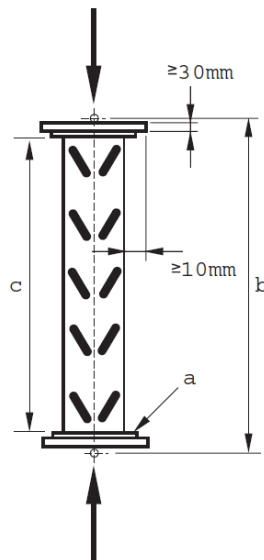


Fig. 2.66 Stub column test arrangement

Annex A.2.2 is focusing on compression tests on uprights, to check for the effects of distortional buckling. The purpose of the test is to determine the influence

of the distortional buckling mode on the axial load capacity of the upright section. The test arrangements have to be similar to those of stub column compression tests. Details are presented in Chapter 3 of the thesis.

Annex A.2.3 presents the compression tests on uprights, to determine the buckling curves. The purpose of this test is to determine the axial load capacity of the upright section for a range of effective lengths in the down-aisle direction, taking account of all buckling effects and the restraint provided by the bracing, its spacing between nodes and its connection to the uprights.

The test arrangement comprises a frame assembly using the maximum frame width specified for the product, in which one of the two uprights is loaded axially, as shown in Fig. 2.67. The bracing pattern, the bracing sections and the bracing connections shall be the components used in the application specific to the buckling curves. The loaded upright shall be loaded through ball bearings and fitted with base and cap plates as described in Annex A.2.1.

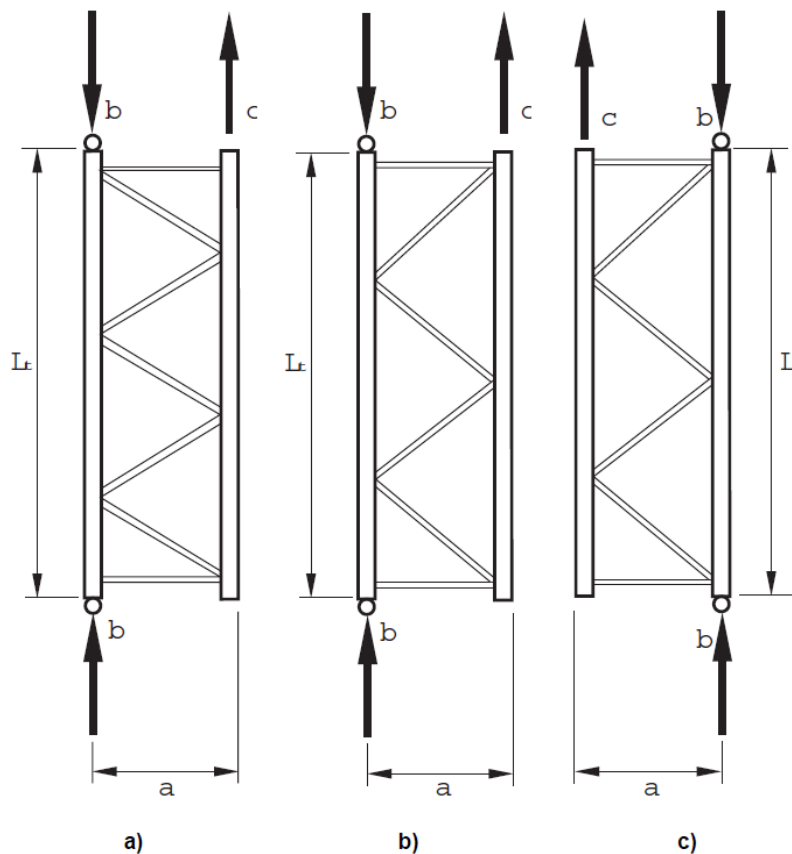
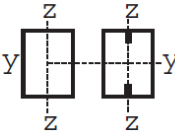
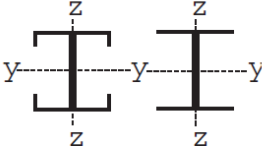
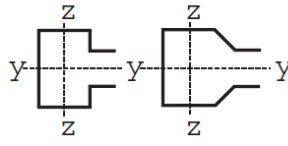
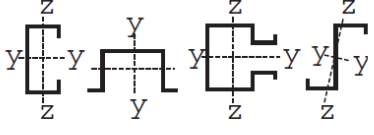
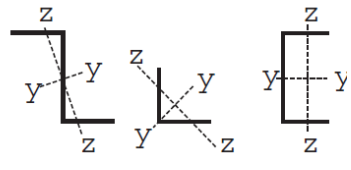


Fig. 2.67 Alternative arrangements for compressive tests on uprights

The overall buckling i.e. flexural must be also considered. Four buckling curves, (i.e. relationships between design stress and slenderness) are available, depending on the type of cross-section and the plane of buckling. The buckling curves are each associated with a value of the imperfection factor α similar to those

presented in EN1993-1-3 and Fig. 2.59 and Table 2.4. The appropriate buckling curve for a particular section shall be determined from Table 2.6.

Table 2.6 Imperfection factor α for different types of cold-formed section

Type of cross-section		Buckling about	
		y - y	z - z
	if f_{yb} is used	$\alpha = 0,34$	$\alpha = 0,34$
	if f_{ya} is used	$\alpha = 0,49$	$\alpha = 0,49$
		$\alpha = 0,21$	$\alpha = 0,34$
		$\alpha = 0,34$	$\alpha = 0,34$
		$\alpha = 0,34$	$\alpha = 0,34$
		$\alpha = 0,49$	$\alpha = 0,49$
<p>NOTE For other types of section not shown above, α may be chosen to correspond to the nearest similar section.</p>			

The buckling length for a given member which is an element of a system shall be determined as the length of a column of the same cross-section and with both ends pinned which has the same Euler critical load as the system under consideration.

If the axial forces and bending moment in the plane of buckling of a member have been determined on the basis of a second-order analysis, they are already enhanced by second-order effects and the buckling length may be

considered as equal to the system length. When second-order global analysis is used, it is permissible to use in-plane buckling lengths for the non-sway mode for member design.

Additional provisions are given for the design strength with respect to torsional and flexural-torsional buckling. The sections geometric properties are calculated for gross section area. The buckling length for torsional and flexural-torsional buckling is dependent on the bracing system. Difference is made between the bracing system connections with large restraint and partial restraint.

2.8 Concluding remarks

Significant research progresses were achieved starting with 1990 in the research field of distortional buckling. Identification and characterisation of distortional buckling is a challenging task, since this buckling mode is not a common failure mode for hot-rolled profiles, characterizing the failure of stiffened singly symmetric cold formed sections.

Starting with 2000 versions of American, Australian and European design code for cold formed sections, the distortional buckling became a specific matter for design checking; on this purpose, adequate calculation procedures have been provided.

Important progresses were also made in the identification of interactive modes and qualitative evaluation of corresponding erosion of theoretical bifurcation load.

Extensive imperfection sensitivity studies were conducted by numerous researchers and several codifications were proposed for computational analysis.

Following the new progresses in understanding the simple and interactive instabilities, new calculation methods were developed, based partially or entirely on numerical tools e.g. GBT, DSM.

The development of ECBL approach as a practical tool, permit the evaluation of the maximum erosion of theoretical bifurcation load, and, on this basis, allow to calibrate the α imperfection factor to adapt the European buckling curves for the interactive buckling modes.

Despite the significant progress in the research field of thin walled sections, with impact in the general design procedures of cold formed steel structures, the technical regulations for design of pallet rack systems and their members still remain at the level of empirical procedures, using almost exclusively the design assisted by testing.

Based on these observations, the objective of this thesis, to provide a design procedure for stability checking of upright members in compression based on the model of EN1993-1-1 approach, seems to be fully justified.

3 EXPERIMENTAL PROGRAM

3.1 Introduction

Racking systems are load bearing structures for the storage and retrieval of goods in warehouses. The goods to be stored are generally on pallets or in box-containers. Racking is constructed from steel components including upright frames, beams and decking. Special beam to column (upright) connections and bracing systems are utilised, in order to achieve a three dimensional steel 'sway' or 'braced' structure with "aisles" to enable order pickers, industrial trucks or stacker cranes to reach the storage positions. Although components are standardised, they are only standard to each manufacturer.

These components differ from traditional column and beam structures in the following regard:

- 1) Continuous perforated columns (uprights).
- 2) Hook-in connections.
- 3) Structural components for racking generally consist of cold formed thin gauge members.

Because of the differences in shape of structural components, detailing and connection types, additional technical information to the Eurocodes are required.

The European Standard, EN15512:2009 [13] specifies the structural design requirements applicable to all types of adjustable beam pallet rack systems fabricated from steel members, intended for the storage of unit loads and subject to predominantly static loads. It gives guidelines for the design of clad rack buildings where requirements are not covered in EN1993.

Pallet racks are standard products for which design by calculation alone aren't enough to characterize the behaviour and capacity of structural members. Test procedures are therefore specified where current analytical methods are not given, or are not appropriate.

The experimental program was developed following the guidelines of Annex A of the EN15512:2009, the European pallet rack design code. The main objective of the experimental program was to observe and characterize the behaviour of pallet rack members in compression. It comprises tests on stub columns specimens and distortional buckling tests of uprights with the length equal with the distance between two subsequent nodes.

The purpose of stub column testing is to observe the influence of such factors as perforations and local buckling on the compressive strength of a short column. This test shall not be used to observe the influence of distortional buckling. It is known that the wavelength for distortional buckling is longer than that for local buckling, meaning that distortional buckling is not usually identified by a conventional stub-column test. Furthermore, if a stub-column test exhibits a distortional failure mode, it is unlikely that the length is sufficient to determine the minimum distortional buckling load.

The purpose of upright testing is to determine the influence of the distortional buckling mode on the axial load capacity of the upright section. The test result provides a means of correcting the theoretically determined axial load capacity. If significant twisting is observed at the ends of the specimen, the ends

should be restrained in order to resist this twisting; this restraint should not offer any additional resistance to distortion of the section.

In order to determine the capacity of a perforated rack section, the European standard [13] requests only tests on stub perforated columns, to determine the effects of local buckling and test on uprights to check the effects of distortional buckling on perforated upright members of length equal with the distance between two subsequent nodes. However, depending on the cross-section dimensions, the distance between two subsequent nodes is often larger than distortional critical buckling length; in such cases the test results correspond rather to the distortional–global interaction, than to pure distortion. A recent study done by Casafont et al. [173] concludes that, for certain rack upright sections, the sectional and global instabilities couples for the range of member lengths used in practice.

None of the tests specified by the norm can characterize the behaviour of the upright sections with respect to pure distortional buckling. For the consistency of testing with the target phenomenon, lengths corresponding to distortional critical buckling length are necessary to be studied. Consequently, the experimental program carried-out within the framework of present thesis, was completed with a series of tests on specimens having the length equal with the half-wave length of distortional buckling, further referred to as “DISTORTIONAL specimens” and a series of tests on specimens having the length in the interactive buckling range, further referred to as “INTERACTIVE specimens”.

In accordance with EN15512:2009 guide lines, the experimental program include tests on two cold formed sections, i.e. RS125x3.2 and RS95x2.6, with and without perforations. The design code requests tests on perforated sections only to determine the effects of local buckling and perforations on axial load capacity of short columns. Also, tests on perforated uprights are requested to determine the influence of the distortional buckling mode on the axial load capacity of the upright section. In order to evaluate the influence of perforations alone, the experimental program was extended to cover sections without perforations as well.

The following abbreviations will be further used to refer specific experimental specimens:

Table 3.1 Specimen codification for considered sections

Section type	RS125x3.2	RS125x3.2	RS125x3.2	RS125x3.2
Test type	Brut Section	Brut Section	Brut Section	Brut Section
STUB				
column test	ST-125B	ST-125N	ST-95B	ST-95B
DISTORTIONAL buckling tests	DIST-125B	DIST-125N	DIST-95B	DIST-95N
UPRIGHT tests	UP-125B	UP-125N	UP-95B	UP-95N
INTERACTIVE buckling tests	INT-125B	INT-125N	INT-95B	INT-95N

As mentioned before, pallet rack upright sections are prone to sectional buckling, local and/or distortional. Theoretically, buckling is caused by a bifurcation in the solution to the equations of static equilibrium. At a certain stage, under an increasing load, further load is able to be sustained in one of two states of equilibrium: an undeformed state or laterally deformed state.

In practice, it is impossible to obtain a column that is perfectly straight, homogeneous and free from initial stress, hence a mathematical approach has little practical application. The main factors that cause deviations from the behaviour of an ideal column, in case of cold formed profiles, are geometrical imperfections. In order to evaluate their influence on the compressive strength of upright sections, the geometric deviations were measured for each tested specimen.

Besides the sectional buckling, local or distortional, as consequence of wall slenderness and sectional shape it is well known that for cold formed profiles, the mechanical properties of base material suffer a series of changes that influences the section's capacity. Mainly, these changes regard the increase of yield and ultimate limit stress with the decrease of the ductility and co-occurrence of significant residual stresses.

In order to take into account these parameters, a supplementary set of tests was conducted to determine:

- yield strength and ultimate strength of base material
- yield strength and ultimate strength distribution on cold formed section
- residual stresses magnitude and distribution due to cold forming
- shape deviations (local and global geometric imperfection)

For the testing of the specimens, numerical controlled (NC) INSTRON 1000KN Dynamic Testing System was used. The entire experimental program was carried-out in the laboratory of the Department of Steel Structures and Structural Mechanics (CEMSIG Research Centre - *cemsig.ct.upt.ro*) at the "POLITEHNICA" University of Timișoara.

The experimental program outcome was further used in the development of a numerical model able to model the behaviour of the real rack upright, including measured geometric imperfection and real material behaviour. The numerical model will be further used to determine the influence of specific imperfections on upright axial load capacity.

3.2 Summary of EN15512 provisions for testing compressed members

Thin walled elements in compression are prone to local buckling. When calculating the load bearing capacity and stiffness, the effect of local buckling shall be taken into account by using the effective cross-sectional properties calculated on the basis of the effective width of individual elements in compression. Effective section properties are used in strength calculations and shall be calculated for non-perforated members in accordance with EN 1993-1-3 [32] or determined by stub column tests according to A.2.1 of the EN15512:2009 [13] design code.

For compression elements with perforations shall be designed on the basis of tests. Compression elements without perforations, however, may be assumed to be fully effective if the width to thickness ratio complies to the following limits:

- a) element supported on two longitudinal edges;

$$\frac{b_p}{t} \leq 1.28 \sqrt{\frac{E}{f_y}} \quad (3.1)$$

- b) element with only one edge supported;

$$\frac{b_p}{t} \leq 0.42 \sqrt{\frac{E}{f_y}} \quad (3.2)$$

The design procedure for perforated compression members shall take proper account of the presence of regular arrays of holes or slots. There are available three alternative procedures:

- a) Design by testing, in accordance with Annex A of the same design code
- b) A fully theoretical procedure which takes rational account of the perforations (e.g. by using finite elements) together with local, global and distortional buckling and imperfections. The way imperfections are taken into account shall be validated by test. It is implicit that the design of continuously perforated members requires testing. This is not intended to restrict the development of analytical procedures (e.g. using finite elements) for predicting the performance of members containing regular arrays of holes or slots. Where rational analysis can be shown to be sufficient, it may be used as an alternative to the use of the relevant test procedures.
- c) A calculation procedure, based on the experimentally-determined effective area, A_{eff} , derived from stub column compression test and modified for distortional buckling. A distortional buckling test shall be carried out on a column length equal to the length of the single bracing panel closest to one metre to give a design strength value $N_{db,Rd}$. The number of tests may be minimized by the use of finite element analysis. The test results shall be used to validate the finite element model.

For perforated pallet rack upright section design by testing, the test arrangement and methods are given in the Annex A of the EN15512:2009 design code.

To observe the influence of local buckling and perforations on the compressive strength of short columns the norm foresees stub column compression tests. The specimens tested according to these specifications will be further referred to as STUB specimens.

Two alternatives are available:

Alternative 1 for test arrangement and method foresees that the length of the stub specimen shall be greater than three times the greatest flat width of the section (ignoring intermediate stiffeners) and it shall include at least five pitches of the perforations. It must be cut normal to the longitudinal axis, midway between two sets of perforations. The base and cap plates shall be bolted or welded to each end of the stub upright. The section may be adjusted for spring back (distortion of the shape of the cross-section after cutting due to residual stresses) by welding to the base plate.

The axial load shall be transmitted to the base and cap plates via pressure pads sufficiently thick to ensure that deformations of the pads under the test load do not influence the test result. The pressure pads shall protrude at least 10 mm beyond the perimeter of the upright section. Base and cap plates shall be positively located on the pressure pads at each end. The pressure pads shall have a small indentation drilled to receive a ball bearing. In Fig. 3.1 is presented the test arrangement for stub column testing.

The initial position of the ball bearing shall be on the same line with the centre of gravity of either the minimum or of the gross cross section or at some

point between them at each end. The specimen shall be placed in the test machine and loaded axially through the ball bearing at each end. The position of the ball bearings in relation to the cross section shall be the same at both ends of the column.

The load shall be increased until the specimen has buckled and will accept no more load. This load shall be recorded as the failure load. The characteristic failure load shall be based on a series of tests with the same load position.

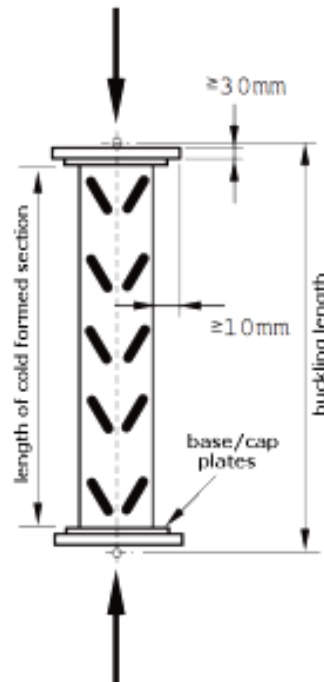


Fig. 3.1 STUB column test arrangement

Alternative 2 is given in order to carry out the stub column compression test using a compression testing machine in which at least one of the loading platens permits rotational adjustment about two horizontal axes and which can be clamped into position as required.

The test specimen shall be mounted with the centroid of its gross cross-section positioned centrally in the testing machine with one loading platen free to rotate in order to take up any lack of alignment of the end plates of the specimen. A small holding load, (e.g. 0,5 % of the expected failure load) is then applied in order to bring the adjustable loading platen of the machine just into full bearing with the end plates of the specimen.

The preparation of the stub column specimens for this test method is the same as in Alternative 1 except that no indentations are required in the pressure pads.

The observed failure load shall be adjusted to take account of the actual thickness and yield stress of the test sample using Eq. (3.3).

$$R_{ni} = R_{ti} \left(\frac{f_y}{f_t} \right)^\alpha \left(\frac{t}{t_t} \right)^\beta \quad (3.3)$$

where, for the specimen:

R_{ni} is the corrected failure load for test number i ,
 R_{ti} is the observed failure load for tested number i
 f_t is the observed yield stress for the specimen
 f_y is the nominal yield stress
 t_t is the observed thickness for the specimen
 t is the design thickness
 α is "0" if $f_y \geq f_t$, or "1" if $f_y < f_t$,

$$\beta \text{ is "0" if } t \geq t_t, \text{ or } \beta = \frac{b_p}{k \sqrt{\frac{E}{f_t}}} - 1, \text{ but } 1 \leq \beta < 2$$

where $k = 0.64$ for stiffened elements or
 $k = 0.21$ for unstiffened elements
 b_p is the nominal plane width

The purpose of the Eq. (3.3) is to limit the capacity of certain series of tests, in order to provide reliable safety coefficients. Considering that the yield strength increase due to cold reducing process is not uniform for different base material sets, the strength is reduced to take into consideration the minimum guaranteed yield strength (f_y).

For the purpose of the present study, the reduction due to the increase in yield strength will be further disregarded, considering the yield strength determined experimentally as the nominal yield strength.

Further on, the characteristic failure load, R_k , is derived using Eq. (3.4).

$$R_k = R_m - k_s s \quad (3.4)$$

where R_m is the mean value of the adjusted test results

$$R_m = \frac{1}{n} \sum_{i=1}^n R_{ni}$$

where R_{ni} is the individual test result corrected for thickness and yield stress
 n is the number of test results in the group ($n \geq 3$);

s is the standard deviation of the adjusted test results, defined by

$$s = \sqrt{\frac{1}{n-1} \sum_{i=1}^n (R_{ni} - R_m)^2}$$

K_s is a coefficient based on 95% fractile at a confidence level of 75%

The effective area of the cross section, A_{eff} , is calculated with:

$$A_{eff} = \frac{R_k}{f_y} \quad (3.5)$$

The effective area is further adjusted if the stub column slenderness exceeds value of $\bar{\lambda} = 0.2$

Compression tests on uprights are foreseen to determine the influence of distortional buckling on the axial load capacity of the upright section. The test results provide a means of correcting the theoretically determined axial load capacity. Test specimens tested in accordance with these provisions will be further called as UPRIGHT specimens.

The test is carried out in the same manner as for stub column tests. The upright length shall be equal to the length of a single bracing panel closest to one metre. If significant twisting is observed at the ends of the specimen, the ends should be restrained in order to resist this twisting; this restraint should not offer any additional resistance to distortion of the section.

The specimen shall be placed in the test machine and loaded axially through the ball bearing at each end. The position of the ball bearings in relation to the cross section shall be the same at both ends of the column, but may be adjusted to the position which gives the maximum failure load.

The results of these tests shall be corrected for yield stress and thickness as follows:

$$R_{ni} = R_{ti} C \alpha \left(\frac{t}{t_t} \right)^\beta$$

where

$$0 \leq \bar{\lambda} \leq 0.2: \quad C = \left(\frac{f_y}{f_t} \right)$$

$$0.2 \leq \bar{\lambda} \leq 1.5: \quad C = \frac{\bar{\lambda} - 0.2 + \frac{f_y}{f_t} (1.5 - \bar{\lambda})}{1.3}$$

$$1.5 \leq \bar{\lambda}: \quad C = 1.0$$

$$\bar{\lambda} = \frac{\lambda}{\pi \sqrt{\frac{E}{f_y}}}$$

λ is the slenderness ratio corresponding to the observed failure mode.

The characteristic failure load, R_{k} , shall be derived as described before.

As mentioned before, the reduction of the axial load capacity due to increase in yield strength will be disregarded.

The norm guidelines presented above created the framework for the experimental program. In addition to tests specified by the norm (tests on stub columns to determine the influence of local buckling and perforations on the compressive strength of short columns and tests on uprights of length equal with the distance between two subsequent nodes) two additional sets of tests were proposed:

- tests on specimens having the length equal with the half-wave length of distortional buckling, and
- tests on specimens having the length in the interactive buckling range.

In European design code for pallet rack structures, EN15512:2009 [13], there are no provisions regarding tests on specimens with critical distortional buckling length.

In accordance with the code provisions, the specimens are bolted or welded to the end plates. By welding, the deformation and warping of the end sections are constrained. Because of this, the specimens can be considered fixed with respect to the distortional buckling mode. It is very difficult to test members with distortional buckling pinned end supports because it is complicated to allow warping of the end cross-sections and to apply a compressive load at the same time.

3.3 Experimental testing program

3.3.1 Geometry and material

There were tested two heavy duty rack upright's sections. The cross sections have extended rear flanges (lipped) with nominal dimensions (provided by the manufacturer) presented in Fig. 3.2 and Fig. 3.3. The sections were provided without any protecting layer (nor galvanized, nor painted). The sectional dimensions were further measured in order to determine geometric deviations and actual base metal thickness.

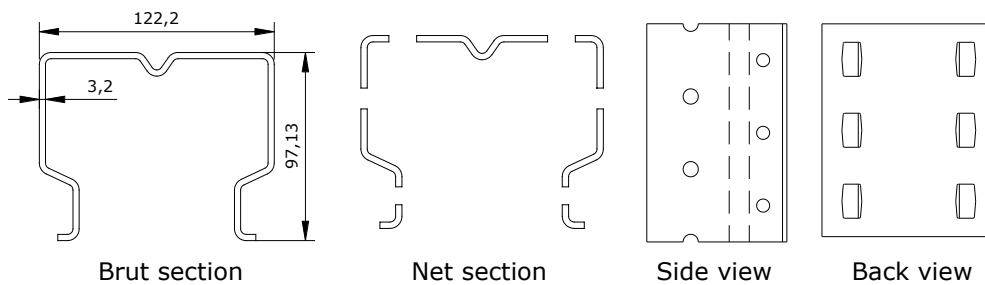


Fig. 3.2 RS125x3.2 cross-section – brut and perforated

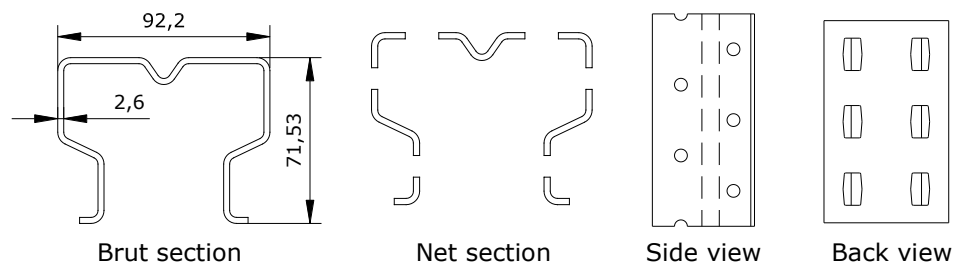


Fig. 3.3 RS95x2.6 cross-section – brut and perforated

The geometry measurements were carried out using a sliding digital calliper with 0.01mm resolution.

The studied sections have the same general geometry. The perforation layout consists in staggered perforations with a pitch (the spacing of the centres of two consecutive holes in the chain measured parallel to the member axis) of 25mm (see Fig. 3.2, side view) and the distance between two identical perforations of 50mm (see Fig. 3.2, back view)

For simplicity, when referring to the whole range of tests for a specific section, the following notations will be further used:

- **RS125B** for RS125x3.2 section without perforations (brut section);
- **RS125N** for RS125x3.2 section with perforations (net section);
- **RS95B** for RS95x2.6 section without perforations (brut section);
- **RS95N** for RS95x2.6 section with perforations (net section).

The usual material for rack uprights is steel. It is provided to the manufacturer in strip rolls of different thicknesses i.e. 5mm in this case. The thickness of steel strips is then reduced using a cold reducing process. By cold reducing, the yield strength is increased from 320-350 N/mm² up to 500-610 N/mm², in some cases. The tensile strength is also increased by cold reducing process. Together with the increase in yield and tensile strength, the material ductility is significantly reduced, from 30% down to 14-15%, even less.

3.3.2 Material testing. Yield strength variation

Material properties play an important role in the performance of thin walled structural members. It is important to be familiar with the mechanical properties of the steel sheets used in cold-formed steel construction before designing this type of steel structural members.

In order to experimentally determine the mechanical properties, a set of samples were cut out from the base material.

The shape and dimensions of testing samples were in accordance with EN10002-1 [177] provisions, function of material thickness.

There were tested a total number of ten samples, five for each type of base material. The INSTRON 1000KN Dynamic Testing System equipped with an optical extensometer was used in order to determine the main mechanical characteristic and establish the behaviour curves (stress-strain diagram) for the of base material together with relevant material properties (e.g. yield strength, ultimate strength).

In Fig. 3.4 a) and b) are presented the stress-strain curves for RS95 base material and for RS125 respectively.

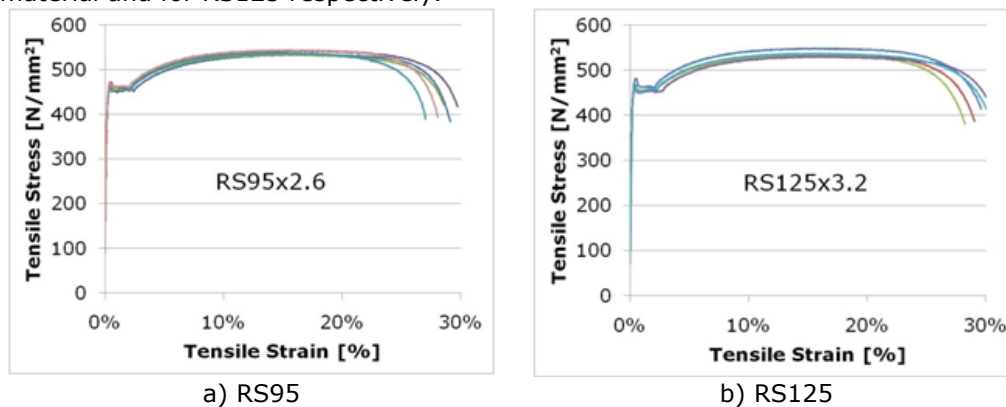


Fig. 3.4 Behaviour curves for base material

The relevant mechanical characteristics of tested material are presented in Table 3.2 and Table 3.3 for RS95 section and RS125 section samples respectively.

Table 3.2 Base material properties for section RS95

Specimen	Yield strength [N/mm ²]	Young modulus [N/mm ²]	Ultimate strength [N/mm ²]	Elongation at maximum load [%]
RS95-1	455.81	210329.96	534.71	15.48
RS95-2	455.67	239613.35	534.31	14.98
RS95-3	463.01	185727.00	543.06	17.45
RS95-4	460.28	203162.70	537.69	15.41
RS95-5	472.27	198485.33	544.71	15.51
Mean	461.41	207463.67	538.90	15.77
Standard Deviation	6.82	20083.63	4.77	0.97

Table 3.3 Base material properties for section RS125

Specimen	Yield strength [N/mm ²]	Young modulus [N/mm ²]	Ultimate strength [N/mm ²]	Elongation at maximum load [%]
RS125-1	478.67	204535.71	548.64	16.01
RS125-2	464.22	222610.55	536.51	14.62
RS125-3	461.51	183831.70	533.50	15.32
RS125-4	457.17	221802.08	530.57	16.35
RS125-5	464.36	181926.37	537.75	15.22
Mean	465.18	202941.28	537.40	15.50
Standard Deviation	8.08	19697.43	6.88	0.68

Due to cold forming process the material properties are modified. The material properties are not constant over the cross-section. The corners area is more affected by plastic deformations and consequently hardening, hence that the changes in material properties are more pronounced in corner area than for flat areas.

In practical design, this increase it is accounted by using average yield strength of the section. Eq. (3.8) presents the procedure defined in EN1993-1-3 [32] and used to determine the average yield strength for a cold formed section.

$$f_{ya} = f_{yb} + f_{yu} - f_{yb} \frac{knt^2}{A_g}, \text{ but } f_{ya} \leq \frac{f_{yu} + f_{yb}}{2} \quad (3.6)$$

where:

- A_g is the gross cross sectional area,
- k is the numerical coefficient that depends on the type of forming (7 for cold rolling, 5 for other methods),
- n is the number of 90° bends in the cross-section with and internal radius $r \leq 5t$,
- t is the nominal core thickness t_{cor} of the steel material before cold forming, exclusive of zinc or organic coatings

In EN1993-1-3 [32] provisions it is specified that the increase in yielding strength due to cold forming shall be taken into account only for the following cases:

- in axially loaded members in which the effective cross-sectional area A_{eff} equals to gross area A_g
- in other cases in which it can be shown that the effects of cold forming lead to an increase in the load carrying capacity

Since the material in the corners of a section is cold-worked to a considerably higher degree than the material in the flat areas, the mechanical properties are different in various parts of the cross section. In order to experimentally determine the yield strength and ultimate tensile strength increase over the cross-section a new series of determinations on coupons cut from specimens without perforations was done for the both of studied sections.

Three cold formed profiles were cut into strips as show in Fig. 3.5. a) and b) for RS95x2.6 section and RS125x3.2 section

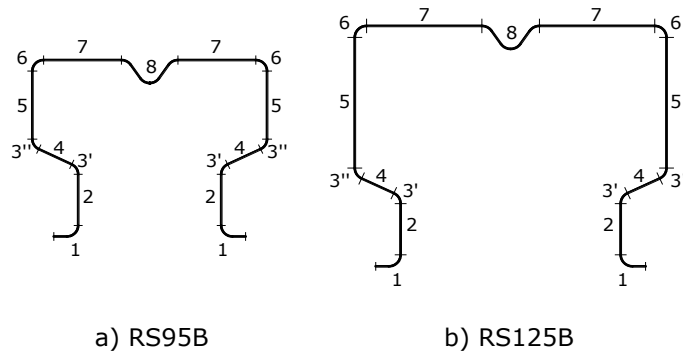


Fig. 3.5 Section partition in strips

The strips were tested using a Static Materials Testing Machine of 250kN capacity produced by Zwick. The behaviour curves for tested strips cut from cold formed sections are presented in Fig. 3.6 for RS95 section material.

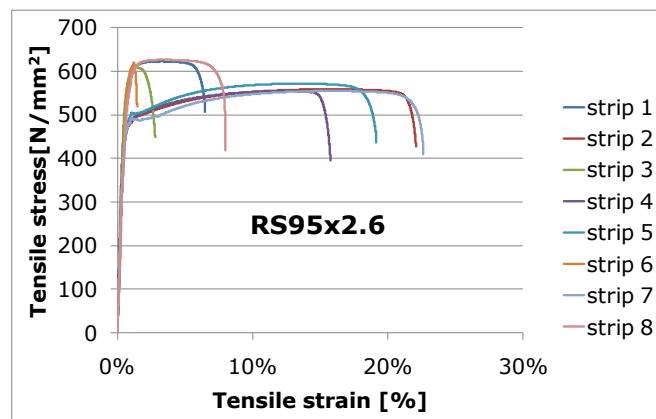


Fig. 3.6 Behaviour curves for RS95 section strips

For RS125 section material, the behaviour curves for tested strips cut from cold formed sections are presented in Fig. 3.7.

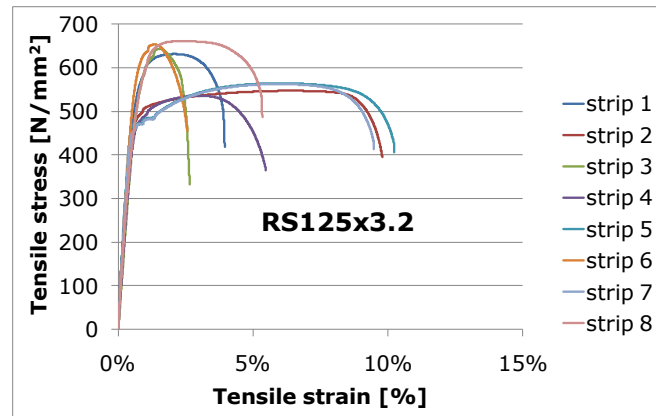


Fig. 3.7 Behaviour curves for RS125 section strips

Comparing the behaviour curves presented in Fig. 3.4 a) and b) with behaviour curves from Fig. 3.6 and Fig. 3.7 it can be observed that the yield and ultimate strength increase is not uniform over the cross section. In the corner areas the yield strength is much more affected by plastic strains and is increased to a value close to the tensile strength.

In the same time, the ductility is reduced down to less than 5%, in some cases. The ductility decrease is more severe in the case of RS125 section and it can be observed for flat walled areas as well. The reduction in ductility is not necessary a problem for thin walled sections. The wall slenderness and cross section's shape imply sectional instabilities that reduce the section's axial compression capacity implying an elastic design of cold formed sections.

In Table 3.4 are presented, comparatively, the yield strength and ultimate strength values of base material, yielding and tensile strength variation over the section and the average limit strength calculated in accordance with EN1993-1-3 for section RS95B. The same comparison is made for section RS125B in Table 3.5.

Table 3.4 Comparison of mechanical characteristics for RS95B section

Strip	$f_{y,Exp}$ [N/mm ²]	f_{yb} [N/mm ²]	f_{ya} [N/mm ²]	$f_{u,exp}$ [N/mm ²]	f_{ub} [N/mm ²]
1 – corner	548.99			615.09	
2 – flat	478.69			557.21	
3' – corner	558.71			601.57	
4 – flat	480.31			559.86	
3'' – corner	558.71	461.41	500.15	601.57	538.9
5 – flat	478.24			559.86	
6 – corner	589.56			631.59	
7 – flat	479.88			558.79	
8 – corner	546.49			620.03	

where $f_{y,Exp}$ is the yield strength of a specific strip

f_{yb} is the yield strength of the base material

f_{ya} is the average yield strength (determined in accordance with EN1993-1-3 provisions, Eq. (3.8))

$f_{u,Exp}$ is the tensile strength of a specific strip

f_{ub} is the tensile strength of base material

Table 3.5 Comparison of mechanical characteristics for RS125B section

Strip	$f_{y,Exp}$ [N/mm ²]	f_{yb} [N/mm ²]	f_{ya} [N/mm ²]	$f_{u,exp}$ [N/mm ²]	f_{ub} [N/mm ²]
1 – corner	571.43			638.40	
2 – flat	485.91			557.80	
3' – corner	570.76			632.43	
4 – flat	475.54			544.85	
3'' – corner	570.76	465.18	501.29	632.43	537.4
5 – flat	464.99			559.94	
6 – corner	608.11			654.35	
7 – flat	469.01			559.84	
8 – corner	572.72			660.73	

3.3.3 Residual stresses

In case of cold formed steel sections beside the increase of yielding and ultimate strength due to cold rolling, another important phenomenon must be considered i.e. the occurrence of residual stresses as a result of the cold forming process.

In hot-rolled steel members, residual stresses do not have a significant variation through the thickness; for cold-formed steel members residual stresses are dominated by a through thickness variation. This variation of residual stresses leads to early yielding on the faces of cold-formed steel plates. The residual stresses can be decisive in the evaluation of the ultimate load. The dominant residual stresses are the flexural or through the thickness residual stresses.

Theoretical residual stresses are composed of two types of residual stresses i.e. membrane and through the thickness (Schafer and Pekoz [187]).

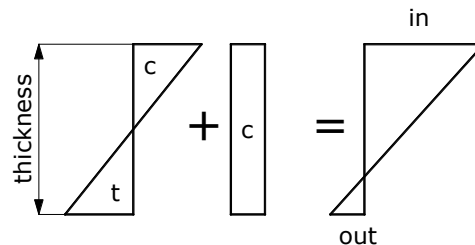


Fig. 3.8 Definition of flexural and membrane residual stress

In order to determine the distribution and magnitude of residual stress, a new set of coupons was prepared by cutting out of four cold formed sections (two for each section). Strips were cut, parallel with sections longitudinal axis, out of cold form profiles without perforations for the two tested sections, as shown in Fig. 3.9.

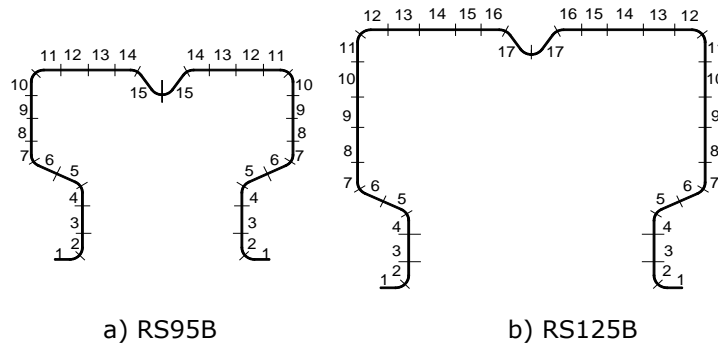


Fig. 3.9 Strips partition for residual stresses measurements

The residual stresses were determined using the method proposed by J. Rondal [178]. The proposed method allows the determination of flexural residual stresses on both interior and exterior faces of cold formed profiles by direct geometric measurements of the curvature of a strip cut off from a profile. The method admits the hypothesis that the membrane residual stresses are zero, assuming a linear variation through the thickness. In reality, the membrane residual stresses exist, but for the case of cold formed sections, due to assumed linear variation through the thickness assumption, they are ignored.

For each cut strip, the curvature was measured using contactless optical measuring system from Limmes GmbH [179] presented in Fig. 3.10. The strip's surface has been prepared with a stochastic pattern.

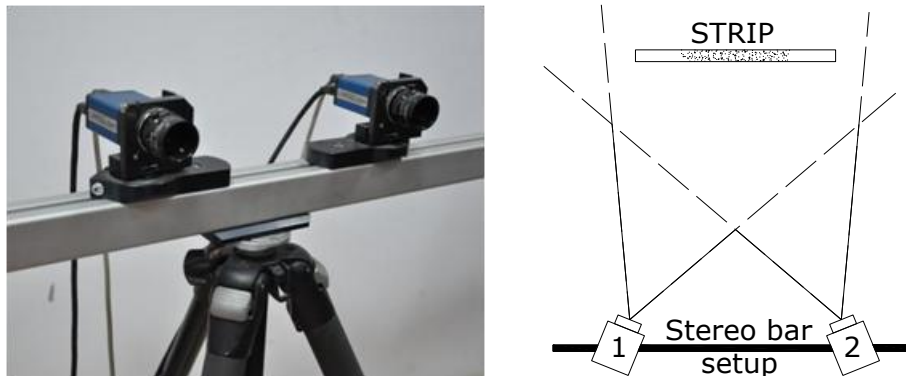


Fig. 3.10 Vic3D measuring system.

Two digital cameras take the pictures of the strips. The images were analysed with accurate image correlation algorithms using Vic3D software for digital image correlation [179] system.

For the curvature determination of the bend strip a second order polynomial function of the neutral surface was used to approximate its deformed shape. Also was considered that the convex and concave edge surface together with the neutral plane have a common curvature. In Fig. 3.11 is presented the stochastic pattern for a strip (a) together with extracted data (b) and the polynomial function that approximates the strip curvature (c) and the calculated deflection. The measurements have been made, considering an 80 mm long chord.

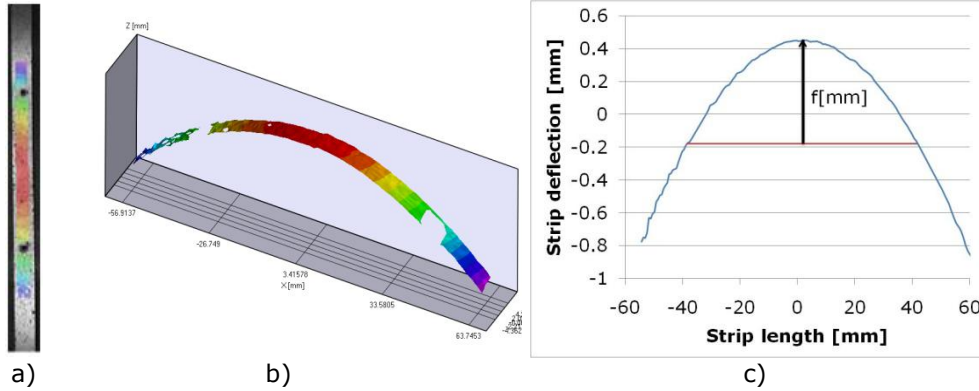


Fig. 3.11 Measured geometry and approximation function for residual stresses measurement

Starting from the above stated hypothesis, an analytical procedure that uses the maximum deflection of the 80 mm long strip (measured at the middle distance) was proposed using the following formula for classic curvature determination:

$$\rho = \frac{l^2}{8 \cdot f} \quad (3.7)$$

where ρ is the strip curvature, l is the chord length (80mm) and f is the strip deflection (distance from the chord to approximation function maximum).

Considering the pure elastic bending theory assumptions, the deformed neutral axis curvature of a bend element may be computed as follow:

$$\frac{1}{\rho} = \frac{M}{E \cdot I_y} \quad (3.8)$$

The second moment of area, for a rectangular strip bend about y-y is:

$$I_y = \frac{l \cdot t^3}{12} \quad (3.9)$$

where: l is the width and t is the thickness of the considered strip.

The maximum longitudinal stress on a strip at the exterior filaments at the location $z = \pm t/2$ (top or bottom of strip), due to pure bending loading can be determined using the well know formula:

$$\sigma = \frac{M}{I_y} \cdot \frac{t}{2} \quad (3.10)$$

By simple replace the expressions (3.7) and (3.10), in equation (3.9) will be obtained the longitudinal stresses that appear in a bent element (of curvature ρ):

$$\frac{E}{\rho} = \frac{M}{I_y} = \frac{2 \cdot \sigma}{t} \Rightarrow \sigma = 4 \cdot f \cdot \frac{E \cdot t}{l^2} \quad (3.11)$$

$$(3.12)$$

The value obtained for bending residual stress is absolute. In order to obtain the corresponding sign (+ for tension and - for compression) at cutting of the strip a special care must be taken to mark curvature sense and establish the interior, respectively the exterior faces of it.

The computed average values of bending residual stresses over the cross-section are presented in Table 3.6.

Table 3.6 Average residual stresses distribution

Strip (see Fig. 3.9)	RS95B r.s. [N/mm ²]	RS125B r.s. [N/mm ²]
1	30.95	19.998
2	185.79	199.69
3	83.60	77.835
4	- 151.4	-40.22
5	-150.7	-69.19
6	-105.4	-55.09
7	-175.6	-96.48
8	-115.3	-76.48
9	-25.95	-59.12
10	-42.33	-51.77
11	-88.62	-47.04
12	-167.5	-173.3
13	-70.93	-196
14	13.356	-114.4
15	26.382	-49.53
16	-	-17.06
17	-	38.965

where “-” sign stands for compression on the outer face of the strip.

3.3.4 Geometrical imperfections

In practice, it is impossible to obtain an upright section that is perfect, from the geometric point of view. The spring-back, as a result of cold working, produces a deviation of the cross section along the member. This is caused by the elastic recovery of the material, upon the release of the forming force.

The European pallet rack design code [13] foresees that for compressed element tests, stubs or uprights with the length equal with the distance between two subsequent nodes, the section may be adjusted for spring-back (distortion of the shape of the cross-section after cutting due to residual stresses) by welding the base plate to the profile’s ends. This adjustment is done at the ends of the profile, while the middle section is left distorted. For studied section the spring-back effect, before welding, is presented in Fig. 3.12.



Fig. 3.12 Spring-back effect

It can be observed that the spring-back effect is more pronounced for sections without perforations. From this point of view, the reduced sectional rigidity due to perforations has a favourable effect, reducing the spring-back.

Additional imperfections were added by welding.

All these geometric imperfections lead to a reduction of the upright compressive strength and to premature failure by local or distortional buckling.

For short length upright sections the overall imperfections can be ignored due to reduced length, while the sectional imperfections together with loading and support eccentricities are of great importance.

In order to determine the influence of sectional geometric imperfections on column compressive strength for each tested STUB and DISTORTIONAL specimens the geometric deviations were measured in three sections, equally spaced along the profile's length. The measured geometry is presented in Fig. 3.13 a). The sectional imperfections are considered to be the deviations from the perfect geometry. They can be positive, the section opens or negative, the section closes.

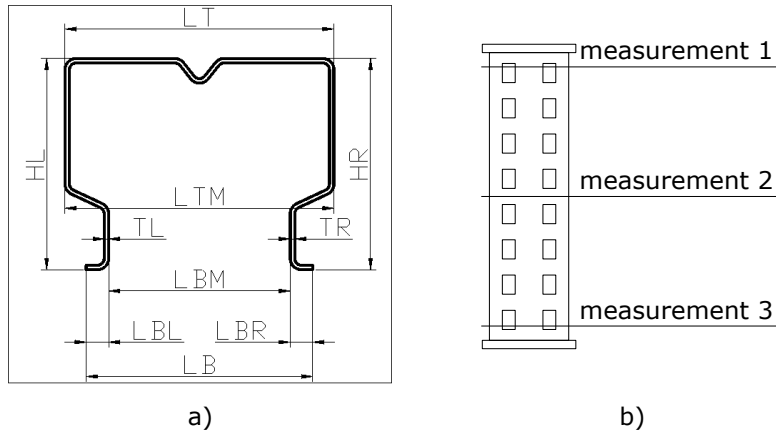


Fig. 3.13 Measured geometry and measurement sections

Schafer and Pekoz [187] (Fig. 3.14 a)) have proposed a set of recommendations for cold formed profiles regarding the geometric sectional imperfections.

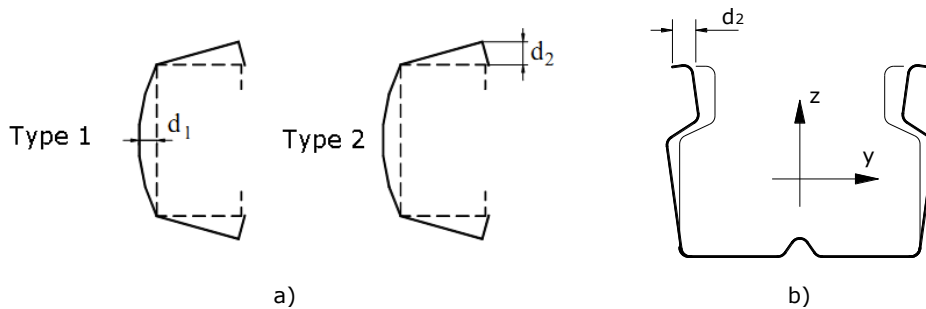


Fig. 3.14 Proposed and considered imperfections

For type 1 imperfection the approximate imperfection magnitude was $d_1=0.006w$, where "w" is the width of the web. An alternative rule based on an exponential curve expressed the imperfection in terms of t, $d_1=6te^{-2t}$ with t and d_1 in

millimetres. For type 2 imperfection the maximum deviation from the straight, is approximated to $d_2=t$.

The thickness has been measured for each tested specimen in each section.

For UPRIGHT specimens, in addition to sectional deviations, the global geometric deviations were measured using a lathe. The measured geometry is presented in Fig. 3.15 and the experimental setup for overall imperfection measurements is presented in Fig. 3.16.

The specimen was mounted between the headstock and tailstock. The movement of the carriage was considered to be rectilinear, providing a perfect straight reference line. A dial gauge was mounted on the carriage in order to record geometrical deviations.

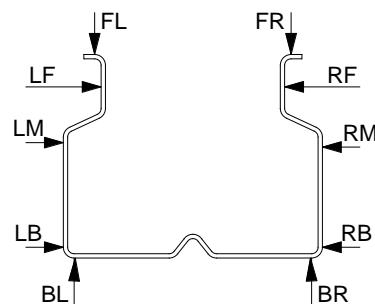


Fig. 3.15 Measured global rectilinear deviations for upright specimens

The deviations were measured in five equidistant sections along the length. The specimen was mounted between the headstock and the tailstock together with its end assembly (end plates, pressure pads and ball bearings). After a measurement was done, the specimen was rotated in order to permit another measurement. The overall imperfections have been measured in the same sections along the specimen's length as the sectional deviations. These values are relative to the upright end, considered as reference.

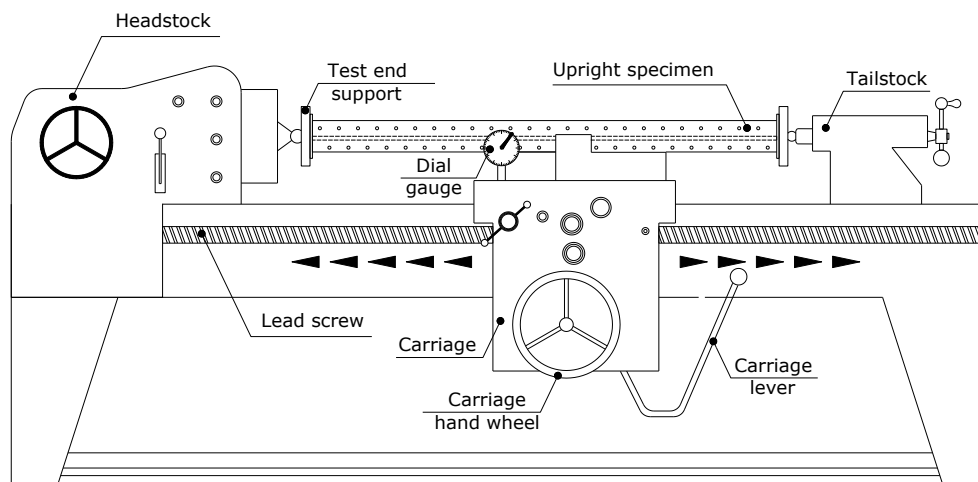


Fig. 3.16 Set up for measuring imperfections of upright specimens

For INTERACTIVE specimens the sectional and global imperfections are of same importance. In order to determine the sectional and global deviations from the straight, a mobile device together with a runway were set up. The mobile device was equipped with displacement transducers connected to a computer. The geometric deviations were measured in sections equally spaced along the specimen's longitudinal axis, placed at 50mm apart. In Fig. 3.17 are presented the arrangement of transducers for the two studied sections together with the measuring device set-up.

Two types of imperfections were recorded and further considered:

- geometric imperfections at cross-section level
- overall geometric imperfections (bar deflections)

The imperfections measured in y direction at the top of the cross-section i.e. LT and RT were considered to be distortional imperfections. These imperfections were identified as *type 2* imperfections (the so called d_2 imperfection - the maximum deviation from the straight, as defined by Schafer and Peköz [187]) (see Fig. 3.18).



Fig. 3.17 Measuring device for geometric imperfections

For INT-125 specimens a maximum measured value for lateral deviations equal with the thickness of walls was obtained for the brut section with a small decrease for perforated section.

For INT-95 specimens a maximum measurement for lateral imperfections equal with 0.86 from the thickness of the wall was obtained for the brut section and slightly decreases for the corresponding perforated section. The measured values of out of straight geometry will be further analyzed in order to compute the values of d_2 imperfections.

It can be observed that, at this point, the measured values for type 2 sectional imperfections are in agreement with the maximum values determined by Schafer & Peköz [187] .

The measured sectional and global imperfections, together with loading and supporting eccentricities have been further analyzed and decomposed in order to be used to calibrate the numerical models.

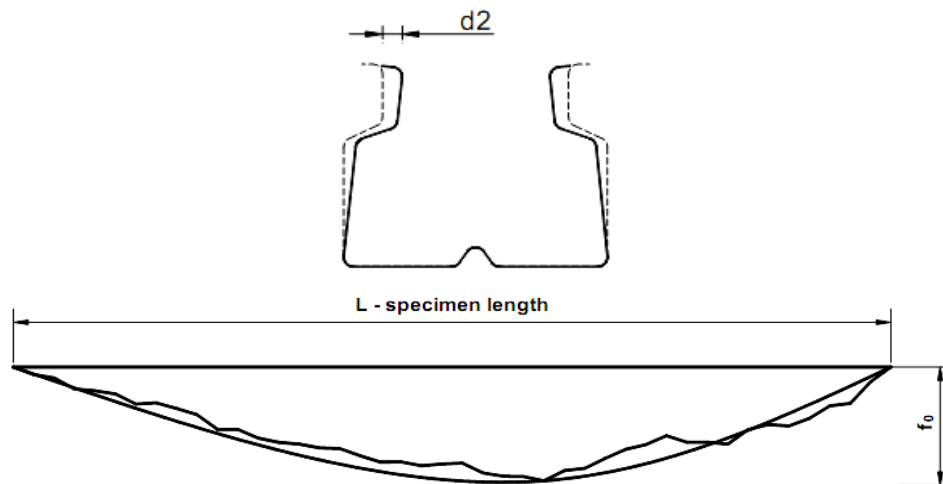


Fig. 3.18 Considered sectional and global bow imperfection

3.3.5 STUB column testing

According to European standard [13] the stub column testing is required in order to experimentally determine the effective area A_{eff} . The tests are performed in order to observe and quantify the influence of perforations and the effects of local buckling on the ultimate strength of a studied member with a specific cross section. The test setup and the testing procedure were in accordance with Annex A.2.1.2 (Alternative 1) of EN15512:2009 [13] design code. The length of specimens was determinate with respect to the code requirements and is summarized below:

- the length of specimen shall be three times the greatest flat width of the section (ignoring intermediate stiffeners); it shall include at least five pitches of the perforations
- the test specimen shall be cut normal to longitudinal axis, midway between two sets of perforations
- the base and cap plates shall be bolted or welded to each end of the stub upright

The section may be adjusted for spring back (distortion of the shape of the cross-section after the cutting due to residual stresses) by welding to the base plates.

Based on the above mentioned criteria, the length of stub upright has resulted as presented in Table 3.7:

Table 3.7 STUB test specimen lengths

Section	fw [mm]	c [mm]	a [mm]	p [mm]	b [mm]
ST-125	125	400	10	30	510
ST-95	95	300	10	30	410

where fw is the greatest flat width of the section, ignoring the intermediate stiffeners, c is the length of the cold formed section, a is the base/cap plate thickness, p is the pressure pad thickness (not considering the ball indentation of

5mm) and b is the buckling length, which includes the length of the cold formed section, base/cap plates, pressure pads (including the ball indentations -5mm x 2) and two halves of ball bearings (2 x 40mm/2).

The compression load was transmitted to the base plates via 30 mm thick pressure pads (to avoid the undesired deformations of the pads during the test). Small deformations of the testing set-up can negatively influence the test result. The pressure pads were prepared with a 5 mm indentation in order to receive a 40mm diameter steel ball bearing. The test setup is presented in detail in Fig. 3.19 (a is base/cap plate, b is buckling length of the specimen and c is the length of the cold formed stub upright).

The European standard does not require tests on specimens without perforations. Tests on specimens without perforations were performed within the framework of this study, in order to quantify the influence of perforations on the capable force of the cross-section.

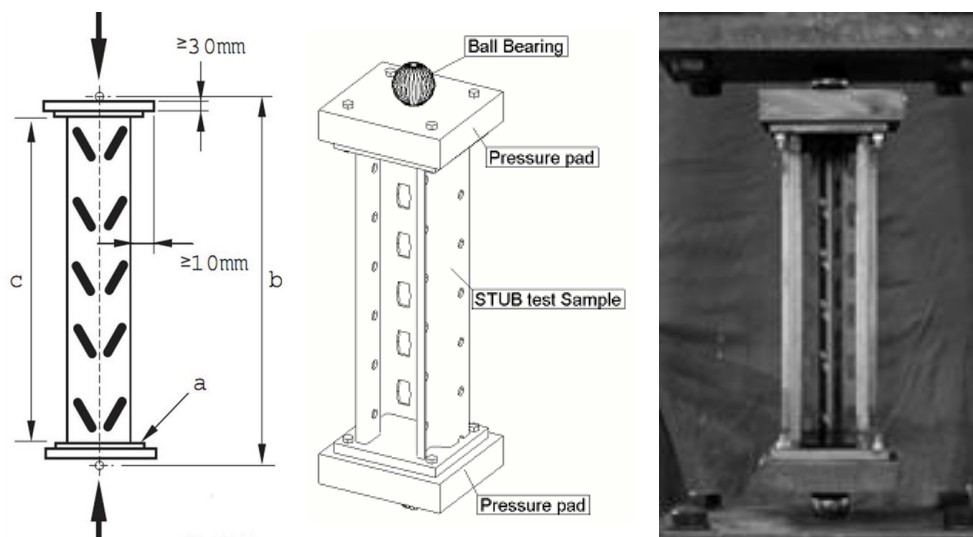


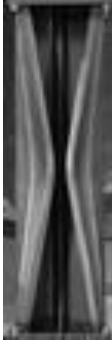




Fig. 3.19 Stub column test setup

The ball bearing was positioned on the symmetry axis of the cross section in between the position of gross and the minimum cross section centres of gravity.

The theoretical position of the ball bearing was on the same line with gravity centres at the both ends, in order to avoid any accidental loads. For obtaining a static load, the specimens were loaded in displacement control at a steady rate of 0.2mm/minute.

In Table 3.8 are presented the failure loads and the observed failure mode for the RS125 stub column specimens, sections without perforations.

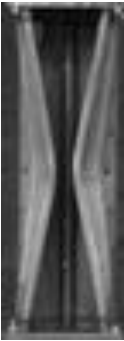




Table 3.8 Maximum loads and failure mode for RS125B stub column specimens

ST-125B		Buckling length: 510mm				
F [kN]	Views					
	Front	Right	Back	Left	ISO	
453.90						
479.43						
463.69						
449.52						
485.38						
487.05						

The failure mode, presented for exemplification in Table 3.8, was observed for all ST-125 specimens without perforations. As it can be observed, no local buckling occurred.

In Table 3.9 are presented the failure loads and the observed failure mode for the SR-125 specimens, section with perforations

Table 3.9 Maximum load and failure mode for ST-125N net stub specimens

ST-125N		Buckling length: 510mm				
F [kN]	Views					
	Front	Right	Back	Left	ISO	
413.28						
407.81						
400.85						
404.03						
402.27						
400.19						
397.46						
409.05						
411.02						
396.51						
395.91						
406.05						

The failure mode presented for exemplification in Table 3.9 for a tested specimen was the one observed for all ST-125 column specimens, section with perforations. As for sections without perforations, no local buckling was observed.

For ST-125B and ST-125N specimens the failure mode was a symmetric distortion of the section. Even if the failure mode was distortional, the length of STUB column test samples is not enough to determine the critical distortional buckling load.

In Fig. 3.20 are presented in terms of axial load vs. axial shortening, the experimental curves for ST-125 specimens for both sections: without perforations (a) and with perforations (b).

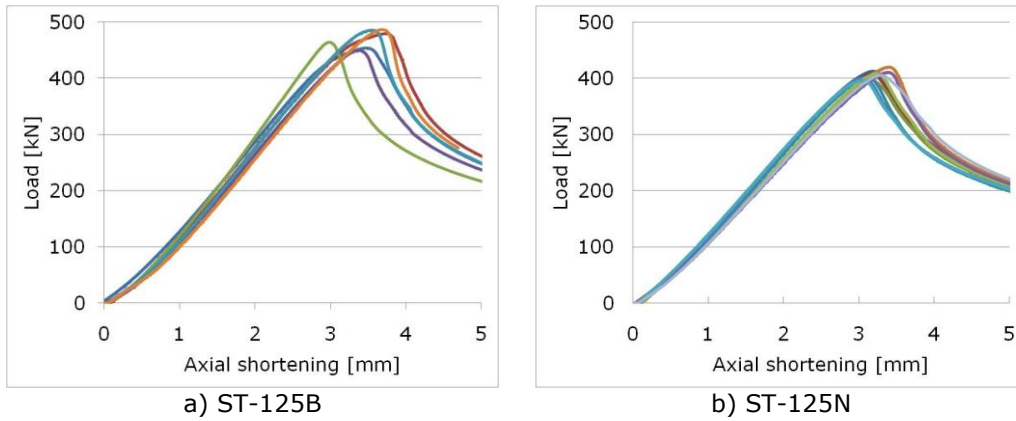





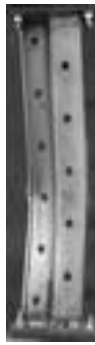

Fig. 3.20 Experimental curves for ST-125 a) brut and b) net stub column specimens.

For ST-95 specimens sections without perforations there were observed two failure modes: (1) symmetric distortional failure mode and (2) asymmetric failure mode presented in Table 3.10. No noticeable variation in failure loads magnitudes was observed.

Table 3.10 Maximum load and failure mode for ST-95B specimens					
ST-95B		Buckling length: 410mm			
F [kN]	Views				
	Front	Right	Back	Left	ISO
Failure mode: symetric distortional					
350.68					
346.44					
346.23					
346.63					
354.30					
338.88					

In Table 3.11 are presented the maximum loads together with observed failure mode for ST-95 specimens with perforations.

Table 3.11 Ultimate load and failure mode for ST-95N specimens

F [kN]	ST-95N				
	Buckling length: 410mm				
	Views				
	Front	Right	Back	Left	ISO
279.82					
276.99					
284.28					
274.33					
278.78					
278.63					
281.63					
278.68					
279.00					
277.92					
277.81					
283.42					

For ST-95 specimens, section with perforations a distortional symmetric failure mode was observed for all tested specimens. No local buckling was observed for ST-95 specimens, sections with and without perforations.

In Fig. 3.21 are presented the axial load vs. axial shortening experimental curves for ST-95 specimens, both sections: a) without perforations and b) with perforations.

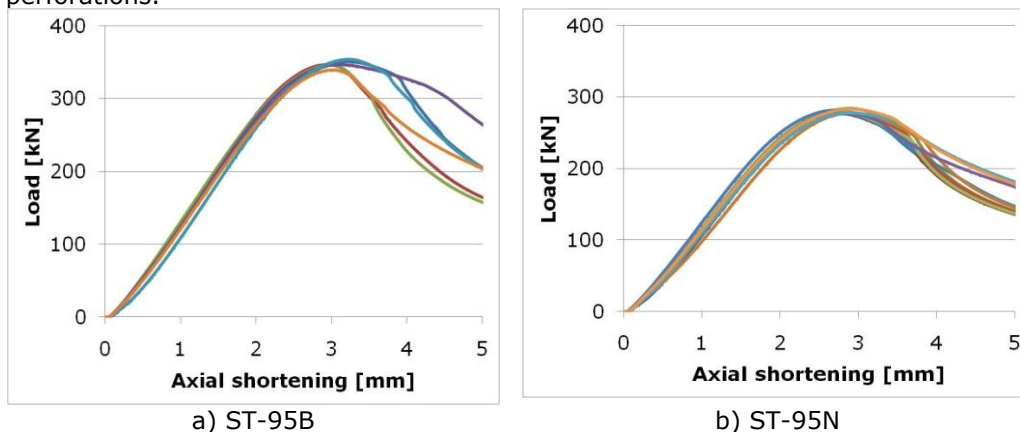


Fig. 3.21 Experimental curves for ST-95 a) brut and b) net stub column specimens.

Considering the maximum experimental load values, it can be said that the failure occurred due to reach of squash load of ST-95 specimens, for both perforated and unperforated sections.

3.3.6 UPRIGHT testing

The EN15512:2009 [13] design code (section 9.7.2, alternative c) states that the influence of distortional buckling mode on the axial load capacity of the upright section shall be determined by tests.

Another series of experimental tests have been conducted to evaluate this effect. The obtained results provide a means of correcting the theoretically obtained axial capacity which can be calculated in accordance with section 9.7.4 and 9.7.5 of the same standard.

The length of the testing specimens, as specified in section 9.7.2 paragraph c), should be the length of a single bracing panel closest to one metre. For tested sections, the length of the bracing panels was 1200mm, which was considered to be the buckling length of the upright specimens (including base plates, pressure pads and the ball bearings).

The experimental setup was the same as for stub column testing and it is presented in Fig. 3.22. The theoretical position of the ball bearing was on the same line with gravity centres at the both ends, in order to avoid any accidental loads. For obtaining a static load, the specimens were loaded in displacement control at a steady rate of 0.2mm/minute.

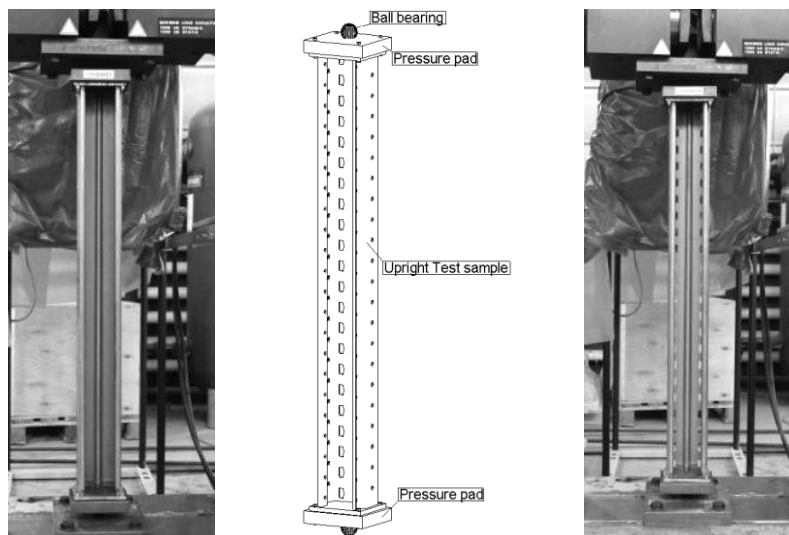


Fig. 3.22 UPRIGHT tests setup

The experimental failure force and the failure mode of RS125 upright specimens are exemplified in Table 3.12 for sections without perforations and in Table 3.13 for sections with perforations.

Table 3.12 Ultimate load and failure mode for UP-125B specimens

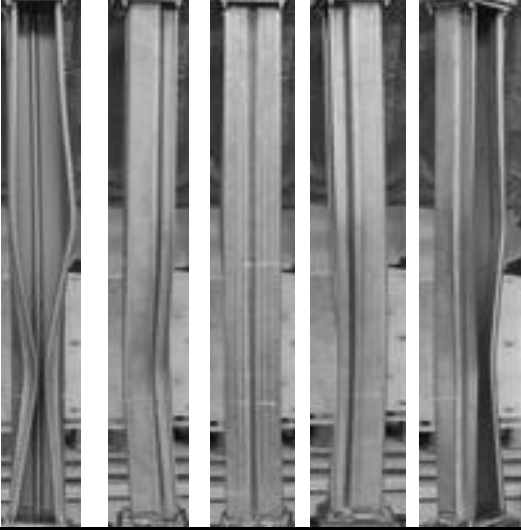

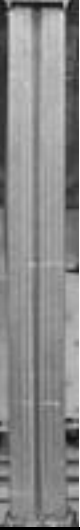

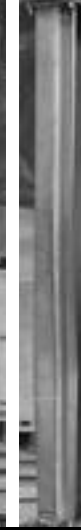
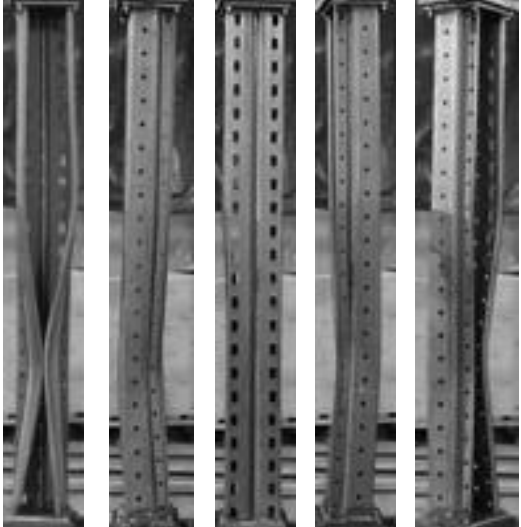


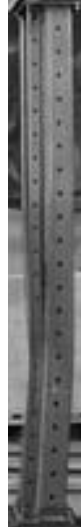

UP-125B		Buckling length: 1200mm				
F [kN]	Views					
	Front	Right	Back	Left	ISO	
386.72						
369.12						
386.90						
373.41						
382.59						

Table 3.13 Maximum load and failure mode for UP-125N upright specimens

UP-125N		Buckling length: 1200mm				
F [kN]	Views					
	Front	Right	Back	Left	ISO	
347.26						
363.48						
350.79						
339.09						
344.46						
337.18						
354.40						
350.45						
340.54						
3454.41						

In Fig. 3.23 are presented the load vs. axial shortening experimental curves for UP-125 upright specimens: a) without perforations and b) with perforations.

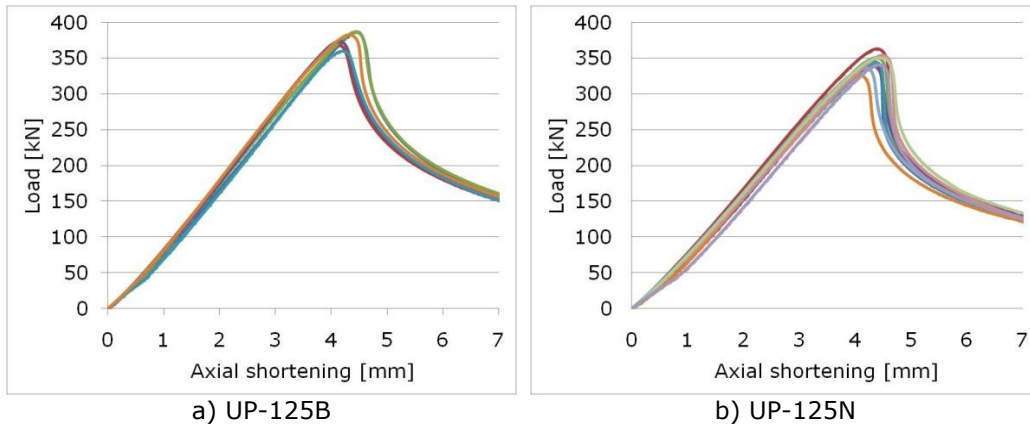


Fig. 3.23 Experimental curves for UP-125 a) brut and b) net upright specimens.

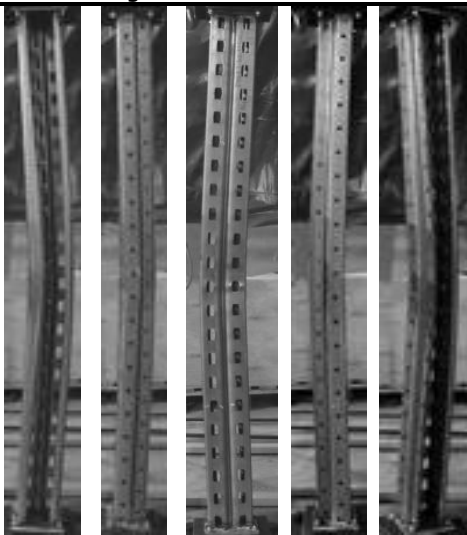
In Table 3.14 are presented the maximum loads and the observed failure mode for the UP-95 section without perforations.

Table 3.14 Maximum load and failure mode for ST-95B upright specimens

F [kN]	UP-95B Buckling length: 1200mm				
	Views				
	Front	Right	Back	Left	ISO
270.35					
270.49					
272.06					
279.65					
269.83					

Initially, at the maximum load the UP-95 upright specimens, section without perforations initiate a distortional failure; the failure mode changed suddenly, jumping to a flexural or flexural-torsional buckling failure mode (distortional buckling is accompanied by flexural or flexural-torsional buckling). The same failure mechanism was observed for RS95 upright specimens, section with perforations as presented in Table 3.15.

Table 3.15 Maximum load and failure mode for UP-95N upright specimens

F [kN]	UP-95N Buckling length: 1200mm				
	Views				
	Front	Right	Back	Left	ISO
207.18					
215.72					
209.87					
211.29					
206.45					
213.24					
223.33					
216.30					
208.90					
209.91					

In Fig. 3.24 are presented the axial load vs. axial shortening experimental curves for UP-125 upright specimens: a) without perforations and b) with perforations.

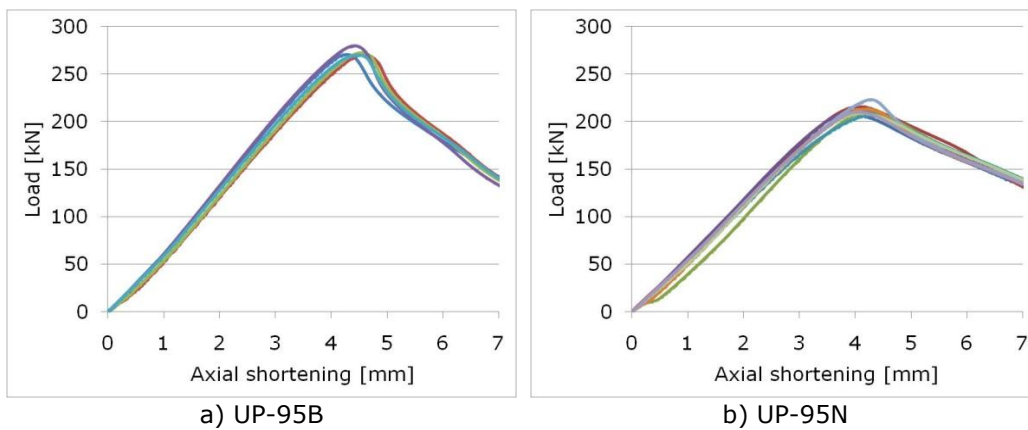


Fig. 3.24 Experimental curves for RS95 a) brut and b) net upright specimens.

3.3.7 DISTORTIONAL buckling specimens testing

Because of the cross section shape and dimensions, pallet rack storage upright members are prone to distortional buckling. As stated before, according to the EN15512:2009 [13] provisions, the effects of distortional buckling are studied for specimens of lengths equal to the distance between two subsequent nodes; for these specimens lengths, the test results correspond rather to the distortional-global interaction, than to pure distortion.

For the consistency of testing with the target phenomena, the lengths corresponding to distortional buckling are necessary to be studied and used after in the interactive buckling inquiry. Consequently, the experimental testing program was completed with a series of tests on specimens having the length equal to the half-wave length of distortional buckling.

There are available a series of software tools able to determine the critical distortional buckling length for various cross-sectional shapes. The problem is more complicated in the case of upright sections due to the perforations arrays. In order to take into account the perforations, the equivalent thickness concept can be used together with CUFSM [183] , [131] software or commercial multipurpose FEM programs, like ABAQUS using an eigenbuckling analysis.

The half-wave length, corresponding to distortional buckling, was determined using the CUFSM software and comparatively, ABAQUS. In order to calculate the half-wave length for members with perforations using CUFSM, an equivalent thickness was determined based on Eq.(3.13):

$$t_{eq,1} = \frac{N_{Dist,Net}}{N_{Dist,Brut}} \cdot t \quad (3.13)$$

where: $t_{eq,1}$ is the equivalent thickness, $N_{Dist,Net}$ and $N_{Dist,Brut}$ are the ultimate axial load capacity of the cross-section, with and without perforations, based on numerical simulations of distortional specimens without imperfections.

Another approach, to take into consideration the effect of perforations, was proposed by Davies [176] . The method consists in determining an equivalent thickness based on the ratios of gross and net effective width, which is then weighted, taking into account the length of the perforations along the axis of the column. The following equation has been used:

$$t_{eq,2} = \left(\frac{L_p}{L} \cdot \frac{b_n}{b_g} + \left(1 - \frac{L_p}{L} \right) \frac{b_g}{b_i} \right) t \quad (3.14)$$

where: $t_{eq,2}$ is the equivalent section thickness, L_p is the length of perforation multiplied by the number of perforations along the length of the plate, L is the length of the plate, b_n is the net effective width of the plate, b_g is the gross effective width of the plate, b_i is the actual width of the plate and t is the actual thickness of the section.

The calculus for effective widths of the perforated plates is based on BS 5950: Part 5 and a method presented by Rhodes and Schneider in their study [184] . A constant stress over the effective areas of the plate was assumed. Where perforations intersect this area, the stress is simply disregarded (see Fig. 3.25).

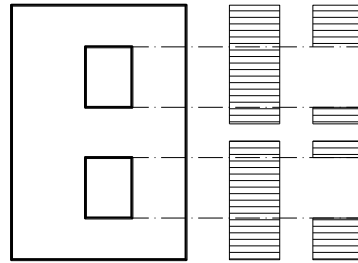


Fig. 3.25 Uniform stress distribution over the effective net section

The net effective width of a plate is given by:

$$b_n = b_g - b_p \tag{3.15}$$

where b_p is the total width of perforations within the effective area
Following, p_{cr} is defined by:

$$p_{cr} = 185000K \left(\frac{t}{b} \right)^2 \tag{3.16}$$

with $K=4$ (buckling factor)

Next, if $p_{cr} < 0.132 \sigma_y$, $b_g = b$, otherwise:

$$b_g = b \left(1 + 14 \left(\sqrt{\frac{\sigma_y}{p_{cr}}} - 0.35 \right)^4 \right)^{-0.2} \tag{3.17}$$

In Table 3.16 are presented the equivalent thicknesses for perforated sections and the half-wave lengths for the elements with and without perforations for the two studied sections determined with finite strip method program, CUFSM, and with finite element package, ABAQUS.

Table 3.16 Distortional critical buckling load and equivalent thickness of perforated sections; half wave lengths of studied sections

Profile		Length [mm]	N_{cr} [kN]	A [mm ²]	t [mm]
DIST-125B	ABAQUS	540 - 550	429.14	1106.6	3.2
	CUFSM	560	435.05	1144.1	3.2
DIST-125 t_{eq1}	CUFSM	620	296.11	965.3	2.7*
DIST-125 t_{eq2}	CUFSM	580	375.15	1072.6	3.0**
DIST-125N	ABAQUS	600	370.48	959.4	3.2 - perforated
DIST-95B	ABAQUS	460 - 470	402.50	692.8	2.6
	CUFSM	480	406.70	721.7	2.6
DIST-95 t_{eq1}	CUFSM	540	255.10	582.9	2.1*
DIST-95 t_{eq2}	CUFSM	500	341.80	666.2	2.4**
DIST-95N	ABAQUS	500	340.78	573.2	2.6 - perforated

* reduced thickness calculated experimentally (Eq. (3.13))

** reduced thickness calculated theoretically (Eq. (3.14))

The length of distortional specimens was chosen based on the values presented in Table 3.16.

Following, in Table 3.17 are presented the specimens length for distortional specimens that were experimentally tested.

Table 3.17 Length for distortional specimens

Section	Specimen length [mm]	Buckling length [mm]
DIST-125B	560	670
DIST-125N	600	710
DIST-95B	480	570
DIST-95N	500	610

The same test setup was used as for STUB and UPRIGHT specimens. In Fig. 3.1 is presented the test setup for distortional specimens.

The ball bearing was positioned on the symmetry axis of the cross section in between the position of gross and the minimum cross section centres of gravity.

The theoretical position of the ball bearing was on the same line with gravity centres at the both ends, in order to avoid any accidental loads. For obtaining a static load, the specimens were loaded in displacement control at a steady rate of 0.2mm/minute.

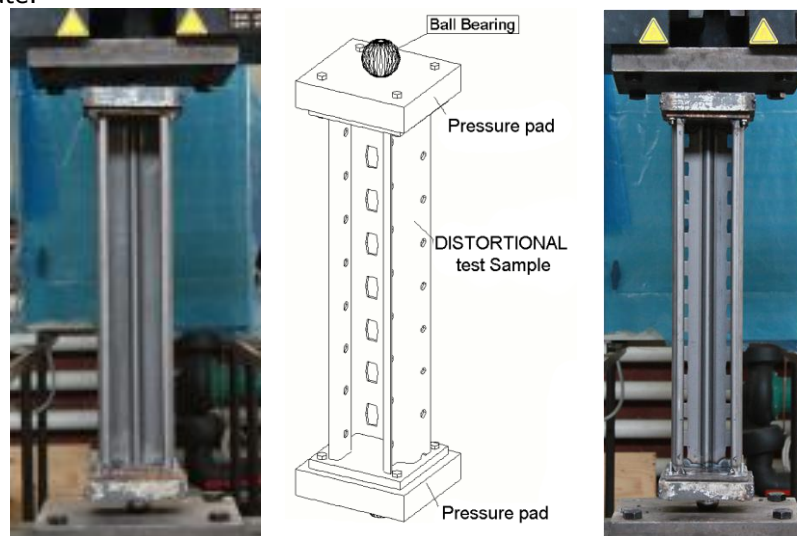







Fig. 3.26 DISTORTIONAL tests setup

In Table 3.18 are presented the maximum loads of the specimens for uniform compression and failure mode for DIST-125 testing specimens, section without perforations. The failure mode was the predicted one, i.e. distortional buckling of the section.

Table 3.18 Maximum load and failure mode for DIST-125B specimens

DIST-125B		Buckling length: 670 mm				
F [kN]	Views					
	Front	Right	Back	Left	ISO	
422.42						
414.33						
432.69						
420.02						
428.28						

In order to quantify the influence of boundary conditions regarding the ball bearing effects on the maximum force and post critic behaviour, two specimens were loaded directly, without the ball bearings at the ends. In Fig. 3.27a, it can be observed that the maximum load was not significant affected by the change of end boundary conditions, but the post-critical behaviour changed together with the change of the support from pinned to fixed.

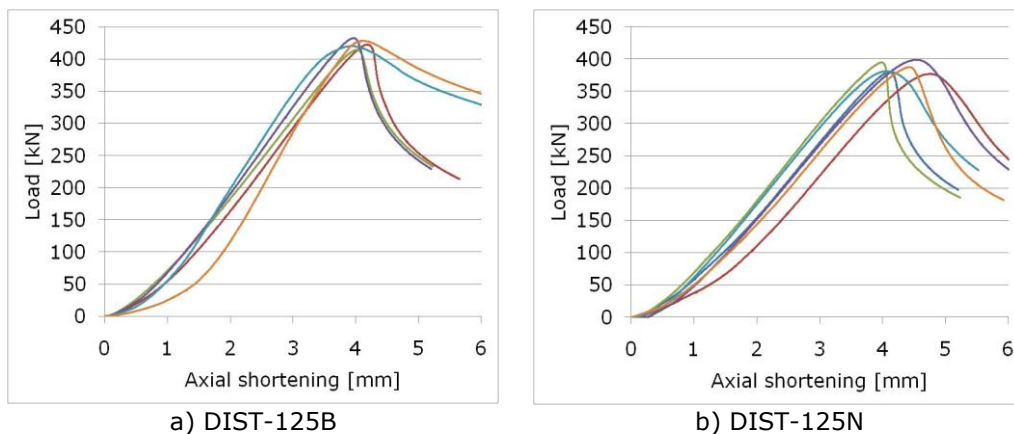

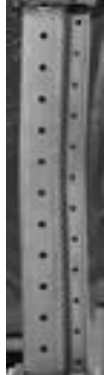





Fig. 3.27 Experimental curves for DIST-125 a) brut and b) net specimens

In Table 3.19 are presented maximum force and failure mode for DIST-125 distortional specimens, sections with perforations. The failure mode was again the expected one, symmetric distortional mode.



Table 3.19 Ultimate load and failure mode for DIST-125N specimens

DIST-125N		Buckling length: 710 mm				
F [kN]	Views					
	Front	Right	Back	Left	ISO	
379.90						
394.62						
398.74						
381.06						
387.43						

For DIST-125 specimens, the test results confirm the software capacity, CUFSM and ABAQUS, to determine the critical buckling load for distortional buckling. It can be observed that the failure mode is distortional buckling for both sections, with and without perforations.

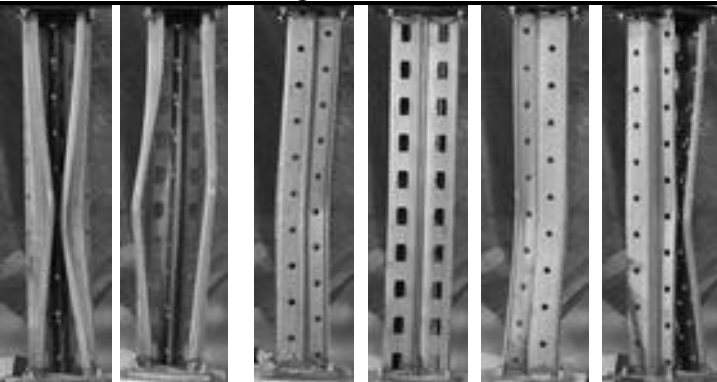
In Table 3.20 are presented the maximum experimental forces for uniform compression and failure mode for DIST-95 distortional specimens, section without perforations. The failure mode was the section's distortion. It can be observed that the distortional failure mechanism can be either inwards or outwards, depending on the geometrical deviation.

Table 3.20 Ultimate load and failure mode for DIST-95B specimens

DIST-95B		Buckling length: 590 mm				
F [kN]	Views					
	Front	Right	Back	Left	ISO	
325.10						
315.36						
328.36			n/a	n/a	n/a	

In Table 3.21 are presented the maximum experimental load and failure modes for DIST-95 distortional specimens, section without perforations. The observed failure mode was a distortional mode. The same failure mode, distortion of the section, was observed for DIST-95 specimens, section with perforations.

Table 3.21 Ultimate load and failure mode for DIST-95N specimens

DIST-95N		Buckling length: 610 mm				
F [kN]	Views					
	Front	Right	Back	Left	ISO	
262.67						
259.67						
260.50						

Even if the observed failure mode for DIST-95 specimens was a symmetric distortion of the section, the observed failure load corresponds rather to the squash load than to critical distortional buckling load.

In Fig. 3.28 are presented the load vs. axial shortening experimental curves for DIST-95 specimens: a) without perforations and b) with perforations.

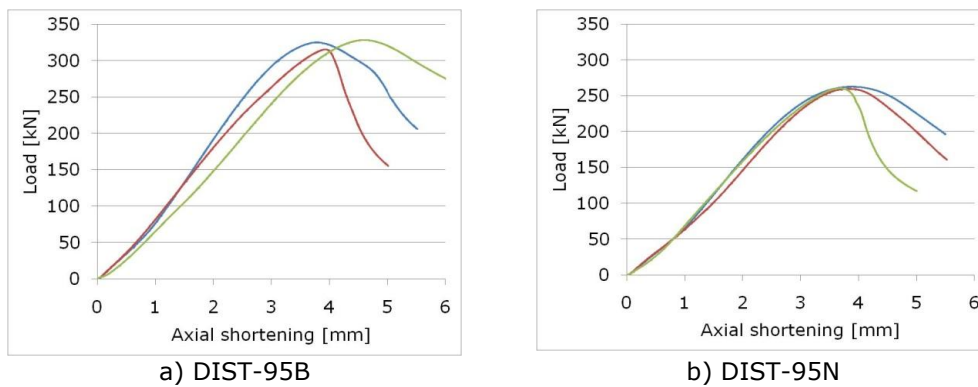


Fig. 3.28 Experimental curves for DIST-95 specimens

3.3.8 INTERACTIVE buckling specimens tests

One of the most interesting aspects of the post-buckling behaviour of thin walled sections is the interaction of multiple buckling modes under the same critical load. This phenomenon is very important, since single stable post-buckling equilibrium paths become unstable when interacting with each other.

The general meaning of coupled instability phenomenon is related, in fact, to nonlinear coupling of simple instability modes. Due to the imperfections and

coupling effect, erosion of the theoretical critical bifurcation load always occurs. The maximum erosion is in the vicinity of the coupling point. For bar members, an interactive slenderness range, within which the sensitivity to imperfections is increased, may be identified.

In Fig. 3.29 are presented the simple instabilities for studied section, obtained with CUFSM [183] , [131] software, together with the considered coupled instability i.e. distortional with flexural about minor inertia axis buckling.

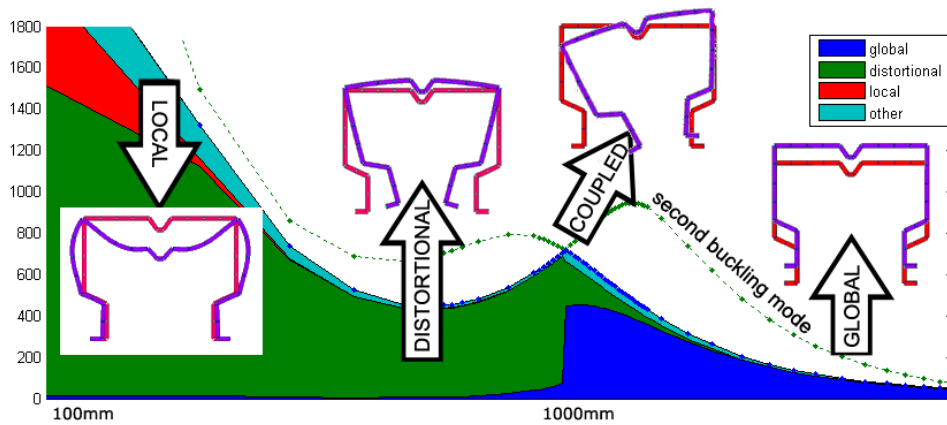


Fig. 3.29 Interactive buckling for studied members in compression

The erosion of critical load is a result of coupled instabilities, geometric and material imperfections. In order to experimentally determine the erosion as a result of global and sectional instability modes coupling, together with the effects of geometric and material imperfections, a new set of specimens having the length in interactive buckling range were tested.

The erosion concept can be implemented in the buckling analysis of thin-walled members via the ECBL (Erosion of Critical Bifurcation Load) Approach, developed by Dubina [28] . This approach can be applied for any type of instability interactions. A summary of this approach for the case of distortional and global flexural buckling was presented in Chapter 2.

Considering the distortional strength of the given section, $\bar{N}_D = N_D/A \cdot f_y$ the interactive length of the member undergoing coupling between distortional and overall buckling is:

$$L = \frac{1}{\sqrt{\bar{N}_{D,u}}} \tag{3.18}$$

Where the corresponding erosion of $\bar{N}_{D,cr}$ is:

$$\psi_D = \bar{N}_{D,u} - \bar{N} \tag{3.19}$$

After, the imperfection factor α_D , for distortional-overall interaction will be obtained with Eq. (2.38).

$$\alpha_{D,cr} = \frac{\psi_D^2}{1 - \psi_D} \frac{\sqrt{N_{D,u}}}{1 - 0.2\sqrt{N_{D,u}}} \quad (3.20)$$

The erosion of critical load is a result of coupled instabilities, geometric and material imperfections. In order to experimentally determine the erosion as a result of global and sectional instability modes coupling, together with the effects of geometric and material imperfections, a new set of specimens having the length in interactive buckling range were tested.

The specimen's length should be reasonably close to the instabilities coupling point (in terms of reduced slenderness). This is leading to the idea of using a "coupling range" defined in terms of reduced slenderness as a vicinity of the coupling point, instead of working strictly in this point. A correct definition of coupling range limits is therefore of great importance for the considered specimens length.

In order to determine the coupling point for interactive instabilities i.e. distortional and global flexural buckling, first the ultimate strength of members with the length corresponding to distortional buckling has to be obtained. Based on numerical results, the sectional strength (corresponding to distortional buckling critical length) was determined for all studied sections (see Table 3.16). Due to the fact that for RS95 sections, the distortional critical buckling load was higher than the squash load, the sectional strength with respect to distortional buckling was limited to the squash load.

The numerical results were confirmed by tests. For DISTORTIONAL specimens it can be observed that for RS125 sections, the failure load is comparable with distortional buckling load, while for RS95 sections, the failure load is almost equal with the squash load.

In Table 3.22 are presented the critical loads corresponding to distortional buckling determined using LBA, together with the experimental failure loads for specimens having the critical length considered for distortional buckling tests.

Table 3.22 Sectional capacity of RS95 and RS125 section

Section	RS125B	RS125N	RS95B	RS95N
Length [mm]	560	600	480	500
Distortional buckling load* ($N_{D,cr}$) [kN]	429.14	370.48	402.50	340.78
Distortional ultimate load** ($N_{D,u}$) [kN]	423.55	388.35	322.94	260.95
Squash load (N_p) [kN]	556.95	483.16	346.51	286.69

* distortional buckling load determined using LBA

** experimental distortional failure load

The buckling length for distortional-flexural interactive buckling has been calibrated using the ECBL approach [28]. It has been determined, based on the experimental failure loads and it is presented in Table 3.23.

Table 3.23 Coupling length for RS95 and RS125 section

Section	RS125B	RS125N	RS95B	RS95N
Coupling length [mm]	2393	2499	1580	1758

Due to the fact that the coupling lengths for sections with perforations and without perforations are different, the length for these specimens has been considered to cover the entire interval.

The buckling length, for the specimens in the interactive buckling interval, has been considered equal, for the sections with and without perforations, in order to better underline the effect of perforations. Moreover, considering the moment of inertia of gross cross-section for global calculations (overall buckling) overestimates the flexural critical buckling loads, increasing unrealistically the coupling length.

The length of tested specimens for both types of cross-sections, with and without perforations, is presented in Table 3.24.

Table 3.24 Specimens length for interactive buckling study

Section	Type	Specimen length	Buckling length	Number of samples
INT-125	brut	2000, 2200, 2400	2110, 2310, 2510	2, 3, 2
	net	2000, 2200, 2400	2110, 2310, 2510	3, 3, 3
INT-95	brut	1400, 1500, 1650	1510, 1610, 1760	3, 3, 3
	net	1400, 1500, 1650	1510, 1610, 1760	3, 3, 3

The test setup was practically the same as for all other tests. During the test, the rotations about minor and major axis were permitted while the torsion was prevented for both ends. All translation were restrained at one end, considered pinned, while for the other, considered simply supported, the axial translation was permitted. For both ends, the torsional degree of freedom was restrained.

The end assembly consists of the same pressure pads of 30mm thick with an indentation of 5mm and the ball bearing of 40mm diameter.

The displacements and rotations of the specimen were monitored in three sections equally spaced along the specimen using five displacement transducers for each section. The global test configuration and displacement transducers arrangement are presented schematically in Fig. 3.31 together with a detailed view of the displacement transducer position on the cross section in Fig. 3.30.

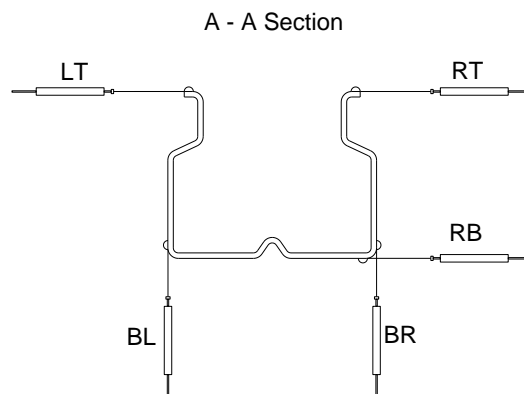


Fig. 3.30 Displacement transducers setup

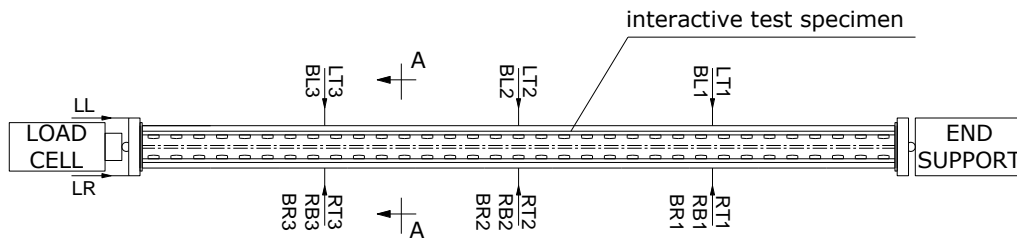


Fig. 3.31 Schematic test setup for interactive buckling specimens

In Fig. 3.32 is presented the actual test setup for interactive buckling specimens testing program.



Fig. 3.32 Test setup for interactive buckling specimens

In Fig. 3.33 are presented the experimental load vs. axial shortening curves for RS125 interactive buckling specimens, section without perforations in a), b), c) and for the section with perforations in d), e) and f).

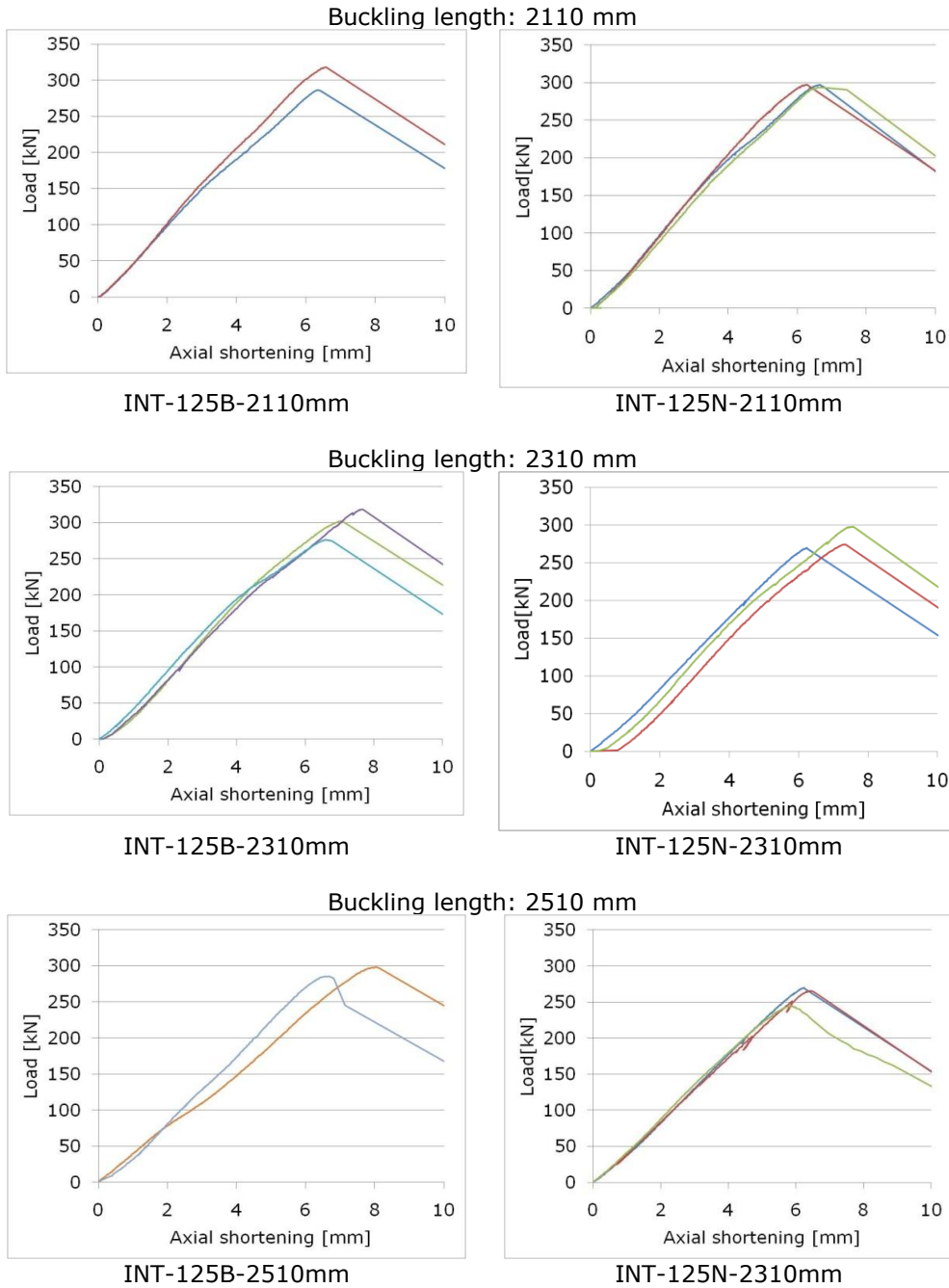


Fig. 3.33 Maximum experimental load vs. axial shortening curves for RS125 interaction specimens

142 **Experimental program – 3**

In Table 3.25 and Table 3.26 are presented the ultimate loads and failure modes for INT-125 interaction specimens, section without and with perforations.

Table 3.25 Failure loads and failure mode for INT-125B specimens



	Buckling length [mm]			
	2110	2310	2510	
Different failure mode				
	Ultimate force [kN]	286.65 317.89	287.34 302.29 318.29	298.22 285.71

Table 3.26 Failure loads and failure mode for INT-125N specimens

	Buckling length [mm]			
	2110	2310	2510	
Different failure mode				
	Ultimate force [kN]	296.73 296.91 293.63	276.15 274.22 298.07	265.44 269.71 244.69

In Fig. 3.34 are presented the experimentally determined load vs. axial shortening curves for INT-95 specimens for the section without perforations in a), b), c) and for the section with perforations in d), e) and f).

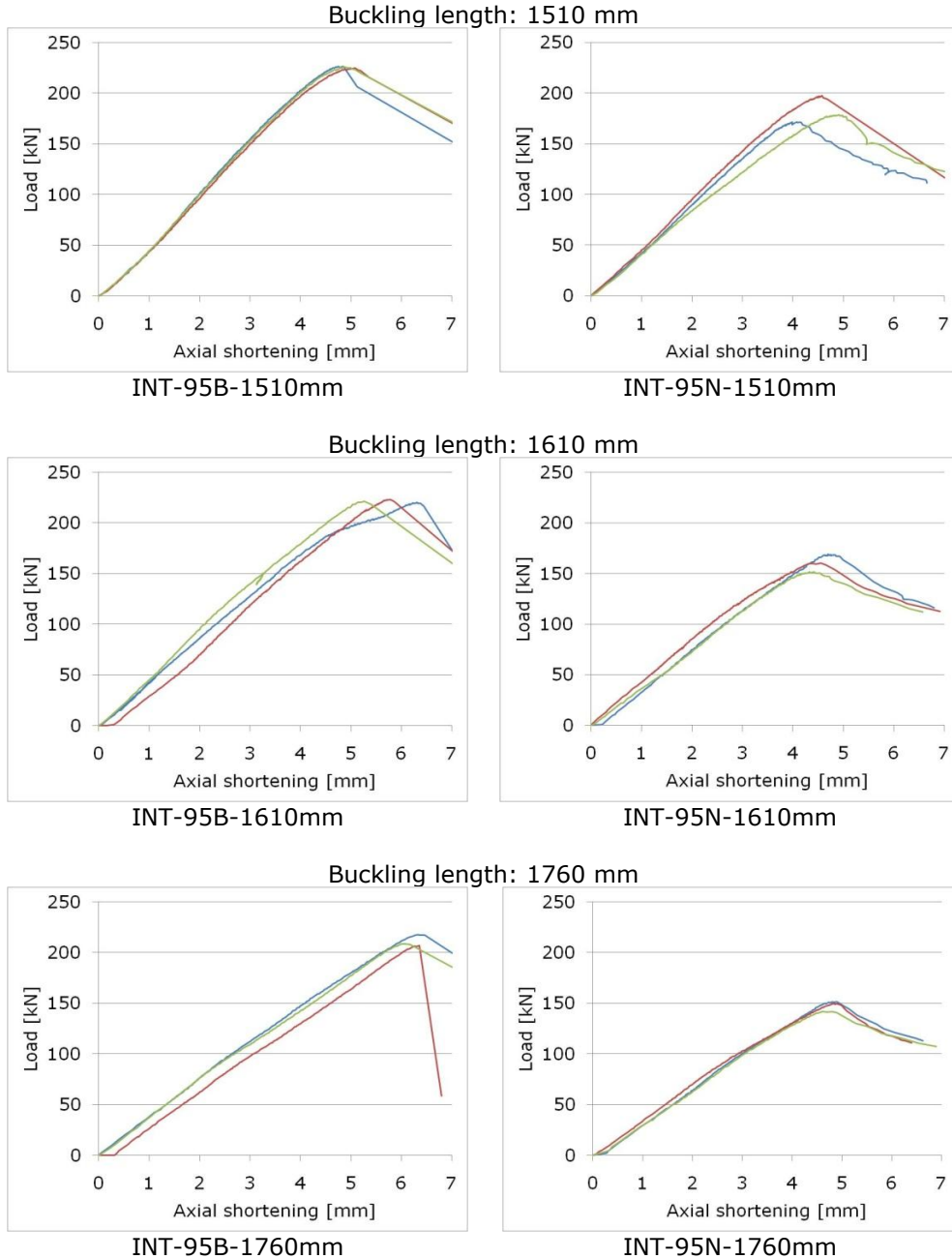


Fig. 3.34 Experimental load vs. axial shortening curves for RS95 interactive buckling specimens

144 **Experimental program – 3**

In Table 3.27 and Table 3.28 are presented the ultimate loads and failure modes for INT-95 interactive specimens, sections with perforations and without perforations.

Table 3.27 Failure load and failure mode for INT-95B specimens

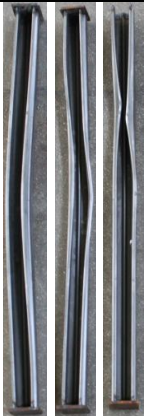





Buckling length [mm]	1510	1610	1760
Different failure mode			
Ultimate force [kN]	226.56 224.65 225.73	220.30 222.91 221.42	217.58 206.96 208.67

Table 3.28 Failure load and failure mode for INT-95N specimens

Buckling length [mm]	1510	1610	1760
Different failure mode			
Ultimate force [kN]	171.50 169.07 178.68	151.69 160.16 168.88	158.41 149.73 151.62

3.4 Tests summary and interpretation

3.4.1 Material properties

There were studied four types of cold formed profiles, RS125 and RS95, sections with and without perforations.

For cold formed profiles, the base material is obtained by cold rolling of thick steel strips, reducing the thickness to the desired value. By this process, the yielding and ultimate strength are increased, together with the ductility decrease. The ductility reduction is not usually a problem for thin walled sections, because the design of these members is usually elastic due to sectional and global instabilities. On the other hand, the yield strength increase can lead to an increase of the critical buckling load up to a value close to the section's elastic capacity.

In Table 3.29 are presented the mean values of base material properties for the two sections, RS125 and RS95.

Table 3.29 Mean value of base material properties

Section	Yield strength [N/mm ²]	Young modulus [N/mm ²]	Ultimate strength [N/mm ²]	Elongation at maximum load [%]
RS125	465.18	202941.28	537.40	15.50
RS95	461.41	207463.67	538.90	15.77

[190] In the cold forming process, the yield and ultimate strength are increased even more, the increase being dependent on the degree of forming. The corner areas are more affected by plastic deformations, hence a higher value for the yield and tensile strength.

Grumbach and Prudhomme [191] determined the yield limit increase due to cold forming for different cross-sections. In Fig. 3.35 are presented the yield strength of base material (f_{yb}), the increase in yield strength due to cold forming (f_y) and the average yield strength (f_{ya}).

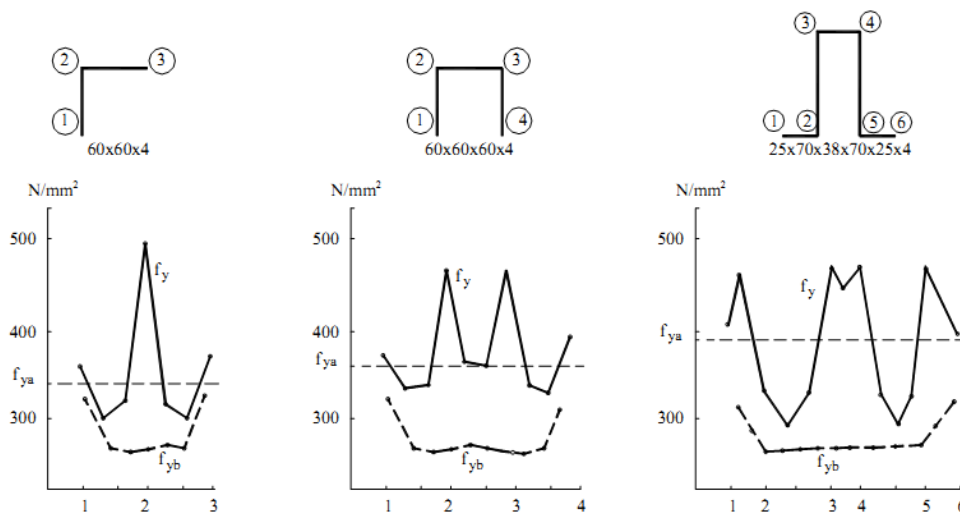


Fig. 3.35 Yield limit increase due to cold forming

A similar yield strength increase was determined for studied upright sections. In Fig. 3.36 is presented the average yield strength increase due to cold forming as percent of yielding strength.

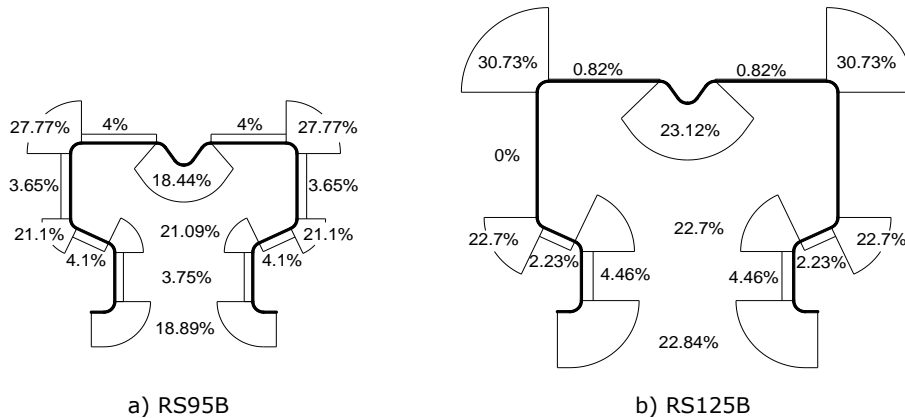


Fig. 3.36 Yield stress increase due to cold forming (% f_y)

Together with yield strength, the tensile strength is also affected by the cold forming process. In Fig. 3.37 is presented the average increase in ultimate strength for the two tested sections, RS95B (a) and RS125B (b).

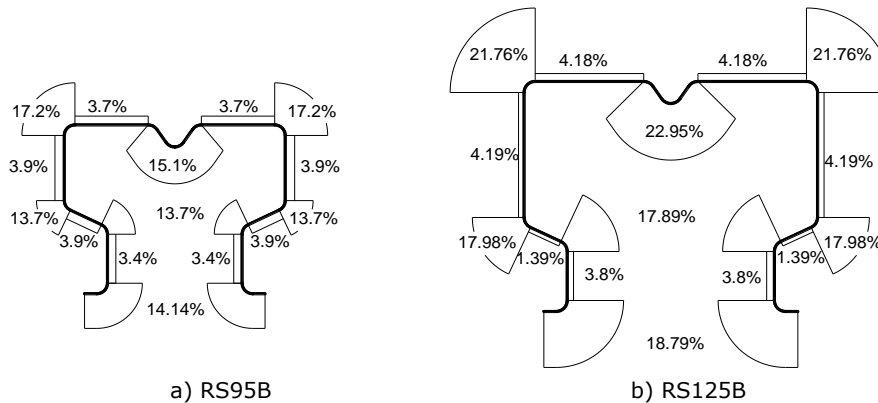


Fig. 3.37 Ultimate strength increase due to cold forming (% f_u)

The increase of yield and tensile strength and the ductility decrease are not the only consequences of the forming process. The residual stresses are an important effect of the forming process.

Because the experimental determination of residual stresses is a laborious and cumbersome procedure, Schafer and Pekoz [187] proposed an average residual stress distribution for cold formed sections

The proposition is based on a conservative approximation of residual stress magnitude. For a roll-formed section, 95% of the residual stresses are lower than $0.67f_y$ in a corner, lower than $0.43f_y$ in an edge stiffened element, and lower than $0.71f_y$ in a stiffened element. In Fig. 3.38 are presented the average residual bending stresses, proposed by Schafer and Pekoz [187] for a roll-formed (a) and for a press-braked section (b).

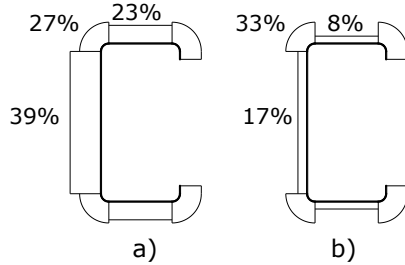


Fig. 3.38 Average bending residual stresses (% f_y)

Rahman and Sivakumaran [192] and Ungureanu [180] (Fig. 3.39) proposed similar codifications based on their research studies on cold formed press braked sections.

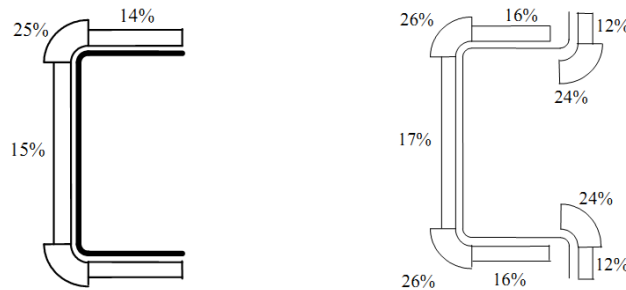


Fig. 3.39 Average residual stresses for press braked sections(%)

In Fig. 3.40 are presented the average residual stresses expressed in percent of f_y for studied sections; a) section RS125B and b) section RS95B. The diagrams are represented on the compressed side of the strip.

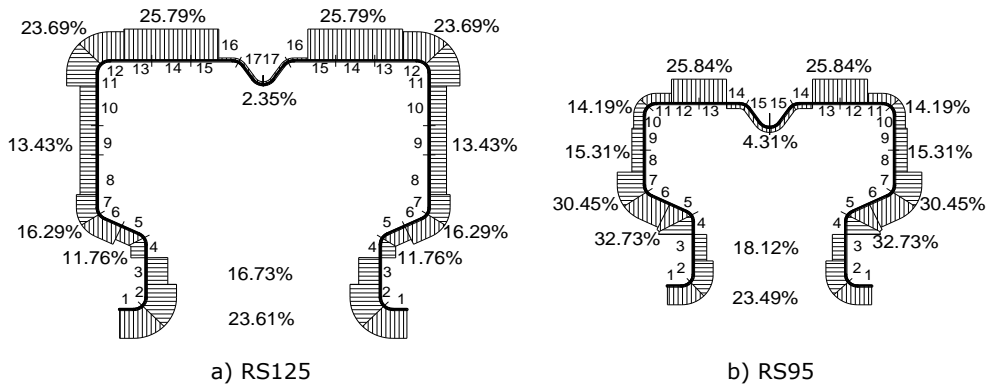


Fig. 3.40 Residual stress distribution (% f_y)

It can be observed that the residual stress distribution and values proposed by Schafer and Pekoz [187] are not exceeded.

3.4.2 Sectional and overall imperfections

The sectional imperfections, for STUB and DISTORTIONAL profiles were measured in three equidistant sections along the specimen's length. Also, loading and support eccentricities were measured for each tested profile. Taking into consideration the sectional imperfections proposed by Schafer and Pekoz [187] together with available measuring instruments, it was decided that only imperfection d_2 will be further considered.

Because of the complex geometry the measured geometry was compared with theoretical perfect geometry. All the measured imperfections are relative to the theoretical perfect section. The d_2 sectional imperfections were determined using the average of the values determined using Eq. (3.21) and (3.22).

$$d_{21} = \frac{(LB - LBL - LBR)_{exp} - (LB - LBL - LBR)_{perfect}}{2} \quad (3.21)$$

$$d_{22} = \frac{(LBM)_{exp} - (LBM)_{perfect}}{2} \quad (3.22)$$

LB, LBL, LBR and LBM are defined in Fig. 3.13 a).

Analyzing the measured values of sectional imperfections, d_2 it was further divided, as follows:

$$\text{if } \begin{cases} d_2 < 0 \rightarrow \text{SECTION CLOSES} \\ d_2 = 0 \rightarrow \text{SECTION IS PERFECT} \\ d_2 > 0 \rightarrow \text{SECTION OPENS} \end{cases}$$

The same d_2 sectional imperfection division is presented in Fig. 3.41.

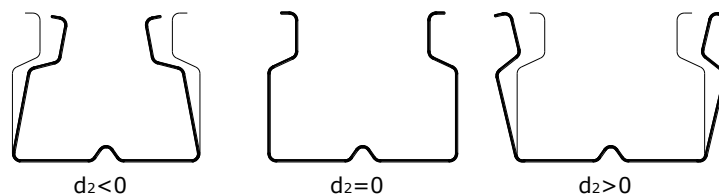


Fig. 3.41 Sectional imperfections

In Table 3.30 are presented the minimum (section closes) and maximum (section opens) values of the d_2 type sectional imperfections measured for different test types.

It must be specified that the measured values are absolute. For numerical simulations, it cannot be considered as d_2 type imperfection the absolute measured value. It must be taken into consideration that if the same value is measured along the specimen's length this will affect only the centroid position.

The absolute values of imperfections, for specific specimens, were further analyzed and processed. The d_2 imperfection considered for the numerical models was computed relative to the specimen ends.

Table 3.30 Sectional measured imperfections (d_2) for short specimens

Test type	Section	$d_2=t$ [mm]		
		Schafer and Pekoz [187]	Minimum [mm]	Maximum [mm]
STUB	RS125B	3.2	2.09	0.00
	RS125N	3.2	2.44	0.00
	RS95B	2.6	1.96	0.00
	RS95N	2.6	2.07	0.00
DIST	RS125B	3.2	1.51	0.00
	RS125N	3.2	2.49	0.00
	RS95B	2.6	0.59	1.19
	RS95N	2.6	2.71	0.00
UPRIGHT	RS125B	3.2	1.36	0.44
	RS125N	3.2	3.10	1.64
	RS95B	2.6	0.00	2.74
	RS95N	2.6	2.93	0.03

It can be observed that average values are in agreement with the values proposed by Schafer and Pekoz [187] .

The higher values of d_2 imperfections are due to (1) elastic spring-back of the sections without perforations (see Table 3.30, Upright RS95B) and (2) additional imperfections induced by the welding process.

Analyzing the values of sectional measurements for INTERACTIVE specimens, the sectional, d_2 , imperfection, relative to profile's end sections were computed. The final values for this type of imperfection are presented in Table 3.31.

Table 3.31 Sectional imperfections d_2 INTERACTIVE specimens

Test type	Section	$d_2=t$ [mm]		
		Schafer and Pekoz [187]	Minimum [mm]	Maximum [mm]
INTERACTIV	RS125B	3.2	0.10	1.21
	RS125N	3.2	0.32	1.45
	RS95B	2.6	1.08	1.38
	RS95N	2.6	1.06	1.38

In what concern the overall imperfections (bar deflection), the maximum recorded values of imperfections, were 1/1416 from the bar total length for INT-95 section, respectively 1/1651 for INT-125 section. The measured magnitude of these imperfection is similar to those available in scientific literature, related to this type of imperfections (overall sinusoidal bow imperfections), and are close to 1/1500 L mentioned in [188] by Bjorhovde. This imperfection magnitude of 1/1500 L corresponds to statistical mean of imperfections of carbon steel columns. Also it is important to mention that this imperfection (1/1500) is lower than the less conservative value proposed by ECCS Recommendation of L/1000 [189] and the one considered in case of European buckling curves. On the other hand, the corresponding tolerance accepted by EN 1090-2 [190] is L/750.

Together with geometrical imperfections there were also measured the support and loading eccentricities for all tested specimens.

The maximum values of eccentricities are presented in Table 3.32.

Table 3.32 Measured loading eccentricities

Section	Eccentricity [mm]			
	z axis		y axis	
	from	to	from	to
RS125B	-0.46	3.06	-0.37	0.96
RS125N	-0.08	3.10	-0.08	1.02
RS95B	-2.29	1.19	-0.84	1.06
RS95N	-3.00	2.65	0.06	1.07

It is very difficult to precisely determine the loading point relative to section centroid due to (1) imperfection of the end section, (2) weldings and (3) measurements relativity.

3.4.3 Compression tests results

The compression tests comprise four pallet rack upright sections, RS125 and RS95, with and without perforations summing a total number of 116 tests, summarized in Table 3.34.

The sections without perforations have been verified according to code provisions [13], formulae (3.1) and (3.2), to establish if the section is fully effective. The ratios were calculated for individual section elements supported on two edges and for elements supported on one edge.

The determined ratios respect the limits imposed by the norm for a section to be fully effective for both considered sections. In Table 3.33 are presented the highest values of the ratios, calculated for the studied upright sections, RS125 and RS95, sections without perforations.

Table 3.33 Local buckling ratios

Section	$\frac{b_p^1}{t}$	$1.28 \sqrt{\frac{E}{f_y}}$	$\frac{b_p^2}{t}$	$0.42 \sqrt{\frac{E}{f_y}}$
RS125	17.7	26.73	2.6	8.77
RS95	13.4	27.14	3.1	8.9

¹elements supported on two edges and ²elements supported on one edge

The stub column test is used to determine the effective area based on tests as described in paragraph 3.2. The effective area accounts the local buckling and the perforations.

Taking into consideration the results of stub column tests, used to observe the influence of local buckling and perforations on the compressive strength of short columns, it can be concluded that none of the tested sections, RS125 and RS95, with and without perforations, are prone to local buckling. For sections without perforations, this is in agreement with the European design code [13] provisions, briefly summarized in paragraph 3.2. (see Table 3.33).

Table 3.34 Experimental test review

Test type	Experimental failure load [kN]				
	RS125B	RS125N	RS95B	RS95N	
<i>Buckling length</i>	<i>510 mm</i>	<i>510 mm</i>	<i>410 mm</i>	<i>410 mm</i>	
STUB		413.28		279.82	
		407.81		276.99	
		400.85		284.28	
		453.90	350.68	274.33	
		479.43	346.44	278.78	
		463.69	346.23	278.63	
		449.52	346.63	281.63	
		485.38	354.30	278.68	
		487.05	338.88	279.00	
			396.51	277.92	
		395.91	277.81		
		406.05	283.42		
Samples tested	6	12	6	12	
<i>Buckling length</i>	<i>1200 mm</i>	<i>1200 mm</i>	<i>1200 mm</i>	<i>1200 mm</i>	
UPRIGHT		347.26		207.18	
		363.48		215.72	
		350.79	270.35	209.87	
		339.09	270.49	211.29	
		344.46	272.06	206.45	
		386.72	279.65	213.24	
		369.12	279.65	223.33	
		386.90	269.83	216.30	
		373.41	350.45	208.90	
		382.59	340.54	209.91	
		345.41			
Samples tested	5	10	5	10	
<i>Buckling length</i>	<i>670 mm</i>	<i>710 mm</i>	<i>590 mm</i>	<i>610 mm</i>	
DISTORTIONAL		422.42		379.90	
		414.33	325.10	262.67	
		432.69	315.36	259.67	
		420.02	328.36	260.50	
		428.28	387.43		
Samples tested	5	5	3	3	
<i>Buckling length</i>	<i>2110 mm</i>	<i>2110 mm</i>	<i>1510 mm</i>	<i>1510 mm</i>	
INTERACTIVE		286.65	226.56	171.50	
		317.89	224.65	169.07	
			225.73	178.68	
		<i>2310 mm</i>	<i>2310 mm</i>	<i>1610 mm</i>	<i>1610 mm</i>
		287.34	276.15	220.30	151.69
		302.29	274.22	222.91	160.16
		318.29	298.07	221.42	168.88
		<i>2510 mm</i>	<i>2510 mm</i>	<i>1760 mm</i>	<i>1760 mm</i>
		298.22	265.44	217.58	158.41
		285.71	269.71	206.96	149.73
		244.69	208.67	151.62	
Samples tested	2, 3, 2	3, 3, 3	3, 3, 3	3, 3, 3	

In order to quantify the effects of perforations and local (sectional) buckling the effective area and the equivalent thickness were determined based on stub column tests. (Table 3.35)

Table 3.35 Effective areas and equivalent thickness for STUB column specimens

Section	Average test load [kN]	f_{ya} [N/mm ²]	Effective area [mm ²]	Equivalent thickness [mm]	Reduction %
RS125B	469.83	501.29	937.30	2.70	-15.64%
RS125N	403.70		805.37	2.32	-27.52%
RS95B	347.19	500.15	694.17	2.60	0.00%
RS95N	279.27		558.37	2.10	-19.40%

The effective area presented in Table 3.35 is informative. The procedure defined by EN15512:2009 takes into account the nominal yield strength, the observed yield strength and the thickness variation together with the standard deviation. Since this is not the main objective, the procedure will not be further detailed.

It can be observed that for RS95 section without perforations, the maximum test load is even bigger than the theoretical section capacity, thus no thickness reduction. For RS125 section the thickness reduction is significant. This reduction reflects (1) the effect of perforations and (2) the effect of sectional buckling. Even if the observed failure mode was the distortion of the section, the length is not enough to determine the critical distortional buckling load.

Using CUFSM [183], [131] software, it can be observed that the failure of the sections is mainly due to distortional buckling. The buckling mode classification, according to CUFSM is presented in Fig. 3.42 and Fig. 3.43 for RS125 section without and with perforations and in Fig. 3.44 and Fig. 3.45 for RS95 section without and with perforations (using t_{eq} , experimentally determined). For all analysed sections, no local minimum corresponding to local buckling was observed on the resulted buckling curves.

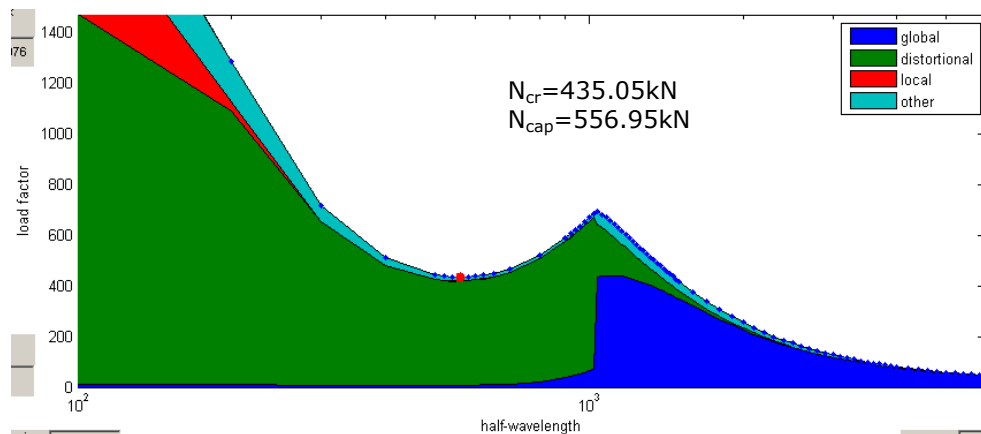


Fig. 3.42 Modal classification for RS125B section

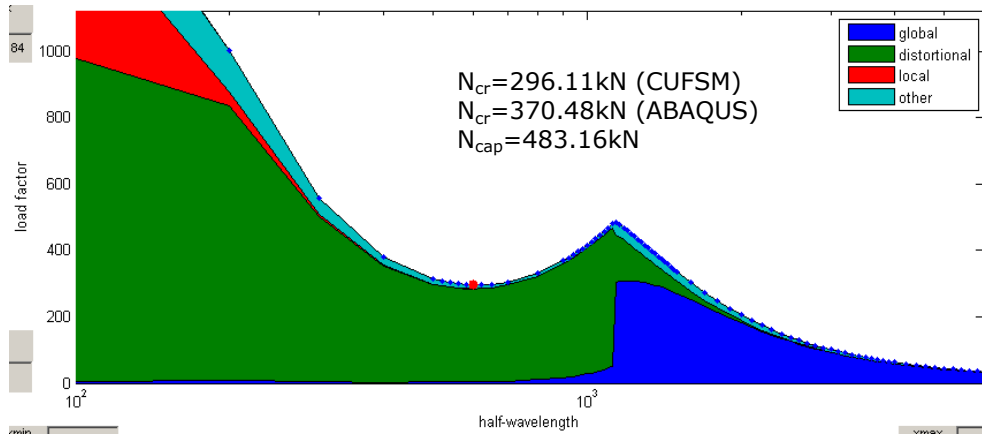


Fig. 3.43 Modal classification for RS125N section (t_{eq} experimental)

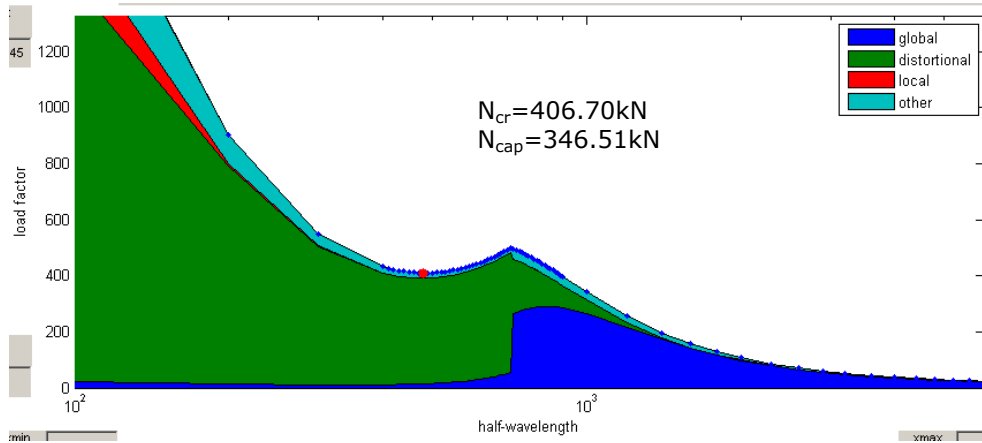


Fig. 3.44 Modal classification for RS95B section

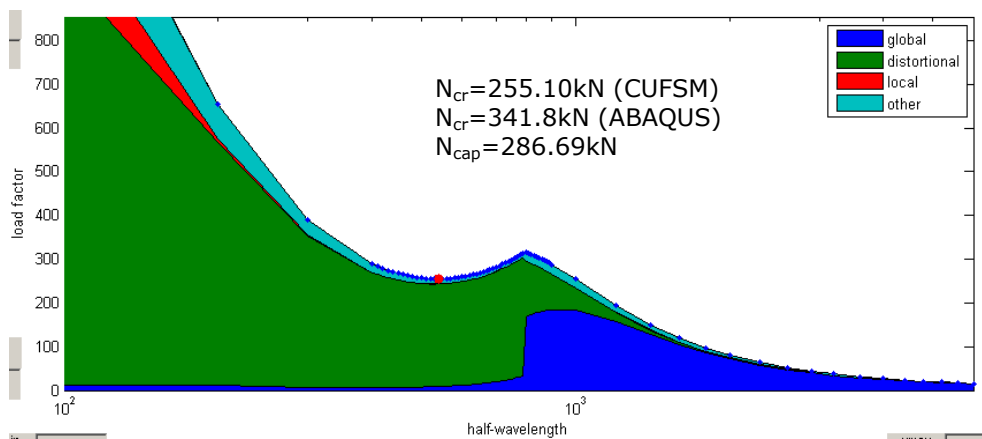


Fig. 3.45 Modal classification for RS95N section (t_{eq} experimental)

For RS125 sections, the dominant failure mode is a symmetric distortional buckling of the section. The optimisation of the section with respect to local buckling (adding supplementary stiffeners to the section) arises, in this case, a distortional problem.

For RS95 sections, with and without perforations, the axial load capacity (squash load) is less than the distortional buckling critical load (Fig. 3.44 and Fig. 3.45). Even if, usually, the process of optimisation of a section with respect to local buckling resistance arise a distortional problem, for this particular section dimensions, the stiffeners increased the critical sectional buckling load (local and distortional) to a value higher than the axial load capacity. The STUB column test results show that the RS95 section fails when reaching the axial load capacity (squash load), even if in some cases, the failure mode seems to be distortional buckling.

For neither of the studied sections, the local buckling was not the expected failure mode. The sections were verified in accordance with the European design code [13] provisions, resulting a full effective area. The failure mode observed for experimental stub column tests confirm the results of these verifications.

The experimental program continued with tests on uprights, with the length equal with the distance between two subsequent nodes, to determine the influence of the distortional buckling mode on the axial load capacity of the upright section.

For both RS125 sections, with and without perforations, the observed failure mode was symmetrical distortion of the section. The failure loads are comparable with the values obtained in distortional buckling test.

For RS95 sections, the failure occurred due to overall buckling, flexural about minimum inertia axis or flexural-torsional buckling.

European norm EN15512, does not foresees experimental tests on upright having the critical length for distortional buckling. The critical length is characteristic for each specific cross sectional shape and, in case of perforated members, is difficult to be determined. To experimentally determine the distortional buckling capacity of the two studied sections, the experimental program was extended to include compression tests on rack upright specimens having the critical length for distortional buckling.

The half-wave length for distortional buckling was determined using FEM and cFSM analyses and is summarized in Table 3.16 for the studied sections, with and without perforations.

In Table 3.36 are presented, comparatively, the distortional critical buckling load obtained using LBA and the sections squash load.

Table 3.36 Distortional critical buckling load and section's capacity

Section	RS125B	RS125N	RS95B	RS95N
Length [mm]	560	600	480	500
Squash load [kN]	556.95	483.16	346.51	286.69
Distortional buckling load [kN]	429.14	370.48	402.50	340.78

For RS125 sections, analytical determined distortional buckling load is smaller than the section's axial load capacity. It can be noted that the results of stub column tests are in between the critical buckling load and axial load capacity of the section.

To determine the critical buckling length for perforated sections an equivalent thickness can be used. Two methods were used to determine the equivalent thickness e.g. (1) using the experimental data and (2) the formula proposed by Davies [176] .

When using the equivalent thickness calculated using experimental data, the critical distortional buckling load is severely underestimated for both, RS125 and RS95 sections. For the case where the equivalent thickness was determined using the analytical method proposed by Davies [176] , the critical distortional buckling load is accurately determined.

The effective area with respect to distortional buckling is presented in for upright test specimens and for specimens with the critical length for distortional buckling.

Table 3.37 Effective areas for distortional and upright tests

Test type	Section	Average test load [kN]	f_{ya} [N/mm ²]	Effective area [mm ²]	Equivalent thickness [mm]	Reduction %
Upright	RS125B	379.75	501.29	757.55	2.18	-31.82%
	RS125N	347.31		692.83	2.00	-37.64%
	RS95B	272.48	500.15	544.80	2.04	-21.36%
	RS95N	212.22		424.31	1.59	-38.75%
Distortional	RS125B	423.55	501.29	844.92	2.43	-23.95%
	RS125N	388.35		774.70	2.23	-30.27%
	RS95B	322.94	500.15	645.69	2.42	-6.80%
	RS95N	260.95		521.74	1.96	-24.69%

The thickness reduction resulted from the upright test is significantly higher than the reduction resulted from the tests done for specimens having the critical distortional buckling length. For RS95 specimens, the observed failure mode for upright specimens was mainly global buckling. The equivalent thickness presented in Table 3.37 is purely informative.

Furthermore, it can be said that the results corresponding to upright tests does not account for distortional buckling alone and are influenced by a instability coupling phenomenon.

For INTERACTIVE buckling specimens the length was calibrated via ECBL approach [28] using the section's distortional capacity obtained numerically. After calibrating a FEM model, the sections were simulated without geometric imperfections and loading eccentricities.

The ECBL approach [28] can be used to determine the erosion as result of coupling effect and/or imperfections. There are three available methods that allow the resolve this problem e.g. (1) analytical approach, based on the stability theory, (2) numerical approach, based on FEM or FSM models that replicate the behaviour of studied member in the coupling point and (3) experimental approach.

Considering the experimental distortional test results as the sections distortional capacity, the resulting erosion is due to the coupling effect only. In Table 3.38 are summarized the experimentally obtained distortional capacities used to determine the erosion as a result of instability coupling.

Table 3.38 Experimental distortional failure loads and section strength

Section	RS125B	RS125N	RS95B	RS95N
Length [mm]	560	600	480	500
Ultimate failure load [kN]	423.55	388.35	322.94	260.95

The ultimate failure load was considered to be the average value obtained from the experimental program. This approach was considered with the purpose to obtain the theoretical point of the interaction of two simple instabilities i.e. distortional and flexural buckling, together with the corresponding value of erosion.

In Table 3.39 and Table 3.40 are presented the failure forces for interactive specimens, together with the erosion coefficients computed based on experimental approach for RS125 sections with and without perforations and RS95 sections respectively.

For the computing of erosion coefficient, the area used for perforated sections was considered to be the minimum cross section area (see Table 3.16) in the section with the maximum reduction due to perforations.

Table 3.39 Erosion coefficient for RS125 sections based on experimental approach

Section/length	Failure load [kN]	Erosion coefficient ψ	Average erosion coefficient
INT-125B/2110	286.65	0.246	0.223
INT-125B/2110	317.89	0.190	
INT-125B/2310	287.34	0.245	
INT-125B/2310	302.29	0.218	
INT-125B/2310	318.29	0.189	
INT-125B/2510	298.22	0.225	
INT-125B/2510	285.71	0.247	0.225
INT-125N/2110	296.73	0.190	
INT-125N/2110	296.91	0.189	
INT-125N/2110	293.63	0.196	
INT-125N/2310	276.15	0.232	
INT-125N/2310	274.22	0.236	
INT-125N/2310	298.07	0.187	
INT-125N/2510	265.44	0.254	
INT-125N/2510	269.71	0.246	
INT-125N/2510	244.69	0.297	

Using the interaction types defined by Gioncu [140] in order to classify the interaction class based on obtained erosion coefficient, it can be observed that for INT-125 specimens the interaction is classified as medium, for both sections with and without perforations ($0.1 \leq \psi \leq 0.3$).

Table 3.40 Erosion coefficient for RS95 sections based on experimental approach

Section/length [mm]	Failure load [kN]	Erosion coefficient	Average erosion coefficient
INT-95B/1510	226.56	0.278	0.299
INT-95B/1510	224.65	0.284	
INT-95B/1510	225.73	0.281	
INT-95B/1610	220.30	0.296	
INT-95B/1610	222.91	0.289	
INT-95B/1610	221.42	0.293	
INT-95B/1760	217.58	0.304	
INT-95B/1760	206.96	0.335	
INT-95B/1760	208.67	0.330	
INT-95N/1510	171.50	0.312	
INT-95N/1510	169.07	0.320	
INT-95N/1510	178.68	0.287	
INT-95N/1610	151.69	0.381	
INT-95N/1610	160.16	0.352	
INT-95N/1610	168.88	0.321	
INT-95N/1760	158.41	0.358	
INT-95N/1760	149.73	0.388	
INT-95N/1760	151.62	0.381	

The same classification has been done for RS95 sections. For RS95 section without perforations the erosion coefficient categorize the section in moderated interaction class ($0.1 \leq \psi \leq 0.3$), while for perforated section the erosion factor corresponds to a strong interaction ($0.3 \leq \psi \leq 0.5$) class.

The classification is in accordance with the classification done in [180] for thin walled section columns, which include them in medium and strong interaction class.

It can be noted that for both upright sections the erosion is increased due to presence of the perforations.

3.5 Concluding remarks

Using the CEMSIG testing facility, there were tested two rack upright sections, RS125 and RS95, with and without perforations summing up a total number of 116 specimens. The purpose was to experimentally determine the buckling strength of cold formed steel sections applied in pallet rack structures.

There were experimentally determined the mechanical properties of base material and the change of these properties due to cold forming process, together with the buckling strength of cold formed section with respect to simple buckling modes e.g. local and distortional and the buckling strength with respect to coupled instabilities i.e. interaction of distortional and Euler bar instability mode.

The uneven increase of yielding strength across the cross-section, together with the residual stresses that occur as a side effect of cold forming, make the study of cold formed sections a demanding task.

There are numerous researchers that proposed various formulae to take into account these modifications. Various codifications for yields strength increase due to

cold forming and residual stresses distribution were proposed by Schafer and Pekoz [187], Rahman and Sivakumaran [192] and Ungureanu [180] for thin walled profiles, cold rolled or press braked formed.

In previous paragraph were presented the yield and tensile strength distribution due to cold forming for two pallet rack upright sections without perforations. It can be observed a high increase of yield and ultimate strength due to cold forming process presented in Fig. 3.36 and Fig. 3.37. Also, the flexural residual stresses were determined for the same sections without perforations. They were determined using a method proposed by Rondal [178]. The method allows the determination of flexural residual stresses, on both interior and exterior faces of cold formed profiles, by direct geometric measurements of the curvature of a strip cut off from a profile. The strip curvature was determined using a contactless optical measuring system [179].

The method admits the hypothesis that the membrane residual stresses are zero, assuming a linear variation through the thickness. In reality, the value of membrane residual stresses is not zero. For thin walled sections, the value of membrane residual stresses is small compared with the value of flexural residual stresses.

Special care must be taken when cutting the strips, because high residual stresses bend the strips and the cuttings tend to be unparallel.

Another key aspect to consider when studying the behaviour of cold formed sections is the geometric imperfections. Dubina and Ungureanu [134] studied the influence of size and shape of sectional geometrical imperfections on the ultimate buckling strength of plain and lipped channel sections, both in compression and bending.

Schafer and Pekoz [187] also proposed a set of maximum magnitudes for sectional imperfections of type 1 and 2.

The maximum magnitudes of sectional geometric imperfections, type 2, for the studied sections, RS125 and RS95, presented in Table 3.30 and Table 3.31 are within the limits suggested by Schafer and Pekoz [187].

The overall imperfections, bow and torsional, measured for INTERACTIVE specimens, were 1/1416 from the bar total length for RS95 section, respectively 1/1651 for RS125 section. The measured magnitude of these imperfection is similar with those available in scientific literature, related to this type of imperfections (overall sinusoidal bow imperfections), and are close to 1/1500 L mentioned in [188] by Bjorhovde. This imperfection magnitude of 1/1500 L corresponds to statistical mean of imperfections of carbon steel columns. Also it is important to mention that this imperfection (1/1500) is lower than the less conservative value proposed by ECCS Recommendation of L/1000 [189] and the one considered in case of European buckling curves. On the other hand, the corresponding tolerance accepted by EN 1090-2 [190] is L/750.

For the case when the base and cap plates are welded to the end of the specimens, special care must be taken to align the centroid of the section and the loading point. The welds can distort the end section of the specimen leading to additional sectional imperfections and load eccentricities due to cool down.

The results of stub column testing revealed that none of the tested sections are sensitive to local buckling.

For RS125 sections, the observed failure mode i.e. symmetric distortion of the section was the expected failure mode, since the critical value of distortional buckling load was lower than the section's squash load. The wall slenderness, even

if reduced due to optimisation for local buckling, lead to a distortional buckling failure.

For RS95 section, the increased section compactness lead to a failure due to reach of capable axial capacity (squash load). It can be observed that the distortional buckling critical load for RS95 sections, with and without perforations, is higher than the squash load.

For distortional buckling test (tests on uprights with critical length for distortional buckling), the test results are as expected. The RS125 failed by distortional buckling, at loads comparable with the load predicted by numerical analyses.

Even if the failure mode, for specific RS95 specimens, can be categorized as distortional failure mode, the maximum force was corresponding rather to the squash load, not to critical distortional buckling load. Due to the fact that the RS95 sections are compact, their sectional capacity is defined by the squash load and not reduced by the local or distortional buckling.

For the upright testing, the results confirmed once again the results on short columns (STUB and DISTORTIONAL) results. Both of the DIST-125 sections failed by distortional buckling (two halfwaves), while for DIST-95 specimens, the failure mode can be defined as a global buckling (flexural or flexural-torsional) for both sections, with and without perforations.

As mentioned before, for section RS125 the section's optimisation for local buckling made the section vulnerable to distortional buckling. This is not the case of RS95 sections. Due to increased number of folds that reduced the wall slenderness, the axial capacity is defined by the squash load.

The study of interactive buckling in the case of thin walled sections is a challenging task. The research regarding interactive buckling for thin walled sections is usually focused on local – global interaction. Nowadays, together with the technological advances, the cold formed sections became more and more stiffened in order to remove local instabilities. This sectional optimization to remove a local instability mode creates a distortional problem.

Due to complicated sectional shapes and cumbersome analytical procedures, FEM or FSM based software packages are usually used to determine the distortional capacity of complicated cold formed sections.

To study the interactive sectional - overall buckling, a correct identification of the sectional mode is imperative. Since distortional buckling capacity of complex sectional shapes i.e. perforated rack uprights cannot be determined analytically all design codes request experimental tests.

Based on ECBL approach [28] one can study the coupling effect of sectional and overall instabilities.

The tests results for slender members of the buckling length calibrated using the ECBL approach [28] within the distortional-overall interactive range, confirm the applied procedure. It is also confirmed the fact that the maximum erosion occurs in the coupling point.

4 NUMERICAL STUDIES

4.1 Introduction

In order to expand the experimental presented in previous chapter study and take into consideration different geometric and material imperfections and combinations of them, a detailed FE (Finite Element) model was developed. On this purpose, the commercial software package ABAQUS 6.7.1 [115] was used to build appropriate FE models for local, distortional and interactive buckling members. The models were calibrated and validated against the experiments.

Following are described the numerical simulations that were run for the four considered sections, RS95x2.6 and RS125x3.2, with and without perforations. All FE simulations were done using the software package ABAQUS 6.7.1.[115]

At the end, interpretation of sensitivity to imperfections in terms of erosion of the theoretical buckling strength and their influence on the corresponding value of α imperfection factor in the European buckling curves are presented.

4.2 Geometrical characteristics of cross-section

A key aspect, when analysing thin walled sections, is represented by the sectional properties. Due to the fact that usual cold formed sections have complex cross-sectional shapes the computation of geometric properties is a cumbersome procedure. In addition to this, for pallet rack upright sections, the perforations make the calculus even more complex.

It is usual practice to approximate the round corners of such a section with right corners in order to simplify the calculus. In accordance with the European pallet rack design code [13] provisions, the following section properties may be calculated on the assumption of sharp corners with no reduction for perforations or for the effective widths of elements of the cross-section in compression:

I_T - St Venant torsion constant of the gross cross-section;

I_w - warping constant of the gross cross section;

y_0 - distance along the y-axis from the shear centre to the centre of gravity of the gross cross-section;

i_y, i_z - radii of gyration of the gross cross-section about the y and z axes respectively;

i_0 - polar radius of gyration of the gross cross-section about the shear centre

Further, the pallet rack design code refers EN1993-1-3 for determining the influence of round corners on other sectional properties.

In order to limit the approximations and to avoid any computational inaccuracies, a CAD software was used to determine the sectional properties for studied sections, accounting for roundness of corners.

For perforated members in compression, the effective design area is determined using the STUB column test. AS 4084 [168] and RMI [169] use an approach based on a form factor (Q), computed using Eq. (4.1), to determine the effective area for perforated sections in compression.

$$Q = \frac{P_u}{A_{net,min} \cdot f_y} \quad (4.1)$$

where P_u is the ultimate compressive strength of the stub column determined by test, f_y is the actual yield strength and $A_{net,min}$ is the minimum cross-sectional area obtained by passing a plane through the column normal to the axis of the column. The value of (Q) form factor is limited to 1.

The European design code [13] adopts a straight foreword method to determine the effective area in compression. (Eq. (4.2))

$$A_{eff} = \frac{R_k}{f_y} \quad (4.2)$$

where R_k is the characteristic failure load and f_y is the yield strength.

Since the main objective of the present study is to limit the experimental testing program by reducing to a minimum the required testing, for cross-sectional resistance of the perforated section the minimum section properties will be further used. For global calculations of internal forces, in accordance with the European design code [13] the gross sections properties were used.

The European design code [13] indicate that the effective area considered in design of perforated sections in compression should be determined by tests i.e. STUB column tests. Also, it stipulates that some upright sections have arrays of perforations which, because of their sizes, number or disposition can cause a significant reduction in the moment of inertia of the section. In such cases the designer should be aware of the implications and an appropriate reduced moment of inertia should be used in the global calculations.

Even if the norm inform about this shortcoming, it does not provide a straight foreword solution to it.

4.3 Model calibration and validation

The first step, in FE simulations, was to calibrate and validate a numerical model based on experimental tests.

In order to obtain a model able to replicate the behaviour observed in experimental tests, the following were taken into account:

- measured imperfections (d_2 type imperfections). For this type of imperfection, it was considered the distortional mode obtained from a buckling analysis, scaled to measured imperfection. The measured imperfections confirmed a distortional buckling mode initial imperfection.
- real material behaviour. It is known that the cold forming process modifies the material behaviour, especially in the corners where the deformation due to cold forming is significantly higher. The material behaviour curves for RS125 section are presented in Fig. 4.1. The material was considered to have a perfectly plastic behaviour after the tensile strength point.
- the presence of residual stresses was modelled as initial stress condition using the real residual stress distribution. (see Chapter 3).

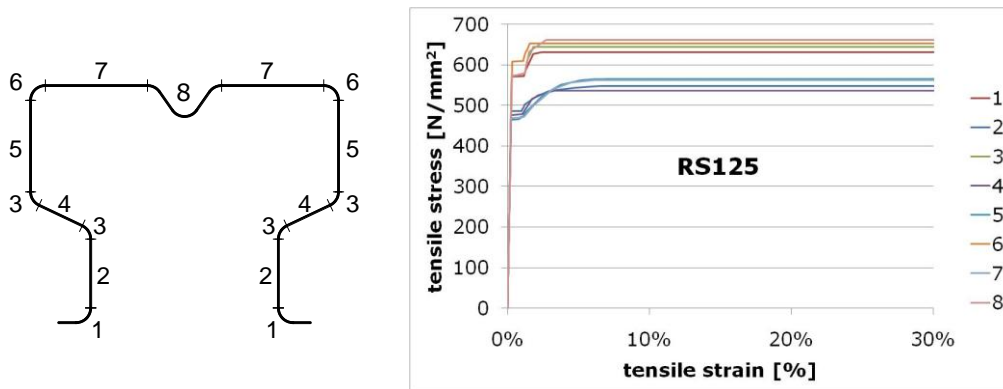


Fig. 4.1 Material behaviour curves defined in FE models for RS125 models

The numerical model was created using 3D deformable shell shape, created by extrusion. A homogeneous shell continuum section using a Simpson integration rule on thickness with 5 points was used.

A RIGID BODY with PINNED nodes constrained was created for each end, in order to model the end assembly. The rigid body constraint allows one to constrain the motion of regions of the assembly to the motion of a reference point. The relative positions of the regions that are part of the rigid body remain constant throughout the analysis. Constraining the end region to the reference point motion, restrained the translational DOFs of the section and, in the same time, allowed the point's rotation. The reference point position was considered in the sections gravity centre, 55mm outside the profile. The 55mm distance accounts the end plates (10mm), the pressure pads (30mm), the ball indentation (-5mm) and half of the ball bearing (40/2=20mm).

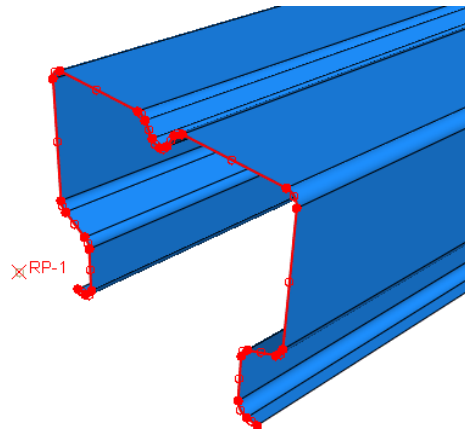


Fig. 4.2 End constrains

In order to create a reliable mesh and to account the holes present along the specimen's length a mesh size of about 5x5mm was chosen. The elements were constrained to a rectangular form and a structured mesh was used.

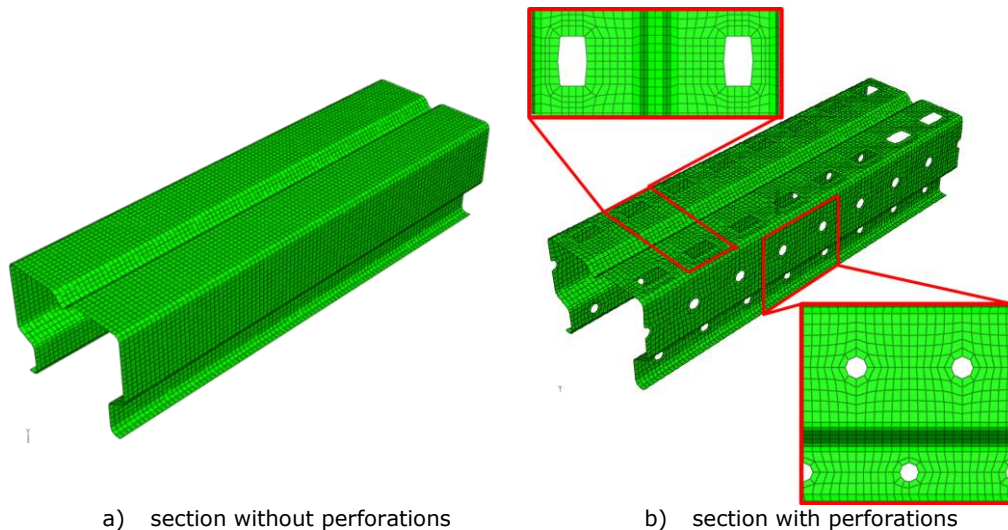


Fig. 4.3 Mesh details for RS125 STUB specimen

To investigate the influence of different element types i.e. S4, S4R, S8R, S8R5 (ABAQUS codification), geometric imperfections, material properties i.e. Young modulus, yield stress and/or residual stresses on ultimate failure load, a parametric study was conducted on RS125 STUB column specimen.

According to [196] the elements are defined as follows:

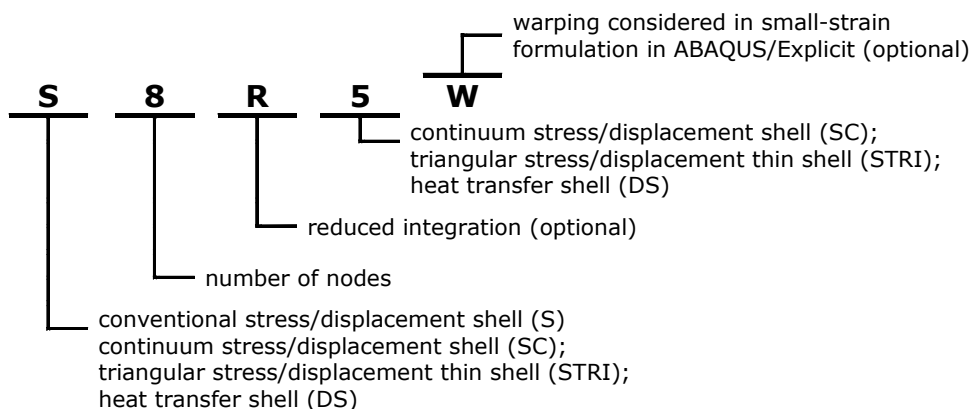
S4 is a 4-noded doubly curved general-purpose shell element, with finite membrane strains;

S4R is a 4-noded doubly curved general-purpose shell element with reduced integration, hourglass control and finite membrane strains;

S8R is an 8-noded doubly curved thick shell, reduced integration

S8R5 is an 8-node doubly curved thin shell with reduced integration, using five degrees of freedom per node

For Abaqus analyses, the element codification respects the following schema:



For numerical simulations, the specimen was considered pinned at one end and simply supported at the other. For the pinned end, all three translations together with the rotation about the longitudinal profile's axis were restrained, while the rotations about maximum and minimum inertia axis were allowed. For the simply supported end, the sectional translations and the rotation about longitudinal profile's axis were restrained, while the rotations about major and minor inertia axis together with longitudinal translation were allowed.

The pinned end was considered to replicate the end support of the real test specimen, while the simply supported end was considered to reproduce the loading machine end, allowing for direct force/displacement specification. For test specimens, the rotation about longitudinal axis was prevented by friction, while for numerical model the rotation was restrained, in order to remove rigid body displacements (rotations in this case).

The FE analysis was conducted in two steps:

- step 1: an eigen buckling analysis (LBA), in order to find a buckling mode or combination of buckling modes, affine with the measured imperfections. A unitary force was applied in the reference point of the simply supported end constraint and the resulting buckling modes were exported as deformed geometry.
- step 2: After imposing the initial geometric imperfection, obtained as a linear combination of eigen buckling modes from previous step, a GMNIA analysis with arc-length (static, Riks) solver was used to determine the profiles capacity. A unit displacement was applied at the simply supported end in order to simulate a displacement controlled experimental test.

In Table 4.1 are presented the considered imperfections, together with the load eccentricities used for numerical model calibration. The multiplication factor for distortional buckling mode, i.e. IMP, considered as initial imperfections, was determined using Eq. (4.3).

Table 4.1 Measured imperfections and load eccentricities for RS125B stub specimen

Specimen	Imperfection d2 [mm]		Loading eccentricities [mm]	
	LBM	LB		
RS125B	End 1	-1.44	-1.51	y axis 0.43
	Mid	-3.98	-4.28	z axis 1.22
Stub 1	End 2	-1.39	-1.25	y axis -0.37
	IMP	1.37		z axis 0.42

where LBL and LB are the sectional imperfection measurements presented in previous chapter.

$$Imp = \frac{\frac{End_1 + End_2}{2} - Mid}{2} \quad (4.3)$$

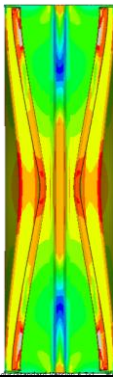
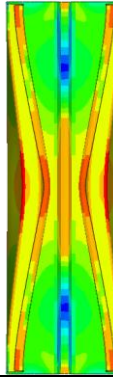
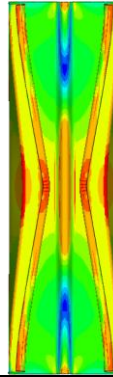
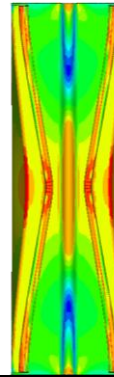
The imperfections were applied in accordance with the positive axis notations in the Fig. 3.14.

The factor used for scaling the model was considered the average value of the two calculated imperfection factors presented in Table 4.1.

In Table 4.2 are presented the failure loads obtained numerically for the considered element types. For these analyses, the material behaviour i.e. yielding

stress distribution across the section and the Young's modulus value were those experimentally obtained.

Table 4.2 Ultimate load and analysis time per element type

Element type	S4	S4R	S8R5	S8R
Observed failure mode				
Ultimate load [kN]	463.06f	461.70	463.02	463.01
Analysis time ¹	0:01:40	0:01:38	0:05:29	0:04:04
Analysis time ²	0:05:46	0:04:00	0:27:04	0:19:14
Total time	0:07:26	0:05:38	0:32:33	0:23:18

¹buckling analysis time and ²static Riks analysis time

It can be observed (see Table 4.2 and Fig. 4.4) that for this specific type of analysis and section, the influence of element type is insignificant. It can be noted that the numerical model behaviour is no influenced by the element type.

Based on these observations, the S4R finite element type was chosen for further analyses. S4R is a robust, general-purpose element that is suitable for a wide range of applications. It is a 4-noded doubly curved quadrilateral, stress/displacement shell element with reduced integration and a large-strain formulation that have 6 DOFs per node.

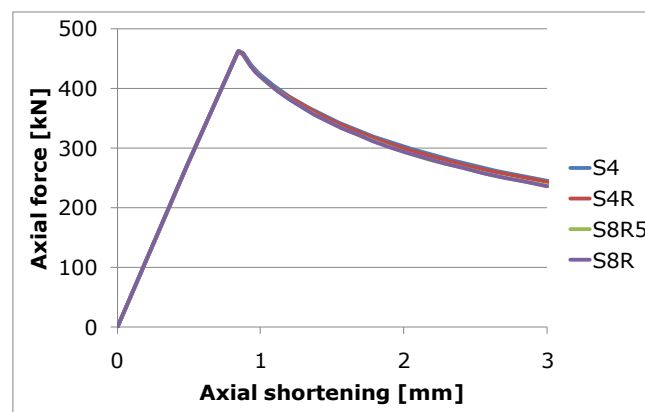
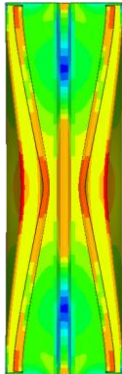
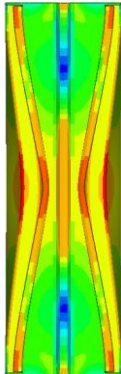



Fig. 4.4 Behaviour curves for different FE types

Following, the effect of residual stresses was considered. The residual stresses were modelled as initial stress state (*INITIAL CONDITIONS – ABAQUS codification) for studied section. As mentioned before, for shell integration method, the Simpson integration rule with five integration points was used. The method used to describe the initial stress state allows for direct specification of stress value for each individual integration point.

In Table 4.3 are presented, comparatively, the numerically obtained values of ultimate loads for the model with no residual stresses considered on section, the model with the residual stresses determined experimentally and considered in the numerical model as initial stress conditions and the experimentally tested specimen.

Table 4.3 Ultimate loads for different imperfection factors

Element type	no residual stresses	with residual stresses	Experimental test
Observed failure mode			
Ultimate load [kN]	461.7	448.63	453.90
Difference [%]	+1.72	-1.16%	

It can be seen that the influence of residual stress is small (less than 3%). Since the effects of residual stresses are not the primary objective of the present study, for further analysis, their effects will be ignored, unless otherwise specified.

It is known that Young's modulus value is difficult to be obtained experimentally. In the same time, it is not common for an extended study regarding the yield stress distribution on a thin walled section to be conducted.

A parametric study regarding the material properties i.e. Young's modulus and real yield stress distribution was done. In Table 4.4 are presented the considerate cases together with the numerically obtained ultimate forces.

Table 4.4 Cases considered for parametric analysis

Case no.	Young's Modulus [N/mm ²]	f_y [N/mm ²]	Residual stresses	Geometric imperfection	Load ecc.	Ultimate force
1	202941	exp¹	yes	yes	yes	448.634
2	202941	exp ¹	Yes	yes	no	460.936
3	202941	exp ¹	Yes	no	yes	526.804
4	202941	exp ¹	no	no	yes	531.583
5	202941	exp ¹	no	no	no	541.873
6	202941	exp ¹	no	yes	yes	461.701
7	202941	f_{va}^2	yes	yes	yes	442.382
8	202941	f_{va}^2	no	yes	yes	455.163
9	210000	f_{va}^2	yes	yes	yes	444.352
10	210000	f_{va}^2	no	yes	yes	457.51
11	202941	f_{yb}^3	yes	yes	yes	415.026
12	202941	f_{yb}^3	no	yes	yes	426.854
13	210000	f_{yb}^3	yes	yes	yes	417.092
14	210000	f_{yb}^3	no	yes	yes	428.657
exp	-	-	-	-	-	453.90

¹experimentally obtained yield stress distribution

²average yield stress, f_{va} , obtained in accordance with EN1993-1-3 [10]

³yield stress of base material, f_{yb} (see Chapter 3)

It can be observed that the model including the residual stresses, the measured imperfections, together with the load eccentricities is able to model accurately ultimate force. Also, the model considering the average yielding stress and the standard Young's modulus ($f_{va}=501.3$ N/mm² and $E=210000$ N/mm²) is accurate enough.

Further, an experimentally tested specimen from a specific test series was chosen to be replicated.

Due to the relativity of the measurements, the dimensions for the numerical model were considered to be those specified by the supplier. The end sections were considered to have specified dimensions and the initial imperfection was applied as the first buckling model i.e. distortional scaled by an imperfection factor.

The imperfection scaling factor, IMP, was calculated based on measured imperfections using Eq. (4.3).


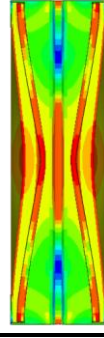

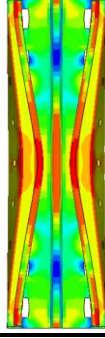

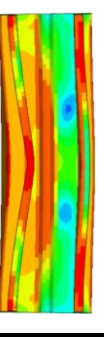

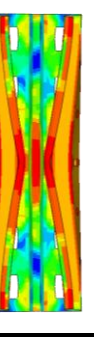
In Table 4.5 are presented the considered scaling factors, load eccentricities, together with the experimental failure load and numerically obtained failure load. The resulted error was determined for each numerically simulated specimen.

Table 4.5 Numerical model validation for STUB specimens

Specimen	Load Eccentricities [mm]		Failure loads [kN]	
	Imperfection factor		Exp	FEM
RS125B Stub	End 1	y axis 0.06 z axis 1.22	463.69	470.55
	End 2	y axis -0.24 z axis 0.25		
	IMP	1.21	1.5%	
RS125N Stub	End 1	y axis -0.35 z axis -1.05	404.03	417.94
	End 2	y axis 0.48 z axis 0.48		
	IMP	0.78	3.4%	
RS95B Stub	End 1	y axis -1.04 z axis -0.64	346.63	335.65
	End 2	y axis -0.35 z axis 0.00		
	IMP	0.35	-3.16%	
RS95N Stub	End 1	y axis 0.00 z axis -0.75	279.00	269.91
	End 2	y axis 0.43 z axis -0.87		
	IMP	0.64	-3.25%	

In Table 4.6 is presented the observed failure mode for STUB column specimens.

Table 4.6 Failure mode for STUB specimens: Experimental vs. numeric

RS125B		RS125N		RS95B		RS95N	
EXP	FEM	EXP	FEM	EXP	FEM	EXP	FEM
							
463.69	470.55	404.03	417.94	346.63	335.65	279.00	269.91
1.5%		3.4%		-3.16%		-3.25%	

Following, the experimental and numerical curves are presented comparatively in Fig. 4.5 for RS125 stub specimens, section without perforations (a)

and section with perforations (b) and in Fig. 4.6 for RS95 stub specimens, section without perforations (a) and section with perforation (b).

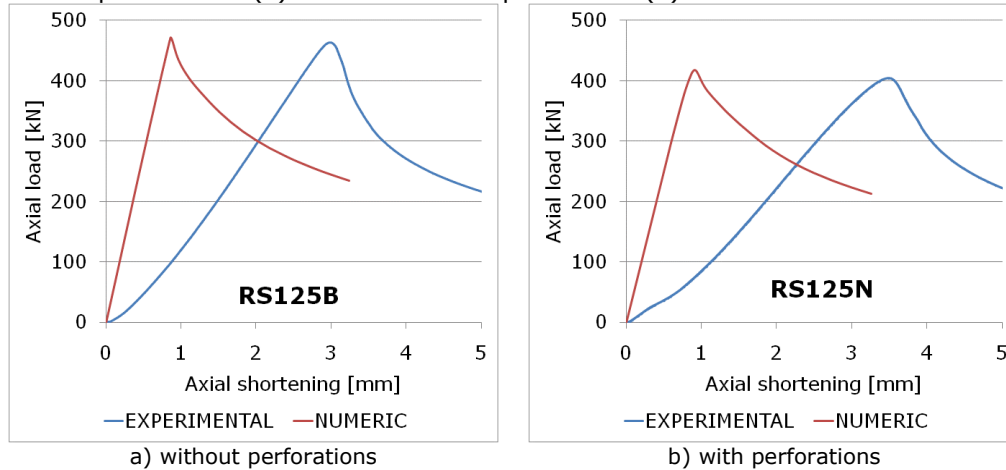


Fig. 4.5 Behaviour curves for RS125 stub specimens

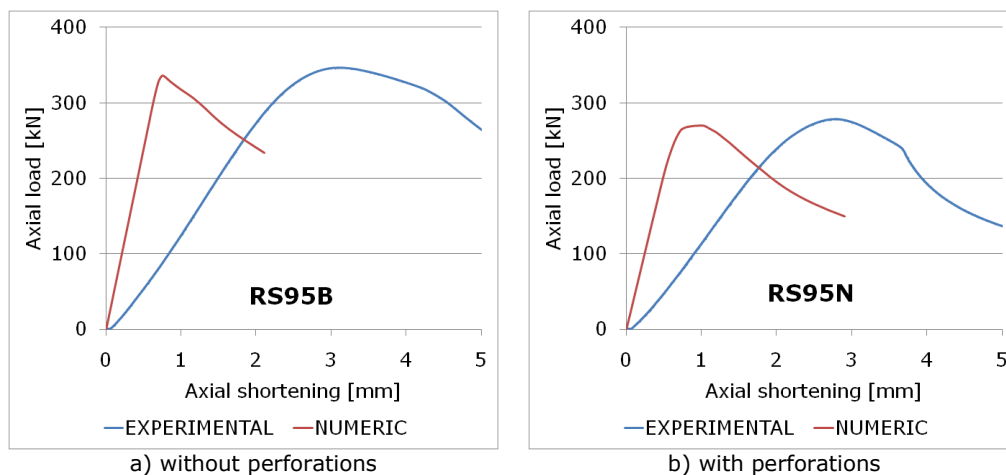


Fig. 4.6 Behaviour curves for RS95 stub specimens

Based on the behaviour curves, presented comparatively in Fig. 4.5 and Fig. 4.6 and failure modes presented in Table 4.6, it can be observed that the numerical model is representative for tested upright sections from the point of view of geometry, initial imperfection, material properties and failure load. The main difference in the results is the initial stiffness of the curve. The slope is function of the axial (vertical) displacement.

For the experimentally tested specimens, the axial displacement is approximately 2mm more at ultimate load for all tested profiles. The additional displacement can be due to bending of the cross-head beam of the testing machine together with the compression of loading plates and end bearings.

For finite element models all the components of the load introduction system (the end plates and pressure pads) were considered fully rigid (RIGID BODY).

Even very small flexibility of load introducing/support system can influence significantly the initial stiffness; the same phenomenon was observed by other researches [115] in similar conditions.

Following, the numerical models was validated for UPRIGHT specimens. For these specimens, the imperfection measurements were considered separately for distortional, type d_2 imperfection, flexural, bow imperfection, and torsional imperfection. The measured imperfections were decomposed in order to determine the scaling factors (used to scale the distortional, flexural and torsional buckling mode). They were determined relative to the end sections, based on the assumption that the ends are not affected by any imperfections. A straight line was assumed to connect the ends and the measurements maximum deviations from the assumed "straight line" were considered to be the maximum imperfection.

In Table 4.7 are presented in imperfections factors together with the load eccentricities considered in numerical models for tested specimens.

Table 4.7 Numerical model validation for UPRIGHT specimens

Specimen	Load eccentricities [mm]		Failure loads [kN]		
	Imperfection factors		Exp	FEM	
RS125B Upright	End 1	y axis	-0.58		
		z axis	0.78		
	End 2	y axis	0.2	382.59	392.58
		z axis	0.42		
	Flexural		0		
	Torsional		0	Error	
Distortional		1.03	2.61%		
RS125N Upright	End 1	y axis	-0.68		
		z axis	0.59		
	End 2	y axis	-0.15	347.26	361.72
		z axis	0.00		
	Flexural		0		
	Torsional		0	Error	
Distortional		0.78	4.16%		
RS95B Upright	End 1	y axis	-1.65		
		z axis	-0.45		
	End 2	y axis	-1.22	272.06	280.09
		z axis	0.39		
	Flexural		0		
	Torsional		2.5*	Error	
Distortional		0.7	2.95%		
RS95N upright	End 1	y axis	-0.45		
		z axis	-0.5		
	End 2	y axis	-0.76	211.29	221.40
		z axis	-1.45		
	Flexural		-0.2		
	Torsional		2.0*	Error	
Distortional		0.4	4.79%		

The torsion was considered to be the maximum absolute value of the difference $|BL - -BR|$, where BL and BR are defined in Fig. 3.15.

The final value of initial imperfection is in fact a linear combination of global flexural, global torsional and distortional buckling modes scaled by corresponding factors. The value of scaling factors was chosen in such a way to replicate as close as possible the initial deformed shape. In addition to this, loading eccentricities were considered.

In Fig. 4.7 is presented the geometrical imperfection of a mid section resulted from the coupling of simple buckling modes i.e. distortional, flexural and torsional. The imperfections are presented exaggeratedly.

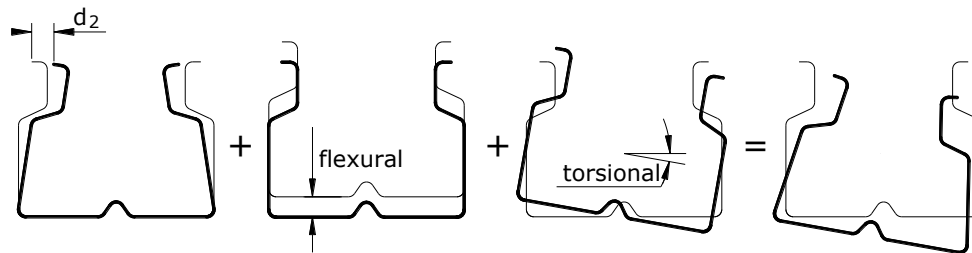


Fig. 4.7 Coupling of simple buckling modes

For RS125 upright specimens, the measured global imperfections were small enough to be ignored (maximum bow imperfection was found to be around $L/5000$, while the torsion was less than 0.1°). For RS95 upright specimens, the bow imperfection was found to be around $L/5000$, while the maximum torsion was found to be 2° .

In Table 4.8 are presented, comparatively, the observed failure mode for upright specimens for experimental tests and numerical model simulations.

The measured imperfections, together with the decomposition have its limitations. Additional measurements would have been required to precisely decompose and determine the actual imperfections shape and magnitudes.

Table 4.8 Failure mode for UPRIGHT specimens: Experimental vs. numeric

RS125B		RS125N		RS95B		RS95N	
EXP	FEM	EXP	FEM	EXP	FEM	EXP	FEM
382.59	392.58	347.26	361.72	272.06	280.09	211.29	221.40
2.61%		4.16%		2.95%		4.79%	

The experimental and numerical curves are presented comparatively in Fig. 4.8 for RS125 upright specimens, section without perforations (a) and section with perforations (b) and in Fig. 4.9 for RS95 upright specimens, section without perforations (a) and section with perforation (b).

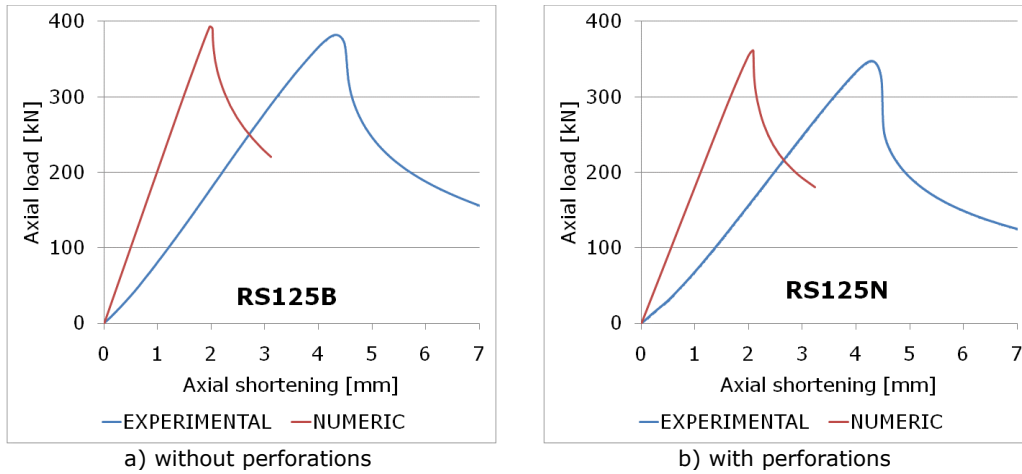


Fig. 4.8 Behaviour curves for RS125 upright specimens

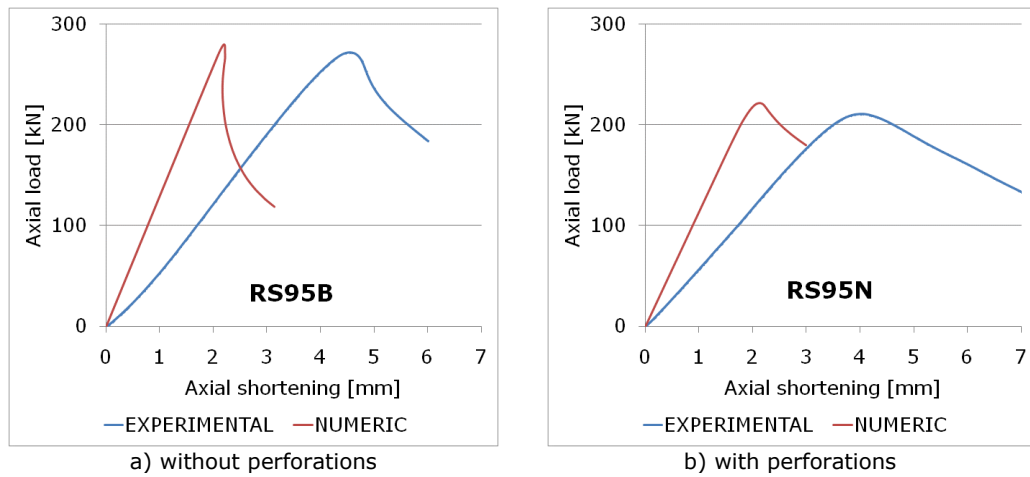


Fig. 4.9 Behaviour curves for RS95 specimens

The same slope difference for experimental specimens and numerical models, as for STUB specimens, can be observed in Fig. 4.8 and Fig. 4.9 for UPRIGHT specimens. The difference in axial displacement (roughly 2mm) is the same as for STUB specimens, confirming the additional displacement sources mentioned before.

For INTERACTIVE specimens, the measured geometrical imperfections are relative to the end sections, considered to have the dimensions specified by supplier. The final values of measured geometrical imperfections were considered to be composed of sectional and overall imperfections. A decomposition procedure was used to determine the best fitted combination of simple buckling modes i.e. distortional, as sectional geometric imperfection, and flexural and torsional, as global imperfections. The resulting values of scaling factors were applied in order to validate the numerical model.

Together with the combined geometrical imperfections, global and sectional, the measured loading and support eccentricities were considered for the numerical model validation

In Table 4.9 are presented the scaling factors obtained for the corresponding simple buckling modes, together with the end support and loading eccentricities.


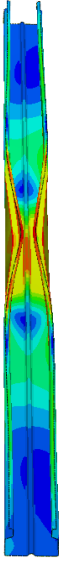

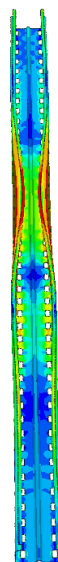

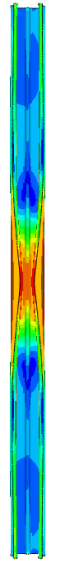

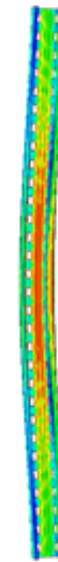
Table 4.9 Numerical model validation for INTERACTIVE specimens

Specimen	Eccentricities [mm] Imperfections		Failure loads [kN]		
			Exp	FEM	
RS125B	End 1	y axis	-0.96		
		z axis	0.47		
	End 2	y axis	-0.48	318.29	331.19
		z axis	-0.10		
		Flexural	0.21		
		Torsional	1.21		Error
	Distortional	0.83		4.05%	
RS125N	End 1	y axis	0.27		
		z axis	1.37		
	End 2	y axis	0.22	274.22	257.65
		z axis	1.53		
		Flexural	0.33		
		Torsional	0.34		Error
	Distortional	1.20		-6.05%	
RS95B	End 1	y axis	0.67		
		z axis	0.78		
	End 2	y axis	0.57	211.42	217.98
		z axis	1.16		
		Flexural	0.01		
		Torsional	0.5		Error
	Distortional	0.89		3.10%	
RS95N	End 1	y axis	0.62		
		z axis	-1.05		
	End 2	y axis	0.19	168.88	177.14
		z axis	-1.02		
		Flexural	0.46		
		Torsional	0.68		Error
	Distortional	0.33		4.98%	

It was observed that imperfections measured along the specimen's length, limited the decomposition method used to determine the scaling factors. A more complex measuring device able to measure, individually, sectional and global imperfections would have been required for a more accurate measuring and decomposition.

The numerical model with initial imperfections (generated as a linear combination of simple buckling modes) seeded into the initial geometry was able to describe symmetric and overall failure modes only. In Table 4.10 are presented the failure modes of experimental tests and the failure modes obtained using the numerical model for specimens having the length, calibrated based on ECBL approach [28] into interactive buckling interval.

Table 4.10 Failure mode for INTERACTIVE specimens: Experimental vs. numeric

RS125B		RS125N		RS95B		RS95N	
EXP	FEM	EXP	FEM	EXP	FEM	EXP	FEM
							
318.29	331.19	274.22	257.65	211.42	217.98	168.88	177.14
4.05%		-6.05%		3.10%		4.98%	

The experimental and numeric curves are presented comparatively in Fig. 4.10 for RS125 specimens and in Fig. 4.11 for RS95 specimens.

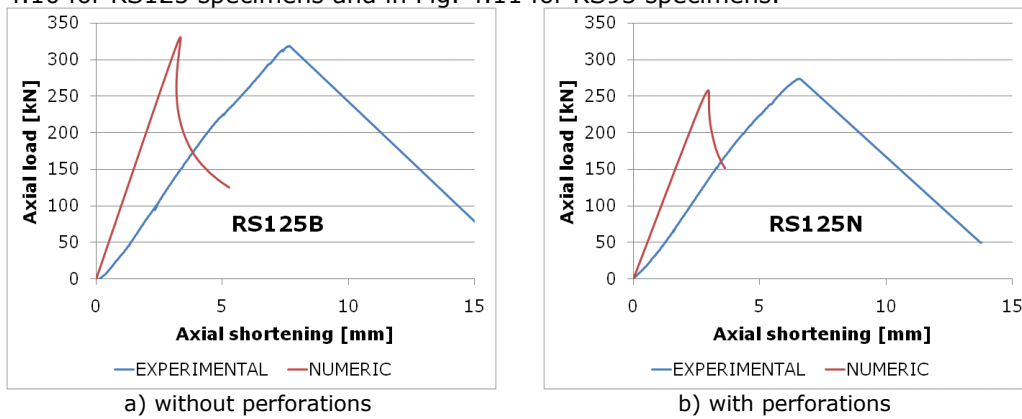


Fig. 4.10 Behaviour curves for RS125 INTERACTIVE specimens

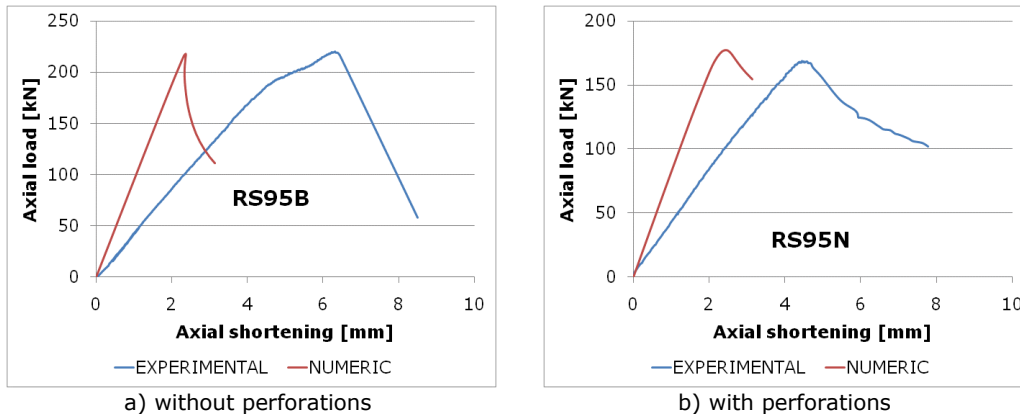


Fig. 4.11 Behaviour curves for RS125 INTERACTIVE specimens

Based on the results obtained from numerical simulations it can be noted that the numerical model for these specific applications is not sensitive to Young's modulus variation (within certain limits). A numerical model that uses average yield strength together with the standard value of Young's modulus is accurate to model the behaviour of studied pallet rack uprights. (see Table 4.4)

From the point of view of maximum load, the numerical model is able to replicate the experimental tests. For specimens with increased length, where global and sectional imperfections are of same importance, a more complex imperfections measurement is recommended. The measurements should allow the decomposition of geometric imperfections into sectional and global components that can afterwards be used to reconstruct the initial deformed shape.

It can be seen that the decomposition method used in this case is limited to symmetric and/or global failure modes. Further development and more complex measuring are required in order to replicate all experimentally obtained failure modes.

4.4 Imperfection sensitivity study

One of the most interesting aspects of the post-buckling behaviour of thin walled sections is the interaction of multiple buckling modes under the same critical load. This phenomenon is very important, since single stable post-buckling equilibrium paths become unstable when interacting with each other.

In accordance with the European design code [13] provisions, the influence of the distortional buckling mode on the axial load capacity of the upright section is determined on uprights with the length equal to the length of a single bracing panel closest to one metre. For this specimen's length, the test results correspond rather to the distortional-global interaction, than to pure distortion.

Following, based on ECBL [28] approach, the coupling point and based on the reduced slenderness which defines it (see Fig. 4.12), the specimen's length were determined. The specimen's length should be reasonably close to the instabilities coupling point (in terms of reduced slenderness). This is leading to the idea of using a "coupling range" defined in terms of reduced slenderness as a vicinity of the coupling point, instead of working strictly in this point. A correct definition of

coupling range limits is therefore of great importance for the considered specimens length.

In order to use the ECBL [28] approach, first the ultimate strength of members with the length corresponding to distortional buckling has to be obtained. Based on experimental results, numerical models were calibrated using ABAQUS in order to obtain the capacity of specimen unaffected by any eccentricities and imperfection, for the two cross-sections studied, with and without perforations. In Table 4.11 are presented the values of ultimate forces obtained numerically for the studied sections together with the obtained coupling length.

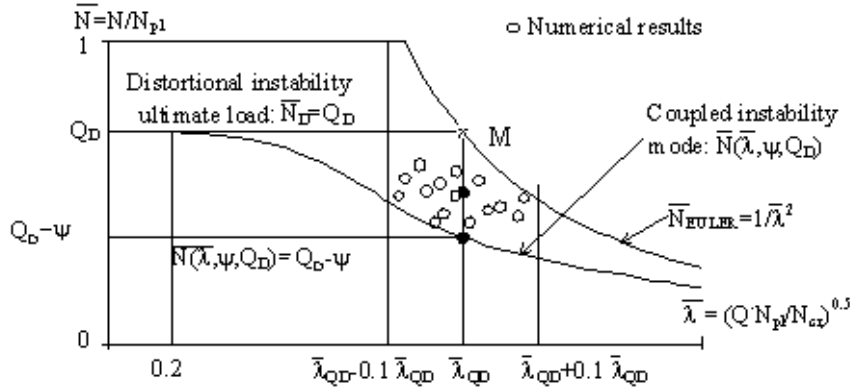


Fig. 4.12 The ECBL interactive buckling model for distortional and Euler bar instabilities

To apply the ECBL approach for interactive buckling i.e. distortional and global flexural instability, the distortional capacity must be determined. In order to determine the distortional capacity of studied sections, compression tests were done on specimens with the length equal with the half-wave length of distortional buckling and based on tests results, the distortional capacity was reconsidered.

In Table 4.11 are presented the critical loads corresponding to distortional buckling, determined using the general purpose finite element package, ABAQUS together with the plastic capacity for the section and the corresponding coupling length.

Table 4.11 “Theoretical” distortional capacity of RS95 and RS125 section

Profile	$N_{D,cr}$ [kN]	N_{pl} [kN]	Q_D	L_c [mm]
RS125B	429.14	556.95	0.771	2378
RS125N	370.48	483.16	0.767	2559
RS95B	402.50	346.51	1.00*	1526
RS95N	340.78	286.69	1.00*	1667

One can observe that for RS95B and RS95N cross-sections, the critical load corresponding to distortional buckling is greater than the cross-section squash load. In this case the Q_D factor has to be limited to 1.00. Based on this limitation, it can be said that for RS95 section with and without perforation there is no interactive buckling.

To calculate the interactive buckling length for perforated sections, the gross section properties are used.

In order to evaluate the effects of geometric imperfections, global, sectional and combined, a new series of numerical models were analysed.

In Fig. 4.13 are presented the geometrical imperfections, considered in the analysis, e.g. distortion (d_{\pm}), flexural about the minor axis (f_{\pm}) and coupling of these two ($f_{\pm}d_{\pm}$). Also, load eccentricities, located on the axis of symmetry, were taken into consideration ($\text{ecc} = -2\text{mm}; -1\text{mm}; +1\text{mm}; +2\text{mm}$). The eccentricity was applied in analysis for specimens alone and together with flexural and distortional imperfections, d , considered in the analyses were taken equal to the thickness of cross-section [187], while for flexural imperfections, the corresponding initial bow tolerance accepted by EN 1090-2 [190], $L/750$, was considered.

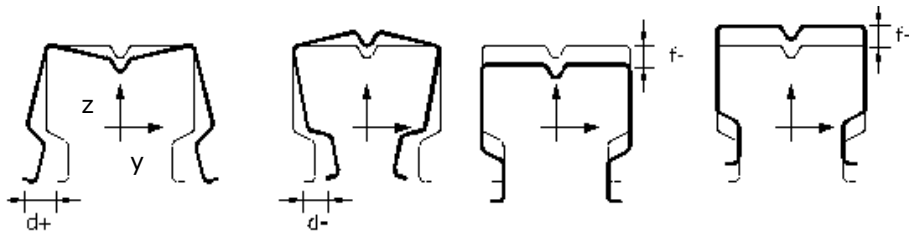


Fig. 4.13 Example of considered simple imperfections (f and d)

Further on, a set of coupled imperfections were considered. In Fig. 4.14 is presented an example where coupled imperfections, distortional and flexural, were applied in the numerical model simulations.

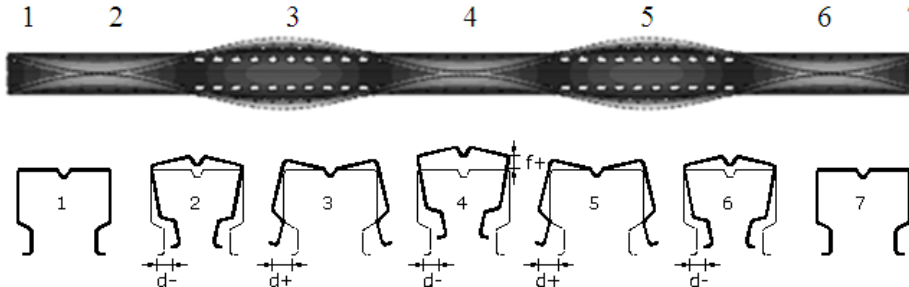


Fig. 4.14 Example of considered coupled imperfections (f and d)

In Table 4.12 are presented the considered cases together with failure loads obtained by numerical simulations. The imperfections were considered in the following manner:

- D+ distortional buckling mode scaled with t , where t is the thickness
- D- distortional buckling mode scaled with $-t$
- F+ flexural buckling mode scaled with $L/750$
- F- flexural buckling mode scaled with $-L/750$
- Ecc_Y load eccentricity in Y direction
- Ecc_Z load eccentricity in Z direction

Table 4.12 The effects of normalized geometric imperfections – absolute values

Considered imperfection	Failure load [kN]			
	RS125B	RS125N	RS95B	RS95N
none	382.740	292.842	339.691	209.838
Ecc_Y 1	374.150	290.592	291.660	199.011
Ecc_Y 2	369.180	284.457	272.523	189.324
Ecc_Z -2	342.644	268.979	231.916	172.788
Ecc_Z -1	363.591	294.708	258.039	188.910
Ecc_Z 1	376.543	275.888	265.708	187.844
Ecc_Z 2	352.367	263.075	243.588	176.356
D+	239.971	209.716	208.606	170.141
D-	240.893	209.702	218.790	176.271
F+	309.577	205.747	235.720	174.648
F-	352.372	255.168	249.510	178.260
F+D+	213.869	179.728	176.878	142.291
F+D-	214.402	181.18	189.896	150.615
F+D+Ecc_Y 1	219.470	179.702	176.701	142.136
F+D+Ecc_Y 2	219.101	179.675	177.254	141.668
F+D+Ecc_Z -2	203.395	166.545	157.104	126.039
F+D+Ecc_Z -1	210.331	172.916	166.130	132.374
F+D+Ecc_Z 1	228.698	187.871	191.973	154.003
F+D+Ecc_Z 2	239.845	197.974	213.241	171.876
F-D+	287.064	260.663	255.465	179.414
F-D-	288.014	260.661	256.260	180.679
F-D+Ecc_Y 1	311.805	260.113	250.629	176.608
F-D+Ecc_Y 2	311.123	257.394	242.561	171.393
F-D+Ecc_Z -2	257.193	214.605	224.616	168.300
F-D+Ecc_Z -1	276.956	235.9	233.953	179.358
F-D+Ecc_Z 1	329.780	249.675	235.343	169.397
F-D+Ecc_Z 2	315.255	240.95	221.837	161.538

The considered load eccentricity was applied at both ends with the same magnitude. For a better understanding, the **F-D+Ecc_Z-2** combined imperfection consists of flexural buckling mode scaled with **L/750** coupled with a distortional buckling mode scaled with **t**, where **t** is the section's thickness and a load eccentricity in Z direction of -2mm.

In order to better view the influence of different imperfections, sectional, overall and coupled, in Table 4.13 are presented the procentual differences of ultimate loads.

Table 4.13 The effects of normalized geometric imperfections – difference

Considered imperfection	Difference [%]			
	RS125B	RS125N	RS95B	RS95N
Ecc_Y 1	-2.24	-0.77	-14.14	-5.16
Ecc_Y 2	-3.54	-2.86	-19.77	-9.78
Ecc_Z -2	-10.48	-8.15	-31.73	-17.66
Ecc_Z -1	-5.00	0.64	-24.04	-9.97
Ecc_Z 1	-1.62	-5.79	-21.78	-10.48
Ecc_Z 2	-7.94	-10.16	-28.29	-15.96
D+	-37.30	-28.39	-38.59	-18.92
D-	-37.06	-28.39	-35.59	-16.00
F+	-19.12	-29.74	-30.61	-16.77
F-	-7.93	-12.86	-26.55	-15.05
F+D+	-44.12	-38.63	-47.93	-32.19
F+D-	-43.98	-38.13	-44.10	-28.22
F+D+Ecc_Y 1	-42.66	-38.64	-47.98	-32.26
F+D+Ecc_Y 2	-42.75	-38.64	-47.82	-32.49
F+D+Ecc_Z -2	-46.86	-43.13	-53.75	-39.94
F+D+Ecc_Z -1	-45.05	-40.95	-51.09	-36.92
F+D+Ecc_Z 1	-40.25	-35.85	-43.49	-26.61
F+D+Ecc_Z 2	-37.33	-32.40	-37.23	-18.09
F-D+	-25.00	-10.99	-24.79	-14.50
F-D-	-24.75	-10.99	-24.56	-13.90
F-D+Ecc_Y 1	-18.53	-11.18	-26.22	-15.84
F-D+Ecc_Y 2	-18.71	-12.10	-28.59	-18.32
F-D+Ecc_Z -2	-32.80	-26.72	-33.88	-19.80
F-D+Ecc_Z -1	-27.64	-19.44	-31.13	-14.53
F-D+Ecc_Z 1	-13.84	-14.74	-30.72	-19.27
F-D+Ecc_Z 2	-17.63	-17.72	-34.69	-23.02

It can be observed that in the case of RS125 sections, the influence of sinusoidal distortional imperfections is significantly higher than the influence of overall bow imperfection, positive or negative. In the case of RS95 section without perforations, the influence of distortional and global bow imperfections is comparable.

When considered as single imperfection, the bow imperfection has the same effect, positive or negative. When coupled with distortional sinusoidal imperfection, the effect of positive and negative bow imperfection is very different. The negative bow imperfection has a stabilizing effect, counteracting the effect of sectional imperfections.

It can be observed that for both RS125 and RS95 sections with and without perforations, considering positive bow imperfection together with positive distortional sinusoidal imperfections gives the most conservative results. The corresponding reduction in section capacity is not real, since, from statistical considerations, in real life sectional and overall imperfections never couples with their maximum magnitudes.

When considering negative bow imperfection, the influence of loading eccentricities is very much increased.

Both tests and numerical simulations confirm the influence of distortional-overall buckling interaction. Also, it seems that considered bow tolerances (imperfection specified in EN1090-2) are significantly higher than the values observed for rolled formed sections. Big attention has to be paid to eccentricity of applied loads, because it can affect significantly the actual capacity of members.

4.5 Erosion of critical bifurcation erosion and imperfection factor evaluation

In order to determine the critical buckling load erosion, ψ , two sets of data can be used i.e. experimentally obtained failure loads and numerically simulated data. When considering the experimental results, the erosion determined includes the effects of all imperfections, geometric and material imperfections and loading eccentricities. Using the numerically determined data, the erosion can be calculated punctually, for a specific type of imperfection (geometric sinusoidal distortional, flexural bow imperfection, load eccentricity) and the influence of these imperfections can be quantified separately.

Considering the imperfections discussed in previous section and the numerically obtained results, the values of erosion factors were calculated for each type of imperfection, simple or coupled, and further compared with the value obtained by using the experimentally tested profiles. The principles of ECBL approach were already presented (see Chapter 2). The erosion of critical bifurcation load was determined using the ECBL scheme (see Fig. 4.15).

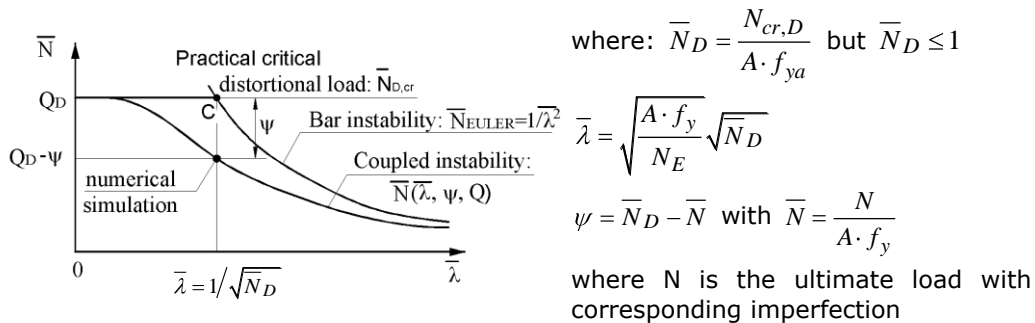


Fig. 4.15 The interactive buckling model based on the ECBL Theory

According to the ECBL approach, the interest is to observe the erosion of practical critical load, this time, the ECBL approach is applied considering the minimum critical load, obtained for the relevant section, in interaction with Euler buckling of the corresponding bar member (see Fig. 4.15).

In Table 4.11 are presented the lengths corresponding to the theoretical interactive buckling (e.g. in the point of $\bar{\lambda} = 1/\sqrt{\bar{N}_D}$) determined via the ECBL approach, in the interactive buckling point, M.

One can observe that for RS95B and RS95N cross-sections, the critical load for distortional buckling is greater than the cross-section capacity and in this case the Q_D factor has to be limited to 1.

Considering the values in Table 4.13 and disregarding the loading eccentricities the most critical imperfection combinations is found to be (F+) + (D+). In principle, the eccentricity is most dangerous when affine with initial bow.

Taking as reference the distortional ultimate load corresponding to the perfect section (see Table 4.11), the ECBL approach is applied once more to get ψ and α factors for the selected imperfection combinations. The obtained results are presented in Table 4.14, for specimens located in the interaction point, M.

Table 4.14 Erosion and imperfection coefficients for considered imperfections

Considered imperfection	Erosion and imperfection coefficient							
	RS125B		RS125N		RS95B		RS95N	
	ψ	α	ψ	α	ψ	α	ψ	α
Ecc_Y 1	0.099	0.012	0.165	0.035	0.158	0.037	0.306	0.168
Ecc_Y 2	0.108	0.014	0.178	0.041	0.214	0.072	0.340	0.218
Ecc_Z -2	0.155	0.030	0.210	0.059	0.331	0.204	0.397	0.327
Ecc_Z -1	0.118	0.017	0.157	0.031	0.255	0.109	0.341	0.221
Ecc_Z 1	0.094	0.010	0.196	0.051	0.233	0.089	0.345	0.227
Ecc_Z 2	0.138	0.023	0.222	0.067	0.297	0.157	0.385	0.301
D+	0.340	0.186	0.333	0.176	0.398	0.329	0.407	0.348
D-	0.338	0.184	0.333	0.176	0.369	0.269	0.385	0.302
F+	0.215	0.062	0.341	0.187	0.320	0.188	0.391	0.313
F-	0.138	0.023	0.239	0.079	0.280	0.136	0.378	0.288
F+D+	0.387	0.259	0.395	0.273	0.490	0.587	0.504	0.639
F+D-	0.386	0.258	0.392	0.268	0.452	0.466	0.475	0.536
F+D+Ecc_Y 1	0.376	0.242	0.395	0.274	0.490	0.589	0.504	0.641
F+D+Ecc_Y 2	0.377	0.243	0.395	0.274	0.488	0.583	0.506	0.647
F+D+Ecc_Z -2	0.405	0.294	0.422	0.327	0.547	0.824	0.560	0.893
F+D+Ecc_Z -1	0.393	0.271	0.409	0.300	0.521	0.707	0.538	0.784
F+D+Ecc_Z 1	0.360	0.215	0.378	0.244	0.446	0.449	0.463	0.498
F+D+Ecc_Z 2	0.340	0.186	0.357	0.210	0.385	0.300	0.400	0.334
F-D+	0.255	0.093	0.227	0.071	0.263	0.117	0.374	0.280
F-D-	0.253	0.092	0.227	0.071	0.260	0.115	0.370	0.271
F-D+Ecc_Y 1	0.211	0.060	0.228	0.072	0.277	0.132	0.384	0.299
F-D+Ecc_Y 2	0.212	0.061	0.234	0.076	0.300	0.161	0.402	0.338
F-D+Ecc_Z -2	0.309	0.147	0.323	0.163	0.352	0.239	0.413	0.363
F-D+Ecc_Z -1	0.273	0.109	0.279	0.114	0.325	0.195	0.374	0.280
F-D+Ecc_Z 1	0.178	0.041	0.250	0.088	0.321	0.189	0.409	0.354
F-D+Ecc_Z 2	0.204	0.056	0.268	0.104	0.360	0.253	0.437	0.423

The Fig. 4.16 to Fig. 4.19 with corresponding tables, Table 4.15 to Table 4.18 show comparatively the theoretical and practical interaction curves, with corresponding interaction points, together with GMNIA curve and test values for the four types of sections studied in this thesis. For the presented curves it was considered the most unfavourable imperfection combination i.e. (F+)+(D+) excepting the load eccentricities. Since for the numerical models, the load eccentricities can be controlled, their effect was excluded.

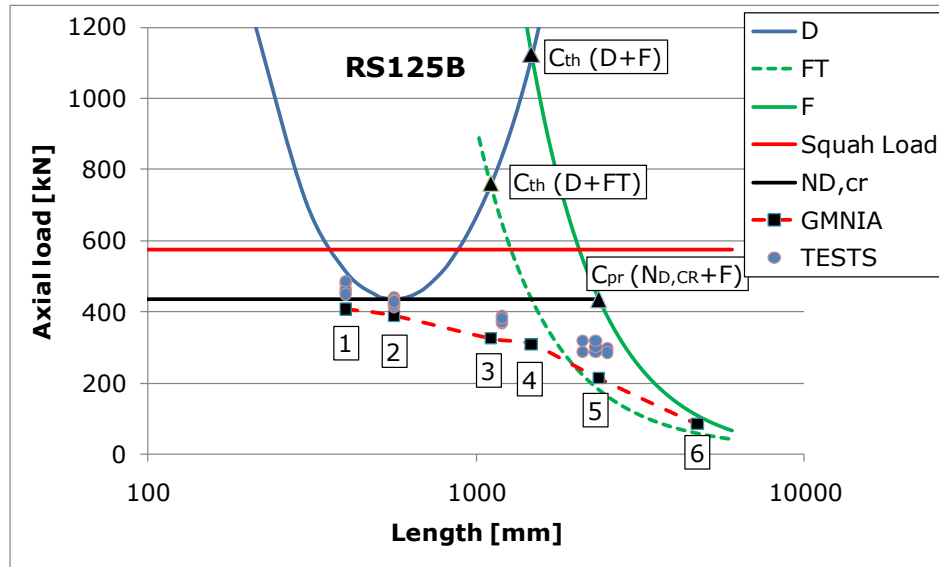


Fig. 4.16 Interaction curves for RS125B section

Table 4.15 Coupling length and resulted erosion for RS125B section

Point number	Ultimate capacity	L [mm]	N _{cr} [kN]	N _u [kN]	Coupling erosion Eq. (4.4) Eq. (4.5)
1	STUB column EN15512:2009	400	510.84	407.58	-
2	Distortional column	560	435.05	388.91	-
3	Upright column Theoretical interaction (D+FT)	1110	761.40	324.86	0.784 57.33%
4	Theoretic interaction (D+F)	1470	1122.57	309.51	1.460 72.43%
5	Practical interaction (N _{D,cr} + F)	2380	429.14	213.87	0.397 50.84%
6	N _{GMNIA} (λ=2)	4710	109.35	85.433	-

where "D" – distortional buckling, "FT" – flexural-torsional buckling, "F" – flexural buckling, C_{Th(D+FT)} – theoretical coupling point for D and FT, C_{Th(D+F)} – theoretical coupling point for D and F, C_{Pr(Npl+FT)} – practical coupling point for N_{pl} and F, N_{pl} – squash load, N_{D,cr} – critical distortional buckling load, N_{cr} – critical buckling load, N_u – plastic strength (GMNIA)

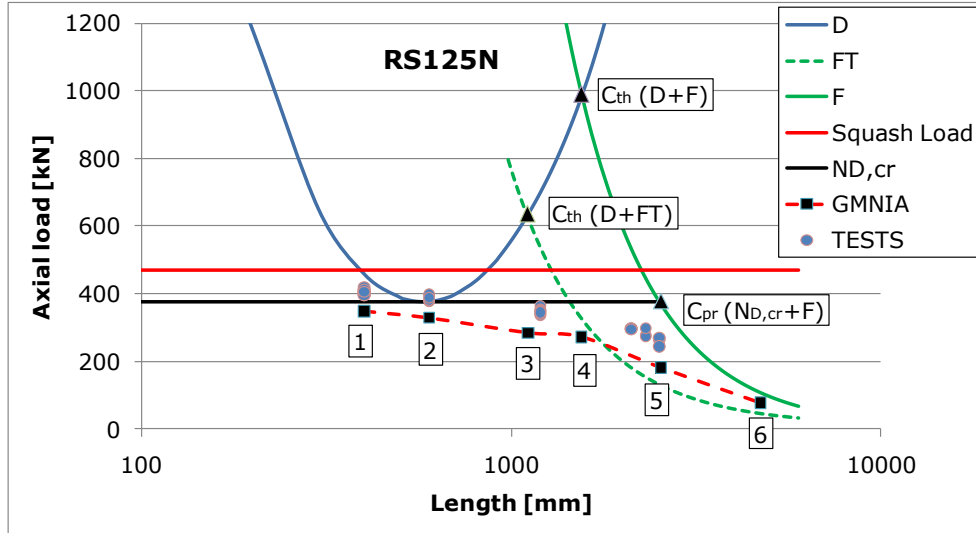


Fig. 4.17 Interaction curves for RS125N section

Table 4.16 Coupling length and resulted erosion for RS125N section

Point number	Ultimate capacity	L [mm]	N_{cr} [kN]	N_u [kN]	Coupling erosion Eq. (4.4) Eq. (4.5)
1	STUB column EN15512:2009	400	456.21	348.82	-
2	Distortional column	600	375.15	328.66	-
3	Upright column Theoretical interaction (D+FT)	1110	636.19	284.76	0.727 55.24%
4	Theoretic interaction (D+F)	1550	990.26	272.56	1.485 72.48%
5	Practical interaction ($N_{D,cr} + F$)	2560	370.48	174.91	0.405 52.79%
6	N_{GMNIA} ($\lambda=2$)	4710	107.24	77.21	-

where "D" – distortional buckling, "FT" – flexural-torsional buckling, "F" – flexural buckling, $C_{Th(D+FT)}$ – theoretical coupling point for D and FT, $C_{Th(D+F)}$ – theoretical coupling point for D and F, $C_{Pr(N_{pl}+FT)}$ – practical coupling point for N_{pl} and F, N_{pl} – squash load, $N_{D,cr}$ – critical distortional buckling load, N_{cr} – critical buckling load, N_u – plastic strength (GMNIA)

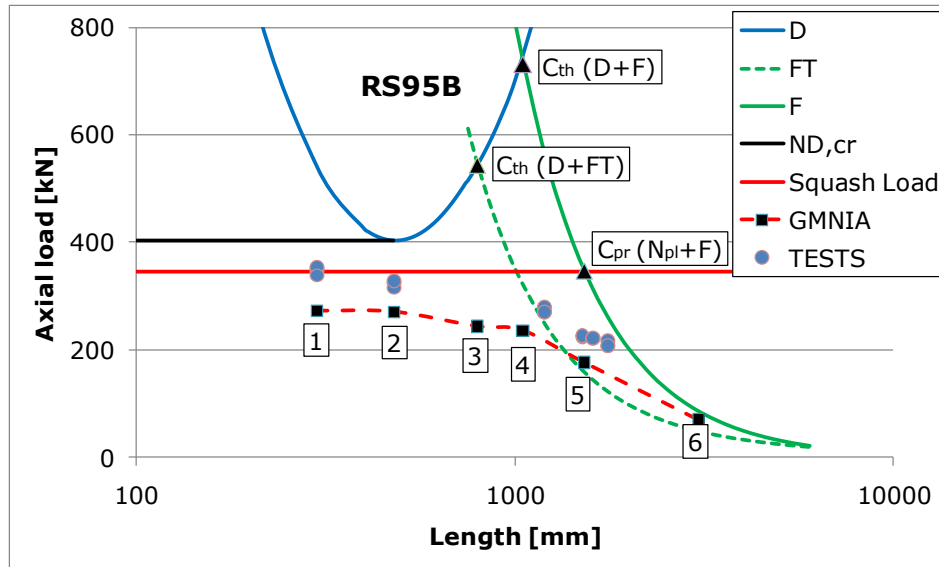


Fig. 4.18 Interaction curves for RS95B section

Table 4.17 Coupling length and resulted erosion for RS95B section

Point number	Ultimate capacity	L [mm]	N_{cr} [kN]	N_u [kN]	Coupling erosion Eq. (4.4) Eq. (4.5)
1	STUB column EN15512:2009	300	539.61	271.98	-
2	Distortional column	480	406.70	270.39	-
3	Upright column Theoretical interaction (D+FT)	795	543.18	243.58	0.865 55.16%
4	Theoretic interaction (D+F)	1050	731.61	236.09	1.430 67.73%
5	Practical interaction ($N_{pl} + F$)	1530	346.51	176.88	0.490 48.95%
6	N_{GMNIA} ($\lambda=2$)	3060	86.14	71.35	-

where "D" – distortional buckling, "FT" – flexural-torsional buckling, "F" – flexural buckling, $C_{Th(D+FT)}$ – theoretical coupling point for D and FT, $C_{Th(D+F)}$ – theoretical coupling point for D and F, $C_{pr(N_{pl}+F)}$ – practical coupling point for N_{pl} and F, N_{pl} – squash load, $N_{D,cr}$ – critical distortional buckling load, N_{cr} – critical buckling load, N_u – plastic strength (GMNIA)

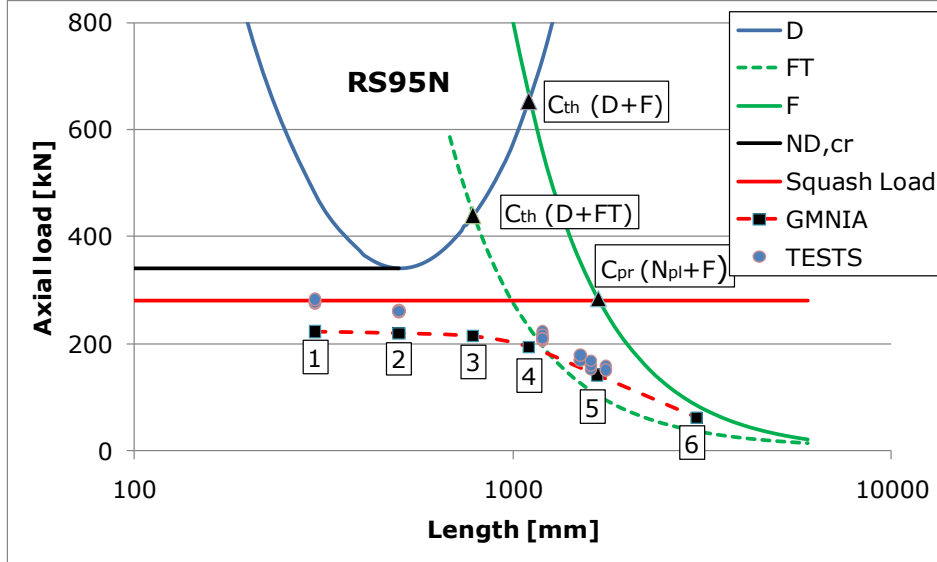


Fig. 4.19 Interaction curves for RS95N section

Table 4.18 Coupling length and resulted erosion for RS95N section

Point number	Ultimate capacity	L [mm]	N_{cr} [kN]	N_u [kN]	Coupling erosion Eq. (4.4) Eq. (4.5)
1	STUB column EN15512:2009	300	477.71	222.68	-
2	Distortional column	500	341.80	219.72	-
3	Upright column Theoretical interaction (D+FT)	785	339.94	214.11	0.439 37.02%
4	Theoretic interaction (D+F)	1105	653.62	194.28	1.602 70.28%
5	Practical interaction ($N_{pl} + F$)	1670	286.66	142.29	0.639 50.36%
6	N_{GMNIA} ($\lambda=2$)	3060	85.82	62.95	-

where "D" – distortional buckling, "FT" – flexural-torsional buckling, "F" – flexural buckling, $C_{Th(D+FT)}$ – theoretical coupling point for D and FT, $C_{Th(D+F)}$ – theoretical coupling point for D and F, $C_{pr(N_{pl}+F)}$ – practical coupling point for N_{pl} and F, N_{pl} – squash load, $N_{D,cr}$ – critical distortional buckling load, N_{cr} – critical buckling load, N_u – plastic strength (GMNIA)

The coupling erosion was determined using the formula:

$$\psi_C = \frac{N_{cr} - N_u}{N_{Pl}} \quad (4.4)$$

$$\psi_C = \frac{N_{cr} - N_u}{N_{cr}} \cdot 100\% \quad (4.5)$$

In section 2.5, a classification of interaction type was done function of the erosion coefficient, ψ , and the following interaction classes were defined:

- class 1: weak interaction (WI): $\psi \leq 0.1$
- class 2: moderate interaction (MI): $0.1 < \psi \leq 0.3$
- class 3: strong interaction (SI): $0.3 < \psi \leq 0.5$
- class 4: very strong interaction (VSI): $\psi > 0.5$

A precise framing for coupled instabilities is very important in order to choose a suitable design strategy. For weak and moderate interaction class, simple design methods based on safety coefficients can be used. In case of strong and very strong interaction, special design methods must be developed.

In Table 4.19 are presented the main coupled instabilities that appear for structural elements together with the corresponding interaction class.

Based on values presented in Table 4.14 and using these interaction classes, a framing can be done for each type of proposed imperfection.

Table 4.19 Coupled instabilities for structural elements

Element type	Interaction class
Mono-symmetric columns	WI to MI
Composed section columns	MI
Thin walled columns	MI to VSI
Thin walled beams	MI

For the case of RS125 section, the maximum value of erosion is 0.515 framing the section into the very strong interaction class. Even if, at first look, for RS95 section, there is no interaction, distortional buckling critical load being higher than section's capacity, the maximum value of 0.504 is framing the section into very strong interaction class. In this classification, the erosion values corresponding to load eccentricities were disregarded.

Based on this classification, it can be concluded that a simple design method, based on safety coefficients alone is not appropriate for the design of such sections, with or without perforations.

When considering different combinations of imperfections, the value of α imperfection coefficient can place a specific section to different buckling curves. In some cases, the coupled imperfections can have a stabilizing effect leading to a lower value for the imperfection coefficient and finally to an unsafe design.

4.6 Concluding remarks

A numerical model was calibrated in order to determine the influence of specific imperfections on ultimate strength of considered sections. In the same time, a numerical model considering the average yield strength (determined using the yield strength of base material and the specifications of EN1993-1-3) is accurate enough (see Table 4.4).

For STUB column specimens, the model is able to model the behaviour and failure mode of experimental tested specimens. The main difference in the results is the initial slope of the curve. For the experimentally tested specimens, the axial displacement is approximately 2mm more at ultimate load for all tested profiles. The additional displacement can be due to bending of the cross-head beam of the testing machine together with the compression of loading plates and end bearings. The same difference was observed for UPRIGHT specimens.

For specimens with the length in interactive buckling range, the numerical model is limited to the modelling of symmetric and overall failure modes. This limitation is a result of the insufficient data for a detailed imperfection decomposition. A more complex and detailed set of geometric imperfection measurements would be required in order to be able to decompose the imperfections in constitutive parts i.e. sectional and global, flexural, torsional, flexural-torsional.

A sensitivity study was conducted in order to determine the effects of initial geometric imperfection on the buckling strength of cold formed steel sections applied in pallet rack structures. Different initial imperfections (distortional and global bow imperfection), simple and combined, were considered together with load loading eccentricities.

Values presented in Table 4.14 prove the negative influence of interaction between distortional and overall buckling in the case of this particular type of rack sections. Considering the maximum values of erosion, the sections can be enclosed in the very strong interaction class. Strong and very strong interaction reduce significantly the capacity in compression of these members.

In principal, the measured geometric imperfection values are lower than those recommended by codes and literature and partially compensate each other. Unfortunately, it cannot be given an absolute value for distortional or overall measured imperfections due to limitations of measuring device used to record the geometric deviations.

The stabilizing effect due to coupling of geometric imperfections can be observed analyzing the values presented in Table 4.13. The ECBL approach [28] has been applied for the same considered cases and the results are presented in Table 4.14. The same stabilizing effects reflect on the reduced erosion and further on the values of the imperfection coefficient, α .

Considering a wide range of simple and combined imperfections, the verification method based on the ECBL approach, proposed by Dubina [28] gives an alternative for determining the axial load capacity of perforated members. This method allows one to adapt the European buckling curves for thin walled perforated sections. The use of ECBL approach [28] together with an extensive FE parametric study can reduce the need of expensive testing.

When studying the influence of coupled imperfections, it is important to consider sufficient imperfection coupling patterns, in order to determine a reliable value for erosion and subsequently, the imperfection factor.

From a statistic point o view, to consider all imperfections that couples with their highest value, lead to over conservative results. It is, for instance, combination pattern considering the positive deflection coupled in the same direction with the load eccentricity; for such a combination the resulting imperfection coefficient is 0.824 for the RS95B section.

A rational consideration of imperfections that are coupled is required in order to best describe the interactive buckling phenomenon. It can be observed that the effect of load eccentricities is more pronounced when coupled with initial bow imperfection.

Truly, the capacity curves obtained with GMNIA, presented in Fig. 4.16 to Fig. 4.19 show the behaviour of simulated specimens considering a GMNIA analysis, with coded imperfections considered. It can be seen that a rational FE analysis, using the code imperfections and a calibrated and validated model, can be used to determine the failure force for perforated cold formed upright sections and, very important, those figures demonstrate that the concept of Erosion of Critical Bifurcation Load is correct!

5 BUCKLING CHECKING OF PERFORATED COLD-FORMED STEEL SECTIONS IN COMPRESSION.

5.1 Introduction

Cold-formed steel structural members used in pallet rack storage systems are commonly manufactured with holes to permit easy beam to column (upright) connection. Current design methods, available to engineers for predicting the strength of perforated thin walled sections, are prescriptive and limited to specific perforation locations, spacings and sizes.

There are available simple design methods, like DSM (Direct Strength Method), validated for cold formed sections without perforations, that predicts the ultimate strength of a general cold formed section, column or beam with the elastic buckling properties of the member cross-section.

The elastic buckling properties of cold-formed steel beams and columns, including the presence of holes, are studied with thin shell finite element eigenbuckling analysis. Parameter studies demonstrate that critical elastic buckling loads either decrease or increase with the presence of holes, depending on the member geometry and perforation size, spacing, and location.

Experiments on cold-formed steel columns with holes are conducted to observe the interaction between elastic buckling, load-deformation response, and ultimate strength. The experimental results are used to validate an ABAQUS nonlinear finite element protocol.

Usually, thin-walled short length sections fail due to material yielding after an elasto-plastic post local buckling phase. Sections with increased length are prone to intermediate or global buckling effects such as distortional buckling or to overall modes e.g. torsional, flexural or torsional-flexural buckling. Furthermore, the interaction between different modes (coupled instabilities) can be encountered in design.

Pallet rack upright sections are usually optimized from the point of view of local buckling, having an increased number of folds. The section optimisation against local buckling, usually, produces a distortional buckling problem.

In accordance with EN15512:2009 [13] specifications, the design of cold formed sections used for palletized storage structures is essentially based on experimental testing.

For thin walled steel section without perforations, when calculating the load bearing capacity and stiffness, the effect of local buckling shall be taken into account by using the effective cross-sectional properties calculated on the basis of the effective width of individual elements in compression. Effective section properties are used in strength calculations and shall be calculated for non-perforated members in accordance with EN 1993-1-3 [32] or determined by stub column tests.

For rack upright sections, the strength with regard to the distortional mode shall be determined by rational analysis which includes for member imperfections or by testing.

Suitable methods of rational analysis include:

- a) second-order finite element analysis;
- b) second-order finite strip analysis;
- c) second-order generalised beam theory.

It must be underlined that the wavelength for distortional buckling is significantly longer than that for local buckling. This means that distortional buckling is not usually identified by a conventional stub-column test. Furthermore, if a stub-column test exhibits a distortional failure mode, it is unlikely that the length is sufficient to determine the minimum distortional buckling load

Casafont [175] studied the influence of interactive distortional – overall buckling on cold formed sections with perforations and concluded that the range of lengths where these modes are combined may include the member lengths used in practice. There is a range of member length where a gradual transition from symmetrical distortional buckling to torsional flexural buckling takes place. In this range, symmetric and anti-symmetric distortional buckling and torsional-flexural modes interact. Consequently, it is useful to know whether the effect of mode combination on the column strength should be considered in design.

As mentioned before, there are several approaches that can be used to study the interactive buckling. Only the ECBL approach [28] will be detailed for the specific case of interactive buckling for thin walled sections used for pallet rack uprights studied herein.

Based on ECBL concept, Dubina [28] proposed a new approach for interactive buckling which express the imperfection coefficient, α , function of erosion coefficient ψ .

Based on this approach, in case of studied pallet rack upright sections, the two theoretical simple instability modes that are coupling, are the Euler bar instability mode, characterized by $\bar{N}_E = 1/\bar{\lambda}^2$, where $\bar{\lambda}$ is the relative member slenderness ($\bar{\lambda}_F$ for flexural and $\bar{\lambda}_{FT}$ for flexural torsional buckling) and the distortional instability mode, characterized by $\bar{Q}_D = \bar{N}_D = N_D/N_{pl}$, the factored distortional ultimate load. The resulted eroded capacity curve for coupled instability modes is $\bar{N}_E(\bar{\lambda}, \bar{Q}_D, \psi)$ (see Fig. 5.1).

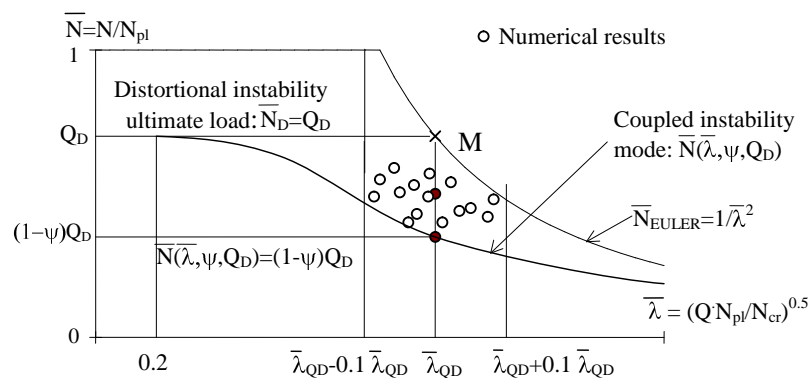


Fig. 5.1 The ECBL interactive buckling model for distortional and Euler bar instabilities

The maximum erosion of critical coupling load, as combined effect of imperfections and coupling, occurs into the coupling point of the two theoretical

instabilities, where the Euler buckling modes becomes equal with the sectional buckling mode i.e. distortional buckling. The coupling point is characterized by:

$$\bar{N}_D = \frac{1}{\bar{\lambda}^2} \quad (5.1)$$

wherefrom the coupling point abscissa is defined by

$$\bar{\lambda} = 1/\sqrt{\bar{N}_D} \quad (5.2)$$

The erosion is defined in the coupling point, by:

$$\psi = \bar{N}_D - \bar{N} \quad (5.3)$$

When distortional buckling occurs before overall buckling, the behaviour of a compressed member can be characterized by an Ayrton-Perry formula (i.e. the equation of European buckling curves [26]), considering $\bar{N} = \bar{N}(\bar{\lambda}, Q_D, \alpha)$. Detailing, the formula becomes:

$$\bar{N}(\bar{\lambda}, Q_D, \alpha) = \frac{1 + \alpha(\bar{\lambda} - 0.2) + Q_D \bar{\lambda}^2}{2\bar{\lambda}^2} - \frac{1}{2\bar{\lambda}^2} \sqrt{\left[1 + \alpha(\bar{\lambda} - 0.2) + Q_D \bar{\lambda}^2\right]^2 - 4Q_D \bar{\lambda}^2} \quad (5.4)$$

In the coupling point, using

$$\bar{N}(\bar{\lambda}, Q_D, \alpha) = 1 - \psi Q_D \quad (5.5)$$

and substituting

$$\bar{\lambda} = \frac{1}{\sqrt{Q_D}} \quad (5.6)$$

for the coupling point abscissa, the formula for imperfection coefficient α , becomes:

$$\alpha = \frac{\psi^2}{1 - \psi} \frac{\sqrt{Q_D}}{1 - 0.2\sqrt{Q_D}} \quad (5.7)$$

This is the new formula for the α imperfection factor that can be used to adapt the European buckling curves in order to better describe the distortional and overall buckling interaction for thin walled sections.

The relations between the imperfection coefficient and the erosion coefficient derived before allow the Ayrton-Perry equation to be modified by using a function of ψ and Q_D , section coefficient. There are three available methods that allow the evaluation of the erosion coefficient:

- Analytical method**, based on elastic stability theory, which determine resolve the problem by determining the minimum axial bar rigidity in the coupling point
- Numerical method**, based on a FE or FS analysis of the bar behaviour in the coupling point
- Experimental method**, based on a statistical analysis of relevant experimental data for specimens included in the coupling interval, in order to determine a calibrated value for the erosion coefficient, ψ .

Based on those mentioned above and considering the EN15512:2009 [13] provisions, compressed upright sections with perforations can be designed using the following alternatives:

- a) a design procedure based on experimental testing
- b) a fully theoretical approach procedure which takes rational account of the perforations (e.g. by using finite elements) together with local, global and distortional buckling and imperfections. The FE model used to replicate the behaviour of real life elements shall be validated and calibrated against experimental results.

5.1.1 Experimentally based design procedure

This design procedure based on experimental testing and requires **three** types of tests:

1. STUB column tests, used to determine the influence of perforations and local buckling on compressive strength of a short column. In case of local buckling an effective area, that defines the section's strength, shall be determined. The STUB column length shall be defined in accordance with EN15512:2009 specifications.
2. DISTORTIONAL buckling tests, used to determine the critical load for section with the critical length for distortional buckling. In order to determine the critical buckling load and corresponding halfwave length any LBA capable software that offers a modal decompositions can be used. It was observed that the CUFEM [131] software package offers a good estimation of buckling modes and it offers an accurate prediction of critical buckling length for distortional buckling for perforated upright sections when used together with the equivalent thickness concept developed by Davies [176]. The member's capacity should still be determined by testing.
3. INTERACTIVE buckling tests. In order to determine the imperfection factor, α , based on an erosion factor determined using experimental data, tests in interactive buckling interval are required. It is recommended that the specimens length to cover the coupling interval, expressed in terms of reduced slenderness. The minimum number of tested specimens shall be equal with 9 (3 specimens with the length equal to the coupling length (L_{cp}) and 3 specimens for each interval limit - $L_{cp} \pm \Delta$). For interactive buckling specimens, correct evaluation of sectional capacity is of paramount importance. The sectional failure mode must be correctly identified e.g. squash load, local buckling or distortional buckling and then after used to determine the coupling point. Also, special care must be taken when defining the coupling interval (usually 10 to 15%).

Based on experimental test results, the design value of ψ erosion coefficient is determined and further used to define the α imperfection coefficient. The Ayrton-Perry model, using the experimentally determined value of α imperfection coefficient, will optimally describe the behaviour of a specific upright section.

In order to be used within the Ayrton-Perry model, the erosion coefficient value must be first calibrated. The methods that can be used to calibrate the value of erosion coefficient include (1) a simplified procedure proposed by Dubina [202] and (2) a detailed procedure based on Annex D of EN1990.

Dubina proposed a simplified method [202] to calibrate the erosion coefficient based on experimental results. The method is summarized in Table 5.1.

Table 5.1 Assumptions for FE-methods

Step	Description	Procedure
1	Definition of coupling interval limits on the axis of reduced slenderness and the selection of n specimens with reduced slenderness in this interval (usually, $\Delta=10\% - 15\%$)	$\bar{\lambda}_c = \frac{1}{\sqrt{N_D}}, \Delta$ $\bar{\lambda}_i \in [\bar{\lambda}_c - \Delta; \bar{\lambda}_c + \Delta]$
2	Experimental determination of the specimen capacity, together with the capacity for the critical length for distortional buckling and the squash load	$N_{i,exp}, N_{pl}, N_{D,cr}$
3	Computation of reduced (adimensional) sectional capacity and the sectional coefficient for distortional buckling	$\bar{N}_{i,exp} = \frac{N_{i,exp}}{N_{pl}}$ $\bar{N}_D = \frac{N_{D,cr}}{N_{pl}}$
4	Computation of average reduced sectional capacity	$m_c = \frac{1}{n} \sum_{i=1}^n \bar{N}_{i,exp}$
5	Computation of the erosion coefficient for each i tested specimen	$\psi_i = \bar{N}_D - \bar{N}_{i,exp}$
6	Computation of average value of erosion coefficient for all n tested specimens	$\psi_m = \frac{1}{n} \sum_{i=1}^n \psi_i$
7	Determination of the erosion coefficients dispersion and the elimination of specimens with unsatisfactory values (usually 50-70%)	$S_\psi = \frac{ \psi_i - \psi_m }{\psi_m} \cdot 100\%, \sigma$
8	For the $n1 < n$ remaining specimens, is computed the value of average erosion and the standard deviation	$\psi_{m1} = \frac{1}{n1} \sum_{i=1}^{n1} \psi_i$
9	Determination of calibrated value for the erosion coefficient: erosion factor	$\psi_d = \psi_{m1} + 2\sigma$

Georgescu [182] analyzed and evaluated this simplified method and concluded that even if the method has its limitations, it gives reliable results and can be used to calibrate the erosion coefficient.

The method detailed method, presented in Annex D of EN1990 [202] introduce a standard procedure to determine the characteristic and design values for element's strength (capacity), together with safety coefficients, based on representative experimental test sets. The statistical uncertainty, due to a limited number of test results, shall be taken into account. Basically, the procedure successively introduces correction factors for a function that express the design strength. The final function will represent the 5% fractile of the considered capacity. The calibrated function can be further used to determine the characteristic values using the procedures from current design code [10]

In order to apply this procedure, there are a few initial conditions that are imposed:

- a. Strength (capacity) function must be function of independent variables
- b. There are sufficient experimental tests available
- c. All material and sectional properties that corresponds to function's variables were determined
- d. All variable have a log-normal distribution. The log-normal distribution, for geometric and capacity type variables, has the advantage that in the theoretical approach no negative values can occur. This is physically correct.
- e. There is no connection (statistic dependency) between the function's variable.

The procedure can be applied to determine the design value for the erosion coefficient and based on its value, the α imperfection coefficient.

5.1.2 FE based design procedure

The second proposed design procedure is based on a numerical model study. Nowadays, the use of FEM based numerical models is common practice. FE analysis offers a reliable alternative to expensive experimental tests. A FEM based approach can be used as an alternative to the design procedure based on laboratory testing. However, the use of numerical models DOES NOT eliminate the need for experimental tests, since the model has to be calibrated and validated for a specific type of section. This procedure reduces to the minimum the required number of experimental tests.

As mentioned before, the total removal of experimental tests is not an option, since each upright section has different characteristics (general dimensions, thickness, and/or perforations array layout) and the model calibration based on existing experimental tests is not possible.

The procedure requires only **one** set of tests used to calibrate and validate a numerical model. The test required is dependent on the cross-sections geometric dimensions.

The base material properties are considered know (provided by supplier). As presented in previous section, the use of average yielding strength distribution over the cross section, gives a good approximation of experimental failure load. In the same time, for the case of pallet rack uprights, the influence of residual stresses is small (less than 3%). A numerical model, using the average yield strength, determined in accordance with EN1993-1-3 provisions, standard value for Young modulus ($E=210000\text{N/mm}^2$) and disregarding the flexural residual stresses should give accurate results.

The first step, for this procedure, is a numerical analysis used to determine the critical sectional mode i.e. local or distortional. For this, a LBA capable software package should be used (CUFSM [131] for instances). The LBA capable software should offer a good estimation of buckling modes and an accurate prediction of critical buckling length for distortional buckling. For perforated rack uprights the equivalent thickness concept developed by Davies [176] can be used to determine the critical buckling mode and corresponding buckling load.

Based on numerical analysis, one can decide if a STUB column test, to determine the influence of local buckling and perforations on the strength of a short column, or a DISTORTIONAL buckling test, on an upright column with the critical length for distortional buckling, is required.

The next step is to calibrate and validate a numerical model against the experiments in order to replicate the behaviour of tested specimens. It is of extreme importance to determine correctly the sectional failure mode (squash load, local or distortional buckling together with the section's strength) and the overall buckling mode (flexural, torsional or flexural-torsional). For this, the end DOF should be analyzed and correctly considered. It should be evaluated the restraint degree set for a specific end and based on this, the overall buckling length should be considered. The buckling length for flexural buckling can differ from the buckling length for torsion and therefore the overall buckling mode should be carefully determined.

Having clearly defined the two simple instabilities, the coupling length can be determined using ECBL approach [28] presented before. Instead of experimental tests for specimens with calibrated length, the numerical model can be used to determine the failure loads for considered specimen's length. Since thin walled sections are extremely sensitive to geometric imperfections (sectional and/or global), it is recommended the use of imperfection magnitudes specified in design codes or literature. There are numerous researchers that studied the geometric imperfections, sectional and global, and recommend a codification for them. ([187] , [134] , [203]).

For thin walled sections, the numerical analyses are usually performed in two steps. Firstly, an eigen buckling analysis (LBA) is used to determine the simple buckling modes, which afterwards, are scaled and combined in order to obtain the initial geometric imperfection. Subsequent, a GMNIA analysis is used to determine the failure load for considered specimen.

It is known that the buckling modes obtained from an eigen buckling analysis are usually periodic functions. Two linear combinations of the same simple buckling modes can give opposite results due to different halfwave lengths. A sensitivity study is recommended in order to determine the dominant imperfections and to generate a reliable set of numerical values.

Attention must be paid to initial imperfection generated as linear combination patterns. Two independent buckling modes combined using a specific pattern can have a stabilizing effect for the considered specimen. Another aspect to be considered concerns the combination of all imperfections scaled to maximum values (statistically speaking, it is impossible for all imperfections to occur in the same time with their maximum value).

Due to the fact that an imperfection measurement needs to be carefully conducted in order to be used for a numerical study, usually, coded imperfections are used. Numerous researchers proposed different values for specific types of imperfections i.e. sectional and global.

For example, Schaffer and Pekoz [203] proposed a codification for sectional imperfections, dividing them into two categories: *type 1*, maximum local imperfection in a stiffened element, and *type 2*, maximum deviation from straightness for a lip stiffened or unstiffened flange.

In terms of t , where t is the section's thickness, the type 1 imperfection, d_1 , is considered $d_1=6te^{-2t}$, while the type 2 imperfection, d_2 is considered $d_2=t$. it is also specified that for type 1 imperfection, the thickness should be less than 3mm.

In what concern the overall imperfections (bar deflection) Bjorhovde [188] proposed a magnitude of 1/1500 times of the member length. In ECCS Recommendations [189] is specified a conservative value of L/1000, value considered for European buckling curves. The corresponding tolerance accepted by EN 1090-2 [190] is L/750.

Considering the maximum values for sectional imperfections proposed by Schaffer and Pekoz [203] in combination with the maximum bar deflection imperfections (tolerance accepted by EN 1090-2 [190]) should lead to an conservative design.

5.2 Proposed design procedure – 1

This design procedure can be used to determine the design strength of perforated and unperforated pallet rack upright sections.

Pallet rack upright sections come in great variety of cross-sectional shapes and dimensions (height, width and thickness). In order to prevent local buckling, intermediate and edge stiffeners are often added to the cross-section walls. This approach leads to a higher strength against local buckling, but also entails the emergence of distortional buckling, a phenomenon caused by "stiffener inefficiency"

As presented before, this design procedure is based on almost exclusively on experimental testing. It requires **three** types of tests:

STUB column tests

The STUB column test setup and specimen's length shall be defined in accordance with EN15512:2009 specifications.

The test shall be used to observe the influence of such factors as perforations and local buckling on the compressive strength of a short column. It should be mentioned that the wavelength for distortional buckling is significantly longer than that for local buckling. This means that distortional buckling is not usually identified by a conventional stub-column test. Furthermore, if a stub-column test exhibits a distortional failure mode, it is unlikely that the length is sufficient to determine the minimum distortional buckling load.

DISTORTIONAL buckling tests

Based on experimental STUB column tests, an equivalent thickness can be determined (when testing perforated and unperforated sections) that accounts for perforations and local buckling. Another approach that accounts only for perforations, was developed by Davies [176] . The two approaches were compared and based on the experimental data presented in chapter 3, it can be concluded that for this particular case, the formula proposed by Davies [176] gives a better estimate.

This difference seems to be because the Davies formula is applied, in principle, to the walls containing perforations and then weighted to the entire section, while the test based evaluation of the equivalent thickness was, in this case, applied by simply reporting the failure load of perforated section to the failure load of brut section.

It is possible, that a weighting procedure to account for the contribution of perforated and unperforated walls would improve the results of experimental procedure.

Due to the fact that the distortional buckling is significantly dependent by the stiffness of inner and outer stiffeners, the equivalent reduced thickness is reducing unrealistically the distortional capacity of corresponding member.

On the other hand, it has to be recognized that the experimental procedure applied to obtain the equivalent thickness characterize mostly the strength of the

section (squash load) and not its behaviour in distortion, which in the end is a nonlinear phenomenon.

Moreover, even if the STUB column specimens are shorter than the critical length for distortional buckling, the observed failure mode was generally distortional. In this case, the equivalent thickness determined experimentally accounts for the perforations and the effects of distortional buckling.

It was observed that a LBA that uses a reduced thickness determined with using the formula proposed by Davies [176] give a good estimate of buckling modes and critical buckling load, together with the corresponding halfwave length.

Since a LBA analysis give the elastic critical buckling load, it is necessary to experimental validate the obtained value. The test setup used for STUB column testing can give reliable results when studying the distortional buckling. (see Chapter3).

INTERACTIVE buckling tests

Casafont [175] studied the influence of interactive distortional – overall buckling on cold formed sections with perforations and concluded that there is a range of member length where a gradual transition from symmetrical distortional buckling to torsional flexural buckling takes place. In this range, symmetric and anti-symmetric distortional buckling and torsional-flexural modes interact. Consequently, it is useful to know whether the effect of mode combination on the column strength should be considered in design. The range of lengths where these modes are combined may include the member lengths used in practice.

It is of paramount importance to correctly determine the sectional failure mode, local or distortional, and corresponding failure load since using the ECBL approach [28] the coupling point is determined based on this value.

Using the procedure proposed by Dubina [28] the value of imperfection coefficient can be determined based on the design value of erosion coefficient in the coupling interval. It is recommended to use an interactive buckling interval instead of a singly coupling point, due to the fact that it is practically impossible to replicate experimentally a test exactly in the coupling point. The factors influencing the experimental test include perforation patterns, end assembly, including cap and pressure plates, considered bearings, cutting imperfections etc.

The coupling point is defined by the reduced slenderness $\bar{\lambda} = 1/\sqrt{Q_D}$. Following, the coupling interval is determined from $\bar{\lambda}_c \pm \Delta$ where, usually, $\Delta \in 10\% - 15\%$. Georgescu [182] had shown that even if an unsymmetrical interval is used, the results are satisfactory (-10% - 5%) and (-15% - 7.5%).

The procedure used to determine the coupling point and corresponding erosion was detailed in previous sections.

The ECBL approach [28] was adapted for the case of distortional – flexural buckling interaction and applied for the case of RS125 sections. The steps followed to apply the procedure are detailed below:

STEP 1. STUB column testing

The test setup and the length of STUB column specimen are determined in accordance with EN15512:2009 [13] provisions. Test arrangement and method, alternative 1 was used.

200 Buckling checking of perforated cold-formed steel sections in compression. – 5

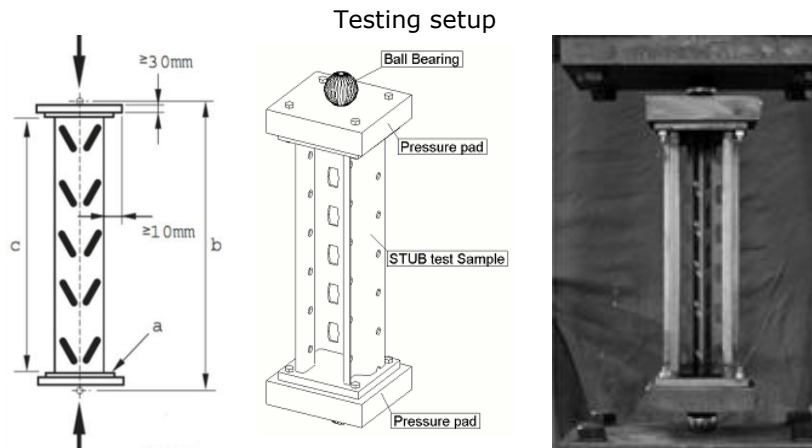
- the length shall be greater than three times the greatest flat width of the section (ignoring intermediate stiffeners). It shall include at least five pitches of the perforations.
- It shall be cut normal to the longitudinal axis, midway between two sets of perforations.
- The base and cap plates shall be bolted or welded to each end of the stub upright.

RS125N

- $3 \times 125 = 375$
- Length increased to 400mm (due to perforations)
- Base and cap plates welded
Specimen length: 400mm
Flexural buckling length: 510mm

RS95N

- $3 \times 95 = 285$
- Length increased to 300mm (due to perforations)
- Base and cap plates welded
Specimen length: 300mm
Flexural buckling length: 410mm



Experimental test – results [kN]			
413.28	397.46	279.82	281.63
407.81	409.05	276.99	278.68
400.85	411.02	284.28	279.00
404.03	396.51	274.33	277.92
402.27	395.91	278.78	277.81
400.19	406.05	278.63	283.42
Average (N_{av}) [kN]	403.70	Average (N_{av}) [kN]	279.27
StDev	5.80	StDev	2.74
Design load [kN]	397.90	Design load [kN]	276.53

Since no local buckling was observed for studied sections, further analysis is required to determine critical sectional buckling mode.

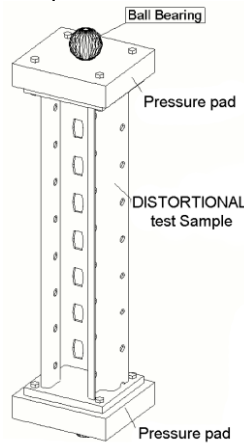
STEP 2. DISTORTIONAL buckling testing

The test setup for DISTORTIONAL buckling test is in accordance with EN15512:2009 [13] provisions for STUB test arrangement and method, alternative 1.

- a. The length was determined using a LBA. Additional, for perforated section, the equivalent thickness approach proposed by Davies [176] was used to account the perforations.
- b. It shall be cut normal to the longitudinal axis, midway between two sets of perforations.
- c. The base and cap plates shall be bolted or welded to each end of the stub upright.

RS125N	RS95N
a. 560mm b. 560mm c. Base and cap plates welded Specimen's length: 560m Flexural buckling length: 670mm	a. 500mm b. 500mm c. Base and cap plates welded Specimen's length: 500m Flexural buckling length: 610mm

Testing setup



Experimental test – results [kN]			
	381.06		262.67
379.90	387.43	259.67	260.50
394.62			
398.74			
Average (N_{av}) [kN]	388.35	Average (N_{av}) [kN]	260.95
StDev (σ)	8.26	StDev (σ)	1.55
Design value (N_D) [kN]	371.84	Design value (N_D) [kN]	257.85

The design value of distortional capacity was obtained with the following formula:

$$N_D = N_{Av} - 2\sigma \tag{5.8}$$

It was observed that the experimental failure load for RS125 perforated section is close to critical distortional load predicted by LBA. The results of LBA indicated that the RS95 section is not prone to distortional buckling. RS95 perforated section the experimental failure load is comparable to the squash load.

Based on this observation, it can be said that the RS95 section is not sensitive to distortional buckling and for this section, the interaction is between the squash load capacity and the considered overall instability.

STEP 3. INTERACTIVE buckling testing

The test setup is similar to the arrangement for STUB column and DISTORTIONAL buckling tests. The ECBL approach [28] was used to determine the coupling point and to define the coupling interval. The following properties were used:

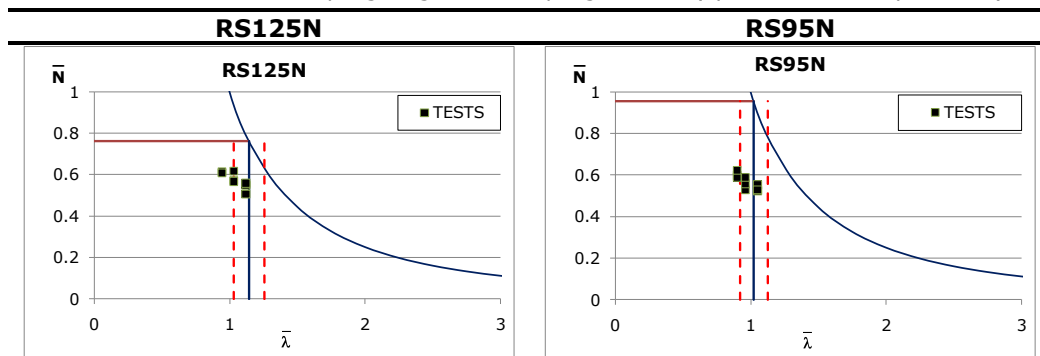
Table 5.2 Properties used for ECBL approach

	RS125N	RS95N
Area [mm ²]	959.4	573.2
Inertia moment [mm ⁴]	1211097	393928.5
f_{va} [N/mm ²]	501.29	500.2
E [N/mm ²]	202941	207467
N_U [kN]	371.84	273.79
N_D	0.770	0.955
λ_c	1.140	1.023
Coupling length, L_c [mm]	2554	1716

The experimentally tested specimens will be used to calibrate the design value of erosion, and further, based on the design value of erosion, the imperfection coefficient will be determined according to simplified method proposed by Dubina [202]. The design value of the

The coupling interval will be considered to be symmetric (-10% to +10%). In Table 5.3 are presented, graphically, the coupling length (coupling point) together with considered coupling interval. Even if considering an

Table 5.3 Considered coupling length and coupling interval (symmetric and asymmetric)



The two situations were considered due to the fact that a symmetric interval ($\lambda_c \pm \Delta$, with $\Delta = \pm 10\%$) excludes a set of specimens. In order to take into account all the tested specimens, the coupling interval was shifted to the left by 6%.

Further, in Table 5.4 is presented the ECBL approach [28] applied for the experimental set of data, (INTERACTIVE buckling test results, for the two considered upright sections with perforations, INT-125N and INT-95N. There were

considered two situations: (1) a symmetric coupling interval and (2) an asymmetric coupling interval.

Table 5.4 INTERACTIVE buckling interval results

RS125N			RS95N		
Length [mm]	Failure load [kN]	Erosion (ψ)	Length [mm]	Failure load [kN]	Erosion (ψ)
2110	296.73	0.155	1510	171.50	0.357
	296.91	0.155		169.07	0.365
	293.63	0.162		178.68	0.332
	276.15	0.198		151.69	0.426
2310	274.22	0.202	1610	160.16	0.396
	298.07	0.153		168.88	0.366
	265.44	0.220		158.41	0.402
2510	269.71	0.211	1760	149.73	0.433
	244.69	0.263		151.62	0.426
	ψ_{aver}	0.208		Symmetric coupling interval	ψ_{aver}
StDev	0.036	StDev	0.025		
ψ_D	0.279	ψ_D	0.459		
α	0.115	α	0.472		

where ψ_{aver} is the average value of erosion, StDev is the computed standard deviation of erosion, ψ_D is the design value of erosion coefficient, determined using Eq. (5.9), α is the imperfection factor computed using Eq.(5.10)

$$\psi_d = \psi_{aver} + 2 \cdot StDev \quad (5.9)$$

$$\alpha = \frac{\psi_d^2}{1 - \psi_d} \frac{\sqrt{\bar{N}_D}}{1 - 0.2\sqrt{\bar{N}_D}} \quad (5.10)$$

with \bar{N}_D defined in Table 5.2

Considering the imperfection coefficient determined using the following method described above, the procedure presented in EN1993-1-1 [32] can be used to determine the buckling capacity curve for considered profiles.

For thin walled sections (class 4 cross sections) the following equation is used to determine the bar buckling capacity:

$$N_{b,Rd} = \frac{\chi A_{eff} f_y}{\gamma_{M1}} \quad (5.11)$$

Since for distortional buckling, there is not the A_{eff} concept, $A_{eff} f_y$ is replaced by N_D . Replacing $A_{eff} f_y$ with N_D Eq. (5.11) becomes:

$$N_{b,Rd} = \frac{\chi N_D}{\gamma_{M1}} \quad (5.12)$$

this is the new formula used to determine the buckling capacity for a member undergoing distortional-overall interactive buckling.

Due to the fact that during the calibration process for α imperfection coefficient the considered design value is affected twice by the standard deviation, it was considered that a safety coefficient $\gamma_{M1}=1$ is sufficient. The χ reduction factor is defined by:

$$\chi = \frac{1}{\Phi + \sqrt{\Phi^2 - \bar{\lambda}^2}}, \text{ but } \chi \leq 1.0 \quad (5.13)$$

where

$$\Phi = 0.5 \left[1 + \alpha \bar{\lambda} - 0.2 + \bar{\lambda}^2 \right] \quad (5.14)$$

and

$$\bar{\lambda} = \sqrt{\frac{N_D}{N_E}} \quad (5.15)$$

where N_D is the experimental failure load for specimens with critical length for distortional buckling and N_E is the critical buckling load for considered global mode, in this case flexural buckling.

In order to compare the results obtained using the proposed method with the results obtained using the procedure defined in EN15512, the design code procedure was applied for considered sections. The methodology proposed by norm consists in four main steps:

- The distortional buckling strength, $N_{db,Rd}$, is determined by means of a test carried out on a column length equal to the length of the single bracing panel closest to one metre.
- The strength, $N_{b,Rd}$, is determined taking into account the effects of local and global buckling test. The effects of local buckling are included through an effective area determined from a STUB column test; the European buckling curves are used to determine the final global buckling strength:

$$N_{b,Rd} = \frac{\chi \cdot A_{eff} \cdot f_y}{\gamma_{M1}} \quad (5.16)$$

where A_{eff} is the effective area determined in the stub column test, and γ_{M1} is the material partial factor ($\gamma_{M1}=1$). χ is the reduction factor for global buckling calculated by means of the European buckling curves

$$\chi = \frac{1}{\phi + \sqrt{\phi^2 - \bar{\lambda}^2}} \quad (5.17)$$

$$\phi = 0.5 \left[1 + \alpha \bar{\lambda} - 0.2 + \bar{\lambda}^2 \right] \quad (5.18)$$

with

$$\bar{\lambda} = \sqrt{\frac{A_{eff} \cdot f_y}{N_E}} \quad (5.19)$$

and N_E is the global elastic buckling load (flexural buckling in this case)

- The ratio $N_{db,Rd}/N_{b,Rd}$ is further computed. If the ratio is greater than one, no adjustment of the effective area is made
- Is the ratio is less than 1, A_{eff} should be reduced to a new value at which the calculated $N_{b,Rd}$ is equal to the value obtained from the distortional buckling tests. The new value for A_{eff} is used in all subsequent calculations.

In the design process, the experimental failure loads are corrected to take into account the yield strength of the material and the thickness of the test specimen.

Following, in Fig. 5.2 and Fig. 5.3 are presented the buckling strength curves determined using the EN15512:2009 procedure (depicted in solid blue line) and the proposed experimental procedure.

For the ECBL proposed procedure, depicted with red lines, two approaches were considered i.e. moment of inertia of the gross cross section (solid line) and moment of inertia of the minimum area cross section (dashed line).

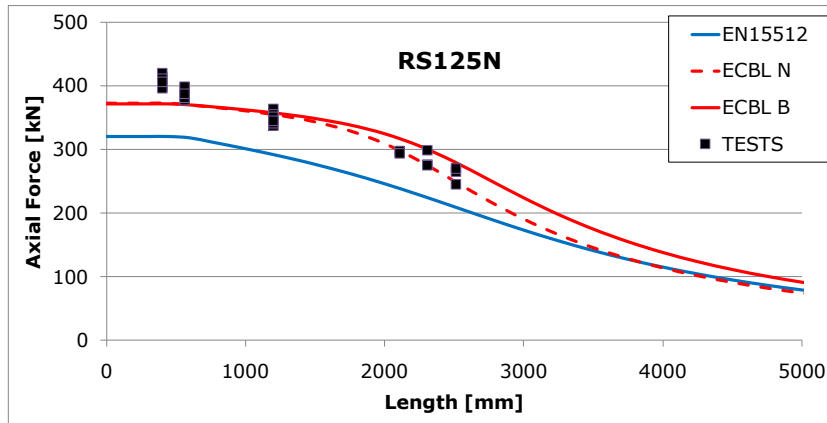


Fig. 5.2 Buckling strength curves for RS125N section

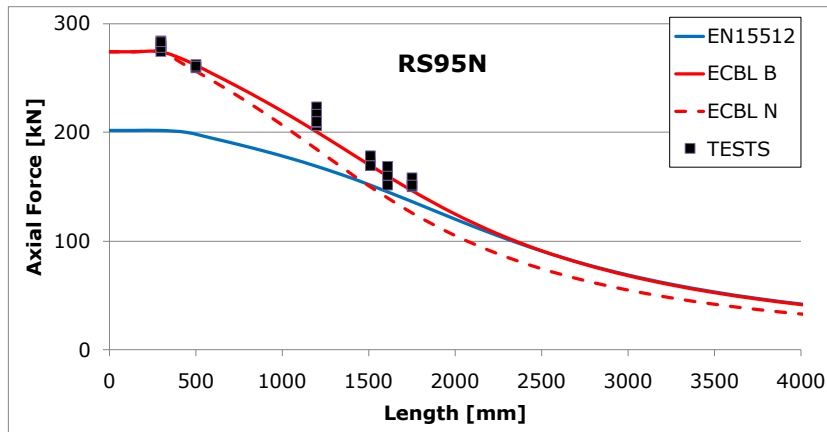


Fig. 5.3 Buckling strength curve for RS95N section

Analyzing Fig. 5.2 and Fig. 5.3 it can be observed that the design procedure defined by EN15512:2009 gives conservative results, mainly for the short length upright sections.

Even though, the purpose of the compression tests on uprights is to determine the influence of the distortional buckling mode on the axial load capacity of the upright section, the actual test results correspond rather to a coupled instability (D+F or D+FT) than to pure distortional buckling. The outcome of this

interactive buckling is altered, once more, by the coupling with overall instability by means χ factor. This last phenomenon is a D.F. + F/FT type of interactive buckling.

The reduction due to the double instability coupling underestimates severely the buckling strength of short length upright sections. In principle, the reduction of the area, in the forth step of the norm procedure, is not theoretically appropriate.

On the other hand, the ECBL approach describes accurately the behaviour of the tested specimens. The negative aspect of the proposed procedure is represented by the safety coefficient resulted from the simplified approach. It is possible to apply the procedure defined in Annex D of EN1990 in order to calibrate properly the γ_{M1} factor, which for this case, has to be greater than one.

5.3 Proposed design procedure – 2

This design procedure reduce to the minimum the experimental part for the design of thin walled members prone to distortional with overall interactive buckling. The procedure requires only **one** set of tests used to calibrate a numerical model. The design is based on rational numerical analysis using a combined GBT or FSM with FEM approach.

The experimental test, used to calibrate the numerical model, is of extreme importance since a correct calibration and validation of the numerical model is required in order to obtain reliable results.

This method is structured in 6 steps, presented below.

STEP1. LBA – Linear Buckling Analysis

In order to determine the critical sectional failure mode i.e. squash load or local / distortional buckling a linear buckling is required. There are available free software packages based on GBT (Generalized Beam Theory) or FSM/cFSM (constraint Finite Strip Method) that offer modal decomposition.

Based on this numerical approach, one can determine the critical failure mode for a specific type of section. The failure mode include:

- a. Failure at squash load
- b. Failure due to local buckling
- c. Failure due to distortional buckling

In order to determine the critical buckling load for perforated sections, the equivalent thickness approach, proposed by Davies [176] can be successfully used in combination with LBA (GBT or cFMS).

STEP2. Experimental testing

If the section failure is determined by a) or b) a STUB column test is recommended to be carried out, in accordance with EN15512:2009 specifications.

If the section is prone to distortional buckling, based on the LBA, the distortional buckling load and corresponding halfwave length should be determined. For this case, the experimental setup should be similar to the test arrangement for STUB column test, excepting the test specimen length. The length for DISTORTIONAL buckling test specimen should be equal with the halfwave length for distortional buckling, determined in the LBA.

This step can be skipped if experimental data is available for an identical section (geometrical dimensions, thickness, perforation pattern, etc.)

STEP3. Numerical model calibration and validation

The experimental test results should be used to calibrate and validate a numerical model, capable to replicate the behaviour of the experimentally tested specimens. In order to calibrate the model, special attention should be paid when measuring the geometric imperfections and the loading and supporting eccentricities. The numerical model should replicate the experimental tests (general geometric dimensions, thickness, perforation arrays pattern, etc).

The base material properties are considered known (provided by supplier). An elastic – perfect-plastic material behaviour, considering the average yielding strength, determined in accordance with EN1993-1-3 [10] provisions and the standard value for Young's modulus are recommended to model the material behaviour for FE model.

For studied pallet rack upright sections, the influence of residual stresses on the ultimate capacity was found to be small (less than 3%). For this particular type of sections, a numerical model that does not model the residual stresses should give accurate results.

STEP4. Coupling length and interactive buckling interval

Following, it is very important to clearly define the end support conditions (free, pinned or fixed) for considered thin walled member. The end restraints can differ for translational, flexural and torsional DOF.

Considering the defined support conditions and the section properties (area, moments of inertia, torsional constant, etc) the critical overall buckling mode can be determined for the considered member e.g. flexural, torsional or flexural-torsional buckling.

Using the ECBL approach [28] the coupling point and corresponding coupling length can be determined for considered interaction, sectional critical failure mode (determined based on LBA) and critical global buckling mode.

This procedure will not be further detailed.

STEP5. Imperfection sensitivity study

Using the calibrated and validated FE model, a new set of numerical analyses should be defined. The numerical model geometry should replicate exactly the considered section, including general geometry dimensions, thickness and perforation pattern along the specimen's length.

The length for the numerical model should be taken to be the coupling length determined in previous step. Since, no geometrical imperfections are available, coded imperfections are recommended to be used (local, distortional and global). Numerous researchers studied the effects of imperfections and proposed a codification for local and/or global imperfections.

Based on the sensitivity study, the critical imperfection combination should be determined. Special attentions should be paid when defining the combinations. It must be considered that, from a statistic point of view, in practice, if two or more imperfections couple, they will not couple with their maximum value. It is still acceptable to consider two imperfections coupled with maximum value, if no load eccentricities are considered.

Using the ECBL approach [28] one can determine the erosion of critical load (buckling or squash load) in the coupling point. The maximum value of the erosion will be considered to be the design value. The imperfection coefficient should be computed using the Eq.(5.10).

STEP6. Buckling Design

Considering the distortional-flexural buckling interaction and using the calibrated and validated numerical model a new FE analysis should be conducted. The specimen that will be analysed should have the critical buckling length, determine using the LBA analysis, and having the coded values as initial geometrical imperfections. The resulted value should be used in the design procedure based on the EN1993-1-1 provisions, described in previous paragraph replacing N_D in Eq. (5.12) with the numerically obtained value.

5.4 Concluding remarks

There were proposed two design procedures for interactive distortional with flexural buckling based on the ECBL approach [28] proposed by Dubina.

In Table 5.5 are presented the outcomes of the two considered procedure.

Table 5.5 Design procedures – results

		Base capacity [kN]	Imperfection coefficient	Global buckling mode
Procedure 1	RS125N	371.84	0.115	Flexural
- experimental-	RS95N	273.79	0.472	Flexural
Procedure 2a	RS125N	370.48	0.273	Flexural
- numeric -	RS95N	286.69	0.639	Flexural
Procedure 2b	RS125N	328.66	0.157	Flexural
- numeric -	RS95N	222.68	0.187	Flexural

In Fig. 5.4 and Fig. 5.5 are presented the buckling capacity curves, for RS125 and RS95 sections with perforations, computed using the EN1993-1-1 [32] buckling check procedure in conjunction with the ECBL approach [28] for interactive distortional – overall flexural buckling considering the experimental approach.

For the numerical procedure, the erosion can be calculated (1) using the LBA results (the resulting erosion accounting for the effect of imperfections and coupling of the two considered instabilities) and (2) using the GMNIA results (the resulting erosion accounting for the coupling effect alone).

It can be observed that the numerical procedure (2a and 2b) gives different values for the α imperfection coefficient. The two approaches are presented in Fig. 5.8 and Fig. 5.9 for RS125 and RS95 sections with perforations.

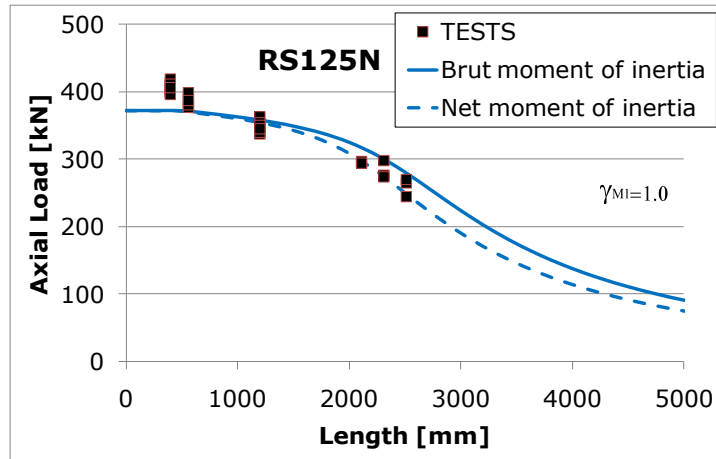


Fig. 5.4 Buckling capacity curve for RS125N section – experimental method, $\gamma_{M1}=1.0$

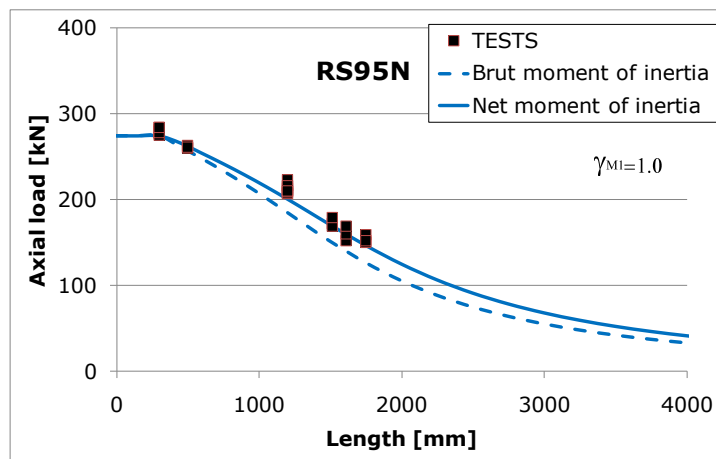


Fig. 5.5 Buckling capacity curve for RS95N section – experimental method, $\gamma_{M1}=1.0$

It can be observed the inconsistency generated by mixed approach; considering the minimum area for sectional strength and the gross section properties for global calculations. From this point of view, considering that the perforations affect only for the section in compression and ignoring it for the section in bending is not an option. Taking this into account, the proposed procedure has certain limitations.

Although, the simplified methodology provides close results, the curves cannot be used for design without applying a safety coefficient, γ_{M1} . It is possible to apply the methodology proposed by Annex D from EN1990 in order to calibrate properly the γ_{M1} factor, which in this case has to be greater than 1.00. For instance, if a $\gamma_{M1}=1.1$ factor is applied, which is the limit accepted by CEN, the buckling curves describe optimally the behaviour of experimentally tested specimens.

The new buckling curves are presented in Fig. 5.6 for RS125 section and in Fig. 5.7 for RS95 section with perforation, using the brut section properties.

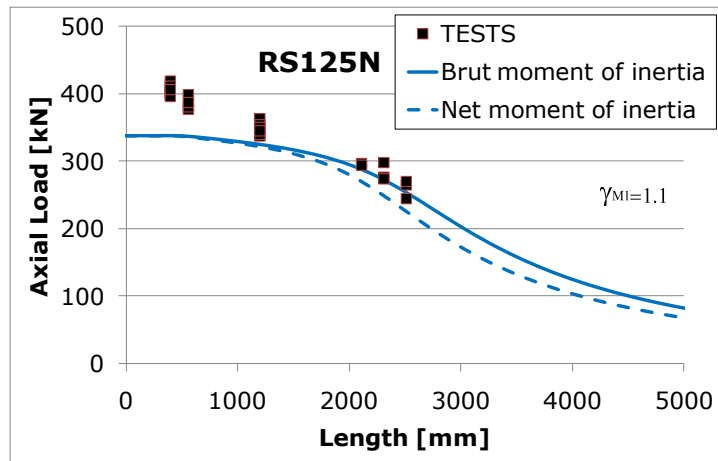


Fig. 5.6 Buckling capacity curve for RS125N section – experimental procedure, $\gamma_{M1}=1.1$

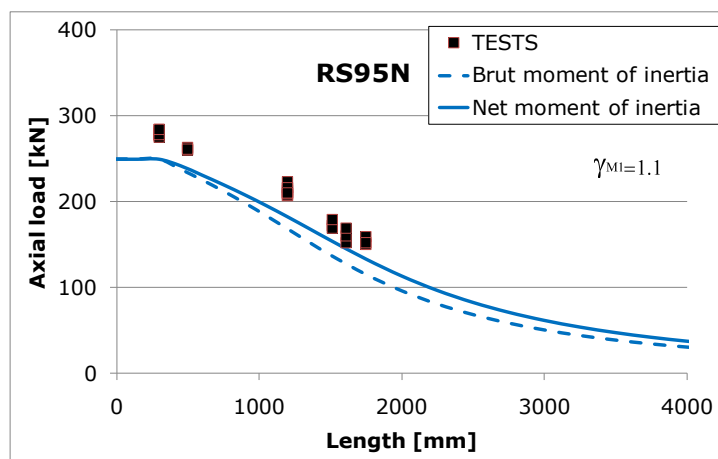


Fig. 5.7 Buckling strength curve for RS95N section – experimental procedure, $\gamma_{M1}=1.1$

The European design code [13] notes that for some upright sections, the arrays of perforations, because their size, number and disposition, can cause a significant reduction in moment of inertia of the section. No further explanation is given regarding the reduction of the value of the moment of inertia.

Based on the Fig. 5.6 and Fig. 5.7 it can be concluded that for studied sections, the moment of inertia value is significantly reduced due the presence of perforations. It can be observed that the proposed design procedure, using the moment of inertia of the minimum area cross-section, defines best the behaviour the experimentally tested specimens.

Following, the buckling strength curves using the α imperfection factor calibrated using the ECBL approach for the numerical method (2a and 2b, see Table 5.5) are presented in Fig. 5.8 and Fig. 5.9 for a safety coefficient $\gamma_{M1}=1.0$.

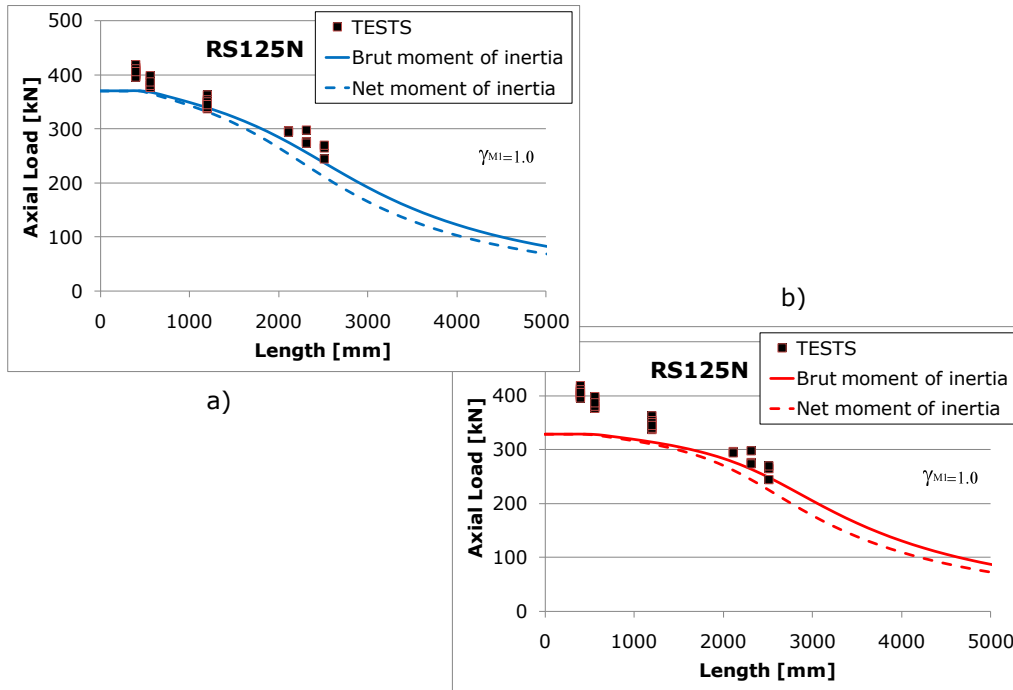


Fig. 5.8 Buckling capacity curve for RS125N section – numerical procedure, $\gamma_{M1}=1.0$

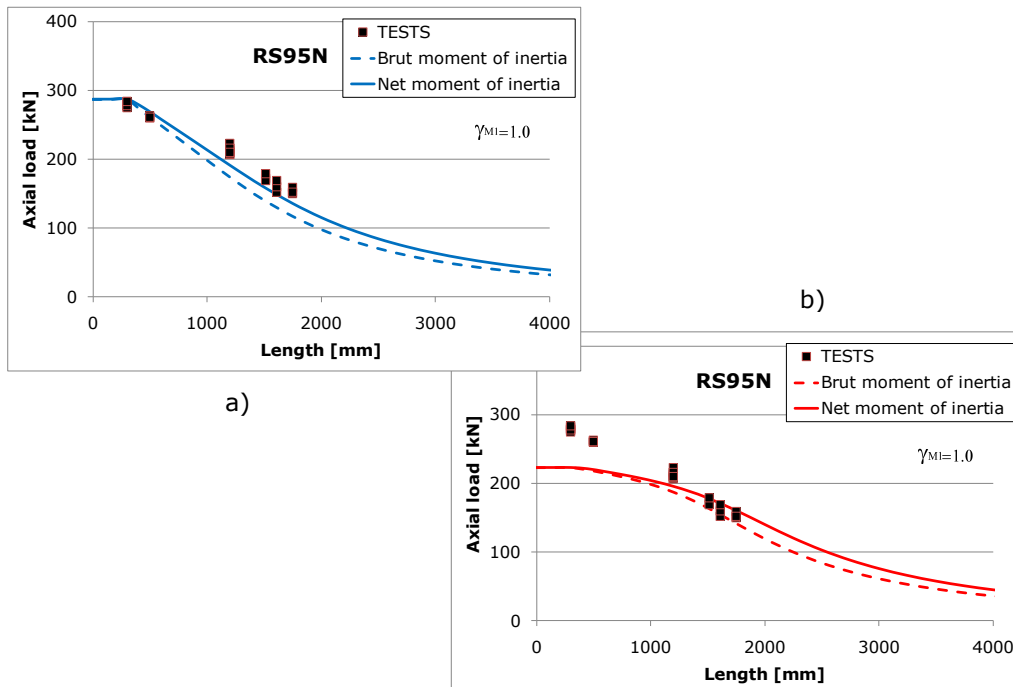


Fig. 5.9 Buckling capacity curve for RS95N section – numerical procedure, $\gamma_{M1}=1.0$

Considering the curves presented in Fig. 5.8 and Fig. 5.9, it can be concluded that the considered sectional imperfection, $d_2=t$, is too severe, especially for RS95N section, where the distortional – flexural interaction is not practical, due to the fact that RS95 section is not prone to distortional buckling.

Moreover, the low value of sectional strength reduces, unrealistic, the erosion coefficient and the corresponding imperfection factor. The resulting buckling strength can overestimates the strength for long length profiles and underestimates the strength for short length profiles.

The differences between the strength curves presented in Fig. 5.6 and Fig. 5.7 on one hand and Fig. 5.8 and Fig. 5.9 on the other hand, can be explained by the fact that the measured imperfections for the tested specimens are lower than the corresponding ones used in numeric analysis, which are codified imperfections presented in Chapter 3. In Fig. 5.10 is presented, qualitatively, for a RS125N distortional specimen, the differences between the considered imperfection for numerical model (in red) and the measured imperfection (in blue). The d_2 imperfection is considered relative to specimen ends (see Fig. 5.10).

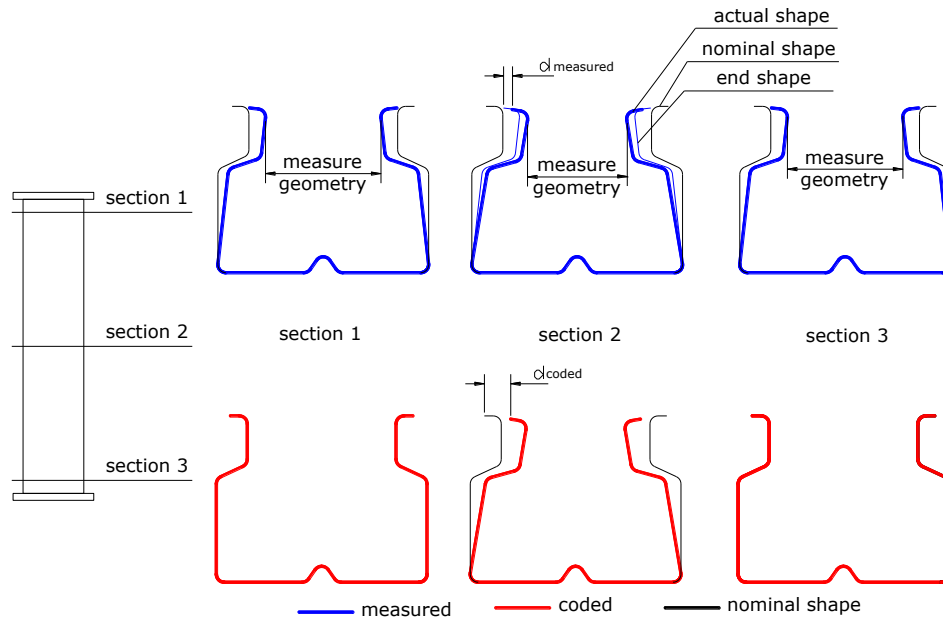


Fig. 5.10 Type 2 sectional imperfection (d_2) for distortional specimens.

In Table 5.6 and Table 5.7 are presented the maximum measured imperfections obtained for interactive specimens, together with the considered (coded) imperfections for the numerical analysis.

Table 5.6 Maximum geometric imperfections for RS125N interactive buckling specimens

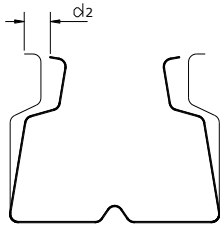
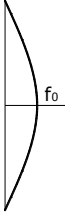
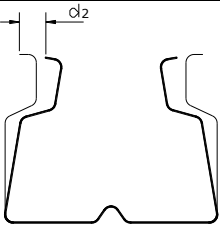
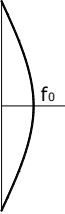
Imperfection	Measured imperfections	Coded imperfections
Sectional 	1.45 (0.45 t)	$d_2=t$ $t=3.2\text{mm}$
Overall 	1/1650	L/750

Table 5.7 Maximum geometric imperfections for RS95N interactive buckling specimens

Imperfection	Measured imperfections	Coded imperfections
Sectional 	1.38 (0.53 t)	$d_2=t$ $t=2.6\text{mm}$
Overall 	1/1416	L/750

It can be observed that for both sections, RS125 and RS95, the considered imperfections for numerical analysis have greater values than those measured for experimentally tested profiles. For RS95 specimens, together with the global bow imperfection a twisting of the section was observed i.e. torsional imperfection. Since the numerical study was conducted for the interactive distortional-flexural buckling, the torsional component of the imperfection was not taken into account.

It must be specified that the flexural and flexural-torsional buckling loads, for the studied sections, are very close, and in real life situations, the imperfections dictate the instability mode, simple and coupled.

In conclusion, procedure defined by the European design code, for stability checking of members in compression can be applied for the perforated upright members. On this purpose, it is necessary to have a proper evaluation, either

214 Buckling checking of perforated cold-formed steel sections in compression. – 5

experimental or numeric, of the distortional capacity for considered sections. Following, the ECBL approach can be applied in order to evaluate the α imperfection coefficient; again, test or numerical simulations of the member buckling strength having the length in the interactive buckling range is required.

Attention has to be paid to the shape and magnitude of imperfection to be used in numerical simulations.

For RS95 section, it can be clearly observed that the interaction between the distortional and flexural buckling is not an actual interaction. The effect of sectional imperfections, when coupled with global bow imperfection, is very small, resulting into a small value of α imperfection factor. Considering a high magnitude for the sectional imperfection can lead to a decrease of the erosion value, and consequently to a small imperfection coefficient.

The considered sectional imperfections, $d_2=t$, lead to over-conservative results for short length specimens, especially for RS95 section, where no distortional buckling was observed.

For both proposed method, it recommended to use Annex D of EN1990 in order to calibrate the γ_{M1} safety coefficients.

6 CONCLUSIONS

6.1 Conclusions

6.1.1 Thesis objective

In the last two decades, the advances in the field of simple and coupled instabilities are of unquestionable value. The understanding of the failure mechanism for distortional buckling, a relatively new instability mode that characterizes stiffened thin walled members, opened new research areas and led to developments of new calculation methods based partially or entirely on numerical tools.

Even if there was recorded a significant progress, the technical regulations for the design of pallet rack uprights in compression is based, almost entirely, on experimental programs which are expensive and time consuming. Moreover, the design codes do not consider the possibility of interactive buckling, sectional and overall.

The main objective of the thesis is to provide a design procedure for stability checking of upright members in compression, accounting for the interactive buckling, distortional and flexural, based on the model of EN1993-1-1/EN1993-1-3 [32], [10] methodology.

6.1.2 Synthesis of chapters conclusions

Chapter 2

Nowadays, the numerical methods based on GBT and/or cFSM can predict the critical buckling mode, the corresponding critical load together with critical halfwave length for thin walled sections with a specific length. The main drawback of these numerical models is represented by the incapacity to incorporate perforations.

Due to this deficiency, a design procedure based entirely on analytical or numerical approach was considered to be precarious for the case of pallet rack upright sections. Technical regulations for design of pallet rack systems and their members still remain at the level of empirical procedures, using almost exclusively the design assisted by testing.

Based on these observations, the objective of this thesis, to provide a design procedure for stability checking of upright members in compression based on the model of EN1993-1-1/EN1993-1-3 approach, seems to be fully justified.

Chapter 3

The output of the experimental program carried out using the CEMSIG testing facility represents the main contribution of the thesis. There have been tested four types of pallet rack upright sections in compression, RS125 and RS95, with and without perforations.

The material properties were also determined from the base material and from the material cut from two cold formed sections, obtaining the yield and ultimate strength of the base material and the increase over the section. Analysing

and processing the results of the material testing program, it can be said that the average yield strength formula recommended by the EN1993-1-3 gives an accurate approximation for the real yield strength distribution.

For the studied sections without perforations, RS125 and RS95, the distribution and magnitude of flexural residual stresses was determined. The values of residual stresses are in accordance with the values found in literature, regarding the cold rolling sections. Special care must be taken when cutting the strip, because due to high residual stresses, the strip bend and the cuttings tend to be unparallel.

Sectional and overall imperfections were measured for tested specimens. The measured values of sectional and overall imperfections for interactive specimens were analyzed and compared to the values found in literature. The overall imperfections, bow and torsional, measured for INTERACTIVE specimens, were 1/1651 for INT-125 section, respectively 1/1416 from the bar total length for INT-95 section, while the sectional *type 2* imperfection (defined by Schafer and Pekoz) were found to have a maximum value of 0.45t for INT-125 specimens and 0.45t for INT-95 specimens. These values are in agreement with the proposed maximum values from literature, 1.00t.

The experimental program for specimens in compression followed the provisions of the European design code for pallet rack storage systems. There were tested four sections, RS125 and RS95, with and without perforations. The STUB column test revealed that none of the studied section is prone to local buckling. For ST-125 specimens a distortional failure type was observed, while for ST-95 specimens, the failure was due to reaching squash load.

For UP-125 specimens, the observed failure was the distortional buckling (two halfwaves), while for UP-95 specimens the observed failure was a global mode i.e. flexural-torsional buckling or flexural buckling about minimum inertia axis.

In order to determine experimentally the failure load of the studied sections with critical length for distortional buckling, the experimental program was extended and consequently, DISTORTIONAL specimens were studied. For DIST-125 specimens, the failure mode was the symmetric distortion of the section and the corresponding failure load was fairly accurate determined by a LBA. For DIST-95 specimens, even if in some cases a distortion of the section was observed, the failure load was corresponding to squash load.

In the case of INTERACTIVE specimens, for all INT-125 specimens, the observed failure mode was characterized by a distortional – flexural or flexural – torsional interaction. The same failure mode was observed for INT-95B specimens. For INT-95N specimens, the dominating failure mode was flexural-torsional.

Due to experimental arrangement, where the torsion was prevented at the ends, the critical buckling loads corresponding to flexural and flexural-torsional buckling were very close. The small difference between the critical buckling loads corresponding to overall buckling modes explains the failure modes observed for INTERACTIVE specimens.

Given the fact that the flexural critical buckling load was slightly lower, this value was considered for the interactive buckling calculations.

Chapter 4

An imperfection sensitivity study was conducted considering the maximum values for sectional and overall imperfections found in design codes and literature.

Considering the coupling of distortional and overall flexural instabilities, the imperfections considered for the numerical study were selected affine with the desired failure mode i.e. distortion of the section and global bow imperfection.

For the sectional imperfection (distortion) the magnitude was taken in accordance with the codification proposed by Schafer and Pekoz [187] ($d_2=t$). For bow imperfection the value was chosen to be the maximum allowed manufacturing tolerance imposed by EN1090.

The imperfection sensitivity study using the calibrated and validated numerical model, reveals that the most critical imperfection combination is a global bow imperfection (F+) combined with a sectional distortional imperfection (D+). It can be said that considering the maximum value of imperfections, $L/750$ (according to EN1090) for bow imperfection and t (according to Schafer and Pekoz [187]) in the case of sectional *type 2* imperfection provide the most conservative results.

Based on the sensitivity study, it was observed that the loading eccentricities can have a significant effect on the ultimate failure load.

When conducting an imperfection sensitivity study, it is recommended to consider a wide range of possible imperfection together with possible/realistic combination. Special attention should be paid when combining imperfections. From a statistic point of view, when several imperfections combine, they do not combine with their peak values.

Chapter 5

The ECBL approach is a newly developed procedure that permits the evaluation erosion of critical bifurcation load as result of interactive buckling. It allows considering the interaction of sectional (local or distortional buckling) with global (flexural, torsional or flexural-torsional) instabilities.

For this study, the distortional-flexural coupled buckling was considered. Using the ECBL approach, two design methods based on EN1993-1-1/EN1993-1-3 buckling strength checking procedure were developed; an experimentally based procedure and a numerically based procedure.

It was observed that the resulting buckling strength curve determined using the experimentally based procedure describe optimally the strength of the tested specimens. The design procedure based on numerical models is more conservative, due to the fact that the imperfections considered for the numerical approach were coupled with their maximum values. This approach was considered due to the fact that the loading eccentricities were disregarded, while in practice they are inerrant.

For both proposed procedures, it is recommended to use the Annex D of EN1990 in order to properly calibrated the γ_{M1} safety coefficient.

6.1.3 Concluding remark

The final conclusion of this study is that it is really possible to adapt the European buckling curves and use the design checking procedure for stability problems from EN1993-1-1 and EN1993-1-3 for verification of upright type members in compression.

On this purpose, either test or numerical simulations results, or a combination of the two, can be used applying the ECBL approach to calibrate appropriate α imperfection factors.

Analyzing the results from the numerical and experimental approach, it seems more logical to use the geometrical properties of the minimum area cross-section, even for global calculations, instead of gross section properties.

It must be mentioned that the UPRIGHT test defined by EN15512:2009 to determine the effects of distortional buckling on axial load capacity of the upright sections does not correspond to pure distortion, but to an interactive buckling. Other

researchers [175] concluded that interactive buckling range can include member lengths used in practice. One suggests completing the code provisions with the relevant procedures.

Taking into account that the imperfection coefficients for the European buckling curves (EN1993-1-1) have been experimentally determined, in the late 1960, for hot-rolled sections and the factor $\alpha \bar{\lambda}^{-0.2}$ have been calibrated by Rondal and Maquoi [26] for the same type of profiles, it is not normal that these values to be used for cold formed steel sections.

The values of imperfection coefficients presented in EN1993-1-1 are influenced by the cross-sectional shape in direct relation with the membrane residual stresses. For the case of thin walled section, the membrane residual stresses are significantly lower than the flexural residual stresses, on one hand, and on the other hand the influence of geometric imperfections, due to wall slenderness has a more pronounced effect than the residual stresses.

Considering these, imperfection coefficients specifically determined for thin walled sections together with a proper calibration of safety coefficient, γ_{M1} , is required.

6.2 Personal contributions

Regarding the research field, based on studies done by the author and the obtained results, the personal contributions include:

- Design and development of an experimental program based on the provisions of European pallet rack structures design code, EN15512:2009.
- Design and development of an extended experimental program with laboratory tests to determine the yield strength distribution due to cold forming process and laboratory tests to determine residual stresses magnitude and distribution over the cross section
- Design and development of an extended experimental program with compression tests on specimens with critical length for distortional buckling and compression tests on specimens with the length, calibrated using the ECBL approach, in interactive buckling range.
- Analysis of experimentally obtained results and, in the same time, emphasizing the need of a detailed design procedure in order to take into account the distortional-flexural buckling interaction for pallet rack upright sections in compression.
- Development of a valid numerical model capable to reproduce the behaviour of pallet rack uprights in compression, from the point of view of failure load and failure mode.
- The calibration and validation of the numerical model against the experimental tests
- Development of a numerical sensitivity study, using the calibrated numerical model, in order to determine the critical imperfections for specimens in the interactive buckling interval.
- Evaluation of the erosion of critical bifurcation load as a result of the coupling effect and geometric imperfections and the computation of the corresponding imperfection coefficients for specimens having the length in the interactive buckling interval.

- The proposal of two design methods, i.e. experimental and FEM based design procedure, for the buckling strength check of perforated pallet rack upright sections.

6.3 Publications

During the research period, the contributions of the author within this thesis have been published and disseminated by means of scientific articles as follows:

1. Viorel Ungureanu, Dan Dubina, **Andrei Crisan**: "Experimental and Numerical Investigation of Ultimate Capacity of Pallet Rack Members" - Presentation of investigation program, ECCS TC7 Meeting, Barcelona, Spain 2010
2. **Andrei Crisan**, Viorel Ungureanu, Dan Dubina: "Ultimate Limit Strength of Perforated Cold-Formed Steel Sections", International Colloquium, "Stability and Ductility of Steel Structures" Rio de Janeiro, Brasil, 2010, Published in VOLUME 2, Proceedings of SDSS' Rio 2010, International Colloquium Stability and Ductility of Steel Structures, Published by Federal University of Rio de Janeiro and State University of Rio de Janeiro, in Brasil in 2010, pg. 937-944, ISBN: 978-85-285-0137-7
3. **Andrei Crisan**, Viorel Ungureanu, Dan Dubina: "Ultimate Limit Strength of Pallet Racks Uprights", Sixth International PhD & DLA Symposium, University of Pecs, Faculty of Engineering, Pecs, Hungary, 2010 (acceptat spre publicare)
4. **Andrei Crisan**, Viorel Ungureanu, Dan Dubina: "Proiectarea si Verificarea Structurilor Pentru Depozite Paletizate", Publicat in lucrarile celei de-a 12-a conferinte nationale de constructii metalice, , pg. 117 – 128, Editura orizonturi universitare, Timisoara, ISBN: 978-973-638-464-6, Timisoara, Romania, 2010
5. Dan Dubina, Viorel Ungureanu, **Andrei Crisan**: "Interactive buckling strength of perforated cold formed steel Sections", Published in Proceedings of EUROSTEEL 2011, 6th International Conference on Steel and Composite Structures, Published by ECCS – European Convention for Constructional Steelwork, ISBN (ECCS): 978-92-9147-103-4, p. 129-134, Budapest, Hungary, 2011
6. **Andrei Crisan**, Viorel Ungureanu, Dan Dubina: "Behaviour of cold-formed perforated sections in compression. Part 1 – experimental investigations, Published in VOLUME 2, Proceedings of ICTWS, 6th International Conference on Thin Walled Structures, Published by ECCS – European Convention for Constructional Steelwork, ISBN (ECCS): 978-92-9147-102-7, p. 795-804, Timisoara, Romania 2011
7. **Andrei Crisan**, Viorel Ungureanu, Dan Dubina: "Behaviour of cold-formed perforated sections in compression. Part 2 – interactive overall-sectional buckling", Published in VOLUME 2, Proceedings of ICTWS, 6th International Conference on Thin Walled Structures, Published by ECCS – European Convention for Constructional Steelwork, ISBN (ECCS): 978-92-9147-102-7, p. 805-812, Timisoara, Romania 2011
8. Dan Dubina, Viorel Ungureanu, **Andrei Crisan**: "Proiectarea și verificarea structurilor pentru depozite paletizate", Revista AICPS nr. 1-2/2011, Romania

9. **Andrei Crisan**, Aurel Stratan: "Overstrength Demands In Multistorey Eccentrically Braced Frames", SUSTAINABILITY in SCIENCE ENGINEERING. Volume II, Proceedings of the 11th WSEAS Int. Conf. on SUSTAINABILITY in SCIENCE ENGINEERING (SSE '09), Timișoara, Romania, May 27-29, 2009, pg. 401-407, ISSN:1790-2769, ISBN:987-960-474-080-2 (**ISI**)
10. Dan Dubina, Viorel Ungureanu, **Andrei Crisan**: "Experimental evidence of erosion of critical interactive distortional–overall buckling load", Special Issue on Cold–formed Steel Structures of Journal of Structural Engineering (ASCE) – sent for publication

6.4 Acknowledgements

This work was partially supported by the strategic grant POSDRU 6/1.5/S/13, (2008) of the Ministry of Labour, Family and Social Protection, Romania, co-financed by the European Social Fund – Investing in People.

The experimental program has been realised with the help of **Dexion Hi-Lo Storage Solutions S.R.L.** (<http://www.dexion.ro/ro/>)

REFERENCES

- [1] Rhodes J & Shanmugam NE: Section VI: "Structural Engineering. Cold-formed steel structures", in The Civil Engineering Handbook, 2nd Edition (WF Chen, JYR Liew editors), CRC Press, 2003.
- [2] Hancock GJ, "Light Gauge Construction", Progress in Structural Engineering and Materials, Vol. I (1), 25-30, 1997.
- [3] Rhodes J (Ed.) Cold-Formed Members in Constructional Steel Design - An International Guide. Elsevier, Oxford, 1992
- [4] AISI (1996). Cold-Formed Steel Design Manual. American Iron and Steel Institute. Washington, D.C., 1996.
- [5] AISI (1999). Specification for the Design of Cold-Formed Steel Structural Members with Commentary. 1996 Edition, Supplement No. 1. American Iron and Steel Institute. Washington, D.C., 1999.
- [6] AISI (2001). North American Specification for the Design of Cold-Formed Steel Structural Members with Commentary. American Iron and Steel Institute. Washington, D.C., 2001.
- [7] AISI (2004). Supplement 2004 to the North American Specification for the Design of Cold-Formed Steel Structural Members, 2001 Edition: Appendix 1, Design of Cold-Formed Steel Structural Members Using Direct Strength Method. American Iron and Steel Institute, Washington, D.C., SG05-1. 2004
- [8] AISI S100-07, North American Specification for the Design of Cold-Formed Steel Structural Members, 2007 edition, American Iron and Steel Institute. 2007
- [9] ECCS - European Convention for Constructional Steelwork. European recommendations for design of light gauge steel members. ECCS TC7, Brussels. 1987
- [10] EN1993-1-3:2006 (European Standard). Eurocode 3: Design of steel structures. Part 1-3: General Rules. Supplementary rules for cold-formed thin gauge members and sheeting. Published by European Committee for Standardization, Brussels, 2006
- [11] AS/NZS 4600 - Australian Standards / New Zealand Standards: Cold-formed Steel Structures, Sydney, 2005
- [12] Yu Wei-Wen "Cold-formed Steel Design (3rd Edition)", John Willey & Sons, New York, 2000
- [13] EN15512:2009, „Steel static storage systems - Adjustable pallet racking systems - Principles for structural design“, CEN, 2009.
- [14] prEN15878, "Steel static storage systems - Adjustable pallet racking - Terms and definitions", 2008.
- [15] Rondal J., "Thin-walled structures - General Report.", Stability of Steel Structures (Ivanyi M. Ed.), Akademiai Kiado, Budapest, Vol. 2, 849-866.
- [16] Chajes, A., Fang, J., Winter, G. (1966). "Torsional Flexural Buckling, Elastic and Inelastic, of Cold Formed Thin Walled Columns". Cornell Engineering Research Bulletin, 66(1). 1988
- [17] Andrei Crisan, Aurel Stratan: "Overstrength Demands In Multistorey Eccentrically Braced Frames", Proceedings of the 11th WSEAS Int. Conf. on Sustainability in Science Engineering (SSE '09), Timișoara, Romania, May 27-29, 2009, pg. 401-407, ISSN:1790-2769, ISBN:987-960- 474-080-2

- [18] Karren, K.W., Winter, G.. "Effects of Cold-Forming on Light-Gage Steel Members". J. of the Structural Div., ASCE, 93(ST1), pp. 433-469., 1987
- [19] Chajes, A., S. J. Britvec, and G. Winter: "Effects of Cold-Straining on Structural Sheet Steels," Journal of the Structural Division, ASCE Proceedings, vol. 89, 1963
- [20] Uribe, J., Winter, G.. "Cold-Forming Effects in Thin-Walled Steel Members". Dept. Of Struct. Eng., Cornell University, 1969
- [21] Rondal J, Dubina D, Bivolaru D. "Residual stresses and the behaviour of cold-formed steel structures." Proceedings of 17th Czech and Slovak International Conference on Steel Structures and Bridges, Bratislava, Slovakia, September 7-9, 193-197, 1994
- [22] Hancock G.J. "Design of Cold-formed Steel Structures, 3rd edition," Australian Institute of Steel Construction, Sydney, 1998
- [23] Karren, K. W.: "Corner Properties of Cold-Formed Steel Shapes," Journal of the Structural Division, ASCE Proceedings, vol. 93, Feb. 1967
- [24] Karren, K. W. and G. Winter: "Effects of Cold-Forming on Light-Gage Steel Members," Journal of the Structural Division, ASCE Proceedings, vol. 93, 1967.
- [25] Sfintesco D. "Fondement expérimental des courbes européennes de flambement." Construction Métallique. 3, 1970.
- [26] Rondal J, Maquoi R. "Formulations d'Ayrton-Perry pour le flambement des barres métalliques." Construction Métallique. 4, p.41-53., 1979
- [27] Batista, E.M. "Essais de profils C et U en acier pliées a froid. Laboratoire de Stabilité des Constructions", Université de Liege, Rapport Nr. 157, Septembre 1986.
- [28] Dubina D. "The ECBL approach for interactive buckling of thin-walled steel members", Steel & Composite Structures. 1(1):75-96., 2001
- [29] Costa Ferreira, C.M. and Rondal, J. "Etude experimental de la stabilité des cornières a parois minces profilées a froid". Université de Liege, Laboratoire de Stabilité des Constructions, Rapport Nr. 149, Janvier. 1985
- [30] Costa Ferreira, C.M. and Rondal, J. "Influence of flexural residual stresses on the stability of compressed angles". Journal of Constructional Steel Research, 9(1988), p. 169-177, 1986
- [31] Costa Ferreira, C.M. "Essais de cornières en acier pliées a froid. Université de Liege", Laboratoire de Stabilité des Constructions, Rapport Nr. 155, 1986.
- [32] EN1993-1-1:2005 (European Standard). Eurocode 3: Design of steel structures - Part 1-1: General rules and rules for buildings. Published by European Committee for Standardization, Brussels, 2005
- [33] EN1993-1-5:2006 (European Standard). Eurocode 3: Design of steel structures - Part 1-5: Plated structural elements. Published by European Committee for Standardization, Brussels, 2006
- [34] Young, B. "The Behaviour and Design of Cold-Formed Channel Columns". Ph.D. Thesis. University of Sydney. Sydney, Australia, 2001
- [35] Rasmussen, K.J.R., Hancock, G.J. "The Flexural Behavior of Thin-Walled Singly Symmetric Columns". Int'l Conf. on Steel and Aluminum Structures. Singapore, 1991
- [36] Schafer, B.W. "Cold-Formed Steel Behavior and Design: Analytical and Numerical Modeling of Elements and Members with Longitudinal Stiffeners". Ph.D. Thesis. Cornell University. Ithaca, New York, 1997.

- [37] Peköz, T., "Post-Buckling Interaction of Plate Elements: Progress Report to Swedish Building Research Council". Dept. of Structural Eng., Cornell University. Ithaca, New York, 1977
- [38] Dubina D., "Coupled instabilities in bar members – General Report. Coupled Instabilities in Metal Structures" – CISM'96 (Rondal J, Dubina D & Gioncu V, Eds.). Imperial College Press, London, 119-132., 1996
- [39] Hancock, G.J. "Design of Cold-formed Steel Structures. 3rd Edition", Australian Institute of Steel Construction, Sydney, 1998
- [40] Murray N.W., "Introduction to the theory of thin-walled structures". Clarendon Press, Oxford, 1985
- [41] Dubina D, Ungureanu V. "Elastic-Plastic Interactive Buckling of Thin-Walled Steel Compression Members." Proceeding of the 15th International Speciality Conference on Cold-Formed Steel Structures, October 19-20, 2000, St. Louis, Missouri, USA, 223-237, 2000
- [42] EN1998-1 (2004) (European Standard). Eurocode 8 – Design of structures for earthquake resistance - Part 1: General rules, seismic actions and rules for buildings. Published by European Committee for Standardization, Brussels, 2004
- [43] Schafer, B.W., Hancock G.J. "Appendix A: Detailed History of Distortional Buckling of Columns", in Distortional Buckling of Cold-Formed Steel Columns, Final Report, AISI, 2000 (http://www.ce.jhu.edu/bschafer/dist_columns/dist_columns.htm).
- [44] Bebiano R., Silvestre N., Camotim D. GBTUL 1.0 β - Code for Buckling and Vibration Analysis of Thin-Walled Members, freely available at <http://www.civil.ist.utl.pt/gbt>, 2008
- [45] Winter, G.. "Tests on Light Studs of Cold-Formed Steel". Third Progress Report. Cornell University. (Unpublished), 1940
- [46] Winter, G. "Tests on Light Studs of Cold-Formed Steel". Second Summary Report. Cornell University. (Unpublished), 1943
- [47] Winter, G. "Performance of Compression Plates as Parts of Structural Members". Research, Engineering Structures Supplement, Colston Papers, vol. II, pp. 179, London, 1949
- [48] Chilver, A.H. "The Behavior of Thin-Walled Structural Members in Compression". Engineering, pp. 281-282, 1951
- [49] Chilver, A.H. "The Stability and Strength of Thin-Walled Steel Struts". The Engineer, pp. 180-183, 1953
- [50] Harvey, J.M. "Structural Strength of Thin-Walled Channel Sections". Engineering, pp. 291-293, 1953
- [51] Karren, K.W. "Effects of Cold-Forming on Light-Gage Steel Members". Ph.D. Thesis, Cornell University. Ithaca, New York, 1965
- [52] Winter, G., and J. Uribe: "Effects of Cold Work on Cold-Formed Steel Members," in Thin-Walled Steel Structures (K. C. Rokey and H. V. Hill, Eds.), Gordon and Breach Science Publishers, New York, 1968.
- [53] Dewolf, J.T., Peköz, T., Winter, G. "Local and Overall Buckling of Cold-Formed Members". J. of the Structural Div., ASCE, 100(ST10), pp. 2017-2036, 1974
- [54] Klöppel, K. Bilstein, W. "Untersuchungen zur linearen und nichtlinearen Beultheorie mit Beulwerttafeln für dünnwandige U, C und Hut-Profile und Tafeln für mitwirkende Breiten und Tragspannungen von dreiseitig und vierseitig gelenkig gelagerten Recktaekplatten nach der nichtlinearen Beultheorie". Stahlbau, 45(2), pp. 33-38, 1976

- [55] Chajes, A., Fang, J., Winter, G. "Torsional Flexural Buckling, Elastic and Inelastic, of Cold Formed Thin Walled Columns". Cornell Engineering Research Bulletin, 66(1), 1966
- [56] Peköz, T. "Torsional Flexural Buckling of Thin-Walled Section Under Eccentric Load". Cornell Engineering Research Bulletin, 69(1), 1969
- [57] Rhodes, J., Harvey, J.M. "Interaction Behaviour of Plain Channel Columns under Concentric or Eccentric Loading". Proc. of the 2nd Int'l. Colloquium on the Stability of Steel Structures. ECCS, Liege, pp. 439-444, 1977
- [58] Lundquist, E.E., Stowel, E.Z. "Principles of Moment Distribution Applied to the Stability of Structures Composed of Bars or Plates". NACA, L-326, 1943
- [59] Timoshenko, S.P., Gere, J.M. "Theory of Elastic Stability". McGraw-Hill, 1936
- [60] von Kármán, T., Sechler, E.E., Donnell, L.H. "The Strength of Thin Plates In Compression". Transactions of the ASME, 54, pp. 53-57, 1932
- [61] Winter, G. "Strength of Thin Steel Compression Flanges." Transactions of ASCE, Paper No. 2305, Trans., 112, 1, 1947
- [62] Divakaran, S. "The Influence of Shape on the Strength of open Thin-Walled Columns". M.S. Thesis. McMaster University. Hamilton, Ontario, Canada, 1964
- [63] Dewolf, J.T., Peköz, T., Winter, G. "Local and Overall Buckling of Cold-Formed Members". J. of the Structural Div., ASCE, 100(ST10), pp. 2017-2036, 1974
- [64] Klöppel, K. Bilstein, W. "Untersuchungen zur linearen und nichtlinearen Beultheorie mit Beulwerttafeln für dünnwandige U, C und Hut-Profile und Tafeln für mitwirkende Breiten und Tragspannungen von dreiseitig und vierseitig gelenkig gelagerten Reckteckplatten nach der nichtlinearen Beultheorie". Stahlbau, 45(2), pp. 33-38, 1976
- [65] Klöppel, K., Unger, B "Das Ausbeulen einer am freien Rand verstüften, dreiseitig momentenfrei gelagerten Platte unter Verwendung der nichtlinearen Beultheorie, Teil II: Experimentelle Untersuchungen, Vergleich der experimentellen mit den theoretischen Ergebnissen". Der Stahlbau, 39, pp. 115-123, 1970
- [66] Cheung, Y.K. "Finite Strip Method in Structural Analysis". Pergamon Press, New York, 1976
- [67] Cheung, Y.K. and Fan, S.C. "Static Analysis of Right Box Girder Bridges by the Spline Finite Strip Method", Proc Inst Civ Engrs, Part 2, 75, June, pp 311 - 323, 1983
- [68] Rhodes, J., Harvey, J.M. "Interaction Behaviour of Plain Channel Columns under Concentric or Eccentric Loading". Proc. of the 2nd Int'l. Colloquium on the Stability of Steel Structures. ECCS, Liege, pp. 439-444. 1977
- [69] Venkataramaiah, K.R. "Optimum Edge Stiffeners for Thin-Walled Structural Elements with Edge Stiffeners". Solid Mechanics Report, 7, University of Waterloo, Ontario, Canada, 1971
- [70] Dwight, J.B. "Aluminum Sections with Lipped Flanges and Their Resistance to Local Buckling". Proc., Symposium on Aluminum in Structural Eng., London, England, 1963.
- [71] Sharp, M.L., "Longitudinal Stiffeners for Compression Members". J. of the Structural Div., ASCE, 92(ST5), pp. 187-211, 1966
- [72] Goldberg, J.E., Bogdanoff, J.L. and Glauz, W.D., "Lateral and Torsional Buckling of Thin-Walled Beams", Proceedings, IABSE, Vol. 24, 1964, pp. 91 -100.
- [73] Wittrick, WH, "General Sinusoidal Stiffness Matrices for Buckling and Vibration Analyses of Thin Flat-Walled Structures", Int. J. Mech Sci, Vol 10, p. 949-966, 1968

- [74] Wittrick, WH "A Unified Approach to the Initial Buckling of Stiffened Panels in Compression", *The Aeronautical Quarterly*, August 1968, pp. 265 - 283, 1968b
- [75] Plank, R.J. and Wittrick, W.H., "Buckling under Combined Loading of Thin, Flat-Walled Structures by a Complex Finite Strip Method, *Int Jour Num Meth in Engg*, Vol 8, pp. 323 -339, 1974
- [76] Lau, S.C.W., and Hancock, G.J., "Distortional Buckling Formulas for Channel Columns", *Journal of Structural Engineering, ASCE*, 1987, 113(5), pp 1063 - 1078, 1987
- [77] Loughlan, J. "Mode Interaction in Lipped Channel Columns under Concentric or Eccentric Loading". Ph.D. Thesis. University of Strathclyde, Glasgow, 1979
- [78] Kalyanaraman, V., Peköz, T., Winter, G.. "Unstiffened Compression Elements". *J. of the Structural Div., ASCE*, 103(ST9), pp. 1833-1848, 1977
- [79] Desmond, T.P. "The Behavior and Strength of Thin-Walled Compression Elements with Longitudinal Stiffeners". Ph.D. Thesis. Cornell University. Ithaca, New York, 1977
- [80] Dat, D.T. "The Strength of Cold-Formed Steel Columns". Ph.D. Thesis. Cornell University. Ithaca, New York, 1980
- [81] Weng, C. "Flexural Buckling of Cold-Formed Steel Columns". Ph.D. Thesis. Cornell University. Ithaca, New York, 1987
- [82] Mulligan, G.P. "The Influence of Local Buckling on the Structural Behavior of Singly-Symmetric Cold-Formed Steel Columns" Ph.D. Thesis. Cornell University. Ithaca, New York, 1983
- [83] Loh, T.S. "Combined Axial Load and Bending in Cold-Formed Steel Members" Ph.D. Thesis, Cornell University. Ithaca, New York, 1985
- [84] Peköz, T. "Development of a Unified Approach to the Design of Cold-Formed Steel Members". American Iron and Steel Institute Research Report, CF 87-1, 1987
- [85] Sharp, M.L., "Longitudinal Stiffeners for Compression Members". *J. of the Structural Div., ASCE*, 92(ST5), pp. 187-211, 1966
- [86] Hikosaka, H., Takami, K. and Maruyama, Y., "Analysis of Elastic Distortional Instability of Thin-Walled Members with Open Polygonal Cross Section", *Proceedings of Japan Society of Civil Engineers, Structural Eng./Earthquake Eng.*, Vol. 4, No. 1, April, pp 31 - 40, 1987
- [87] Takahashi, K., "A New Buckling Mode of Thin-Walled Columns with Cross-Sectional Distortions", *Solid Mechanics*, - 2 (eds Tooth, A.S. and Spencer, J.), 25, Elsevier, pp 553 - 573, 1988
- [88] Batista, E., Rondal, J., Maquoi, R. "Column Stability of Cold-Formed U and C Sections". *Proc. of the Int'l Conf. on Steel and Aluminum Structures*. Cardiff, U.K., 1987
- [89] Zaras, J., Rhodes, J. "Carefully Controlled Compression Tests on Thin-Walled Cold-Formed Sections". *Applied Solid Mechanics*, Elsevier, 2, pp. 519-551, 1987
- [90] Lim, B.S. "Buckling behaviour of asymmetric edge stiffened plates". Ph.D. Thesis, University of Strathclyde, Glasgow, 1985
- [91] Lim, B.S., Rhodes, J. "Buckling Behaviour of Asymmetric Edge Stiffened Plates". *Applied Solid Mechanics*, Elsevier, 1, pp. 351-375, 1986
- [92] Hancock, G.J. "Distortional Buckling of Steel Storage Rack Columns". *J. of Structural Eng., ASCE*, 111(12), pp. 2770-2783, 1985

- [93] Lau, S.C.W., and Hancock, G.J, "Distortional Buckling Formulas for Channel Columns", *Journal of Structural Engineering*, ASCE, 1987, 113(5), pp. 1063 – 1078, 1987
- [94] Hikosaka, H., Takami, K. and Maruyama, Y. "Analysis of Elastic Distortional Instability of Thin-Walled Members with Open Polygonal Cross Section", *Proceedings of Japan Society of Civil Engineers, Structural Eng./Earthquake Eng.*, Vol. 4, No. 1, April, pp. 31 – 40, 1987
- [95] Takahashi, K. "A New Buckling Mode of Thin-Walled Columns with Cross-Sectional Distortions", *Solid Mechanics*, - 2 (eds Tooth, A.S. and Spencer, J.), 25, Elsevier, pp. 553 – 573, 1988
- [96] Sridharan, S. "A Semi-Analytical Method for the Post-Local-Torsional Buckling Analysis of Prismatic Plate Structures", *Int Jour Num Meth in Engg*, Vol 18, pp 1685 – 1697, 1982
- [97] Moldovan, A. "Compression Tests on Cold-Formed Steel Columns with Monosymmetrical Section". *Thin-Walled Structures*, Elsevier, 20(1-4), pp. 241-252, 1994
- [98] Salmi, P. and Talja, A. "Design of Cold-Formed HSS Channels for Bending and Eccentric Compression", *VTT Research Notes*, 1505, Technical Research Centre of Finland, Espoo, 1993
- [99] Miller, T.H., Peköz, T. "Load-Eccentricity Effects on Cold-Formed Steel Lipped-Channel Columns." *J. of Struct. Eng.*, ASCE, 120(3), pp. 805-823, 1994
- [100] Polyzois, D., Sudharmapal, A.R. "Cold-Formed Steel Z-Sections with Sloping Edge Stiffness under Axial Load". *J. of Struct. Eng.*, ASCE, 116(2), pp. 392-406, 1990
- [101] Purnadi, R.W., Tassoulas, J.L., Polyzois, D. "Study of Cold-Formed Z-section Steel Member under Axial Loading". 10th Int'l. Spec. Conf. on Cold-Formed Steel Structures. University of Missouri-Rolla, St. Louis, Missouri, 1990
- [102] Polyzois, D., Charnvarnichborikarn, P. "Web-Flange Interaction in Cold-Formed Steel Z-Section Columns". *J. of Struct. Eng. ASCE*, 119(9), pp. 2607-2628, 1993
- [103] Kwon, Y.B. "Post-Buckling Behaviour of Thin-Walled Channel Sections". Ph.D. Thesis. University of Sydney. Sydney, Australia, 1992
- [104] Kwon, Y.B., and Hancock, G.J., "Strength Tests of Cold-Formed Channel Sections undergoing Local and Distortional Buckling", *Jour Struct Engg*, ASCE, 117(2), pp. 1786 – 1803.
- [105] Rasmussen, K.J.R., Hancock, G.J. "The Flexural Behavior of Thin-Walled Singly Symmetric Columns". *Int'l Conf. on Steel and Aluminum Structures*. Singapore, 1991
- [106] Young, B. "The Behaviour and Design of Cold-Formed Channel Columns". Ph.D. Thesis. University of Sydney. Sydney, Australia, 1997
- [107] Seah, L.K. "Buckling behaviour of edge stiffeners in thin-walled sections". Ph.D. Thesis. University of Strathclyde, Glasgow, 1989
- [108] Seah, L.K., Rhodes, J. "Simplified Buckling Analysis of Plate with Compound Edge Stiffeners". *J. of Eng. Mech.*, ASCE, 119(1), pp. 19-38, 1993
- [109] Seah, L.K., Rhodes, J., Lim, B.S., "Influence of Lips on Thin-Walled Sections". *Thin-Walled Structures*. Elsevier, 16(1-4), pp. 145-178, 1993
- [110] Chou, S.W., Seah, L.K., Rhodes, J. "Accuracy of Some Codes of Practice in Predicting the Load Capacity of Cold-Formed Columns". *J. of Constructional Steel Research*, Elsevier, 37(2), pp. 137-172, 1996
- [111] Schardt, R. "Verallgemeinerte Technische Biegetheorie". Springer-Verlag, Germany, 1989

- [112] Davies, J.M., Leach, P., Heinz, D. "Second-Order Generalised Beam Theory". *J. of Constructional Steel Research*, Elsevier, 31(2-3), pp. 221-242, 1994
- [113] Schardt, R. "Generalized Beam Theory - An Adequate Method for Coupled Stability Problems". *Thin-Walled Structures*, Elsevier, 19(2-4), pp. 161-180, 1994
- [114] Rotter J.M. "Challenges in the generalisation of structural buckling assessments to all structures and load cases", *The 6th International Conference on Thin Walled Structures*, Timisoara, Romania, 2011
- [115] Koen D., "Structural capacity of light gauge steel storage rack uprights", Thesis presented for the degree of Master of Engineering, School of Civil Engineering, The University of Sydney, 2008
- [116] Panangelis, J.P. and Hancock G.J. "Computer analysis of thin walled structural members, V.2.1", Centre for advanced structural engineering, University of Sydney, NSW Australia
- [117] Davies, J.M., Jiang, C. "Design of Thin-Walled Columns for Distortional Buckling". *Proc. of the 2nd Int'l Conf. on Coupled Instabilities in Metal Structures*, Imperial College Press, Liege, Belgium, 1996
- [118] Hancock, G.J., Kwon, Y.B., Bernard, E.S. "Strength Design Curves for Thin-Walled Sections Undergoing Distortional Buckling". *J. of Constructional Steel Research*, Elsevier, 31(2-3), pp. 169-186, 1994
- [119] von Kármán, T., "Festigkeitsproblem im Maschinenbau," *Encyk. D. Math. Wiss.* **IV**, 311-385, 1910
- [120] Marguerre, K.: "Zur Theorie der gekrummten Platte grosser Formänderung, in *Proceedings*", Fifth International Congress for Applied Mechanics, 93-101, 1938.
- [121] Bourrier P., Brozzetti J.: *Construction metallique et mixte acier-beton*, Tome 2, Conception et mise en oeuvre, Editions Eyrolles, APK et ACIER, Paris, 1996.
- [122] Moen C.D., Schafer B.W. "Direct strength design of cold-formed steel members with perforations", Research report, AISI, 2009
- [123] Dinis PB, Camotim D. 'Post-Buckling Behaviour and Strength of Cold-Formed Steel Lipped Channel Columns Experiencing Distortional/Global Interaction', *Computers and Structures*, 89 422-434, 2011
- [124] Schafer, B.W. "A Correction to AISI Specification B2.3 and B4.2 in order to partially alleviate the unconservative prediction of members with edge stiffened elements." *Commentary on Ballot S98-90A*, American Iron and Steel Institute. (Unpublished), 1998
- [125] Silvestre N, Camotim D "First-order generalised beam theory for arbitrary orthotropic materials". *Thin-Walled Structures*, 40 (9) 755-789, 2002
- [126] Silvestre N, Camotim D. "Second-order generalised beam theory for arbitrary orthotropic materials. *Thin-Walled Structures*, 40 (9) 791-820, 2002
- [127] Silvestre N, Camotim D., "Nonlinear Generalized Beam Theory for Cold-formed Steel Members", *International Journal of Structural Stability and Dynamics*. 3 (4) 461-490, 2003
- [128] Camotim D., Silvestre N., Gonçalves R. and Dinis P.B., "GBT analysis of thin-walled members: new formulations and applications", *Thin-Walled Structures: Recent Advances and Future Trends in Thin-Walled Structures Technology (Loughborough, 25/6)*, J. Loughlan (ed.), Canopus Publishing, Bath, 137-168, 2004.
- [129] Camotim D., Silvestre N., Gonçalves R. and Dinis P.B., "GBT-based structural analysis of thin-walled members: overview, recent progress and future

- developments", *Advances in Engineering Structures, Mechanics and Construction (Waterloo, 14-17/5)*, M. Pandey, W.C. Xie, L. Xu (eds.), Springer, Dordrecht, 187-204, 2006.
- [130] Camotim D., Basaglia C. and Silvestre N. "GBT buckling analysis of thin-walled steel frames: A state-of-the-art report", *Thin-Walled Structures*, Volume 48, Issues 10-11, pp. 726-743, 2010
- [131] Schafer BW, Ádány S "Buckling analysis of cold-formed steel members using CUFSM: conventional and constrained finite strip methods". Eighteenth International Specialty Conference on Cold-Formed Steel Structures, Orlando, FL. October 2006.
- [132] Ádány, S., Schafer, B.W. "A full modal decomposition of thin-walled, single-branched open cross-section members via the constrained finite strip method". *Journal of Constructional Steel Research*, 64, pp. 12-29, 2008
- [133] Dubina D. "Recent research advances and trends on coupled instability of bar members, General Report – Session 3: Bar Members", *Coupled Instabilities in Metal Structures - CIMS'2000 (Camotin D, Dubina D & Rondal J, Eds.)*. Imperial College Press, London, 131-144, 2000
- [134] Dubina, D., Ungureanu, V. "Effect of imperfections on numerical simulation on instability behaviour of cold-formed steel members", *Thin Walled Structures*, Vol. 40, No. 3, 239-262, 2002
- [135] Dubina, D., Ungureanu, V., Rondal, J. "Numerical modelling and codification of imperfections for cold-formed steel members analysis", *Steel & Composite Structures*, Volume 5, Number 6, December 2005, pp. 315-332, 2005
- [136] Gioncu, V. "Instabilities and Catastrophes in Structural Engineering", Bucharest, Editura Academiei (in Romanian), 2004
- [137] Gioncu, V. "Coupled instabilities under dynamic loading. General report", In J. Rondal, D. Dubina and V. Gioncu, eds. *Coupled Instabilities in Metal Structures*, London, Imperial College Press, 469-481, 1996
- [138] Gioncu, V. "Stable and unstable components of the critical load". In J.Szabo, Zs. Caspar and T.Tarnai, eds. *Post-Buckling of Elastic Structures*, Budapest, Akademiai Kiado, 93-117, 1986
- [139] Lau, S.C.W. and Hancock, G.J., "Inelastic Buckling of Channel Columns in the Distortional Mode", *Thin-Walled Structures*, 10(1), pp. 59-84.
- [140] Gioncu, V. "General theory of coupled instabilities. General report". *Thin-Walled Structures*, Vol. 19, No. 2-4, 81-127, 1994
- [141] Schafer B.W. "Review: the direct strength method of cold-formed steel member design", *Journal of Constructional Steel Research*, 64(7-8), 766-778, 2008
- [142] Bebiano R., Silvestre N. and Camotim D. "GBTUL – a code for the buckling analysis of cold-formed steel members", *Proceedings of 19th International Specialty Conference on Recent Research and Developments in Cold-Formed Steel Design and Construction (St. Louis, 14-15/10)*, R. LaBoube, W.-W. Yu (eds.), pp. 61-79, 2008
- [143] AISI S100-07-C, *Commentary on North American Specification for the Design of Cold-Formed Steel Structural Members*, 2007 edition, American Iron and Steel Institute, 2007
- [144] AISI S200-07, *Standard for Cold-Formed Steel Framing – General Provisions*, 2007 edition, American Iron and Steel Institute, 2007
- [145] Burstand H "Light Gauge Steel Framing for Housing", SBI – Swedish Institute of Steel Construction, Publication 170, Stockholm, Sweden, 2000

- [146] Canadian Standards Association (1994). S136 - Specification for Cold Formed Steel Structural Members, Toronto, Ontario, Canada, 1994.
- [147] Dubina D, Rondal J, Vayas I (Eds), "Design of Steel Structures; EUROCODE 3-Worked Examples", Bridgeman Ltd., Timisoara, Romania. 1997
- [148] ECCS - European Convention for Constructional Steelwork (European Recommendations for the Application of Metal Sheeting acting as a Diaphragm, Publication No.88, Brussels, 1995
- [149] ECCS - European Convention for Constructional Steelwork Worked examples according to EN1993-1-3. ECCS TC7, TWG 7.5, Brussels, 2008
- [150] Hancock G.J. "Design of cold-formed steel structures (to AS/NZS 4600:2005). 4th edition", Australian Institute of Steel Construction, Sydney, 2007.
- [151] Lawson RM, Grubb PJ, Prewer J, Trebilcock PJ "Modular construction using light steel framing: An architect's guide", SCI Publication P272. Steel Construction Institute, Ascot, Berkshire, United Kingdom, 1999
- [152] Makelainen P, Kesti J "Advanced method for lightweight steel joining". Journal of Constructional Steel Research, No. 49, 107-116, 1999
- [153] Predeschi RF, Sinha BP, Davies R "Advanced connection techniques for cold-formed steel structures", Journal of Structural Engineering (ASCE), vol. 123(2), 138-144, 1997
- [154] Schafer BW "Designing Cold-Formed Steel Using the Direct Strength Method", Proceeding of the 18th International Specialty Conference on Cold-Formed Steel Structures, October 26-27, 2006, Orlando, Florida, 2006
- [155] Cheung, Y.K. "Finite Strip Method in Structural Analysis", Pergamon Press, New York, 1976
- [156] Cheung, Y.K. and Fan, S.C. "Static Analysis of Right Box Girder Bridges by the Spline Finite Strip Method", Proc Inst Civ Engrs, Part 2, 75, June, pp. 311 - 323, 1983
- [157] Comite Europeen de Normalisation "Eurocode 3: Design of Steel Structures, Part 1.3: General Rules", European Prestandard ENV 1993-1-3, 1996
- [158] Kassab, M., Pan, C.L., Yu, W.W. "Effect of Strain Rate on Cold-Formed Steel Stub Columns". J. of Structural Eng., ASCE, 118(11), pp. 3151-3168, 1992
- [159] Klöppel, K., Unger, B. "Das Ausbeulen einer am freien Rand verstüfteten, dreiseitig momentenfrei gelagerten Platte unter Verwendung der nichtlinearen Beultheorie, Teil II: Experimentelle Untersuchungen, Vergleich der experimentellen mit den theoretischen Ergebnissen". Der Stahlbau, 39, pp. 115-123, 1970
- [160] Lau, S.C.W. "Distortional Buckling of Thin-Walled Columns". Ph.D. Thesis, University of Sydney. Sydney, Australia, 1988
- [161] Peköz, T. "Torsional Flexural Buckling of Thin-Walled Section Under Eccentric Load". Cornell Engineering Research Bulletin, 69(1), 1969
- [162] Rhodes, J., Loughlan, J. "Simple Design Analysis of Lipped Channel Columns". 5th Int'l. Spec. Conf. on Cold-Formed Steel Structures. University of Missouri-Rolla, St. Louis, Missouri, 1980
- [163] Schafer, B.W. "Distortional Buckling of Cold-Formed Steel Columns". Research Report. Committee on Specifications for the Design of Cold-Formed, Steel Structural Members. American Iron and Steel Institute, 2006
- [164] Schafer B.W. "Designing Cold-Formed Steel Using the Direct Strength Method". 18th International Specialty Conference on Cold-Formed Steel Structures, October 26-27, Orlando, Florida, 2006
- [165] Standards Australia (1993). "Steel Storage Racking", AS4084.

- [166] Standards Australia/Standards New Zealand (1996), "Cold-Formed Steel Structures", AS/NZS4600.
- [167] Thomasson, P. "Thin-walled C-shaped Panels in Axial Compression". Swedish Council for Building Research. D1:1978, Stockholm, Sweden, 1978
- [168] AS4048. Steel Storage Racking.. Standards Australia, Sydney, 1993
- [169] MH16.1:2008, "Specification for the Design, Testing and Utilization of Industrial Steel Storage Racks", Rack Manufacturing Institute, 2008.
- [170] EN1998 – Eurocode 8 – "Design of structures for earthquake resistance", CEN, 2005.
- [171] Lecce, M. and Rasmussen, K. Distortional Buckling of Cold-Formed Stainless Steel Sections: Experimental Investigation. Journal of Structural Engineering 2006; 132:497-504, 2006
- [172] Lecce, M. and Rasmussen, K. "Distortional Buckling of Cold-Formed Stainless Steel Sections: Finite-Element Modelling and Design". Journal of Structural Engineering 2006; 132:505-514, 2006
- [173] Crisan A., Ungureanu. V, Dubina D.: "Ultimate Limit Strength of Perforated Cold-Formed Steel Sections", International Colloquium, "Stability and Ductility of Steel Structures" Rio de Janeiro, Brasil, 2010, Published in VOLUME 2, Proceedings of SDSS' Rio 2010, International Colloquium Stability and Ductility of Steel Structures, Published by Federal University of Rio de Janeiro and State University of Rio de Janeiro, in Brasil in 2010, pg. 937-944, ISBN: 978-85-285-0137-7, 2010
- [174] Andrei Crisan, Viorel Ungureanu, Dan Dubina: "Proiectarea si Verificarea Structurilor Pentru Depozite Paletizate", a 12a Conferinta nationale de constructii metalice, Facultatea de Constructii, Timisoara, Romania, 2010, Lucrarile celei de-a 12-a Conferinta Nationale de Constructii Metalice, Timisoara, 26-27 noiembrie 2010, p. 117 – 128, Editura orizonturi universitare, Timisoara, ISBN: 978-973-638-464-6, 2010
- [175] Casafont. M, Pastor M.M., Roure F., Pekoz T., "An experimental investigation of distortional buckling of steel storage rack columns" Thin-Walled Structures 49,p. 933 –946, 2011
- [176] Davies, J.M., Leach, P., Taylor, A., "The design of perforated cold-formed steel sections subject to axial load and bending", Thin-Walled Structures, 29(1-4): 141-157, 1997.
- [177] EN10002-1, "Tensile testing of metallic materials. Method of test at ambient temperature", Published by European Committee for Standardization, Brussels, 2001.
- [178] Rondal, J. "Determination theoretique des contraintes residuelles dans les elements en acier profiles a froid". Ce travail a recu le prix N.V. BEKAERT S.A. 1992, octroye par le Fonds National de la Recherche Scientifique, 1992
- [179] LIMESS Messtechnik und Software GmbH, Gripswaldstr. 37, 47804 Krefeld, Germany, <http://www.limess.com>
- [180] Ungureanu V., "Contribuții la studiul flambajului prin încovoiere-răsucire a grinzilor din profile cu pereți subțiri", Universitatea "POLITEHNICA" din Timisoara, Romania, 2003
- [181] Dubina D., "Structural analysis and design assisted by testing of cold-formed steel structures", Thin-Walled Structures 46, p. 741 – 764, 2008
- [182] Georgescu M., "Probleme de intabilitate la bare cu pereti subtiri", Teza de doctorat, UP Timisoara, Romania, 1998
- [183] CUFSM: Elastic Buckling Analysis of Thin-Walled Members by Finite Strip Analysis. CUFSM v3.12, 2006. <http://www.ce.jhu.edu/bschafer/cufsm>.

- [184] Rhodes, J. and Schneider, F. D., "The compressional behaviour of perforated elements". Proc. Twelfth International Speciality Conference on Cold-Formed Steel Structures, St. Louis, MO, 1994.
- [185] Becque J., "The interaction of local and overall buckling of cold formed stainless steel columns", The University of Sydney, School of Civil Engineering, Australia, 2008
- [186] Crisan A., Ungureanu V., Dubina D.: "Behaviour of cold-formed perforated sections in compression. Part 1 – Experimental Investigations, International conference on thin-walled structures", Timisoara, Romania, 2011, Published in VOLUME 2, Proceedings of ICTWS Timișoara, 2011, 6th International Conference on Thin Walled Structures, Published by ECCS – European Convention for Constructional Steelwork, ISBN (ECCS): 978-92-9147-102-7, p. 795-804, 2011
- [187] Schafer B.W, Peköz T. "Computational modelling of cold-formed steel characterising geometric imperfections and residual stresses", Journal of Constructional Steel Research, 47, 193-210, 1998.
- [188] Bjorhovde R. "Deterministic and probabilistic approaches to the strength of steel columns", PhD Dissertation, Lehigh University, PA, 1972.
- [189] European Recommendations for the Design of Light Gauge Steel Members, ECCS, Brussels, 1978.
- [190] EN1090-2:2008. Execution of steel structures and aluminium structures - Part 2: Technical requirements for steel structures, CEN, Brussels, 2009
- [191] Grumbach, M., Prudhomme, M.. "Proprietes des Profiles a Froid." Construction Metallique, No. 1.1974
- [192] Abdel-Rahman, N. Sivakumaran, K.S.: Material properties models for analysis of cold-formed steel members. Journal of Structural Engineering, Vol. 123, No. 9, pp. 1135-1143, 1997
- [193] Rondal J., Dubina D., Ungureanu V., "Imperfections and computational modelling of cold-formed steel members",
- [194] ABAQUS software package, Desault systems, 2007
- [195] ABAQUS. "Theory manual", Hibbit, Karlson and Sorenson Inc., 2007
- [196] ABAQUS, "Analysis User's Manual. Volume IV: Elements", V.6.7
- [197] EN 1993-1-6: "Strength and stability of shell structures", 2008
- [198] SCHAFFER B.W., "Computational modeling of cold-formed steel", Fifth International Conference on Coupled Instabilities in Metal Structures, Sydney, Australia, 2008
- [199] AS4100-1990: Australian Standard: Steel Structures, Homebush, Australia.
- [200] Loughlan J., Yidris N., Jones K., "The failure of thin-walled lipped channel Compression members due to coupled local-distortional interactions and material yielding", The 6th International Conference on Thin Walled Structures, Timisoara, Romania, 2011
- [201] Dubina D., Goina D., "Interactive buckling approach of thin-walled cold formed members via an Ayrton-Perry formula and based on the Critical Load Erosion Theory", Romanian Academy of Science, Timisoara branch, Research Report, 1995
- [202] EN1990, "Eurocode - Basis of structural design", 2002
- [203] Bjorhovde R. "Evolution and state-of-the-art of column stability criteria" Journal of civil engineering and management, p. 159 - 165, 2010
- [204] Silvestre N, Camotim D. "On the mechanics of distortion in thin-walled open sections". Thin Walled Structures, doi:10.1016/j.tws.2010.02.001, 2010

- [205] Andrei Crisan, Viorel Ungureanu, Dan Dubina: "Behaviour of cold-formed perforated sections in compression. Part 2 – Numerical Investigations", Timisoara, Romania, 2011, Published in VOLUME 2, Proceedings of ICTWS Timișoara, 2011, 6th International Conference on Thin Walled Structures, Published by ECCS – European Convention for Constructional Steelwork, ISBN (ECCS): 978-92-9147-102-7, p. 805-812, 2011
- [206] Dan Dubina, Viorel Ungureanu, Andrei Crisan: "Interactive buckling strength of perforated cold formed steel Sections", Published in Proceedings of EUROSTEEL 2011, 6th International Conference on Steel and Composite Structures, Published by ECCS – European Convention for Constructional Steelwork, ISBN (ECCS): 978-92-9147-103-4, p. 129-134, Budapest, Hungary, 2011